Hybrid and Multifield Inflation

by

Evangelos I. Sfakianakis

Submitted to the Department of Physics
in partial fulfillment of the requirements for the degree of

Doctor of Philosophy

at the

MASSACHUSETTS INSTITUTE OF TECHNOLOGY

June 2014

Author .....
Department of Physics
May 22, 2014

Certified by .....
Alan H. Guth
Victor F. Weisskopf Professor of Physics
Thesis Supervisor

Certified by .....
David I. Kaiser
Germeshausen Professor of the History of Science
and Senior Lecturer, Department of Physics
Thesis Supervisor

Accepted by .....
Krishna Rajagopal
Associate Department Head for Education

Hybrid and Multifield Inflation

by

Evangelos I. Sfakianakis

Submitted to the Department of Physics
on May 22, 2014, in partial fulfillment of the
requirements for the degree of
Doctor of Philosophy

Abstract

In this thesis I study the generation of density perturbations in two classes of inflationary models: hybrid inflation and multifield inflation with nonminimal coupling to gravity.

- In the case of hybrid inflation, we developed a new method of treating these perturbations that does not rely on a classical trajectory for the fields. A characteristic of the spectrum is the appearance of a spike at small length scales, which could conceivably seed the formation of black holes that can evolve to become the supermassive black holes found at the centers of galaxies. Apart from numerically calculating the resulting spectrum, we derived an expansion in the number of waterfall fields, which makes the calculation easier and more intuitive.

- In the case of multifield inflation, we studied models where the scalar fields are coupled non-minimally to gravity. We developed a covariant formalism and examined the prediction for non-Gaussianities in these models, arguing that they are absent except in the case of fine-tuned initial conditions. We have also applied our formalism to Higgs inflation and found that multifield effects are too small to be observable. We compared these models to the early data of the Planck satellite mission, finding excellent agreement for the spectral index and tensor to scalar ratio and promising agreement for the existence of isocurvature modes.

Thesis Supervisor: Alan H. Guth
Title: Victor F. Weisskopf Professor of Physics

Thesis Supervisor: David I. Kaiser
Title: Germeshausen Professor of the History of Science
and Senior Lecturer, Department of Physics

Acknowledgments

I am grateful to my supervisors, Prof. Alan Guth and Prof. David Kaiser, for their support and mentoring. I thank my thesis readers, Prof. Hong Liu and Prof. Max Tegmark for their advice. I also thank my collaborators, Prof. Ruben Rosales, Prof. Edward Farhi, Prof. Iain Stewart, Dr. Mark Hertzberg, Dr. Mustafa Amin, Ross Greenwood, Illan Halpern, Matthew Joss, Edward Mazenc and Katelin Schutz for their contribution to this thesis and beyond.

I would like to thank my family and friends for their continued support and Angeliki for being there for me during the last two years.

I am indebted to my fellow students, the staff of the CTP, Joyce Berggren, Scott Morley and Charles Suggs and the staff of the Physics Department for creating a vibrant environment. I thank the undergraduate students who worked with us, since they reminded me why I wanted to be a physicist, at a time when I needed it the most. I would not be here without the teachers and professors, in Greece and the US, who inspired me and I hope I have met their expectations.

Last but not least I would like to thank George J. Elbaum and Mimi Jensen for their generosity that gave me the opportunity to pursue a PhD at MIT.

This thesis is dedicated to the memory of my beloved grandmother.

Contents

List of Figures

List of Tables

Chapter 1

Introduction

1.1 Inflation

Inflation was introduced by Alan Guth in 1980 [1], and developed into a full working model by Linde [2] and Albrecht and Steinhardt [3] in 1981 and 1982. We will start the thesis by listing what can be considered the four main supporting pieces of evidence for inflation. We will not include the absence of monopoles from our universe, although this was one of the initial motivations.

1. **Uniformity at large scales:** If one examines the universe at large scales, one can see that it is approximately homogenous. From the CMB to the distribution of galaxies, the universe looks the same no matter "which way we look". Based on the standard big bang theory and the fact that information travels at the speed of light at most, opposite parts of the universe were not in causal contact in the past, hence they are not expected to be uniform to that degree (1 in $100,000$). Inflation solves this problem by starting with a very small uniform patch and doubling it 100 times to create our observable universe.

2. **Flatness of the universe:** To explain the flatness problem of the old big bang theory, we should start from an isotropic universe governed by the Friedman-

Robertson-Walker metric

$$ds^2 = dt^2 - a(t)^2 \left[\frac{dr^2}{1-kr^2} + r^2(d\theta^2 + \sin^2\theta d\phi^2) \right], \tag{1.1}$$

where $a(t)$ is the scale factor and k defines the curvature of the universe. Let us define the ratio

$$\Omega = \frac{\text{mass density}}{\text{critical mass density}}. \tag{1.2}$$

The parameter $|\Omega - 1|$ defines the departure from flatness ($\Omega = 1$ for a flat universe). However $|\Omega - 1|$ is increasing after the big bang. In fact, in order for the observed value of $\Omega = 1 + 0.0010 \pm 0.0065$ [4] to be possible, Ω had to be exponentially close to unity at the big bang. Indeed inflation shows that

$$\frac{|\Omega_{\text{end}} - 1|}{|\Omega_{\text{init}} - 1|} = \left(\frac{a_{\text{init}}}{a_{\text{end}}} \right)^2 = e^{-2N_e} \lesssim 10^{-50}, \tag{1.3}$$

meaning that inflation can start with a patch of some curvature and the resulting universe will be approximately flat to a high degree.

3. **Perturbations:** Although the universe is made uniform by inflation, we can see non-uniformities all around us, from planets to solar systems, from galaxies to galaxy clusters and of course in the CMB. This can also be explained quite naturally by inflation. One has to take a step back and realize that quantum mechanics demands that field values are fluctuating on very short scales. During inflation these fluctuations are stretched along with the rest of the universe, so they reach cosmological dimensions. These fluctuations are observable in the CMB, and they also provide the seeds of all structure around us, as they are then enhanced by the unstable nature of gravitational systems. Inflationary predictions agree with the measured spectrum of these fluctuations to an excellent degree [5].

4. **Tensor modes:** Inflation has the ability to stretch fluctuations of the gravitational field that exist at the quantum level to cosmological scales. The am-

plitude of the resulting primordial gravity waves is proportional to the energy scale during inflation. Suppression of gravity waves would not rule out inflation, but rather point to models of "low-scale" inflation. However a detection of primordial gravity waves (through B-modes in the CMB) has been considered a smoking gun for inflation. Such a discovery was announced as the present thesis was being written [6]. Although there are claims that primordial gravity waves can be generated by other sources (e.g. phase transitions), such models are more complicated and not widely accepted as a viable alternative.

1.1.1 Simple Single field inflation

It is worth presenting the simplest model of inflation (which became hugely relevant after the latest BICEP2 data [6]), which is a model of a single inflaton field ϕ coupled minimally to gravity with the potential $V(\phi) = \frac{1}{2}m^2\phi^2$.

The action for this model is

$$S = \int d^4x\sqrt{-g}\left[\frac{M_{\rm Pl}^2}{2}R - \frac{1}{2}g^{\mu\nu}\partial_\mu\phi\partial_\nu\phi - \frac{1}{2}m^2\phi^2\right], \tag{1.4}$$

leading to the following equation of motion

$$\ddot{\phi} + 3H\dot{\phi} + m^2\phi = 0\,, \tag{1.5}$$

where the Hubble parameter is defined as

$$H^2 = \frac{1}{3M_{\rm Pl}^2}\left(\frac{1}{2}\dot{\phi}^2 + V\right). \tag{1.6}$$

During slow roll the dynamics is dominated by the potential energy and the Hubble

parameter remains almost constant, giving

$$\frac{1}{2}\dot{\phi}^2 \ll V(\phi), \tag{1.7}$$

$$|\dot{H}| \ll H^2, \tag{1.8}$$

$$|\ddot{\phi}| \ll |3H\dot{\phi}|\,. \tag{1.9}$$

The above slow roll conditions are equivalent to $\epsilon \ll 1$ and $|\eta| \ll 1$, where ϵ and η are the slow-roll parameters defined by

$$\epsilon \equiv \frac{M_{\rm Pl}^2}{2}\left(\frac{V'}{V}\right)^2 \simeq -\frac{\dot{H}}{H^2}\,, \tag{1.10}$$

$$|\eta| \equiv M_{\rm Pl}^2\left|\frac{V''}{V}\right| \simeq \left|\epsilon - \frac{\ddot{\phi}}{H\dot{\phi}}\right|\,. \tag{1.11}$$

During slow-roll we can neglect the $\ddot{\phi}$ term in the equation of motion for the inflaton, which gives

$$\dot{\phi} = -\frac{m^2\phi}{3H} = -\sqrt{\frac{2}{3}}mM_{\rm Pl}\,, \tag{1.12}$$

where

$$H^2 \simeq \frac{1}{3M_{\rm Pl}^2}V = \frac{m^2}{6M_{\rm Pl}^2}\phi^2\,. \tag{1.13}$$

Using this we can calculate the number of efolds of inflation (the number of times that the universe expands by a factor of $e \approx 2.72$)

$$\begin{aligned} dN = Hdt \Rightarrow N &= \int_{t_i}^{t_{end}} H(t)dt = \int_{\phi_i}^{\phi_{end}} Hdt = \int_{\phi_i}^{\phi_{end}} H\frac{dt}{d\phi}d\phi = \\ &= \int_{\phi_i}^{\phi_{end}} \frac{-3H^2}{V'}d\phi \Rightarrow N = \frac{\phi_i^2 - \phi_{end}^2}{4M_{\rm Pl}^2} \Rightarrow N \approx \frac{1}{4}\frac{\phi_i^2}{M_{\rm Pl}^2}\,. \end{aligned} \tag{1.14}$$

In order for inflation to solve the flatness and horizon problems we need $N_e = 60 - 70$.

1.1.2 Inflationary Perturbations

At this point we will present a simple description of the standard perturbation theory for single field inflation. Since the thesis aims at extending these methods, this is a

good place to start. Since there are numerous books and review articles on inflationary perturbations, we will not attempt to present a complete discussion here, but rather a very simple introduction to make the comparison of the standard methods with our new results easier.

We start by considering linear perturbations in the field and the metric

$$\phi(x,t) = \phi(x) + \delta\phi(x,t), \tag{1.15}$$

$$g_{\mu\nu}(x,t) = \bar{g}_{\mu\nu}(x,t) + h_{\mu\nu}(x,t). \tag{1.16}$$

The line element in the longitudinal gauge in terms of the gauge-invariant Bardeen potentials is

$$ds^2 = -(1+2\Phi)dt^2 + a^2(1-2\Psi)dx^i dx^j \delta_{ij}. \tag{1.17}$$

In a single field model the anisotropic pressure vanishes, leading to the equality of the two Bardeen potentials

$$\Phi = \Psi\,. \tag{1.18}$$

The equations of motion for the field and metric perturbations are

$$\delta\ddot{\phi} + 3H\delta\dot{\phi} - \frac{1}{a^2}\nabla^2\delta\phi + V_{,\phi\phi}\delta\phi = -2\Psi V_{,\phi} + 4\dot{\phi}\dot{\Psi}\,, \tag{1.19}$$

$$\dot{\Psi} + H\Psi = 4\pi G\dot{\phi}\delta\phi, \tag{1.20}$$

supplemented by the constraint equation

$$\left(\dot{H} - \frac{1}{a^2}\nabla^2\right)\Psi = 4\pi G(-\dot{\phi}\delta\dot{\phi} + \ddot{\phi}\delta\phi)\,. \tag{1.21}$$

Studying the evolution of perturbations becomes easier if one uses the gauge invariant form

$$\mathcal{R} = \psi + \frac{H}{\dot{\phi}}\delta\phi\,. \tag{1.22}$$

The spectrum of the scalar perturbations defined by

$$\mathcal{P}_{\mathcal{R}}(k) \equiv \frac{k^3}{2\pi^2} \int d^3x e^{-i\vec{k}\cdot\vec{x}} \langle \mathcal{R}(\vec{x},t)\mathcal{R}(\vec{0},t)\rangle. \tag{1.23}$$

Skipping the analysis, the spectrum of the scalar perturbations is

$$\mathcal{P}(k) = A_s \left(\frac{k}{k_*}\right)^{n_s-1} \tag{1.24}$$

where the amplitude is calculated to be

$$A_s = \left(\frac{H^2}{2\pi\dot{\phi}}\right)^2 \tag{1.25}$$

and the spectral tilt

$$n_s = 1 - 6\epsilon + 2\eta\,. \tag{1.26}$$

Both A_s and n_s are evaluated at the time that an arbitrary pivot wave number k_* crosses the Hubble length (i.e., when $k_*/a = H$). The Planck Collaboration uses $k_* = 0.05$ Mpc^{-1}. A similar analysis for the tensor modes gives for the ratio r of tensor to scalar modes

$$r = 16\epsilon\,. \tag{1.27}$$

This means that the amplitude of tensor modes directly probes the value of the Hubble parameter during inflation.

1.2 Beyond the single field

Modern theories of particle physics, including Supersymmetry and String Theory, generally contain multiple scalar fields at high energies. Considering that some of those scalars are relevant for inflation provides a model-building framework, where one can deviate from the simple picture of a single slow rolling scalar field presented above. And more than that multi-field models offer possibilities to extend beyond the simplest case of purely adiabatic and Gaussian perturbations. They provide levers

with which to address some subtle features of state-of-the-art CMB measurements. So there are both high-energy theory and empirical / phenomenological motivations to look at multi-field models. We will study two classes of models, where a revision or extension of the standard tools was needed to study inflationary perturbations.

1.2.1 Hybrid Inflation

As we saw for the single field inflation model, the same field is responsible for the expansion of the universe (since its potential energy dominates the Hubble parameter) and the creation of the perturbations that are relevant for the CMB and structure formation. Inflation ends when the field starts accelerating near the end of the potential. Hybrid inflation employs two fields with distinct roles.

1. The timer field produces the observable large scale perturbations.

2. The waterfall field provides the potential energy that drives the expansion and once the timer field reaches a particular value, it is destabilized and ends inflation.

A pictorial representation of the hybrid potential is given in Fig. 1-1. The field rolls along the valley (form right to left) and once it finds itself on top of the ridge is destabilized by quantum perturbations and rolls towards its minimum. More details regarding the transition are given in Chapter 2.

1.2.2 Non-minimal coupling

When we wrote the action for the simple model of inflation, the gravity term was $\frac{1}{2}M_{\rm Pl}^2 R$. However one can modify this, by essentially making Newton's constant be a function of the field amplitude at each point in space. In fact, renormalization of scalar fields in a curved background generates terms of the form $\xi\phi^2 R$ [7, 8], where ξ is a dimensionless parameter, called the non-minimal coupling. We will describe briefly here the physics of a single non-minimally coupled inflaton field (for more look for example [9, 10]), since in the main part of the thesis we study multiple non-minimally

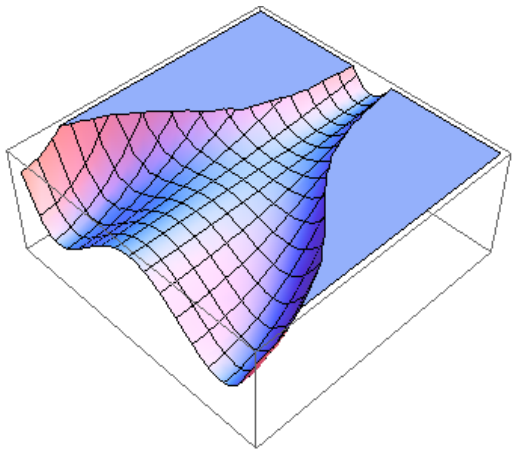

Figure 1-1: A pictorial form of the hybrid potential.

coupled fields in detail. The general form of the action we will consider is

$$S = \int d^4x\sqrt{-g}\left[f(\phi)R - \frac{1}{2}g^{\mu\nu}\partial_\mu\phi\partial_\nu\phi - V(\phi)\right]. \tag{1.28}$$

A conformal transformation is possible that will bring the gravity term to the usual form of Einstein gravity $\frac{1}{2}M_{\rm Pl}^2 R$

$$\tilde{g}_{\mu\nu} = \frac{2f}{M_{\rm Pl}^2}g_{\mu\nu}\,. \tag{1.29}$$

In addition we can make a field redefinition from ϕ to φ, in order for the kinetic term to be canonical.

$$\frac{d\varphi}{d\phi} = \frac{M_{\rm Pl}}{2f(\phi)}\sqrt{\frac{2f(\phi)+6(f'(\phi))^2}{2f^2(\phi}}\,, \tag{1.30}$$

$$\tilde{V} = \frac{V(\phi)}{(2f(\phi))^2}\,. \tag{1.31}$$

With the conformal transformation and the field redefinition the action becomes

$$S = \int d^4x\sqrt{-\tilde{g}}\left[\frac{M_{\rm Pl}^2}{2}\tilde{R} - \frac{1}{2}\tilde{g}^{\mu\nu}\partial_\mu\varphi\partial_\nu\varphi - \tilde{V}\right]. \tag{1.32}$$

In the case of multiple fields (more than two) the conformal transformation does not change, but a field redefinition that makes the kinetic term canonical is not possible.

1.3 Organization of the thesis

The thesis is divided in two main parts, each consisting of a number of chapters and dealing with two main classes of inflationary models. Each chapter is meant to be self-contained and can be read separately. However Chapters 2 and 4 extensively discuss the framework developed for the two model types that were studied and it can be helpful to the reader to study them before proceeding to Chapters 3 and 5-7 respectively.

Chapters 2 and 3 deal with a new method of calculating density perturbations in Hybrid Inflation. They are based on [11, 12] respectively. Regarding my contribution, I did all numerical calculations and wrote most of the text for [11], and I assisted in the analysis and wrote an early draft of [12].

Chapters 4-7 deal with calculating density perturbations in inflationary models where multiple fields are coupled to each other and non-minimally to gravity. They are based on [13, 14, 15, 16] respectively. Regarding my contribution, I did most numerical calculations and a big part of the analytics and assisted in writing the final version of the papers.

Bibliography

[1] A. H. Guth, "The Inflationary Universe: A Possible Solution to the Horizon and Flatness Problems," Phys. Rev. D **23** (1981) 347.

[2] A. D. Linde, "A New Inflationary Universe Scenario: A Possible Solution of the Horizon, Flatness, Homogeneity, Isotropy and Primordial Monopole Problems," Phys. Lett. B **108**, 389 (1982).

[3] A. Albrecht and P. J. Steinhardt, "Cosmology for Grand Unified Theories with Radiatively Induced Symmetry Breaking," Phys. Rev. Lett. **48**, 1220 (1982).

[4] P. A. R. Ade *et al.* [Planck Collaboration], "Planck 2013 results. XVI. Cosmological parameters," arXiv:1303.5076 [astro-ph.CO].

[5] P. A. R. Ade *et al.* [Planck Collaboration], "Planck 2013 results. XXII. Constraints on inflation," arXiv:1303.5082 [astro-ph.CO].

[6] P. A. R. Ade *et al.* [BICEP2 Collaboration], "BICEP2 I: Detection Of B-mode Polarization at Degree Angular Scales," arXiv:1403.3985 [astro-ph.CO].

[7] N. D. Birrell and P. C. W. Davies, *Quantum Fields in Curved Space* (New York: Cambridge University Press, 1982).

[8] I. L. Buchbinder, S. D. Odintsov, and I. L. Shapiro, *Effective Action in Quantum Gravity* (New York: Taylor and Francis, 1992).

[9] D. I. Kaiser, "Primordial spectral indices from generalized Einstein theories," Phys. Rev. D **52**, 4295 (1995) [astro-ph/9408044].

[10] A. Linde, M. Noorbala and A. Westphal, "Observational consequences of chaotic inflation with nonminimal coupling to gravity," JCAP **1103**, 013 (2011) [arXiv:1101.2652 [hep-th]].

[11] A. H. Guth and E. I. Sfakianakis, "Density Perturbations in Hybrid Inflation Using a Free Field Theory Time-Delay Approach," arXiv:1210.8128 [astro-ph.CO]

[12] A. H. Guth, I. F. Halpern, M. P. Hertzberg, M. A. Joss and E. I. Sfakianakis, "Hybrid Inflation with $\mathcal{N}$ Waterfall Fields: Density Perturbations and Constraints", to appear.

[13] D. I. Kaiser, E. A. Mazenc and E. I. Sfakianakis, "Primordial Bispectrum from Multifield Inflation with Nonminimal Couplings," Phys. Rev. D **87**, 064004 (2013)

[14] R. N. Greenwood, D. I. Kaiser and E. I. Sfakianakis, "Multifield Dynamics of Higgs Inflation," Phys. Rev. D **87**, 064021 (2013) [arXiv:1210.8190 [hep-ph]]

[15] D. I. Kaiser and E. I. Sfakianakis, "Multifield Inflation after Planck: The Case for Nonminimal Couplings," Phys. Rev. Lett. **112**, 011302 (2014) [arXiv:1304.0363 [astro-ph.CO]]

[16] K. Schutz, E. I. Sfakianakis and D. I. Kaiser, "Multifield Inflation after Planck: Isocurvature Modes from Nonminimal Couplings," Phys. Rev. D **89**, 064044 (2014) [arXiv:1310.8285 [astro-ph.CO]]

Chapter 2

Density Perturbations in Hybrid Inflation Using a Free Field Theory Time-Delay Approach

We introduce a new method for calculating density perturbations in hybrid inflation which avoids treating the fluctuations of the "waterfall" field as if they were small perturbations about a classical trajectory. We quantize only the waterfall field, treating it as a free quantum field with a time-dependent m^2, which evolves from positive values to tachyonic values. Although this potential has no minimum, we think it captures the important dynamics that occurs as m^2 goes through zero, at which time a large spike in the density perturbations is generated. We assume that the time-delay formalism provides an accurate approximation to the density perturbations, and proceed to calculate the power spectrum of the time delay fluctuations. While the evolution of the field is linear, the time delay is a nonlinear function to which all modes contribute. Using the Gaussian probability distribution of the mode amplitudes, we express the time-delay power spectrum as an integral which can be carried out numerically. We use this method to calculate numerically the spectrum of density perturbations created in hybrid inflation models for a wide range of parameters. A characteristic of the spectrum is the appearance of a spike at small length scales, which can be used to relate the model parameters to observational data. It is

conceivable that this spike could seed the formation of black holes that can evolve to become the supermassive black holes found at the centers of galaxies.

2.1 Introduction

Inflation [1] remains the leading paradigm for the very early universe. It naturally solves the cosmological flatness and horizon problems and is consistent with high precision measurements of the cosmic microwave background radiation [2, 3]. Numerous models of inflation have been proposed, each adding features to the predictions of a scale invariant spectrum derived from single-field slow-roll inflation. Their motivation can be either some particle physics ideas coming from the standard model [4] or supersymmetric theories [5, 6], the need to explain some observation such as glitches in the CMB or supermassive black holes in galactic centers, or simply the extension of a theorist's toolbox in anticipation of the next set of high precision data, such as the upcoming Planck satellite measurements.

Hybrid inflation was first proposed by A. Linde [7] and the name was chosen because this class of models can be thought of as being a hybrid between chaotic inflation and inflation in a theory with spontaneous symmetry breaking. The simplest hybrid inflation model requires two fields that we will call the timer and waterfall fields. The timer field corresponds the usual slow rolling field and is responsible for the scale invariant spectrum of perturbations observed in the CMB. The waterfall field is confined to its origin by the interaction with the timer field, giving a large constant contribution to the potential, which is also the main contribution to the energy density and hence the Hubble parameter. The potential governing the waterfall field changes as the timer field evolves, and at some point the minimum of the potential turns into a local maximum, and the waterfall field rolls down its tachyonic potential to its new minimum, where inflation ends. A characteristic feature of the density perturbation spectrum of hybrid inflation is the appearance of a large spike generated at the time when the waterfall potential turns tachyonic. The spike is generically at small length scales, and can potentially seed primordial black holes [8]. Primordial black hole

formation and evolution has been studied in the past [9, 10, 11, 12], but whether these black holes grow to become the supermassive black holes currently found in galactic centers is an open and intriguing possibility that we will address in a future publication.

Usual inflationary perturbation theory is based on the study of quantum fluctuations around a classical trajectory in field space. However, in a purely classical formulation the waterfall field of hybrid inflation would remain forever at the origin, even after the waterfall transition, due to symmetry. It is quantum fluctuations that destabilize it and lead to the end of inflation, so in a sense the classical trajectory has a quantum origin. Numerous papers have used various analytical approaches or numerical simulations to overcome this difficulty and approximate the spectrum of density perturbations [5, 6, 15, 16, 17, 18, 19, 20, 21, 13, 14].

The method we use here has evolved from the early work in Kristin Burgess' thesis [13], in which she studied a free-field model of the waterfall field in one space dimension, focusing on the time delay of the scalar field as a measure of perturbations. As in the model considered here, the waterfall field was described by a Lagrangian with a time-dependent m^2, caused by the interaction with the timer field. m^2 evolved from positive values at early times to negative (tachyonic) values at late times. Such models are unnatural, since the potential is not bounded from below, but they nonetheless appear to be useful toy models, since the dynamics that generate the spike in the fluctuation spectrum occur during the transition from positive to negative m^2. The evolution in the bottomless potential is realistic enough to give a well-defined time delay. Burgess studied the evolution of the waterfall field by means of a numerical simulation on a spatial lattice, using 262,000 points, calculating the power spectrum of the time delay by Monte Carlo methods. The method was slow, but for one choice of parameters she accumulated 5000 runs, giving a very reliable graph of the time-delay spectrum for this model. This line of research was pursued further in the thesis of Nguyen Thanh Son [14], who repeated Burgess' numerical simulations with a new code (with excellent agreement). More importantly, Son and one of us (AHG), with some crucial input from private communication with Larry Guth, developed a method

to short-circuit the Monte Carlo calculation. Instead of determining the power spectrum by repeated random trials, it was possible to express the expectation value for the random trials as an explicit expression involving integrals over mode functions, which could be evaluated numerically. The speed and numerical precision were dramatically improved. While Son's work was still limited to one spatial dimension, the possibility of extending it to three spatial dimensions was now a very realistic goal. In this chapter we extend the calculation of the time-delay power spectrum in free-field models of hybrid inflation to three spatial dimensions, calculating the spectrum for a wide range of model parameters.

In Section II we define the free-field model for the timer and waterfall fields that we will use to calculate fluctuations. We set up the equations of motion, define the notation of the mode expansion, and discuss the behavior of the mode functions. We make contact with a class of supersymmetric models that support hybrid inflation in Section III, presenting the form of their potential and the range of parameters that they allow. Section IV gives a brief summary of the time delay formalism, and presents an approximation for calculating perturbations, developed earlier by Randall, Soljačić, and Guth. In Section V we develop a new method for calculating density perturbations in hybrid inflation that avoids any need to consider small fluctuations about a classical solution. Instead we show how the time delay power spectrum can be calculated essentially exactly in the context of the free field theory description. The result is given in the form of an integral over the modes which makes use of their known Gaussian probability distribution. In section VI we present an extensive set of numerical results over the parameter space of our model, where we are able to isolate the main factors that influence the density perturbation spectrum. In the limit of a light timer field, all quantities of interest are determined by the product of the timer and waterfall masses. We examine the models discussed in Section II as examples of realistic versions of hybrid inflation, and provide graphs showing the predictions of these models. Concluding remarks and directions of future work follow in Section VII.

2.2 Model

As we noted in the Introduction, the model consists of two fields with different behavior: the timer and waterfall fields. The timer field dominates the initial slow-roll inflation phase and we take it to be a single scalar field. The waterfall field becomes tachyonic and rolls to its minimum ending inflation. We take the waterfall field to be a complex scalar, so as to avoid the creation of domain walls after the waterfall transition. The action of this two-field system with minimal coupling to gravity is

$$S = \int d^4x\sqrt{-g}\left[\frac{M_{\rm Pl}^2}{2}R - \frac{1}{2}g^{\mu\nu}\partial_\mu\psi\partial_\mu\psi - \frac{1}{2}g^{\mu\nu}\partial_\mu\phi^\dagger\partial_\nu\phi - V(\psi,\phi)\right], \tag{2.1}$$

where the potential is comprised of a constant term, the potentials of the waterfall and timer fields and an interaction terms.

$$V(\psi,\phi) = V_0 + V_\psi(\psi) + V_\phi(\phi) + V_{\rm int}(\psi,\phi). \tag{2.2}$$

2.2.1 Field set-up

Our first assumption is related to the expansion rate. We consider the metric to be exactly De-Sitter, even though this is only approximately correct. However, it changes only weakly during the slow roll inflation era, and we will terminate our calculation once the approximation loses its validity. This is equivalent to requiring the constant term V_0 to dominate the potential. Defining the Hubble constant during inflation through

$$H^2 \approx \frac{V_0}{3M_{\rm pl}^2}, \tag{2.3}$$

the scale factor is written as

$$a(t) = e^{Ht}. \tag{2.4}$$

Our second approximation concerns the potential of the two fields $V_\psi(\psi)$ and $V_\phi(\phi)$. We will take both to be purely quadratic. Physically this can only be an accurate approximation close to the transition time. However we will take this potential to hold for all times. Since the important dynamics happens close to the time of the

transition, we believe that this approximation makes the dynamics tractable without introducing large errors. Work is already under way to extend out method to more realistic potentials.

We will split the action in two parts for each of the fields. We neglect the interaction term from the Lagrangian of the timer field and consider it a part of the waterfall field Lagrangian. This means that there is no back-reaction from the waterfall to the timer field. Physically this is a reasonable approximation before the waterfall transition, as well as afterwards, for as long as the waterfall field remains close to the origin. Mathematically, neglecting this term makes the equation of motion for the timer field de-coupled and in our quadratic approximation analytically solvable.

The Lagrangian density for the waterfall field ϕ is

$$\mathcal{L}_\phi = e^{3Ht}\left[|\dot{\phi}|^2 - e^{-2Ht}|\nabla\phi|^2 - m_\phi^2(t)|\phi|^2\right]. \tag{2.5}$$

The usual 1/2 factors can be restored, if one writes $\phi = \frac{1}{\sqrt{2}}(\phi_1 + i\phi_2)$ where ϕ_1 and ϕ_2 are real scalar fields. The waterfall field must be complex, otherwise it will create domain walls as it rolls down from its initial value. The time-dependent mass of the ϕ field is controlled by a real scalar field, subsequently called the timer field. The important property of the squared mass of ϕ is that it has to be positive initially and as ψ evolves become negative. A general form is the following

$$m_\phi^2(t) = -m_0^2\left[1 - \left(\frac{\psi(t)}{\psi_c}\right)^r\right]. \tag{2.6}$$

We will choose $r = 4$ for most of our simulations. The lagrangian density of the timer field ψ is

$$\mathcal{L}_\psi = e^{3Ht}\left[\frac{1}{2}\dot{\psi}^2 - \frac{1}{2}e^{-2Ht}(\nabla\psi)^2 - \frac{1}{2}m_\psi^2\psi^2\right]. \tag{2.7}$$

We do not examine perturbations arising from quantum fluctuations of the timer field. Before the waterfall transition they will give the nearly scale invariant spectrum that can be matched to the CMB observations. Apart from making sure that the long wavelength tail of the waterfall field perturbations does not contradict CMB

data, we will not consider these scales. After the waterfall transition the timer field perturbations will continue to be of the order of 10^{-5}, hence they will be subdominant to the perturbations of the waterfall field by a few orders of magnitude, as we will see. We will not worry about matching the *Plack* observations for the spectral index of the CMB, but we will restrict ourselves to a quadratic timer field potential. Comments on the modification needed to turn the blue spectrum of this model to one compatible with *Planck* are deferred for [25].

The equations of motion are

$$\ddot{\phi} + 3H\dot{\phi} - e^{-2Ht}\nabla^2\phi = -m_\phi^2(t)\phi, \tag{2.8}$$

$$\ddot{\psi} + 3H\dot{\psi} - e^{-2Ht}\nabla^2\psi = -m_\psi^2\psi. \tag{2.9}$$

If we take the timer field to be spatially homogenous, we get

$$\psi(t) = \psi_c e^{pt} \tag{2.10}$$

with the exponent

$$p_\pm = H\left(-\frac{3}{2} \pm \sqrt{\frac{9}{4} - \frac{m_\psi^2}{H^2}}\right). \tag{2.11}$$

The value of the constant of integration was chosen so that $\psi(t) = \psi_c$ and $m_\phi^2(t) = 0$ at $t = 0$. Both roots are negative, but the long time behavior is dominated by the larger of the two roots, which is

$$p = p_+ = -H\left(\frac{3}{2} - \sqrt{\frac{9}{4} - \frac{m_\psi^2}{H^2}}\right). \tag{2.12}$$

We will always choose $\frac{m_\psi}{H} < \frac{3}{2}$ and not consider the case of a complex root. In fact, hybrid inflation models usually require the mass of the timer field to be well below the Hubble parameter, as in [5] and [6]. We choose to measure time in number of e-folds, hence we use $N = Ht$. We rescale the masses similarly as $\mu_\psi = m_\psi/H$ and $\mu_\phi = m_0/H$. Furthermore the finite box size that we will use in our simulations is

measured in units of $\frac{1}{H}$ and the field magnitude in units of H. We also define

$$\tilde{\mu}_\psi^2 = -\frac{rp}{H} = r\left(\frac{3}{2} - \sqrt{\frac{9}{4} - \frac{m_\psi^2}{H^2}}\right). \tag{2.13}$$

For a light timer field the reduced mass $\tilde{\mu}_\psi$ is proportional to the actual timer mass, $\tilde{\mu}_\psi = \sqrt{\frac{r}{3}}\left(\frac{m_\psi}{H}\right) = \sqrt{\frac{r}{3}}\mu_\psi$.

2.2.2 Fast Transition

Let's consider the speed of the transition. The transition happens at $m_\phi^2 = 0$. In order to quantify the speed of the transition, we will use the basic scale of our system, the Hubble scale. We will consider the transition duration to be the period for which $|m_\phi| \leq H$, meaning that the mass term in the equation of motion of the waterfall field is negligible. Assuming that $\tilde{\mu}_\phi > 1$ we get

$$\pm 1 = \mu_\phi^2\left(1 - e^{-\tilde{\mu}_\psi^2 N}\right) \Rightarrow \Delta N = \frac{1}{\tilde{\mu}_\psi^2}\log\left(\frac{\mu_\phi^2 + 1}{\mu_\phi^2 - 1}\right). \tag{2.14}$$

In the limit of $\tilde{\mu}_\phi \gg 1$

$$\Delta N = \frac{2}{(\tilde{\mu}_\psi \mu_\phi)^2}. \tag{2.15}$$

Another measure of the speed of the transition is given by derivative of the waterfall field mass at $N = 0$.

$$\frac{1}{H^2}\frac{dm_\phi^2(N)}{dN}|_{N=0} = (\tilde{\mu}_\psi \mu_\phi)^2 \Rightarrow \Delta N \sim \frac{1}{(\tilde{\mu}_\psi \mu_\phi)^2}. \tag{2.16}$$

This shows that as long as the product $\mu_\phi \mu_\psi$ is somewhat larger than unity, the duration of the transition will be less than a Hubble time, meaning that the transition is fast!

2.2.3 Mode expansion

For purposes of our numerical calculations, we think of the universe as a finite box with periodic boundary conditions and a discrete spatial lattice. We choose the lattice to be cubic with length b and Q^3 points. This means that

$$\vec{x} = \frac{b}{Q}\vec{l} \ , \quad \vec{k} = \frac{2\pi}{b}\vec{n} \ , \tag{2.17}$$

where $\vec{l}$ is a triplet of integers between 0 and $Q-1$ and $\vec{n}$ is a triplet of integers between $-Q/2$ and $(Q/2)-1$. We can move between the finite discrete set of points and the continuous limit using the usual substitutions

$$\int d^3x \to \left(\frac{b}{Q}\right)^3 \sum_{\vec{x}} \ , \quad \int d^3k \to \left(\frac{2\pi}{b}\right)^3 \sum_{\vec{k}} \ . \tag{2.18}$$

Our convention for the Fourier transform is

$$\begin{aligned} f(\vec{x}) &= \int d^3k e^{i\vec{k}\cdot\vec{x}} f(\vec{k}) = \left(\frac{2\pi}{b}\right)^3 \sum_{\vec{k}} e^{i\vec{k}\cdot\vec{x}} f(\vec{k}), \\ f(\vec{k}) &= \left(\frac{1}{2\pi}\right)^3 \int d^3x e^{i\vec{k}\cdot\vec{x}} f(\vec{x}) = \left(\frac{1}{2\pi}\right)^3 \left(\frac{b}{Q}\right)^3 \sum_{\vec{x}} e^{i\vec{k}\cdot\vec{x}} f(\vec{x}) \ . \end{aligned} \tag{2.19}$$

We will expand the waterfall field in modes in momentum space,

$$\phi(\vec{x},t) = \frac{1}{(2\pi)^{3/2}} \left(\frac{2\pi}{b}\right)^{3/2} \sum_{\vec{k}} [c(\vec{k}) e^{i\vec{k}\cdot\vec{x}} u(\vec{k},t) + d^\dagger(\vec{k}) e^{-i\vec{k}\cdot\vec{x}} u^*(\vec{k},t)] \ , \tag{2.20}$$

which with Eq. (2.8) gives

$$\ddot{u}(\vec{k},N) + 3\dot{u}(\vec{k},N) + e^{-2N}\tilde{k}^2 u(\vec{k},N) = \mu_\phi^2 (1 - e^{-\tilde{\mu}_\psi^2 N}) u(\vec{k},N) \ , \tag{2.21}$$

where $\tilde{k} = \frac{|\vec{k}|}{H}$ and an overdot denotes a derivative with respect to the time variable $N = Ht$.

2.2.4 Solution of the mode function

Early time behavior

At asymptotically early times the $\tilde{k}^2$ term dominates over the mass term provided that $\tilde{\mu}_\psi^2 < 2$. For $r = 2$ this is the case for $\mu_\psi < \sqrt{2}$, and for $r = 4$ it holds for $\mu_\psi < \sqrt{5/4}$. These inequalities will hold throughout the parameter space of the models that we will examine, so we can neglect the mass term for $N \to -\infty$. We then define a new function, following [22] as

$$u(\vec{k}, N) = \frac{1}{2}\sqrt{\frac{\pi}{H}} e^{-3N/2} Z(z) \quad , \quad z = \tilde{k} e^{-N} \ . \tag{2.22}$$

Neglecting the mass term in Eq. (2.21), we find

$$z^2 \frac{d^2 Z}{dz^2} + z \frac{dZ}{dz} + \left(z^2 - \frac{9}{4} \right) Z = 0 \ , \tag{2.23}$$

which is the equation for a Bessel function of order 3/2. At early times the solution should look like a harmonic oscillator in its ground state, or equivalently the ground state of a free field in flat space, which is composed of negative frequency complex exponentials. This choice of initial conditions is the well known Bunch–Davies vacuum. For a review of scalar field quantization in de Sitter space and the corresponding vacuum choice see for example Ref. [23]. At early times the solution is given by

$$u \sim \frac{1}{2}\sqrt{\frac{\pi}{H}} e^{-3N/2} H^{(1)}_{3/2}(z) \ , \tag{2.24}$$

where

$$H^{(1)}_{3/2}(z) = -\sqrt{\frac{2}{\pi z}} e^{iz} \left(1 - \frac{1}{iz} \right) \tag{2.25}$$

is a Hankel function, a linear combination of Bessel functions. (The phase is arbitrary, and the normalization is fixed by insisting that the field and the creation and annihilation operators obey their standard commutation relations.) Rewriting the

original mode equation in terms of the new variable z, it simplifies to

$$\frac{\partial^2 u}{\partial z^2} - \frac{2}{z}\frac{\partial u}{\partial z} + u = \frac{\mu_\phi^2}{z^2}\left[1 - \left(\frac{z}{\tilde{k}}\right)^{\tilde{\mu}_\psi^2}\right] u \ . \tag{2.26}$$

The $\vec{k} = 0$ mode is not captured by the procedure described here and is presented in detail in Appendix 2.9.1.

General Solution

We will now examine the general solution in a form that will be more appropriate for the numerical calculations that we have to perform. We can write the solution as

$$u(\vec{k}, t) = \frac{1}{\sqrt{2\tilde{k}H}} R(\vec{k}, t) e^{i\theta(\vec{k},t)} \tag{2.27}$$

and the differential equation separates in real and imaginary parts

$$\ddot{R} - R\dot{\theta}^2 + 3\dot{R} + e^{-2N}\tilde{k}^2 R = \mu_\phi^2 (1 - e^{-\tilde{\mu}_\psi^2 N}) R, \tag{2.28}$$

$$2\dot{R}\dot{\theta} + R\ddot{\theta} + 3R\dot{\theta} = 0. \tag{2.29}$$

Integrating the second equation gives

$$\dot{\theta} = const \frac{e^{-3N}}{R^2}. \tag{2.30}$$

By comparing this with the early time behavior of the analytic solution

$$u \sim \frac{1}{2H\sqrt{\tilde{k}}} e^{-N} e^{i\tilde{k}e^{-N}}. \tag{2.31}$$

The phase equation becomes

$$\dot{\theta} = -\frac{\tilde{k}e^{-3N}}{R^2}, \tag{2.32}$$

while the initial condition for the amplitude is given by the same asymptotic term to be

$$R \to e^{-N}. \tag{2.33}$$

Inserting this expression in the equation for the amplitude function R

$$\boxed{\ddot{R} - \frac{\tilde{k}^2 e^{-6N}}{R^3} + 3\dot{R} + e^{-2N}\tilde{k}^2 R = \mu_\phi^2(1 - e^{-\tilde{\mu}_\psi^2 N})R}. \tag{2.34}$$

A closer look at the mode behavior

Let us rewrite the equation of motion (Eq. 2.21) in a way that makes the time dependence of the solution more transparent

$$\ddot{u}_k(t) + 3\dot{u}_k(t) + \mu_{eff}^2 = 0 \quad , \quad \mu_{eff}^2(k) = \tilde{k}^2 e^{-2N} + \mu_\phi^2 e^{-\tilde{\mu}_\psi^2 N} - \mu_\phi^2. \tag{2.35}$$

We can distinguish different time windows with different behavior of the mode functions, based on the effective waterfall field mass. We will list these time windows here and then proceed to examine them one by one.

1. $N \ll 0$, many efolds before the waterfall transition, in the asymptotic past
2. $N_{dev}(k) < N < 0$, a few efolds before the transition, where $N_{dev}(k)$ is the time at which a mode starts deviating significantly from the e^{-N} behavior, in particular starts decaying faster.
3. $0 < N < N_{tr}(k)$ a few efolds after the transition, where $N_{tr}(k)$ is the time at which each mode starts growing.
4. $N \gg 0$, the asymptotic future

Now let us look at each of those time scales more closely. The asymptotic past is well described in the previous section and we see that all modes decay like e^{-N}. More precisely their magnitude behaves as $|u_k| \sim \sqrt{\frac{1}{2k}}e^{-N}$. The first time scale N_{dev} appears only for low wavenumbers. For $N < 0$ we can keep only two of the three terms in the effective mass. Since $\mu_\phi^2 e^{-\tilde{\mu}_\psi^2 N} > \mu_\phi^2$ we will drop the μ_ϕ^2 term, leaving the

effective mass as $\mu_{eff}^2(k) = \tilde{k}^2 e^{-2N} + \mu_\phi^2 e^{-\tilde{\mu}_\psi^2 N}$. The time at which the two dominant terms become equal is

$$N_{dev}(k) = \frac{2}{2 - \tilde{\mu}_\psi^2} \log\left(\frac{\tilde{k}}{\mu_\phi}\right). \tag{2.36}$$

For $\tilde{k} \geq \mu_\phi$ this time is not negative, hence we cannot drop μ_ϕ^2 and our analysis fails. This transition, which happens only for $\tilde{k} < \mu_\phi$ signals a deviation of the behavior of the modes, which do not evolve as e^{-N}, but instead decay faster.

Next we move to the actual waterfall transition time for each mode, which happens when the effective squared mass changes sign and becomes negative, or

$$\tilde{k}^2 e^{-2N} = \mu_\phi^2 \left(1 - e^{-\tilde{\mu}_\psi^2 N}\right). \tag{2.37}$$

We will approximate the right hand side of the above equation with a piecewise linear function as follows

$$\mu_\phi^2 \left(1 - e^{-\tilde{\mu}_\psi^2 N}\right) = \begin{cases} \mu_\phi^2 \tilde{\mu}_\psi^2 N & : N < 1/\mu_\psi^2 \\ \mu_\phi^2 & : N > 1/\mu_\psi^2 \end{cases}. \tag{2.38}$$

For $\tilde{k} < \mu_\phi e^{1/\mu_\psi^2}$ the solution is found on the first branch and is

$$N_{tr}(k) = \frac{1}{2} W\left(\frac{2\tilde{k}^2}{\mu_\phi \tilde{\mu}_\psi^2}\right). \tag{2.39}$$

where W is known as the Product Logarithm, or Lambert W function and is defined as the solution to the equation $z = W(z)e^{W(z)}$. For small values of the wavenumber we can write the solutions as a Taylor series in $\tilde{k}$

$$N_{tr}(\tilde{k} \ll \sqrt{\mu_\phi \tilde{\mu}_\psi}) = \frac{\tilde{k}^2}{\mu_\phi^2 \tilde{\mu}_\psi^2} + O(\tilde{k}^4). \tag{2.40}$$

For $\tilde{k} > \mu_\phi e^{1/\mu_\psi^2}$ we operate on the second branch and the transition time for each mode is

$$N_{tr}(k) = \log\left(\frac{\tilde{k}}{\mu_\phi}\right). \tag{2.41}$$

The behavior of the modes after the transition is different for different ranges of the timer field mass. If we consider the late time behavior of the mode equation, we can see two timescales introduced by the time dependent exponential coefficients. One is $O(1)$ and the other $O(1/\tilde{\mu}_\psi^2)$. We distinguish two cases: They can both be O(1) or the second one can be larger than the first. The first timescale defines the time at which the equation becomes k-independent, meaning that all modes behave (grow) in the same way. The second time scale defines the time, after which the equation becomes time independent, meaning that after that all modes behave as pure exponentials.

Let us first deal with the case of $\tilde{\mu}_\psi \ll 1$ meaning that the second time scale is much larger than the first one. Between the two timescales, that is $1 < N < -1/\tilde{\mu}_\psi^2$, the equation is independent of $\tilde{k}$

$$\ddot{R} + 3\dot{R} = \mu_\phi^2 (1 - e^{-\tilde{\mu}_\psi^2 N}) R. \tag{2.42}$$

Since the evolution of the exponential term on the right hand side is by far slowest than the other timescales in the problem, we will treat $1 - e^{-\tilde{\mu}_\psi^2 N}$ adiabatically. This leads immediately to the solution

$$R = R_0 e^{\int_0^N \lambda(N')dN'} \quad , \quad \lambda(N) = \frac{-3 + \sqrt{9 + 4\mu_\phi^2 (1 - e^{-\tilde{\mu}_\psi^2 N})}}{2}. \tag{2.43}$$

After a long time the growth rate would mathematically settle to

$$\frac{1}{R}\frac{dR}{dN} \to \lambda_\infty = \frac{-3 + \sqrt{9 + 4\mu_\phi^2}}{2}. \tag{2.44}$$

However, this is far beyond the time when inflation will have ended, hence it would physically never have time to happen (plus it is well outside the validity of our constructed potential).

Let us choose $\mu_\phi = 10$ and $\tilde{\mu}_\psi = 1/10$ to demonstrate our analysis. Some characteristic mode functions are presented in Fig. 2-1

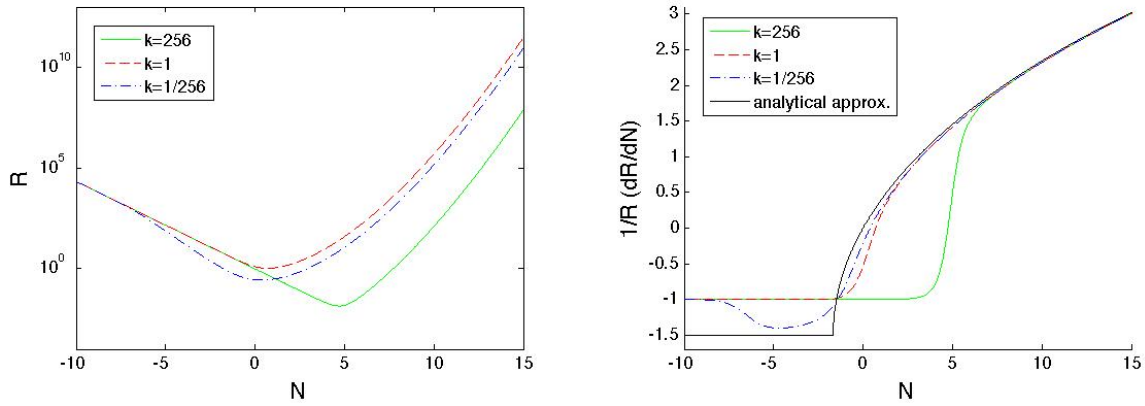

Figure 2-1: Mode functions for different comoving wavenumbers as a function of time in efolds. The model parameters are $\mu_\psi = \frac{1}{10}$ and $\mu_\phi = 10$. We can see the modes following our analytic approximation for the growth rate. Our analysis gives $N_{dev}(1/256) \approx -7.9$ and $N_{tr}(256) \approx 4.76$, which are very close to the values that can be read off the graph.

We see that all modes behave similarly at late times, independent of their wavenumber, as they should based on our late time analysis. Specifically, we can plot the ratio of the time derivative of each mode to its magnitude, as in Fig. 2-1. We call this the growth rate $\lambda \equiv \left(\frac{\dot{R}_k}{R_k}\right)$. We can see both phenomena. First, after $N \approx 6$ the modes behave identically. Second, the behavior of the mode approaches that of an exponential function (whose logarithm is a constant), but at a slower rate. In this example time needs to go on for several hundreds of efolds for the growth rate to set to a constant, which is calculated to be $\lambda(t \to \infty) = 8.6119$ for $\mu_\phi = 10$ and $\mu_\psi = 1/10$.

It is important to test our analytical approach to the late time behavior of the growth rate of mode function. As seen in Fig. 2-1 once the mode functions evolve in a k - independent way, our simple analytical estimate for their growth rate is accurate to within a few percent, which gives us a very accurate expression for the growth rate and leads to the terms evolving as $u \sim e^{\lambda(t)t}$, where the time-dependent growth rate $\lambda(t)$ is slowly changing.

As a test of our analysis, we can calculate the two important transition times $N_{dev}(1/256) = -7.9005$ and $N_{tr}(256) = 4.76457$. We see that the calculated values

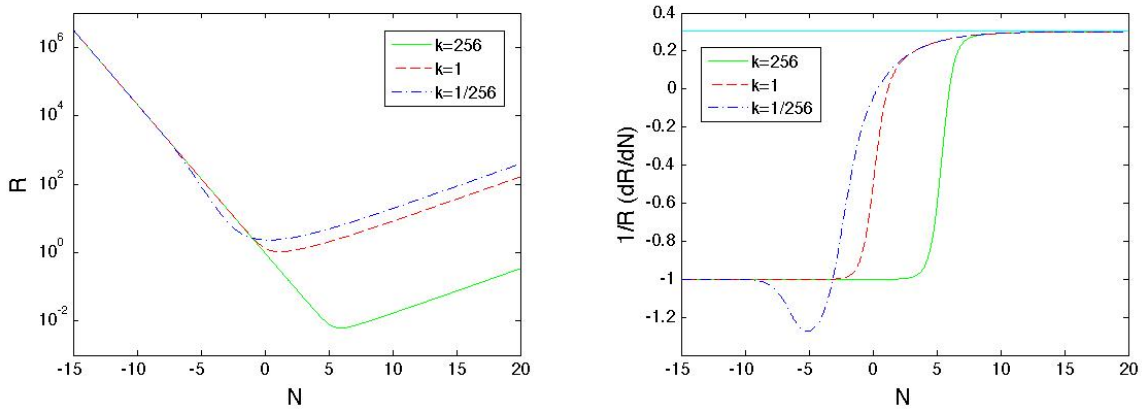

Figure 2-2: Mode functions for different comoving wavenumbers as a function of time in efolds. The model parameters are $\mu_\psi = \frac{1}{2}$ and $\mu_\phi = 1$. The horizontal line corresponds to the asymptotic value of the growth factor λ. We can see how the mode functions reach their asymptotic behavior after 10 efolds. Our analysis gives $N_{dev}(1/256) \approx -7.84$ and $N_{tr}(256) \approx 5.4$, which are very close to the values that can be read off the graph.

agree very well with the behavior of the plotted modes.

Let us briefly examine the situation where $\tilde{\mu}_\psi^2 \leq 2$. In this case the mode equation becomes k-independent and time independent at about the same time, that is a few e-folds after the waterfall transition. We choose $\mu_\psi = \frac{1}{2}$ and $\mu_\phi = 1$ and plot the results in Fig. 2-2. It is clear that the modes become both k-independent and pure exponential (having a constant growth rate) at about the same time ($N \approx 10$). The asymptotic growth rate in this case is $\lambda(t \to \infty) = 0.3028$.

Again we can calculate the two important transition times $N_{dev}(1/256) = -7.8377$ and $N_{tr}(256) = 5.39554$, which agree once more with the behavior of the plotted modes.

2.3 Supernatural Inflation models

It is interesting to make contact between our abstract model and specific potentials inspired form particle theory. In general inflation models require small parameters in order to ensure slow roll inflation and produce the correct magnitude of density perturbations. It was shown in [5, 6] that supersymmetric theories with weak scale

Quadratic Approximation	V_0	m_0	r	ψ_c	m_ψ
SUSY Model 1	M^4	$\frac{M^2}{\sqrt{2}f}$	4	$\frac{M\sqrt{2M'}}{\sqrt{f}}$	m_ψ
SUSY Model 2	M^4	$\frac{M^2}{\sqrt{2}f}$	2	$\frac{\sqrt{2}M^2}{f\lambda}$	m_ψ

Table 2.1: Parameters of SUSY models and their counterparts in our quadratic approximation

supersymmetry breaking can give models where such small parameters emerge "naturally" as ratios of masses already in the theory. We will not go into the details of such theories, but instead give the forms of the constructed potentials and use them as an application of our formalism.

$$V = M^4 \cos^2(\phi/\sqrt{2}f) + \frac{m_\psi^2}{2}\psi^2 + \frac{\psi^4\phi^2 + \phi^4\psi^2}{8M'^2} \tag{2.45}$$

for what we will call model 1 and will be the primary focus of this work and

$$V = M^4 \cos^2(\phi/\sqrt{2}f) + \frac{m_\psi^2}{2}\psi^2 + \lambda^2\frac{\psi^2\phi^2}{4} \tag{2.46}$$

which we will call model 2.

The first model can be taken with M' at one of three regions: the Planck scale, the GUT scale or an intermediate scale ($\sim 10^{10}\ GeV$). At each scale the rest of the parameters are adjusted accordingly to produce sufficient inflation and agree with CMB data.

We will approximate the potential with a pure quadratic one with a time varying waterfall mass, of the form

$$V(\phi,\psi) = V_0 - m_0^2\left[1 - \left(\frac{\psi}{\psi_c}\right)^r\right]|\phi|^2 + m_\psi^2\psi^2, \tag{2.47}$$

where $r = 4$ for model 1 and $r = 2$ for model 2, as can be easily seen by the form of the interaction terms in both cases. The correspondence between the exact SUSY potential and our quadratic counterpart is shown in Table 2.1.

The parameters of the two models are restricted to fit CMB data, as shown in Fig. 2-3.

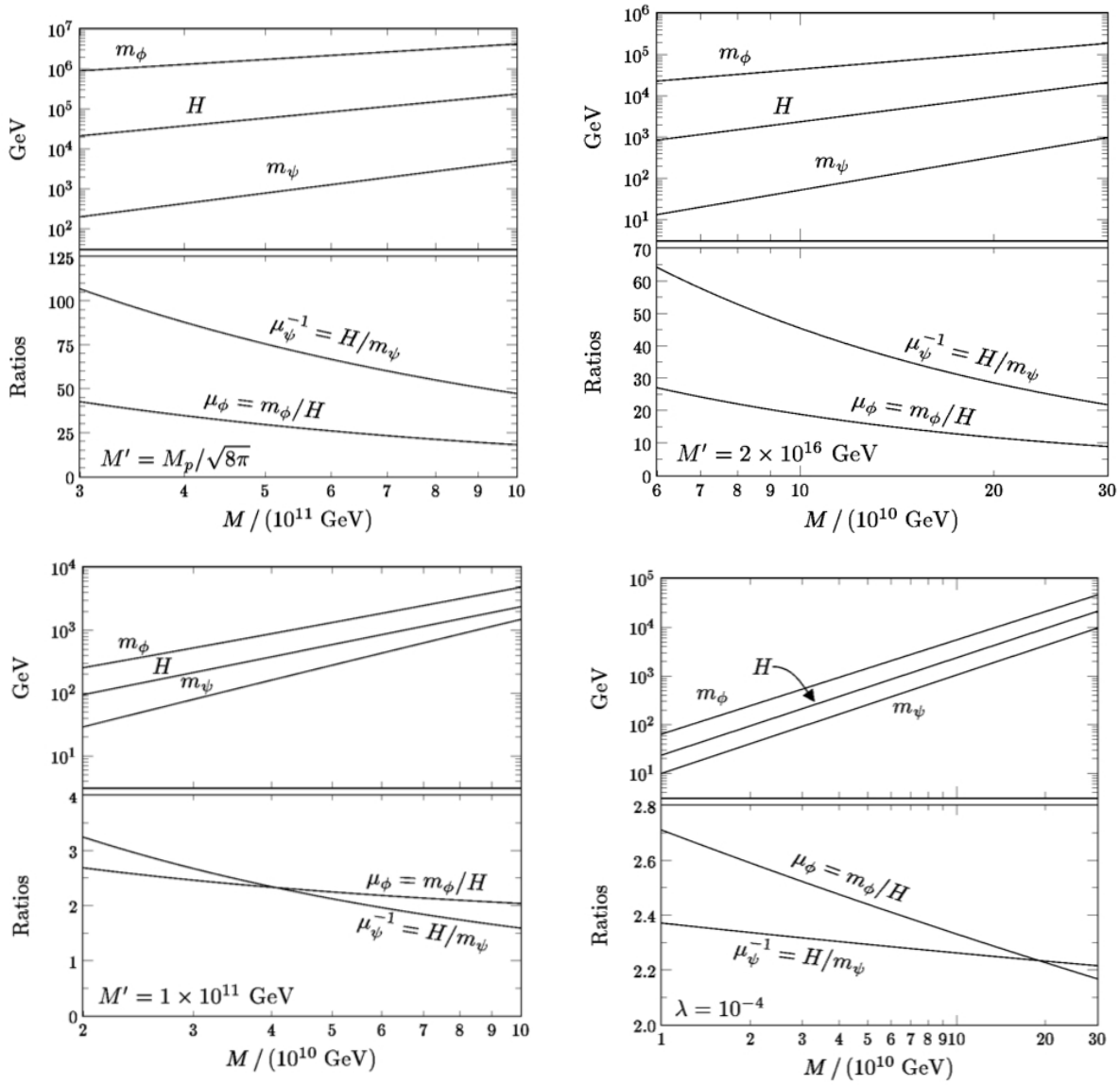

Figure 2-3: Parameter space for the two supernatural inflation models. The bottom right corner shows the parameter for model 2, while the other three show parameters for model 1, for different ranges of the mass scale M'

To lowest order, in this potential dominated model, the Hubble parameter is constant and equal to

$$H = \sqrt{\frac{8\pi}{3}}\frac{M^2}{M_p} = \sqrt{\frac{8\pi}{3}}\frac{\sqrt{V_0}}{M_p}. \tag{2.48}$$

2.3.1 End of Inflation

In our simplified quadratic model inflation will never end. The waterfall field will roll forever down its tachyonic potential. However, we shall not forget that this is a mere Taylor expansion of more realistic potentials, which have a well defined minimum. We will use the supersymmetric potentials of [5, 6] as a concrete example to connect our purely quadratic potential to ones with more realistic shapes. In these supersymmetric models the potential has a cosine-like form and the minimum occurs at $\frac{\phi}{\sqrt{2}f} = \frac{\pi}{2}$, where the inflaton will oscillate, terminating inflation and giving rise to (p)reheating. By making contact between the parameters of our potential and the physical parameters of the actual supersymmetric models, we can estimate the field value at which inflation ends.

There are two strategies for defining $\phi_{\rm end}$, the field value at which inflation ends. We can either pretend that the quadratic potential can be followed up to the end field value of the corresponding SUSY potential, or we can choose to end our calculation when the quadratic potential departs significantly from the actual SUSY potential that we are trying to approximate.

In the first case the end field value is at $\phi_{\rm end} = f\pi/\sqrt{2}$. To calculate the end field value for the latter case we will note that the cosine potential is accurately approximated by a quadratic as long as $\phi/f \ll 1$. We will call this ratio ϵ and in this case we will end our calculations when ϵ ceases being small. We can write these two cases in a unified manner, as

$$\phi_{\rm end} = \epsilon f, \tag{2.49}$$

where $\epsilon = \pi/\sqrt{2}$ if we follow the quadratic potential all the way to the field value corresponding to the minimum of the SUSY potential and $\epsilon < 1$ if we stop our calculation at the point where the quadratic potential deviates significantly from the

supersymmetric one.

Using the values of the parameters taken from the supersymmetric models, we can estimate the end field value to be

$$\phi_{\rm end} \sim \epsilon \ 10^{15} H \tag{2.50}$$

within one or two orders of magnitude for all cases of models considered in [5, 6].

We will be using field values of this order of magnitude in our numerical calculations, whether we are dealing with the supersymmetric potentials or not. We will however examine the effects of changing the end value of the field and show that it is minimal, easily understandable, and calculable.

2.4 Perturbation theory basics

2.4.1 Time delay formalism

The time delay formalism provides an intuitive and straightforward way to calculate primordial perturbations. Its basic principle is that inflation ends at different places in time at different times, due to quantum fluctuations. This leads some of the regions of the universe to have inflated more than others, creating a difference in their densities. The time-delay formalism was first introduced by Hawking [24] and by Guth and Pi [26], and has recently been reviewed in Ref. [27].

We will briefly describe the method here for the case of a single real scalar field. The universe is assumed to be described by a de-Sitter space-time, since the Hubble parameter is taken to be a constant. The equation of motion for the scalar field $\phi(\vec{x}, t)$ is

$$\ddot{\phi} + 3H\dot{\phi} = -\frac{\partial V}{\partial \phi} + \frac{1}{a(t)^2}\nabla^2\phi, \tag{2.51}$$

where the last term is suppressed by an exponentially growing quantity, so at late times it becomes negligible. We will omit the last term from now on.

We call the homogenous (classical) solution $\phi_0(t)$ and write the full solution, in-

cluding a space dependent small perturbation $\delta\phi \ll \phi_0$ as

$$\phi(\vec{x},t) = \phi_0(t) + \delta\phi(\vec{x},t). \tag{2.52}$$

Plugging this into the equation of motion and working to linear order in $\delta\phi$ one can show that the quantity $\delta\phi$ obeys the same differential equation as $\dot{\phi}_0$. Furthermore the presence of a damping term implies that any two solutions approach a time independent ratio at large times. Thus, at large times we have (to first order in $\delta\tau$)

$$\delta\phi(\vec{x},t) \to -\delta\tau(\vec{x})\dot{\phi}_0(t) \Rightarrow \phi(\vec{x},t) \to \phi_0(t - \delta\tau(\vec{x})). \tag{2.53}$$

This is the formulation of the intuitive picture of the time delay method.

2.4.2 Randall-Soljacic-Guth approximation

The usual calculation of density perturbations in inflation considers small quantum fluctuations around a classical field trajectory. In the case of hybrid inflation such a classical trajectory does not exist, since classically the field would stay forever on the top of the inverted potential. It is the quantum fluctuations that push the field away from this point of unstable equilibrium. One way to overcome this difficulty is to consider the RMS value of the field as the classical trajectory. This was done for example in [5] and [6] and is a recurring approximation in the study of hybrid inflation.

Using the Bunch-Davies vacuum in the definition of the RMS value of the waterfall field $\phi_{\rm rms} = \sqrt{\langle 0|\phi(x,t)\phi^*(x,t)|0\rangle}$ it it straightforward to calculate it using the mode expansion

$$\phi^2_{\rm rms}(t) = \frac{1}{b^3}\sum_{\vec{k}\ ,\ \vec{k}'} e^{i(\vec{k}-\vec{k}')\cdot x}\left\langle 0|(c_{\vec{k}}u_{\vec{k}} + d^\dagger_{-\vec{k}}u^*_{-\vec{k}})(c^\dagger_{\vec{k}'}u^*_{\vec{k}'} + d_{-\vec{k}'}u_{-\vec{k}'})|0\right\rangle = \frac{1}{b^3}\sum_{\vec{k}}|u_k(t)|^2. \tag{2.54}$$

The mean fluctuations are measured by

$$\Delta\phi(\vec{k}) = \left[\left(\frac{k}{2\pi}\right)^3 \int d^3x e^{i\vec{k}\cdot\vec{x}} \left\langle \phi(x)\phi^*(0)\right\rangle\right]^{1/2} = \left[\left(\frac{k}{2\pi}\right)^3 |u_{\vec{k}}|^2\right]^{1/2} \tag{2.55}$$

resulting in what will be called the RSG approximation for the time delay field

$$\Delta\tau_{RSG}(\vec{k}) \approx \frac{\Delta\phi(\vec{k},t)}{\dot{\phi}_{\rm rms}} = \left(\frac{kb}{2\pi}\right)^{3/2} |u_{\vec{k}}| \frac{\sqrt{\sum_{\vec{k}} |u_{\vec{k}}(t)|^2}}{\sum_{\vec{k}} \dot{u}_{\vec{k}}(t) u_{\vec{k}}(t)} \ . \tag{2.56}$$

There is an important comment to be made about the quantum mechanical nature of these density perturbations. In regular models of inflation quantum perturbations are scaled by $\hbar$. We can think of them as modes with initial conditions that are of the order of $\hbar$. The classical trajectory on the other hand does not have any quantum mechanical origin, hence does not scale with $\hbar$. This means that in the limit of $\hbar \to 0$ the perturbations vanish, as one would expect will happen if one could "switch off" quantum mechanical effects.

In the case of hybrid inflation on the other hand, what we call the classical trajectory (be it the RMS value or something else) is comprised of modes that originated as quantum fluctuations, hence is scaled by $\hbar$ itself. This means that even in the limit of $\hbar \to 0$, the density perturbations in hybrid inflation remain finite! By explicitly restoring $\hbar$ in the formulas of this chapter, the reader can formally arrive to the same conclusion.

Some plots of the time delay field calculated using the RSG approximation are shown in Fig. 2-4. The reduced mass of the timer field was taken to be $\mu_\psi = \frac{1}{20}$ while we varied the waterfall field mass. We fixed the time at which inflation ended to be 15 e-folds after the waterfall transition.

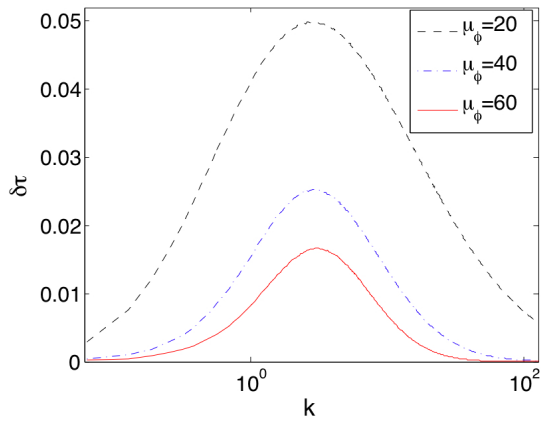

Figure 2-4: The time delay field calculated using the RSG formalism. The end time was taken to be 15 e-folds after the waterfall transition and $\mu_\psi = \frac{1}{20}$ for all curves, while we varied μ_ϕ.

2.5 Calculation of the Time Delay Power Spectrum

The usual method to calculate the primordial perturbation spectrum would involve either making some approximations (more or less similar to the RSG) or using a Monte Carlo simulation. The former suffers from the lack of a classical trajectory that invalidates the usual perturbation method, while the latter would be computationally costly in three spatial dimensions. We will therefore implement an alternate method that reduces the calculation of the spectrum of the time delay field to the evaluation of a two dimensional integral and does not need a classical trajectory to do so.

As discussed at the end of Sec. 2.2.4, the behavior of the mode functions at asymptotically late times ($t \to \infty$) is given by

$$u(\vec{k}, t \to \infty) \sim e^{\lambda_\infty t} u(\vec{k}) \ , \tag{2.57}$$

where λ_∞ is given by Eq. (2.44). If we define for all times

$$\lambda(t) \equiv \frac{\dot{\phi}_{\rm rms}(t)}{\phi_{\rm rms}(t)} = \frac{\sum_{\vec{k}} \frac{R(\vec{k},t)\dot{R}(\vec{k},t)}{2|k|}}{\sum_{\vec{k}} \frac{|R(\vec{k},t)|^2}{2|k|}} \ , \tag{2.58}$$

then at late times $\lambda(t) \to \lambda_\infty$. Since $\lambda(t)$ changes very slowly, we can take it as a constant around the time of interest.

To discuss fluctuations in the time at which inflation ends, we begin by defining t_0 as the time when the rms field reaches the value $\phi_{\rm end}$, which we have chosen to define the nominal end of inflation:

$$\phi^2_{\rm rms}(t_0) = \phi^2_{\rm end} \ . \tag{2.59}$$

Since at late times all modes, to a good approximation, grow at the same exponential rate $\lambda(t)$, we can express the field $\phi(\vec{x}, t)$ at time $t = t_0 + \delta t$ in terms of the field $\phi(\vec{x}, t_0)$ by

$$|\phi(\vec{x}, t)|^2 = |\phi(\vec{x}, t_0)|^2 e^{2\int_{t_0}^{t_0+\delta t} \lambda(t')dt'} = |\phi(\vec{x}, t_0)|^2 e^{2\lambda(t_0)\delta t}. \tag{2.60}$$

We will drop the argument of $\lambda(t_0)$ from now on. If t is chosen to be the time $t_{\rm end}(\vec{x})$ at which inflation ends at each point in space, then $\phi\big(\vec{x}, t_{\rm end}(\vec{x})\big) = \phi_{\rm end} = \phi_{\rm rms}(t_0)$, and the above equation becomes

$$\phi^2_{\rm rms}(t_0) = |\phi(\vec{x}, t_0)|^2 e^{2\lambda\delta t} \ , \tag{2.61}$$

which can be solved for the time delay field $\delta t(\vec{x}) = t_{\rm end}(\vec{x}) - t_0$:

$$\delta t(\vec{x}) = \frac{-1}{2\lambda} \log\left(\frac{|\phi(\vec{x}, t_0)|^2}{\phi^2_{\rm rms}(t_0)}\right) \ . \tag{2.62}$$

Rescaling by the rms field

$$\tilde{\phi}(\vec{x}, t) \equiv \frac{\phi(\vec{x}, t)}{\phi_{\rm rms}(t)} \ , \tag{2.63}$$

we can write

$$\delta t(\vec{x}) = \frac{-1}{2\lambda} \log|\tilde{\phi}(\vec{x}, t_0)|^2 \ . \tag{2.64}$$

Using this expression, we can write the two-point function of the time delay field as

$$\Big\langle \delta t(\vec{x}) \delta t(\vec{0}) \Big\rangle = \frac{1}{4\lambda^2} \Big\langle \log|\tilde{\phi}(\vec{x}, t_0)|^2 \log|\tilde{\phi}(\vec{0}, t_0)|^2 \Big\rangle \ , \tag{2.65}$$

which can be evaluated, since the probability distributions are known. To continue, we can decompose the complex scalar field in terms of the real fields X_i:

$$\tilde{\phi}(\vec{x},t) = X_1 + iX_2 \quad , \quad \tilde{\phi}(\vec{0},t) = X_3 + iX_4 \ . \tag{2.66}$$

The average value of a function F of a random variable X with probability distribution function $p(X)$ is given by

$$\langle F[X] \rangle = \int dX p(X) F[X] \ . \tag{2.67}$$

Since this is a free field theory, we can take the four random variables $X_i(\vec{x})$ to follow a joint Gaussian distribution with

$$p(X) = \frac{1}{(2\pi)^2 \sqrt{\det(\Sigma)}} \exp\left(-\frac{1}{2} X^T \Sigma^{-1} X\right) \quad , \quad \Sigma_{ij} = \langle X_i X_j \rangle \ . \tag{2.68}$$

A function of the $X_i's$ then has the expected value

$$\langle F[X] \rangle = \int \prod_{i=1}^{4} dX_i \frac{1}{(2\pi)^2 \sqrt{\det(\Sigma)}} \exp\left(-\frac{1}{2} X^T \Sigma^{-1} X\right) F[X] \ . \tag{2.69}$$

The new fields X_i can be written in terms of the original complex field ϕ as

$$\begin{aligned} X_1 &= \frac{1}{2}\left[\tilde{\phi}(\vec{x}) + \tilde{\phi}^*(\vec{x})\right] \ , \ X_2 = \frac{1}{2i}\left[\tilde{\phi}(\vec{x}) - \tilde{\phi}^*(\vec{x})\right], \\ X_3 &= \frac{1}{2}\left[\tilde{\phi}(\vec{0}) + \tilde{\phi}^*(\vec{0})\right] \ , \ X_4 = \frac{1}{2i}\left[\tilde{\phi}(\vec{0}) - \tilde{\phi}^*(\vec{0})\right]. \end{aligned} \tag{2.70}$$

The components of the variance matrix Σ can be easily calculated using the commutation relations for the creation and annihilation operators in $\phi(\vec{x},t)$, from Eq. (2.20).

Due to the high degree of symmetry the matrix itself has a very simple structure:

$$\Sigma = \begin{pmatrix} \frac{1}{2} & 0 & \Delta & 0 \\ 0 & \frac{1}{2} & 0 & \Delta \\ \Delta & 0 & \frac{1}{2} & 0 \\ 0 & \Delta & 0 & \frac{1}{2} \end{pmatrix} , \tag{2.71}$$

where

$$\Delta(\vec{x}, t_0) = \langle X_1 X_3 \rangle = \langle X_2 X_4 \rangle = \frac{1}{2} \left\langle \phi^*(\vec{x}, t_0) \phi(\vec{0}, t_0) \right\rangle = \frac{1}{2b^3} \sum_{\vec{k}} |\tilde{u}(\vec{k}, t_0)|^2 e^{i\vec{k}\cdot\vec{x}} , \tag{2.72}$$

where

$$\tilde{u}(\vec{k}, t) = \frac{u(\vec{k}, t)}{\phi_{\rm rms}(t)} . \tag{2.73}$$

Since $\tilde{u}(\vec{k}, t)$ actually depends only on the magnitude of the wavenumber, because of the isotropy of the problem, we can do the angular calculations explicitly in Δ and leave only the radial integral to be calculated numerically. Then

$$\begin{aligned} \left\langle \delta t(\vec{x}) \delta t(\vec{0}) \right\rangle &= \frac{1}{4\lambda^2} \frac{1}{(2\pi)^2 [\frac{1}{4} - \Delta^2]} \int dX_1 dX_2 dX_3 dX_4 \log(X_1^2 + X_2^2) \log(X_3^2 + X_4^2) \\ &\quad \times \exp\left\{ -\frac{1}{4[\frac{1}{4} - \Delta^2]} \Big[X_1^2 + X_2^2 + X_3^2 + X_4^2 - 4(X_1 X_3 + X_2 X_4)\Delta \Big] \right\} . \end{aligned} \tag{2.74}$$

Changing to polar coordinates

$$\begin{aligned} X_1 = r_1 \cos\theta_1 \ , \ X_2 = r_1 \sin\theta_1 \ , \\ X_3 = r_2 \cos\theta_2 \ , \ X_4 = r_2 \sin\theta_2 \ , \end{aligned} \tag{2.75}$$

the integral becomes

$$\begin{aligned} \left\langle \delta t(\vec{x}) \delta t(\vec{0}) \right\rangle &= \frac{2}{\pi\lambda^2(1 - 4\Delta^2)} \int_0^{2\pi} d\theta \int_0^\infty r_1 dr_1 \int_0^\infty r_2 dr_2 \log(r_1) \log(r_2) \\ &\quad \times \exp\left[-\frac{r_1^2 + r_2^2 - 4\Delta r_1 r_2 \cos\theta}{1 - 4\Delta^2} \right] , \end{aligned} \tag{2.76}$$

where we redefined the angular variables as $\theta = \theta_1 - \theta_2$ and $\tilde{\theta} = \theta_1 + \theta_2$ and integrated over $\tilde{\theta}$. Changing also the radial variables

$$r_1 = r\cos\phi \ , \ r_2 = r\sin\phi \ , \tag{2.77}$$

$$\begin{aligned}\left\langle \delta t(\vec{x})\delta t(\vec{0})\right\rangle &= \frac{1}{\pi\lambda^2(1-4\Delta^2)}\int_0^{2\pi} d\theta \int_0^{\frac{\pi}{2}} d\phi \, \sin 2\phi \int_0^{\infty} dr\, r^3 \, \log(r\,\cos\phi)\log(r\,\sin\phi) \\ &\times \exp\left[-\frac{(1-2\Delta\sin 2\phi\,\cos\theta)\,r^2}{1-4\Delta^2}\right] \ . \end{aligned} \tag{2.78}$$

The radial integration can be performed analytically

$$\begin{aligned}&\int_0^{\infty} dr\ r^3\ \log(ar)\log(br)e^{-cr^2} = \\ &\frac{1}{8c^2}\left[(\gamma-2)\gamma + \frac{\pi^2}{6} - 2\log(ab)(\gamma - 1 + \log(c)) + 4\log(a)\log(b) + \log(c)(2\gamma - 2 + \log(c))\right],\end{aligned} \tag{2.79}$$

where $a = \cos\phi$, $b = \sin\phi$, $c = \frac{1}{(1-4\Delta^2)}(1 - 2\Delta\ \sin 2\phi\ \cos\theta)$ and γ is the Euler constant $\gamma \approx 0.57721$.

Finally, the spectrum of the time delay field is defined by

$$\delta\tau(\vec{k}) = \left[\left(\frac{k}{2\pi}\right)^3 \int d^3x\, e^{i\vec{k}\cdot\vec{x}} \left\langle \delta t(\vec{x})\delta t(\vec{0})\right\rangle\right]^{1/2} \ . \tag{2.80}$$

Calculation in the two limiting cases $x \to 0$ and $x \to \infty$ (or $x \to b$ in our case) can be done analytically.

1. For $x \to 0$ several terms in the integral diverge, since $\Delta \to \frac{1}{2}$. In this case we have only two degrees of freedom instead of four, since we consider a complex scalar field at one point in space. The integral becomes

$$\begin{aligned}\left\langle \delta t(\vec{0})\delta t(\vec{0})\right\rangle &= \frac{1}{4\lambda^2}\int \frac{dX_1 dX_2}{\pi} e^{-(X_1^2+X_2^2)}\log^2(X_1^2+X_2^2) = \\ &= \frac{1}{4\pi\lambda^2}\int_0^{2\pi} d\theta \int_0^{\infty} dr\ re^{-r^2}\log^2(r^2) = \frac{1}{4\lambda^2}\left(\gamma^2 + \frac{\pi^2}{6}\right).\end{aligned} \tag{2.81}$$

2. The $x \to \infty$ limit is much easier to handle. We recognize that $\Delta(\vec{x})$ is simply the Fourier transform of $|u_k|^2$. Since u_k is smooth, $\Delta(x \to \infty) \to 0$, and therefore $\delta t(\infty)$ is uncorrelated with $\delta t(\vec{0})$. Eq. (2.74) can be seen to factorize, giving $\left\langle \delta t(\infty)\delta t(\vec{0}) \right\rangle = \left\langle \delta t(\vec{0}) \right\rangle^2$, where

$$\begin{aligned} \left\langle \delta t(\vec{0}) \right\rangle &= \frac{-1}{2\pi\lambda} \int dX_1 dX_2 \log(X_1^2 + X_2^2) \exp\left[-(X_1^2 + X_2^2)\right] \\ &= -\frac{1}{\pi\lambda} \int_0^{2\pi} d\theta \int_0^{\infty} r\, dr\, \log r e^{-r^2} = \frac{\gamma}{2\lambda} \ . \end{aligned} \tag{2.82}$$

Combining these results, we see that the probability distribution for $\delta t(\vec{0})$ has a standard deviation $\sigma = \sqrt{\left\langle \delta t(\vec{0})^2 \right\rangle - \left\langle \delta t(\vec{0}) \right\rangle^2} = \pi/(2\sqrt{6}\lambda)$. While the first limit above is needed for programming the numerical calculations, since the integral of Eq. (2.74) cannot be numerically evaluated at $\vec{x} = \vec{0}$, the second limit can be used as a numerical check.

The same method can be applied to the exact calculation of any higher order correlation functions. Especially the non-Gaussian part of the power spectrum f_{NL} can be read off from the momentum space Fourier transform of the three-point correlation function in position space $\langle \delta t(\vec{x}_1)\delta t(\vec{x}_2)\delta t(x_3)\rangle = \langle \delta t(\vec{x}_1)\delta t(\vec{x}_2)\delta t(0)\rangle$. Taking the Fourier transform we can compute $\left\langle \delta t(\vec{k}_1)\delta t(\vec{k}_2)\delta t(k_3) \right\rangle$, from which we can extract the properties of the bispectrum.

The form of the three point function in position space is

$$\langle \delta t(\vec{x}_1)\delta t(\vec{x}_2)\delta t(0)\rangle = \frac{-(2\pi)^2}{\lambda^3} \int_0^{2\pi} d\gamma_1 d\gamma_2 \int_0^{\pi} \sin\theta d\theta \int_0^{2\pi} d\phi F(\gamma_1, \gamma_2, \theta, \phi) \ , \tag{2.83}$$

where $F(\gamma_1, \gamma_2, \theta, \phi)$ is a function of four angular variables. Calculations regarding the form of the bispectrum are given in the next chapter of the present thesis.

2.6 Numerical Results and Discussion

Let us begin by plotting one example of the free field theory (FFT) calculation of the time delay power spectrum, from Eqs. (2.78) and (2.80), along with the corresponding

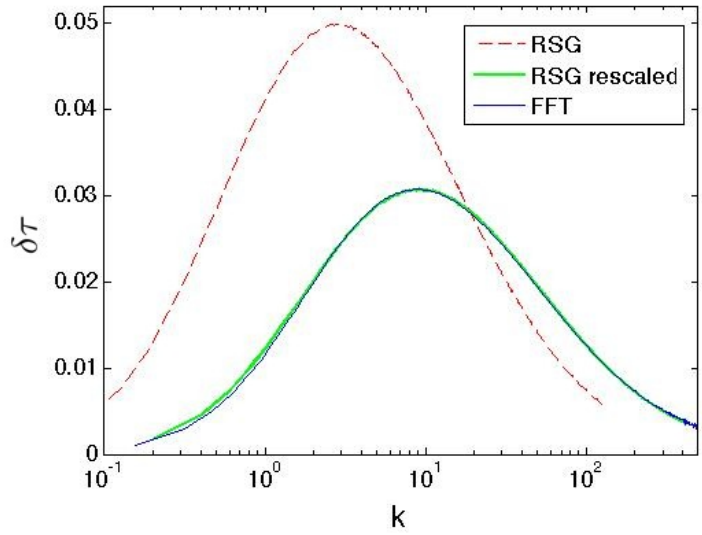

Figure 2-5: Comparison between the RSG and FFT methods. The end time was taken to be 15 e-folds after the waterfall transition and $\mu_\phi = 20$ and $\mu_\psi = 1/20$. We can see that the spectrum of the time delay field calculated in the free field theory agrees very well with the rescaled version of the RSG approximation $A\,\delta\tau_{RSG}\,(Bk)$.

curve derived using the RSG approximation, Eq. (2.56). We use the sample parameters $\mu_\psi = \frac{1}{20}$ and $\mu_\phi = 20$. Both calculations give a spike, but a spike of different width, different height and different position. Let us rescale the RSG result as follows

$$\delta\tau_{\rm RSG,rescaled}(k) = A\,\delta\tau_{\rm RSG}\,(Bk)\ , \tag{2.84}$$

where A and B are $O(1)$ constants calculated by requiring the peaks of the FFT and RSG distributions to match in position and amplitude. The results are plotted in Fig. 2-5. We can see that the FFT and RSG curves do not seem similar. However the rescaled RSG curve seems to follow the FFT curve very well, as was first noticed by Burgess [13]. Based on our simulations the curves generally tend to agree better for low wavenumbers, up to and including the peak, and start deviating after the peak. The rescaling parameters vary with the field masses chosen and for the particular choice of Fig. 2-5 were calculated to be $A = 0.6152$ and $B = 3.25$. We do not yet fully understand this behavior, but we are studying it both analytically and numerically and will present our findings in a subsequent paper.

We will now do an extensive scan of parameter space $\{\mu_\phi, \mu_\psi\}$ in order to have reliable estimates on the magnitude and wavelength of the perturbations. This is important both to make sure that CMB constraints can be satisfied as well as to study the formation of primordial black holes that might lead to the supermassive black holes found in the centers of galaxies. Since the original motivation for this work has been the supersymmetric models first presented in [5] and [6], we will present the results for the perturbations in these models. However, our quadratic approximation holds for more general hybrid inflation models. Hence it is important to make a model-independent parameter sweep. This will provide a more general set of predictions of this class of models. We will give both exact power spectra, as well as try to isolate the dominant features and provide a qualitative understanding of their dependence on the model's parameters.

2.6.1 Model-Independent Parameter Sweep

There are several model-dependent parameters that give us some control over the properties of the resulting power spectrum. Initially we will fix the value of the field at the end of inflation to be $|\phi_{\rm end}| = 10^{14}$ in units of the Hubble parameter. With this assumption (which will be relaxed later), we can calculate the properties of the power spectrum as a function of the masses. Initially we fix the reduced timer field mass to be $\mu_\psi = \frac{1}{20}$ and vary the mass of the waterfall field. The results are shown in Fig. 2-6. We have plotted (clockwise from the top left)

1. The end time of inflation, defined as the time when the RMS value of the field reaches the end value.

2. The maximum amplitude of the spectrum of the time delay.

3. The comoving wavenumber at which the aforementioned maximum value occurs. Thinking about black holes, this is the scale at which black holes will be most likely produced.

4. The width of the time delay distribution in the logarithmic scale, taken as

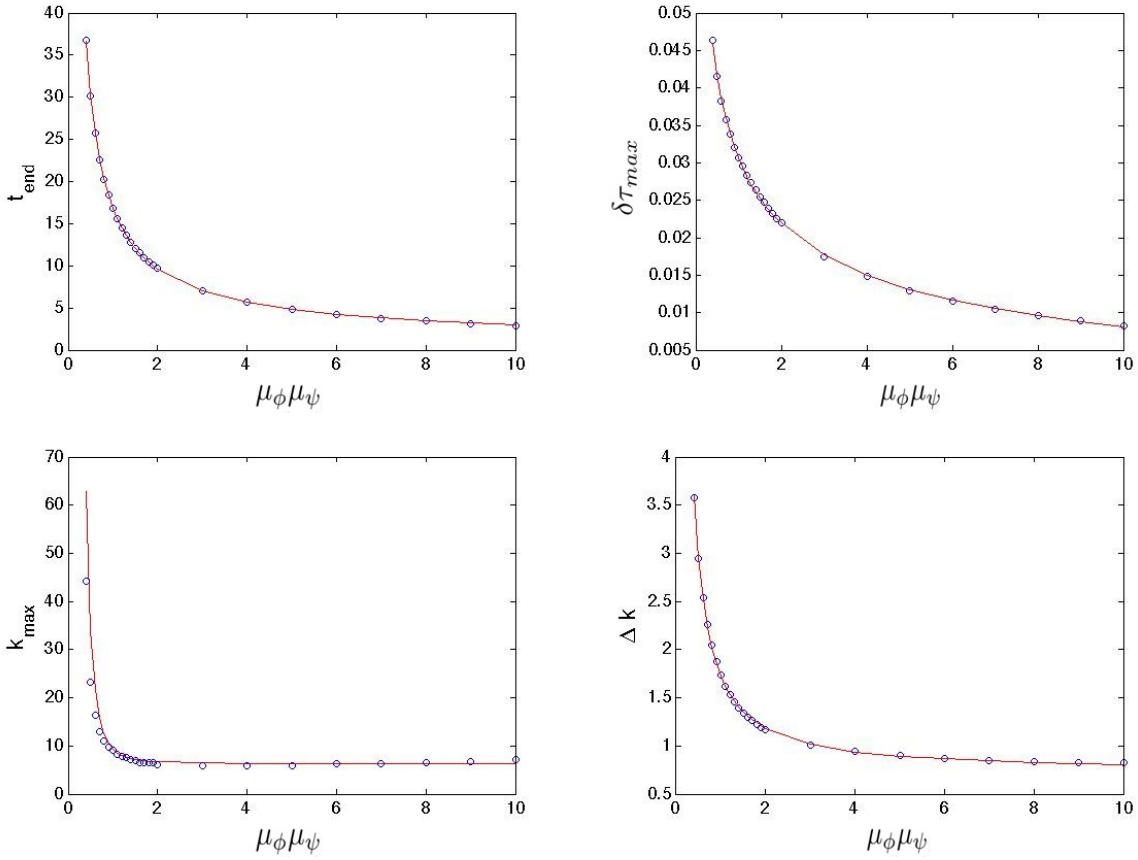

Figure 2-6: Parameter sweep for constant timer field mass $\mu_\psi = 1/20$ and constant end field value $\phi_{\text{end}} = 10^{14}$. Data points are plotted along with a least square power law fit. The same trend is evident in all curves. The time delay spectrum grows in amplitude and width and is shifted towards larger momentum values as the mass product decreases. Also inflation takes longer to end for low mass product.

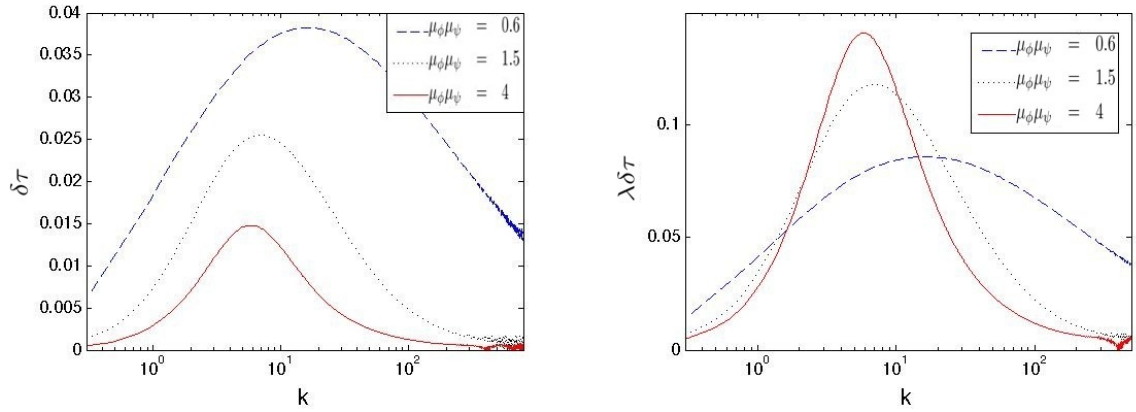

Figure 2-7: Time delay spectra for different values of the mass product, keeping the timer field mass fixed at $\mu_\psi = \frac{1}{20}$

$\Delta k = \log_{10}\left(\frac{k_{+1/2}}{k_{-1/2}}\right)$ where $k_{\pm 1/2}$ are the wavenumbers at which the distribution reaches one half of its maximum value.

We see that all the plotted quantities show a decreasing behavior as one increases the mass product. In order to quantify this statement, we fitted each set of data points with a power law curve of the form $y = ax^b + c$. The scaling exponent b for the various quantities was $b_{t_{\rm end}} \approx -0.88$, $b_{\delta\tau_{max}} \approx -0.34$, $b_{kmax} \approx -3.219$, $b_{\Delta k} \approx -1.17$. As a comparison, the corresponding best fit exponent of the growth rate λ as a function of the mass product is $b_\lambda \approx -0.85$.

In order to get a better understanding of what these parameters actually mean, we plot three characteristic spectra for three values of the mass ratio in Fig. 2-7. We also rescale the spectra by the growth factor λ. This probes the actual form of the two point correlation function, as seen in momentum space. That is, it shows the evaluation of the spectrum in Eq. (2.80), while ignoring the factor of $1/\lambda^2$ in the evaluation of $\left\langle \delta t(\vec{x})\delta t(\vec{0})\right\rangle$ from Eq. (2.78).

Before continuing to a more thorough examination of parameter space, let us understand how changing the field value at the end of inflation will change our results. Fixing the product of the reduced masses equal to 2 ($\mu_\psi = \frac{1}{20}$ and $\mu_\phi = 40$), we let the field value $\phi_{\rm end}$ vary by four orders of magnitude. The results are shown in Fig. 2-8. It is evident that the curves for $\delta\tau(k)$ are of identical form and slightly

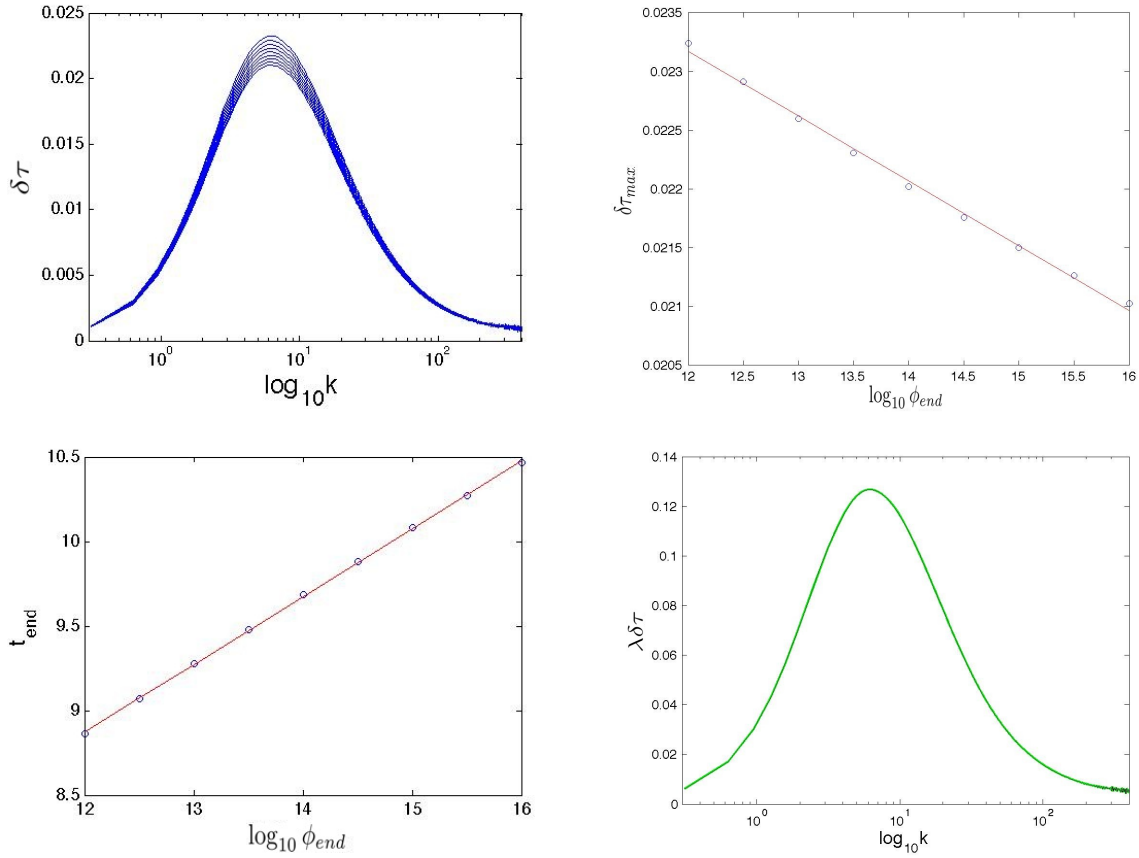

Figure 2-8: Perturbation spectrum for varying field value at $t_{\rm end}$ for constant masses. The time delay curves are identical in shape and differ only in amplitude. This variation is entirely due to the different value of the time dependent growth factor λ, which differs for each case because inflation simply takes longer to end for larger end field values.

different magnitude. The last graph shows the product $\lambda \cdot \delta\tau(k)$ for the two curves at $\phi_{\rm end} = 10^{12}$ and $\phi_{\rm end} = 10^{16}$, plotted respectively as a green thick and a black thin line. It is seen, that once rescaled the two curves fall exactly on top of each other, meaning that the actual integral that gives us the two point function in position space is time independent, once we enter the region where all modes behave identically. Furthermore if one takes the product of the maximum value of the time delay times the growth parameter ($\delta\tau_{max}\cdot\lambda$) for the different values of $\phi_{\rm end}$ the result is constant for the range explored here to better than 1 part in 10^6, meaning that they are identical within the margins of numerical error. Thus, changing the value of the field at which inflation ends can affect the resulting perturbation spectrum only by changing the growth parameter λ, for which we have a very accurate analytical estimate in the form of Eq. (2.43). From this point onward, we will keep the end field value fixed at $\phi_{\rm end} = 10^{14}$ and keep in mind that the fluctuation magnitude can change by 10% or so if this field value changes.

Once we fix the field magnitude at the end of inflation we have two more parameters to vary, namely the two masses: the actual timer field mass and the asymptotic tachyonic waterfall field mass. The two masses can be varied either independently on a two dimensional plane or along some line on the plane, in a specific one-dimensional way. Fixing one of the two masses is such a way of dimensional reduction of the available parameter space, as we did before. Another way to eliminate one of the variables is to fix the mass product and change the mass ratio. This will prove and quantify the statement, that (at least for heavy waterfall and light timer fields) the result is controlled primarily by the mass product.

We fix the mass product at $\mu_\phi\mu_\psi = 2$. The results are shown in Fig. 2-9. The curves are of identical form and everything is again controlled only by λ. On the top left figure we plotted $\lambda\ \delta\tau$ for the two extreme values and the curves fall identically on top of each other (color-coding is as before). Furthermore if we calculate the product $\lambda\cdot\delta\tau_{max}$ for different values of the mass ratio we get a constant result $0.1225 \pm 2\cdot 10^{-5}$ where the discrepancy can be attributed to our finite numerical accuracy. The second

feature of this calculation is the extremely flat part of the end-time, growth factor and maximum time delay curves for large values of the mass ratio and the abrupt change as the mass ratio gets smaller. For the value of the mass product that we have chosen, this transition happens as the timer field mass approaches unity. Let us look at the expansion of the effective waterfall field mass

$$\mu_{\phi,eff}^2 = \mu_\phi^2 \left(1 - e^{-\tilde{\mu}_\psi^2 N}\right) = \mu_\phi^2 \tilde{\mu}_\psi^2 N(1 - \tilde{\mu}_\psi^2 N + ...) \ . \tag{2.85}$$

When the second term in the expansion cannot be neglected, the dynamics of the problem stops being defined by the mass product alone. This explains the abrupt change we see as we lower the mass ratio. By doing the same simulation for different values of the fixed mass product we get similar results.

We can now do the opposite, that is fix the ratio and change the mass product. The results are shown as the open circles in the top two diagrams of Fig. 2-10, and in the lower diagrams of the figure. There are two main comments to be made. First of all, in the case of a fixed ratio, the growth rate λ does not solely determine the results. Rescaling the spectrum by λ not only fails to give a constant peak amplitude (Fig. 2-10, lower left), but the result are spectra of different shapes (Fig. 2-10, lower right). On the other hand, the data points taken with a constant mass ratio and a constant timer field mass ($\mu_\psi = \frac{1}{20}$), as shown by the +'s on the upper diagrams of Fig. 2-10, fall precisely on the same curve! This clearly demonstrates that the only relevant parameter, at least for a light timer field, is the mass product!

We see that contrary to the fixed product case, the results for fixed mass ratio do not depend solely on λ. We have established that the the most important factor in determining the time delay field is the product of the waterfall and timer field masses, especially for a light timer field.

2.6.2 Supernatural Inflation

We now turn our attention to the supernatural inflation models that were studied in [5] and [6]. We will examine each of the four cases separately.

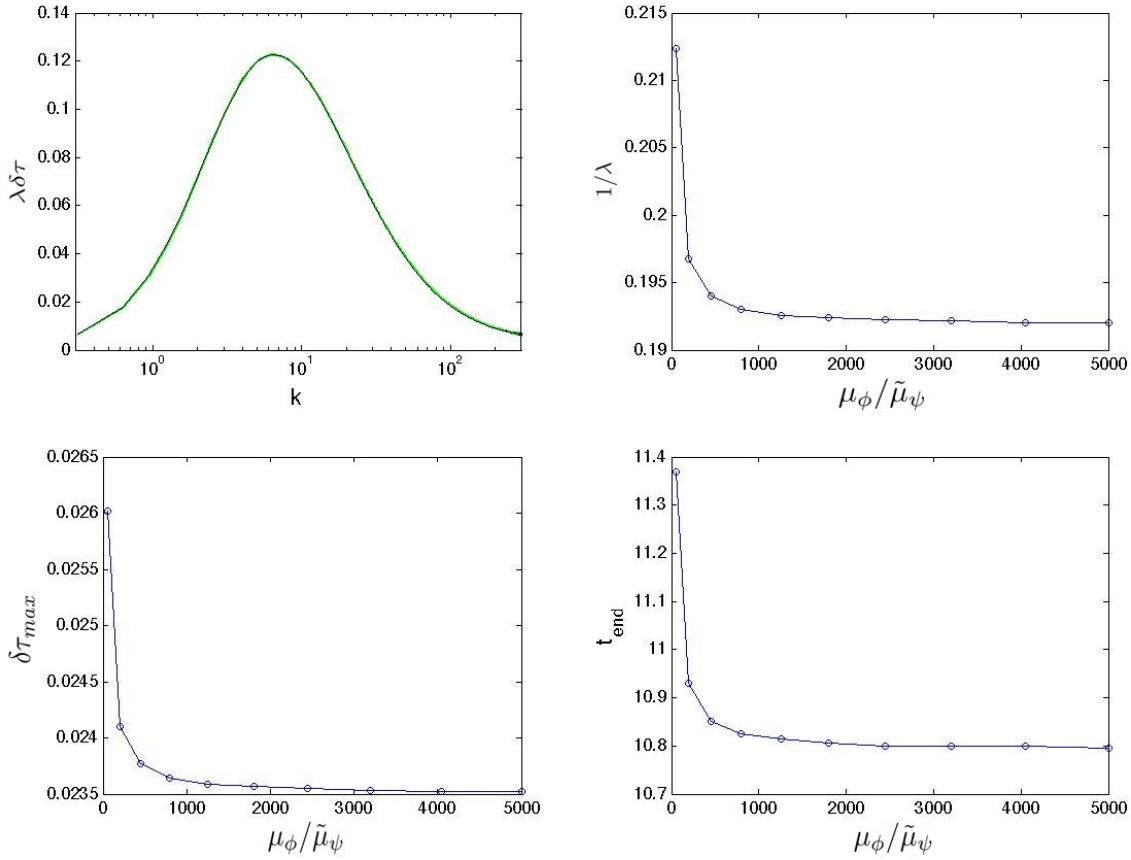

Figure 2-9: Fixing the mass product at 2 and varying the mass ratio. There is significant variation only for low mass ratio, when the light timer field approximation loses its validity. Furthermore the curves of maximum time delay amplitude and $1/\lambda$ follow each other exactly up to our numerical accuracy. Finally by rescaling the spectra by the growth factor λ they become identical for all values of the mass ratio.

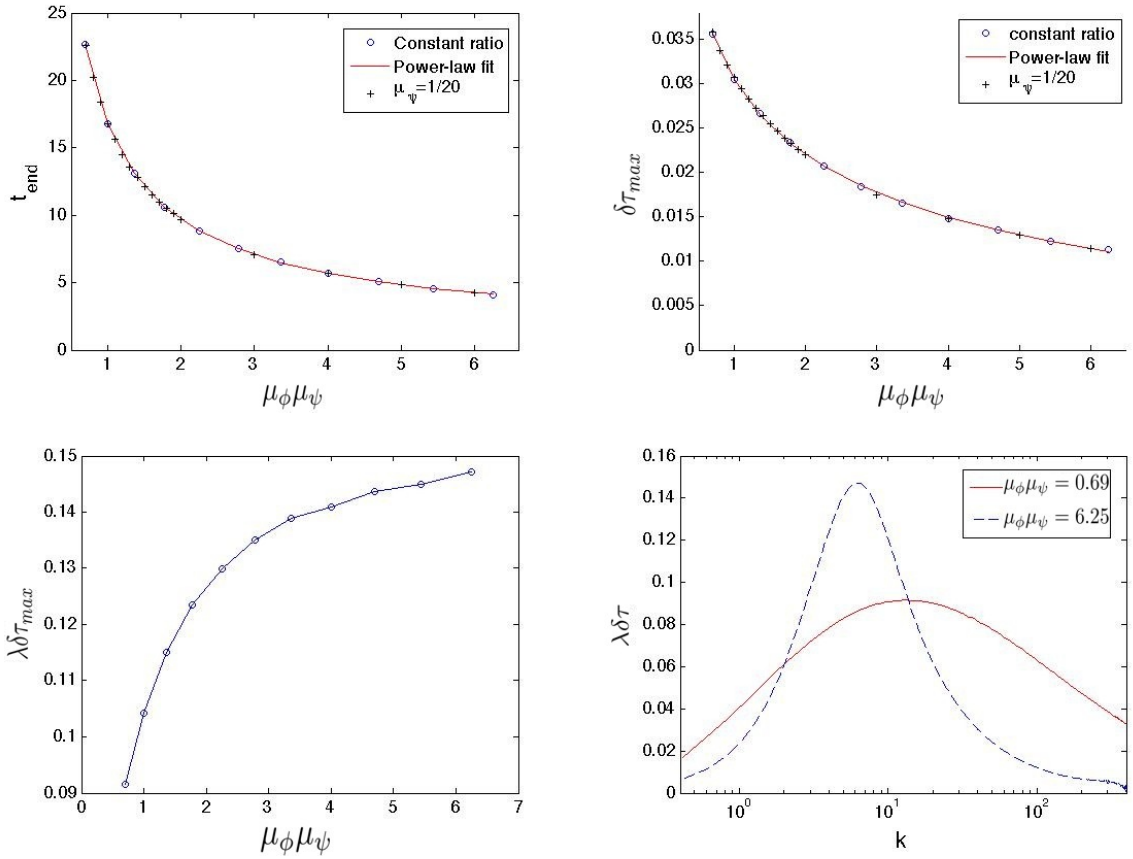

Figure 2-10: Fixing the mass ratio at 900 (open circles) or the timer mass at $\mu_\psi = 1/20$ (+'s). The time delay spectra for different mass products show no common shape characteristics and remain different even when rescaled by λ. Furthermore the end time and maximum perturbation amplitude curves are identical for constant mass ratio and constant timer field mass, proving that indeed the mass product is the dominant parameter.

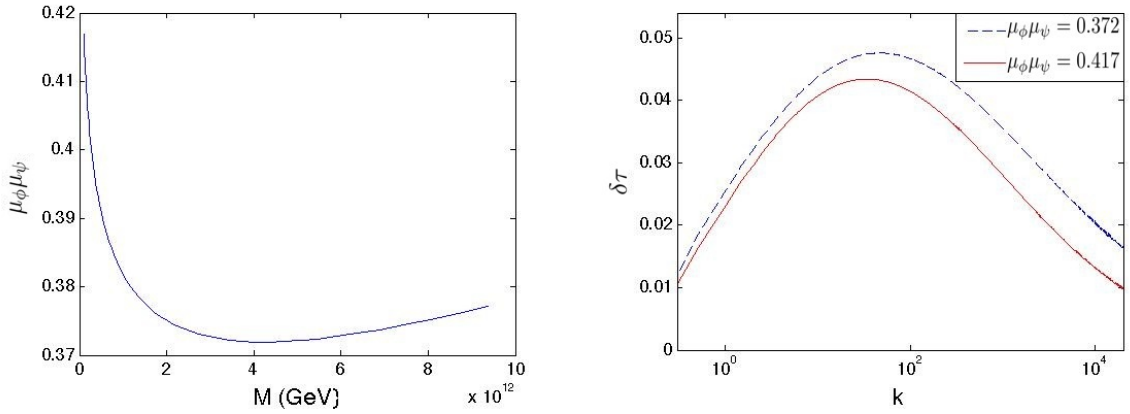

Figure 2-11: First Supernatural inflation model with M' at the Planck scale. The spectra corresponding to the maximum and minimum mass product are shown. We observe good agreement with the results of the model independent parameter sweep of the previous section, because the timer field mass is much smaller than the Hubble scale.

Let us start with the first SUSY model (described by Eq. (2.45)) with the interaction-suppressing mass scale M' set at the Planck scale. The mass of the timer field was calculated to be 50 to 100 times less than the Hubble scale, while the asymptotic waterfall field mass was more than 20 times the Hubble scale. This means that the model is well into the region where the two masses are separated by a few orders of magnitude. According to the analysis of the previous section, we expect the mass product to be the dominant factor in the generation of density perturbations. In the left part of Fig. 2-11 we see the mass product for this model. We can see that the mass product varies less than 15%. It is hence enough to calculate the time delay spectra for the two extreme values and say that all other values of the mass product will fall between the two, as shown in 2-11.

Putting the mass scale M' of the first SUSY model at the GUT scale changes the masses as well as the Hubble scale by one order of magnitude. However the reduced masses and their product have very similar values as before. This is shown in Fig. 2-12

It is worth noting that these two SUSY models contain a very light timer field, hence the results should be the same as our previous parameter space sweep with a

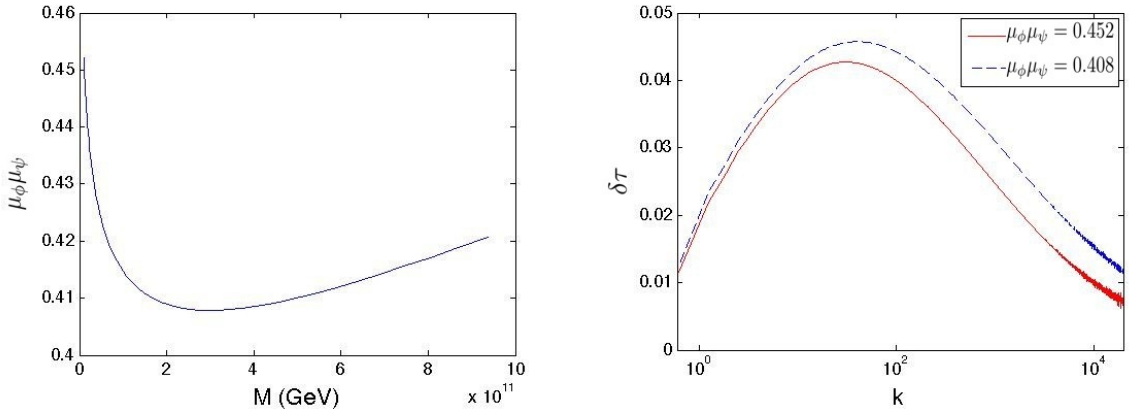

Figure 2-12: First Supernatural inflation model with M' at the GUT scale. The spectra corresponding to the maximum and minimum mass product are shown. There is again good agreement with the results of the previous section.

constant light timer field. If one compares Fig. 2-11 and Fig. 2-12 with Fig. 2-6, we indeed see excellent agreement for the amplitude and width of the time delay spectrum.

When setting the mass scale M' at some lower scale of 10^{11} GeV, the reduced timer and waterfall masses become $O(1)$. This means that in this case the parameter λ saturates faster and the perturbation spectrum reaches its asymptotic limit earlier and becomes time-independent from that point onward. Furthermore the actual value of the growth parameter λ is smaller, leading to an enhanced perturbation amplitude, the largest among the models studied here. The mass product changes by a factor of 2.5 as seen in Fig. 2-13. We choose five points in the allowed interval of mass values and calculate the corresponding curves. The specific values of the mass parameter M are $M = 1.06\cdot10^{10}$ GeV, $2.4\cdot10^{10}$ GeV, $5.42\cdot10^{10}$ GeV, $1.23\cdot10^{11}$ GeV, $2.77\cdot10^{11}$ GeV. The corresponding pairs of reduced waterfall and timer masses are $\{\mu_\phi, 1/\mu_\psi\} = \{3.19, 4.48\}$, $\{2.58, 2.97\}$, $\{2.22, 2.05\}$, $\{1.99, 1.47\}$, $\{1.83, 1.09\}$. The points on the mass product graph are color coded to match the corresponding time delay curve in Fig. 2-13. We can see that since the mass products have a larger variation, the resulting spectra have quite different time delay spectra. Also, since the timer is not much lighter than the Hubble scale, the curves do not scale according to our previous analysis.

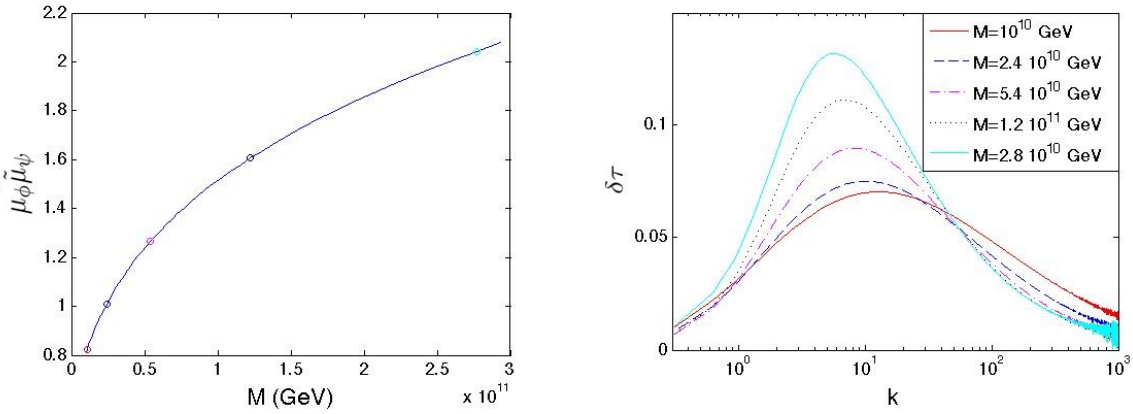

Figure 2-13: First Supernatural inflation model with M' at the intermediate scale. Five representative pairs of masses were chosen and the corresponding time delay curves are shown. This model can give maximum time delay of more than 0.1.

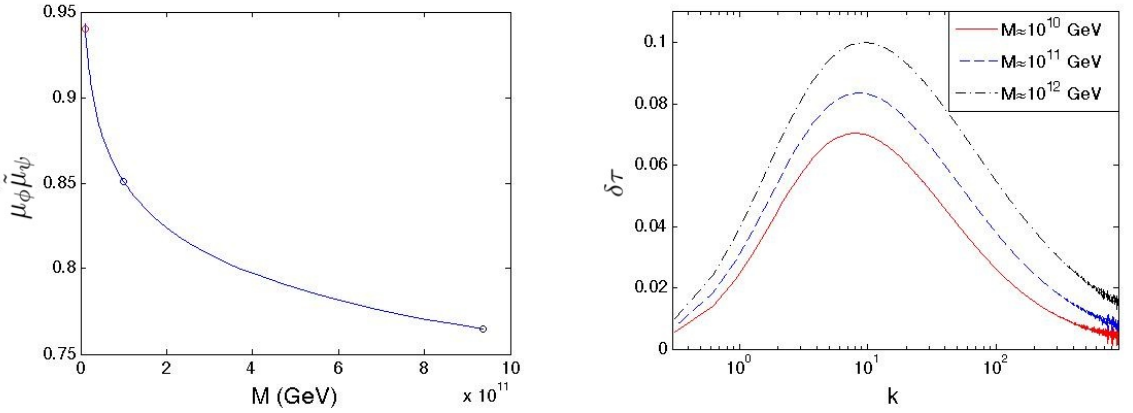

Figure 2-14: Second Supernatural inflation model. Three representative pairs of masses were chosen and the corresponding time delay curves are shown.

We finally consider SUSY model 2, Eq. (2.46), with the $\psi^2\phi^2$ interaction term. Again the reduced masses are $O(1)$, so we expect a small λ leading to a large amplitude perturbation spectrum. The mass product varies around 1 by less than $\pm 15\%$. We choose three values of the mass product (the two extrema and an intermediate one) and plot the resulting curves in Fig. 2-14. The specific values of the mass parameter M are $M = 1.080 \cdot 10^{10}$ GeV, $1.006 \cdot 10^{11}$ GeV, $9.376 \cdot 10^{11}$ GeV and the corresponding pairs of reduced waterfall and timer masses are $\{\mu_\phi, 1/\mu_\psi\} = \{2.697, 2.367\}$, $\{2.330, 2.262\}$, $\{2.007, 2.170\}$.

2.7 Conclusions

We presented a novel method for calculating the power spectrum of density fluctuations in hybrid inflation, one that does not suffer from the non-existence of a classical field trajectory. We used this method to numerically calculate the power spectrum for a wide range of parameters and concluded that in the case of a light timer field, all characteristics of the power spectrum are controlled by the product of the masses of the two fields. In particular the amplitude was fitted to a power law and found to behave as $\delta\tau_{max} \sim 0.03(\mu_\phi\mu_\psi)^{-0.34}$ and the width in log-space as $\Delta k \sim 1.7(\mu_\phi\mu_\psi)^{-1.17}$. Furthermore we made connection to SUSY inspired models of hybrid inflation and gave numerical results to their power spectra as well. For the SUSY models with a light timer field the numerical results were in excellent agreement with our fitted parameters.

Work is currently under way in refining and extending the formalism. Understanding the rescaling properties between the RSG approximation and the exact result could provide further insight into the physics of the problem and provide quasi-analytical approximation of well controlled accuracy. We will also apply our results to estimating the number and size of primordial black holes and try to make contact with astrophysical observations regarding supermassive black holes in galactic centers. Finally we are examining the predictions of our model for the non-Gaussian part of the perturbation spectrum.

2.8 Acknowledgements

We thank Kristin Burgess and Nguyen Thanh Son, whose earlier work on this subject paved the way for the current project. We also thank Larry Guth, who helped us understand that this problem does not require a Monte Carlo calculation, and Mark Hertzberg, who helped us understand the dynamics of the waterfall transition. We also thank Alexis Giguere, Illan Halpern, and Matthew Joss for helpful discussions. The work was supported in part by the DOE under Contract No. DE-

FG02-05ER41360.

2.9 Appendix

2.9.1 Zero mode at early times

The $\vec{k} = 0$ mode is not captured by the procedure described in the main text. If we consider this mode alone for asymptotically early times, so that we keep only the exponential in the mass term

$$\ddot{u} + 3\dot{u} = -\mu_\phi^2 e^{-\tilde{\mu}_\psi^2 N} u \ . \tag{2.86}$$

This can again be solved in terms of Bessel functions by defining a new variable and a new function as

$$\tilde{z} = \alpha e^{-\tilde{\mu}_\psi^2 N/2} \quad , \quad u(0,N) = \tilde{z}^\beta \tilde{Z}(\tilde{z}) \ . \tag{2.87}$$

The mode function becomes

$$\tilde{z}^2 \frac{d^2\tilde{Z}}{d\tilde{z}^2} + \tilde{z}\frac{d\tilde{Z}}{d\tilde{z}}\left(1 + 2\beta - \frac{6}{\tilde{\mu}_\psi^2}\right) + \tilde{Z}\left(\beta^2 - \frac{6\beta}{\tilde{\mu}_\psi^2} + \frac{\mu_\phi^2 \tilde{z}^2 4}{\alpha^2 \tilde{\mu}_\psi^4}\right) = 0 \ . \tag{2.88}$$

The standard form of the differential equation that gives Bessel functions is

$$z^2 \frac{d^2 Z_\nu}{dz^2} + z\frac{dZ_\nu}{dz} + (z^2 - \nu^2) Z_\nu = 0 \ . \tag{2.89}$$

By appropriately choosing the constants α,β and ν the two equations can be made identical. The choices are

$$\beta = \frac{3}{\tilde{\mu}_\psi^2} \ , \ \alpha = \frac{2\mu_\phi}{\tilde{\mu}_\psi^2} \ , \ \nu = \frac{3}{\tilde{\mu}_\psi^2} \ . \tag{2.90}$$

Finally introducing an arbitrary constant of normalization N_0, the solution for the zero mode at asymptotically early times becomes

$$u(0,N) = N_0 e^{-3N/2} H_\nu^{(1)}(\tilde{z}) \quad , \quad \tilde{z} = \frac{2\mu_\phi}{\tilde{\mu}_\psi^2} e^{-\tilde{\mu}_\psi^2 N/2} \ . \tag{2.91}$$

The normalization factor N_0 can be defined using the Wronskian at early times. The Wronskian at all times is defined as

$$W(\vec{k},t) = u(\vec{k},t)\frac{\partial u^*(-\vec{k},t)}{\partial t} - \frac{\partial u(\vec{k},t)}{\partial t} u^*(-\vec{k},t) \ . \tag{2.92}$$

Taking the time derivative and using the equation of motion

$$\begin{aligned} \frac{\partial W(\vec{k},t)}{\partial t} &= u(\vec{k},t)\frac{\partial^2 u^*(-\vec{k},t)}{\partial t^2} - \frac{\partial^2 u(\vec{k},t)}{\partial t^2} u^*(-\vec{k},t) = -3HW(\vec{k},t) \\ &\Rightarrow W(\vec{k},t) = f(\vec{k}) e^{-3Ht} \ . \end{aligned} \tag{2.93}$$

Since $f(\vec{k})$ is by definition independent of time, we will compute it at approximately early times, where we know the solution in analytic form and the solution is

$$W(\vec{k} \neq 0) = i e^{-3N} \quad , \quad W(\vec{k}=0) = \frac{2ir\mu_\psi^2 H}{pi} N_0^2 e^{-3N} \ . \tag{2.94}$$

Requiring that the Wronskian be a continuous function of $\vec{k}$ at all times we can extract the value of N_0.

$$N_0 = \sqrt{\frac{3\pi}{2r\mu_\psi^2 H}} \ . \tag{2.95}$$

2.9.2 Initial Conditions

We can rewrite the mode equation as a system of three coupled first order differential equations.

$$\frac{d\theta}{dN} = -\frac{\tilde{k}e^{-3N}}{R^2} , \tag{2.96}$$

$$\frac{dR}{dN} = \dot{R} , \tag{2.97}$$

$$\frac{d\dot{R}}{dN} = \frac{\tilde{k}^2 e^{-6N}}{R^3} - 3\dot{R} - e^{-2N}\tilde{k}^2 R + \mu_\phi^2(1 - e^{-\tilde{\mu}_\psi^2 N})R . \tag{2.98}$$

In this notation, $\dot{R}$ is one of the three independent functions.

This is not a system of three coupled ODE's in the strict sense. We can first solve the two equations $\frac{dR}{dN}$ and $\frac{d\dot{R}}{dN}$ as they do not contain any terms involving θ or its derivative. We can then integrate $\frac{d\theta}{dN}$ forward in time, using the calculated values of $R(N)$. Furthermore it is clear that the equations needed to calculate the spectral quantities of the time delay field only depend on the magnitude of the wavenumber, as was expected due to the isotropy of the problem, so we need only solve the mode equations for one positive semi-axis.

We know from the analytical solution at early times that

$$R(N \to -\infty) \to e^{-N} . \tag{2.99}$$

Since we have to start the numerical integration at some finite negative time without losing much in terms of accuracy, we refine the initial condition by including extra terms in the above expression. We will then start numerically integrating when our expansion violates the desired accuracy bound. We define the correction to the asymptotic behavior as $\delta R(N)$ such that

$$R(N) \equiv e^{-N} + \delta R(N) . \tag{2.100}$$

We will plug this into Eq. (2.34) and expand δR in powers of μ_ϕ^2 and e^N .

$$\begin{aligned}\delta R \quad &= \left(\frac{e^N}{2\tilde{k}^2} - \frac{e^{3N}}{8\tilde{k}^4} + \frac{e^{5N}}{16\tilde{k}^6}\right) + \mu_\phi^2\left(\frac{e^N}{4\tilde{k}^2}\left[1 - e^{-\tilde{\mu}_\psi^2 N}\right] + \frac{e^{3N}}{16\tilde{k}^4}\left[4 + e^{-\tilde{\mu}_\psi^2 N}(\tilde{\mu}_\psi^4 - 6\tilde{\mu}_\psi^2 - 4)\right]\right. \\ &\left. -\mu_\phi^2\frac{e^{5N}}{64\tilde{k}^6}\left[86 + e^{-\tilde{\mu}_\psi^2 N}(\tilde{\mu}_\psi^8 - 14\tilde{\mu}_\psi^6 + 53\tilde{\mu}_\psi^4 - 25\tilde{\mu}_\psi^2 - 86)\right]\right) \\ &+5\mu_\phi^4\left(\frac{e^{3N}}{32\tilde{k}^4}\left[1 - e^{-\tilde{\mu}_\psi^2 N}\right]^2 - \frac{e^{5N}}{64\tilde{k}^6}\left[29 - e^{-\tilde{\mu}_\psi^2 N}(9\tilde{\mu}_\psi^4 - 65\tilde{\mu}\psi^2 + 58)\right.\right. \\ &\left.\left. +e^{-2\tilde{\mu}_\psi^2 N}(14\tilde{\mu}_\psi^4 - 65\tilde{\mu}\psi^2 + 29)\right]\right) + 15\mu_\phi^6\frac{e^{5N}}{128\tilde{k}^6}\left[1 - e^{-\tilde{\mu}_\psi^2 N}\right]^3 + \mathcal{O}\left(e^{7N}, \mu_\phi^8\right) \ . \quad (2.101)\end{aligned}$$

We can now use the initial value expansion for $R(N)$ to calculate the corresponding expansion for the phase $\theta(N)$ through Eq. (2.32).

The asymptotic behavior, given by the standard definition of the Hankel functions is

$$\theta(N \to -\infty) = \tilde{k}e^{-N} - \pi \Leftrightarrow \theta(N \to -\infty) + \pi = \tilde{k}e^{-N} \ . \quad (2.102)$$

We define $\tilde{\theta} \equiv \theta(N) + \pi \Rightarrow \dot{\tilde{\theta}} = \dot{\theta}$, in order to keep track of the constant phase factor without carrying it through the perturbation expansion.

Defining the corrections to the early time behavior of the phase as

$$\tilde{\theta} = e^{-N}[\tilde{k} + \delta\theta(N)] \ , \quad (2.103)$$

we can construct a similar expansion as the one for δR. Since our formalism does not require knowledge of $\theta(N)$ we will not report the full expansion. It can be calculated in a straightforward way following the definition of Eq. (2.103), the evolution of Eq. (2.32) and the expansion for δR given in Eq. (2.101).

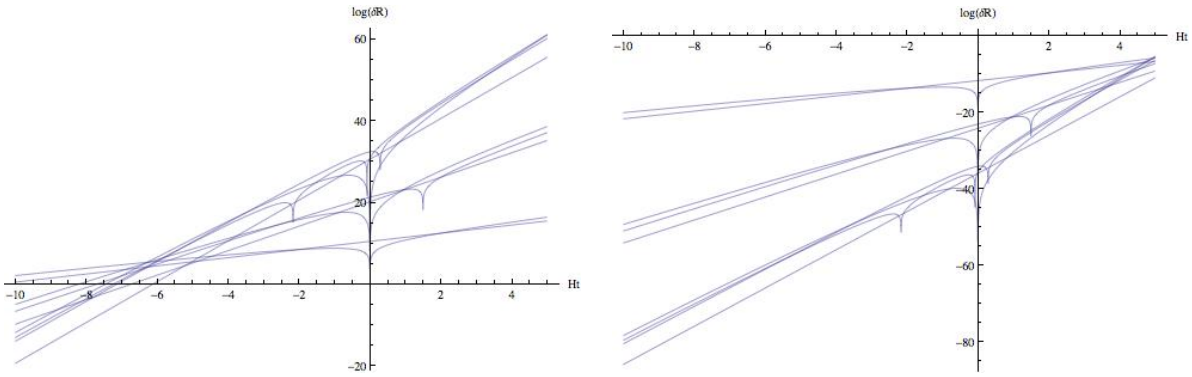

Figure 2-15: Mode functions for $\mu_\phi = 22$ and $\tilde{m}u_\psi = 1/18$. The left column is calculated for $\tilde{k} = 1/256$ and the right for $\tilde{k} = 256$

Bibliography

[1] A. H. Guth, "The inflationary universe: a possible solution to the horizon and flatness problems," Phys. Rev. D **23**, 347 (1981);
A. D. Linde, "A new inflationary universe scenario: a possible solution of the horizon, flatness, homogeneity, isotropy and primordial monopole problems," Phys. Lett. B **108**, 389 (1982);
A. Albrecht and P. J. Steinhardt, "Cosmology for grand unified theories with radiatively induced symmetry breaking," Phys. Rev. Lett. **48**, 1220 (1982).

[2] A. H. Guth and D. I. Kaiser, "Inflationary cosmology: Exploring the universe from the smallest to the largest scales," Science **307**, 884 (2005) [arXiv:astro-ph/0502328].

[3] E. Komatsu et al. [WMAP collaboration], "Seven-year Wilkinson Microwave Anisotropy Probe (WMAP) observations: Cosmological interpretation," Astrophy. J. Suppl. **192**, 18 (2011) [arXiv:1001.4538 [astro-ph.CO]].

[4] F. L. Bezrukov and M. E. Shaposhnikov, "The Standard Model Higgs boson as the inflaton," Phys. Lett. B **659**, 703 (2008) [arXiv:hep-th/0710.3755].

[5] L. Randall, M. Soljacic, and A.H. Guth,"Supernatural Inflation," arXiv:hep-ph/9601296v1.

[6] L. Randall, M. Soljacic, and A.H. Guth,"Supernatural Inflation: Inflation from Supersymmetry with No (Very) Small Parameters," Nucl. Phys. B **472**, 377-408 (1996) [arXiv:hep-ph/9512439v3].

[7] A. Linde, "Hybrid Inflation," Phys. Rev. D **49**, 748-754 (1994) [arXiv:astro-ph/9307002].

[8] J. G. Bellido, A. Linde, and D. Wands, "Density Perturbations and Black Hole Formation in Hybrid Inflation," Phys. Rev. D **54**, 6040-6058 (1996). [arXiv:astro-ph/9605094].

[9] B.J. Carr, "Primordial Black Holes as a Probe of Cosmology and High Energy Physics," Lect. Notes Phys. **631**, 301 (2003) [arXiv: astro-ph/0310838].

[10] B.J. Carr, "Primordial Black Holes–Recent Developments," 22nd Texas Symposium at Stanford, 12-17 December 2004, eConf C **041213**, 0204 (2004) [arXiv:astro-ph/0504034].

[11] B.J. Carr, "Primordial Black Holes: Do They Exist and Are They Useful?" to appear in Proceedings of "Inflating Horizon of Particle Astrophysics and Cosmology," Universal Academy Press Inc and Yamada Science Foundation (2005) [arXiv:astro-ph/0511743].

[12] B.J. Carr, "Primordial black hole formation and hybrid inflation," arXiv:1107.1681 [astro-ph.CO].

[13] K.M. Burgess, "Early Stages in Structure Formation," Ph.D. Thesis, Massachusetts Institute of Technology, 2004.

[14] N.T. Son, "Density Perturbations in Hybrid Inflation," Master's Thesis, Massachusetts Institute of Technology, 2009.

[15] D. Lyth, "Issues concerning the waterfall of hybrid inflation," Prog. Theor. Phys. Suppl. **190**, 107-119 (2011) [arXiv:1005.2461].

[16] D. Lyth, "The hybrid inflation waterfall and the primordial curvature perturbation," [arXiv:astro-ph/1201.4312].

[17] D. Lyth, "Contribution of the hybrid inflation waterfall to the primordial curvature perturbation," JCAP **1107**, 035 (2011) [arXiv:1012.4617].

[18] J. Martin, and V. Vennin, "Stochastic Effects in Hybrid Inflation," Phys. Rev. D **85**, 043525 (2012) [arXiv:1110.2070].

[19] A.A. Abolhasani, H. Firouzjahi, and M. Sasaki, "Curvature perturbation and waterfall dynamics in hybrid inflation," JCAP **1110**, 015 (2011) [arXiv:1106.6315].

[20] H. Kodama, K. Kohri, and K. Nakayama, "On the waterfall behavior in hybrid inflation" [arXiv:1102.5612].

[21] J. Fonseca, M. Sasaki, and D. Wands, "Large-scale Perturbations from the Waterfall Field in Hybrid Inflation," Prog. Theor. Phys. **126**, 331-350 (2011) [arXiv:1005.4053].

[22] A.H. Guth and S.Y. Pi, "Quantum Mechanics of the scalar field in the new inflationary universe," Phys. Rev. D **32**, 1899 (1985).

[23] V. Mukhanov and S. Winitzki, "Introduction to Quantum Effects in Gravity," 2007, Cambridge University Press.

[24] S.W. Hawking, "The development of irregularities in a single bubble inflationary universe," Phys. Lett. B **115**, 295 (1982).

[25] A. H. Guth, I. F. Halpern, M. P. Hertzberg, M. A. Joss and E. I. Sfakianakis, "Hybrid Inflation with $\mathcal{N}$ Waterfall Fields: Density Perturbations and Constraints," , to be submitted

[26] A.H. Guth and S.Y. Pi, "Fluctuations in the new inflationary universe," Phys. Rev. Lett. **49**, 1110 (1982).

[27] A.H. Guth, "Quantum fluctuations in cosmology and how they lead to a multiverse," to be published in the Proceedings of the 25th Solvay Conference in Physics, *The Theory of the Quantum World,* Brussels, October 2011.

Chapter 3

Hybrid Inflation with $\mathcal{N}$ Waterfall Fields: Density Perturbations and Constraints

Hybrid inflation models are especially interesting as they lead to a spike in the density power spectrum on small scales, compared to the CMB. They also satisfy current bounds on tensor modes. Here we study hybrid inflation with $\mathcal{N}$ waterfall fields sharing a global $SO(\mathcal{N})$ symmetry. The inclusion of many waterfall fields has the obvious advantage of avoiding topologically stable defects for $\mathcal{N} > 3$. We find that it also has another advantage: it is easier to engineer models that can simultaneously (i) be compatible with constraints on the primordial spectral index, which tends to otherwise disfavor hybrid models, and (ii) produce a spike on astrophysically large length scales. The latter may have significant consequences, possibly seeding black hole formation. We calculate correlation functions of the time-delay, a measure of density perturbations, produced by the waterfall fields, as a convergent power series in both $1/\mathcal{N}$ and the field's correlation function $\Delta(x)$. We show that for large $\mathcal{N}$, the two-point function is $\langle \delta t(\mathbf{x})\, \delta t(\mathbf{0}) \rangle \propto \Delta^2(|\mathbf{x}|)/\mathcal{N}$ and the three-point function is $\langle \delta t(\mathbf{x})\, \delta t(\mathbf{y})\, \delta t(\mathbf{0}) \rangle \propto \Delta(|\mathbf{x}-\mathbf{y}|)\Delta(|\mathbf{x}|)\Delta(|\mathbf{y}|)/\mathcal{N}^2$. In accordance with the central limit theorem, the density perturbations on the scale of the spike are approximately Gaussian for large $\mathcal{N}$ and non-Gaussian for small $\mathcal{N}$.

3.1 Introduction

Inflation, a phase of accelerated expansion in the very early universe thought to be driven by one or several scalar fields, is our paradigm of early universe cosmology [1, 2, 3, 4]. It naturally explains the large scale homogeneity, isotropy, and flatness of the universe. Moreover, its basic predictions of approximate scale invariance and small non-Gaussianity in the $\sim 10^{-5}$ level departures from homogeneity and isotropy are in excellent agreement with recent CMB data [5, 6] and large scale structure.

While the basic paradigm of inflation is in excellent shape, no single model stands clearly preferred. Instead the literature abounds with various models motivated by different considerations, such as string moduli, supergravity, branes, ghosts, Standard Model, etc [7, 8, 9, 10, 11, 12, 13, 14]. While the incoming data is at such an impressive level that it can discriminate between various models and rule out many, such as models that overpredict non-Gaussianity, it is not clear if the data will ever reveal one model alone. An important way to make progress is to disfavor models based on theoretical grounds (such as issues of unitarity violation, acausality, etc) and to find a model that is able to account for phenomena in the universe lacking an alternate explanation. It is conceivable that some version of the so-called "hybrid inflation" model may account for astrophysical phenomena, for reasons we shall come to.

The hybrid inflation model, originally proposed by Linde [15], requires at least two fields. One of the fields is light and another of the fields is heavy (in Hubble units). The light field, called the "timer", is at early times slowly rolling down a potential hill and generates the almost scale invariant spectrum of fluctuations observed in the CMB and in large scale structure. The heavy field, called the "waterfall" field, has an effective mass that is time-dependent and controlled by the value of the timer field. The waterfall field is originally trapped at a minimum of its potential, but as its effective mass-squared becomes negative, a tachyonic instability follows, leading to the end of inflation; an illustration is given in Figure 3-1. The name "hybrid inflation" comes from the fact that this model is a sort of hybrid between a chaotic inflation model and a symmetry breaking inflation model.

As originally discussed in Refs. [16, 17], one of the most fascinating features of hybrid models is that the tachyonic behavior of the waterfall field leads to a sharp "spike" in the density power spectrum. This could seed primordial black holes [18, 19, 20, 21, 22]. For generic parameters, the length scale associated with this spike is typically very small. However, if one could find a parameter regime where the waterfall phase were to be prolonged, lasting for many e-foldings, say $N_w \sim 30 - 40$, then this would lead to a spike in the density perturbations on astrophysically large scales (but smaller than CMB scales). This may help to account for phenomena such as supermassive black holes or dark matter, etc. Of course the details of all this requires a very careful examination of the spectrum of density perturbations, including observational constraints.

Ordinarily the spectrum of density perturbations in a given model of inflation is obtained by decomposing the inflaton field into a homogeneous part plus a small inhomogeneous perturbation. However, for the waterfall fields of hybrid inflation, this approach fails since classically the waterfall field would stay forever at the top of a ridge in its potential. It is the quantum perturbations themselves that lead to a non-trivial evolution of the waterfall field, and therefore the quantum perturbations cannot be treated as small. Several approximations have been used to deal with this problem [16, 17, 25, 26, 27, 28, 29, 30, 31, 23, 24]. Here we follow the approach presented by some of us recently in Ref. [32], where a free field time-delay method was used, providing accurate numerical results.

In this chapter, we generalize the method of Ref. [32] to a model with $\mathcal{N}$ waterfall fields sharing a global $SO(\mathcal{N})$ symmetry. A model of many fields may be natural in various microscopic constructions, such as grand unified models, string models, etc. But apart from generalizing Ref. [32] to $\mathcal{N}$ fields, we also go much further in our analysis: we derive explicit analytical results for several correlation functions of the so-called time-delay. We formulate a convergent series expansion in powers of $1/\mathcal{N}$ and the field's correlation function $\Delta(x)$. We find all terms in the series to obtain the two-point correlation function of the time-delay for any $\mathcal{N}$. We also obtain the leading order behavior at large $\mathcal{N}$ for the three-point function time-delay, which provides a

measure of non-Gaussianity. We find that the non-Gaussianity is appreciable for small $\mathcal{N}$ and suppressed for large $\mathcal{N}$.

We also analyze in detail constraints on hybrid inflation models. We comment on how multiple fields avoids topological defects, which is a serious problem for low $\mathcal{N}$ models. However, the most severe constraint on hybrid models comes from the requirement to obtain the observed spectral index n_s. We show that at large $\mathcal{N}$, it is easier to engineer models that can fit the observed n_s, while also allowing for a prolonged waterfall phase. This means that large $\mathcal{N}$ models provide the most plausible way for the spike to appear on astrophysically large scales and be compatible with other constraints.

The organization of this chapter is as follows: In Section 3.2 we present our hybrid inflation model and discuss our approximations. In Section 3.3 we present the time-delay formalism, adapting the method of Ref. [32] to $\mathcal{N}$ fields. In section 3.4 we derive a series expansion for the two-point function, we derive the leading order behavior of the three-point function, and we derive results in k-space. In Section 3.5 we present constraints on hybrid models, emphasizing the role that $\mathcal{N}$ plays. In Section 3.6 we discuss and conclude. Finally, in the Appendices we present further analytical results.

3.2 $\mathcal{N}$ Field Model

The model consists of two types of fields: The timer field ψ that drives the first slow-roll inflation phase, and the waterfall field ϕ that becomes tachyonic during the second phase causing inflation to end. In many hybrid models, ϕ is comprised of two components, a complex field, but here we allow for $\mathcal{N}$ real components ϕ_i. We assume the components share a global $SO(\mathcal{N})$ symmetry, and so it is convenient to organize them into a vector

$$\vec{\phi} = \{\phi_1, \phi_2, \ldots, \phi_{\mathcal{N}}\}. \tag{3.1}$$

For the special case $\mathcal{N} = 2$, this can be organized into a complex field by writing $\phi_{complex} = (\phi_1 + i\,\phi_2)/\sqrt{2}$.

The dynamics is governed by the standard two derivative action for the scalar

fields $\psi, \vec{\phi}$ minimally coupled to gravity as follows (signature $+---$)

$$S = \int d^4x\sqrt{-g}\Bigg[\frac{1}{16\pi G}R \quad + \quad \frac{1}{2}g^{\mu\nu}\partial_\mu\psi\partial_\nu\psi \\ +\frac{1}{2}g^{\mu\nu}\partial_\mu\vec{\phi}\cdot\partial_\nu\vec{\phi} - V(\psi,\phi)\Bigg]. \tag{3.2}$$

The potential V is given by a sum of terms: V_0 providing false vacuum energy, $V_\psi(\psi)$ governing the timer field, $V_\phi(\phi)$ governing the waterfall field, and $V_{int}(\psi,\phi)$ governing their mutual interaction, i.e.,

$$V(\psi,\phi) = V_0 + V_\psi(\psi) + V_\phi(\phi) + V_{int}(\psi,\phi). \tag{3.3}$$

During inflation we assume that the constant V_0 dominates all other terms.

The timer field potential V_ψ and the waterfall field potential V_ϕ can in general be complicated. In general, they are allowed to be non-polynomial functions as part of some low energy effective field theory, possibly from supergravity or other microscopic theories. For our purposes, it is enough to assume an extremum at $\psi = \phi = 0$ and expand the potentials around this extremum as follows:

$$V_\psi(\psi) = \frac{1}{2}m_\psi^2\psi^2 + \ldots \tag{3.4}$$

$$V_\phi(\phi) = -\frac{1}{2}m_0^2\,\vec{\phi}\cdot\vec{\phi} + \ldots \tag{3.5}$$

The timer field is assumed to be light $m_\psi < H$ and the waterfall field is assumed to be heavy $m_0 > H$, where H is the Hubble parameter. In the original hybrid model, this quadratic term for V_ψ was assumed to be the entire potential. This model leads to a spectrum with a spectral index $n_s > 1$ and is observationally ruled out. Instead we need higher order terms, indicated by the dots, to fix this problem. This also places constraints on the mass of the timer field m_ψ, which has important consequences. We discuss these issues in detail in Section 3.5.

As indicated by the negative mass-squared, the waterfall field is tachyonic around

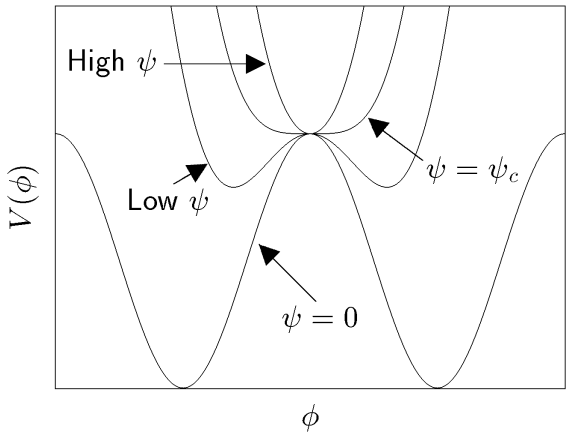

Figure 3-1: An illustration of the evolution of the effective potential for the waterfall field ϕ as the timer field ψ evolves from "high" values at early times, to $\psi = \psi_c$, and finally to "low" values at late times. In the process, the effective mass-squared of ϕ evolves from positive, to zero, to negative (tachyonic).

$\phi = \psi = 0$. This obviously cannot be the entire potential because then the potential would be unbounded from below. Instead there must be higher order terms that stabilize the potential with a global minimum near $V \approx 0$ (effectively setting the late-time cosmological constant).

The key to hybrid inflation is the interaction between the two fields. For simplicity, we assume a standard dimension 4 coupling of the form

$$V_{int}(\psi, \phi) = \frac{1}{2} g^2 \psi^2 \, \vec{\phi} \cdot \vec{\phi}. \tag{3.6}$$

This term allows the waterfall field to be stabilized at $\phi = 0$ at early times during slow-roll inflation when ψ is displaced away from zero, and then becomes tachyonic once the timer field approaches the origin; this is illustrated in Figure 3-1.

3.2.1 Approximations

We assume that the constant V_0 is dominant during inflation, leading to an approximate de Sitter phase with constant Hubble parameter H. By assuming a flat FRW

background, the scale factor is approximated as

$$a = \exp(Ht). \tag{3.7}$$

At early times, ψ is displaced from its origin, so $\phi = 0$. This means that we can approximate the ψ dynamics by ignoring the back reaction from ϕ. The fluctuations in ψ establish nearly scale invariant fluctuations on large scales, which we shall return to in Section 3.5. However, for the present purposes it is enough to treat ψ as a classical, homogeneous field $\psi(t)$. We make the approximation that we can neglect the higher order terms in the potential V_ψ in the transition era, leading to the equation of motion

$$\ddot{\psi} + 3H\dot{\psi} + m_\psi^2 \psi = 0. \tag{3.8}$$

Solving this equation for $\psi(t)$, we insert this into the equation for ϕ_i. We allow spatial dependence in ϕ_i, and ignore, for simplicity, the higher order terms in V_ϕ, leading to the equation of motion

$$\ddot{\phi}_i + 3H\dot{\phi}_i - e^{-2Ht}\nabla^2\phi_i + m_\phi^2(t)\phi_i = 0. \tag{3.9}$$

Here we have identified an effective mass-squared for the waterfall field of

$$m_\phi^2(t) \equiv -m_0^2 \left(1 - \left(\frac{\psi(t)}{\psi_c}\right)^2\right), \tag{3.10}$$

where the dimension 4 coupling g has been traded for a coupling ψ_c as $g^2 = m_0^2/\psi_c^2$. The quantity ψ_c has the physical interpretation as the "critical" value of ψ such that the effective mass of the waterfall field passes through zero. So at early times for $\psi > \psi_c$, then $m_\phi^2 > 0$ and ϕ_i is trapped at $\phi_i = 0$, while at late times for $\psi < \psi_c$, then $m_\phi^2 < 0$ and ϕ_i is tachyonic and can grow in amplitude, depending on the mode of interest; Figure 3-1 illustrates these features.

3.2.2 Mode Functions

Since we ignore the back-reaction of ϕ onto ψ and since we treat ψ as homogeneous in the equation of motion for ϕ (eq. (3.9)), then by passing to k-space, all modes are decoupled. Each waterfall field ϕ_i can be quantized and expanded in modes in momentum space as follows

$$\phi_i(\vec{x},t) = \int \frac{d^3k}{(2\pi)^3}\left[c_{k,i}e^{i\mathbf{k}\cdot\mathbf{x}}u_k(t) + c^\dagger_{k,i}e^{-i\mathbf{k}\cdot\mathbf{x}}u^*_k(t)\right], \tag{3.11}$$

where $c^\dagger_k$ (c_k) are the creation (annihilation) operators, acting on the $\phi_i = 0$ vacuum. By assuming an initial Bunch-Davies vacuum for each ϕ_i, the mode functions u_k are the same for all components due to the $SO(\mathcal{N})$ symmetry. To be precise, we assume that at asymptotically early times the mode functions are the ordinary Minkowski space mode functions, with the caveat that we need to insert factors of the scale factor a to convert from physical wavenumbers to comoving wavenumbers, i.e.,

$$u_k(t) \to \frac{e^{-i\,k\,t/a}}{a\sqrt{2k}}, \quad \text{at early times.} \tag{3.12}$$

At late times the mode functions behave very differently. Since the field becomes tachyonic, then the mode functions grow exponentially at late times. The transition depends on the wavenumber of interest. The full details of the mode functions were explained very carefully in Ref. [32], and the interested reader is directed to that paper for more information.

Now since we are approximating ϕ_i as a free field, then its fluctuations are entirely Gaussian and characterized entirely by its equal time two-point correlation function $\langle\phi_i(\mathbf{x})\,\phi_j(\mathbf{y})\rangle$. Passing to k-space, and using statistical isotropy and homogeneity of the Bunch-Davies vacuum, the fluctuations are equally well characterized by the so-called power spectrum $P_\phi(k)$, defined through

$$\langle\phi_i(\mathbf{k}_1)\,\phi_j(\mathbf{k}_2)\rangle = (2\pi)^3\delta(\mathbf{k}_1+\mathbf{k}_2)\,\delta_{ij}\,P_\phi(k_1). \tag{3.13}$$

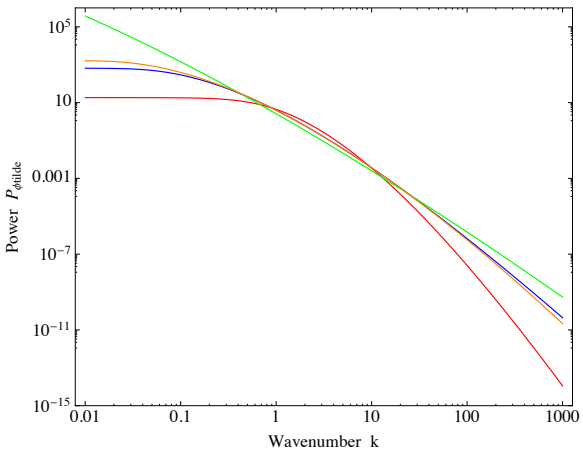

Figure 3-2: A plot of the (re-scaled) field's power spectrum $P_{\tilde{\phi}}$ as a function of wavenumber k (in units of H) for different masses: blue is $m_0 = 2$ and $m_\psi = 1/2$, red is $m_0 = 4$ and $m_\psi = 1/2$, green is $m_0 = 2$ and $m_\psi = 1/4$, orange is $m_0 = 4$ and $m_\psi = 1/4$.

This means the power spectrum is

$$\delta_{ij}\, P_\phi(k) = \int d^3x\, e^{-i\mathbf{k}\cdot\mathbf{x}} \langle \phi_i(\mathbf{x}) \phi_j(\mathbf{0}) \rangle. \tag{3.14}$$

It is simple to show that the power spectrum is related to the mode functions by

$$P_\phi(k) = |u_k|^2. \tag{3.15}$$

In Figure 3-2 we plot a rescaled version of P_ϕ, where we divide out by the root-mean-square (rms) of ϕ as defined in the next Section.

3.3 The Time-Delay

We would now like to relate the fluctuations in the waterfall field ϕ to a fluctuation in a physical observable, namely the density perturbation. An important step in this direction is to compute the so-called "time-delay" $\delta t(\mathbf{x})$; the time offset for the end of inflation for different parts of the universe. This causes different regions of the universe to have inflated more than others, creating a difference in their densities (though we will not explicitly compute $\delta\rho/\rho$ here). This basic formalism was first introduced by

Hawking [33] and by Guth and Pi [34], and has recently been reviewed in Ref. [35]. In the context of hybrid inflation, it was recently used by some of us in Ref. [**?**]. It provides an intuitive and straightforward way to calculate primordial perturbations and we now use this to study perturbations established by the $\mathcal{N}$ waterfall fields.

In its original formulation, the time-delay formalism starts by considering a classical homogeneous trajectory $\phi_0 = \phi_0(t)$, and then considers a first order perturbation around this. At first order, one is able to prove that the fluctuating inhomogeneous field $\phi(\mathbf{x}, t)$ is related to the classical field ϕ_0, up to an overall time offset $\delta t(\mathbf{x})$,

$$\phi(\mathbf{x}, t) = \phi_0(t - \delta t(\mathbf{x})). \tag{3.16}$$

In the present case of hybrid inflation, the waterfall field is initially trapped at $\phi = 0$ and then once it becomes tachyonic, it eventually falls off the hill-top due to quantum fluctuations. This means that there is no classical trajectory about which to expand. Nevertheless, we will show that, to a good approximation, the field $\phi(\mathbf{x}, t)$ is well described by an equation of the form (3.16), for a suitably defined ϕ_0. The key is that all modes of interest grow at the same rate at late times. Further information of the time evolution of the mode functions is in Ref. [32].

To show this, we need to compute the evolution of the field ϕ according to eq. (3.9). This requires knowing $m_\phi(t)$, which in turn requires knowing $\psi(t)$. By solving eq. (3.8) for the timer field and dispensing with transient behavior, we have

$$\psi(t) = \psi_c \, \exp\left(-\, p\, t\right), \tag{3.17}$$

where

$$p = H\left(\frac{3}{2} - \sqrt{\frac{9}{4} - \frac{m_\psi^2}{H^2}}\right), \tag{3.18}$$

(note $p > 0$). We have set the origin of time $t = 0$ to be when $\psi = \psi_c$ and assume $\psi > \psi_c$ at early times.

Substituting this solution into $m_\phi(t)$, we can, in principle, solve eq. (3.9). In general, the solution is somewhat complicated with a non-trivial dependence on

wavenumber. However, at late times the behavior simplifies. Our modes of interest are super-horizon at late times. For these modes, the gradient term is negligible and the equation of motion reduces to

$$\ddot{\phi}_i + 3H\dot{\phi}_i + m_\phi^2(t)\phi_i = 0. \tag{3.19}$$

So each mode evolves in the same way at late times. Treating $m_\phi(t)$ as slowly varying (which is justified because the timer field mass $m_\psi < H$ and so p is small), we can solve for ϕ_i at late times t in the adiabatic approximation. We obtain

$$\phi_i(\mathbf{x}, t) = \phi_i(\mathbf{x}, t_0) \exp\left(\int_{t_0}^{t} dt'\, \lambda(t')\right), \tag{3.20}$$

where

$$\lambda(t) = H\left(-\frac{3}{2} + \sqrt{\frac{9}{4} + \frac{m_0^2}{H^2}\left(1 - e^{-2\,p\,t}\right)}\right). \tag{3.21}$$

Here t_0 is some reference time. For $t > 0$, we have $\lambda(t) > 0$, so the modes grow exponentially in time. Later in Section 3.5 we explain that in fact λ is roughly constant in the latter stage of the waterfall phase, i.e., the $\exp(-2\,p\,t)$ piece becomes small.

We now discuss fluctuations in the time at which inflation ends. For convenience, we define the reference time t_0 to be the time at which the rms value of the field reaches ϕ_{end}; the end of inflation

$$\mathcal{N}\phi_{\rm rms}^2(t_0) = \phi_{\rm end}^2, \tag{3.22}$$

where we have included a factor of $\mathcal{N}$ to account for all fields, allowing ϕ_{rms} to refer to fluctuations in a single component ϕ_i, i.e., $\phi_{rms}^2 = \langle \phi_i^2(0) \rangle$. In terms of the power spectrum, it is

$$\phi_{rms}^2 = \int \frac{d^3k}{(2\pi)^3} P_\phi(k). \tag{3.23}$$

If we were to include arbitrarily high k, this would diverge quadratically, which is the usual Minkowski space divergence. However, our present analysis only applies to

modes that are in the growing regime. For these modes, $P_\phi(k)$ falls off exponentially with k and there is no problem. So in this integral, we only include modes that are in the asymptotic regime, or, roughly speaking, only super-horizon modes.

Using eq. (3.20), we can express the field $\phi_i(\mathbf{x}, t)$ at time $t = t_0 + \delta t$ in terms of the field $\phi_i(\mathbf{x}, t_0)$ by

$$\phi_i(\mathbf{x}, t) = \phi_i(\mathbf{x}, t_0) \exp\left(\lambda(t_0)\, \delta t\right). \tag{3.24}$$

If t is chosen to be the time $t_{\rm end}(\mathbf{x})$ at which inflation ends at each point in space, then $\vec{\phi}\cdot\vec{\phi}\big(\mathbf{x}, t_{\rm end}(\mathbf{x})\big) = \phi^2_{\rm end} = \mathcal{N}\phi^2_{\rm rms}(t_0)$, and the above equation becomes

$$\mathcal{N}\phi^2_{\rm rms}(t_0) = \vec{\phi}(\mathbf{x}, t_0)\cdot\vec{\phi}(\mathbf{x}, t_0) \exp\left(2\,\lambda(t_0)\, \delta t\right), \tag{3.25}$$

which can be solved for the time-delay field $\delta t(\mathbf{x}) = t_{\rm end}(\mathbf{x}) - t_0$ as

$$\delta t(\mathbf{x}) = \frac{-1}{2\lambda(t_0)} \ln\left(\frac{\vec{\phi}(\mathbf{x}, t_0)\cdot\vec{\phi}(\mathbf{x}, t_0)}{\mathcal{N}\phi^2_{\rm rms}(t_0)}\right). \tag{3.26}$$

This finalizes the $\mathcal{N}$ component analysis of the time-delay, generalizing the two component (complex) analysis of Ref. [32].

3.4 Correlation Functions

We now derive expressions for the two-point and three-point correlation functions of the time-delay field. To do so, it is convenient to introduce a re-scaled version of the correlation function $\Delta(x)$ defined through

$$\langle \phi_i(\mathbf{x})\phi_j(\mathbf{0})\rangle = \Delta(x)\phi^2_{rms}\delta_{ij}. \tag{3.27}$$

By definition $\Delta(0) = 1$, and as we vary x, Δ covers the interval $\Delta(x) \in (0, 1]$. (Ref. [32] used a different convention where Δ covers the interval $\Delta(x) \in (0, 1/2]$).

In Figure 3-3, we show a plot of Δ at t_{end} as a function of x, measured in Hubble lengths (H^{-1}), for a choice of masses.

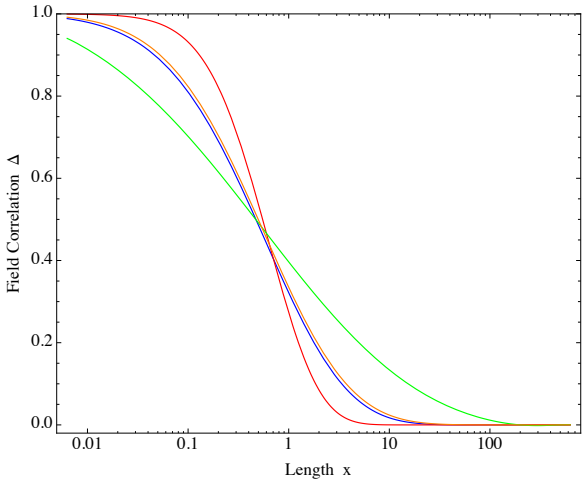

Figure 3-3: A plot of the field's correlation Δ as a function of x (in units of H^{-1}) for different masses: blue is $m_0 = 2$ and $m_\psi = 1/2$, red is $m_0 = 4$ and $m_\psi = 1/2$, green is $m_0 = 2$ and $m_\psi = 1/4$, orange is $m_0 = 4$ and $m_\psi = 1/4$.

3.4.1 Two-Point Function

We now express the time-delay correlation functions as a power series in Δ and $1/\mathcal{N}$. An alternative derivation of the power spectra of the time-delay field in terms of an integral, which is closer to the language of Ref. [32], can be found in Appendix 3.8.3.

Using the above approximation for δt in eq. (3.26), the two-point correlation function for the time-delay is

$$(2\lambda)^2\langle\delta t(\mathbf{x})\delta t(\mathbf{0})\rangle = \left\langle \ln\left(\frac{\vec{\phi}_x\cdot\vec{\phi}_x}{\mathcal{N}\phi_{rms}^2}\right)\ln\left(\frac{\vec{\phi}_0\cdot\vec{\phi}_0}{\mathcal{N}\phi_{rms}^2}\right)\right\rangle, \tag{3.28}$$

where we have used the abbreviated notation $\vec{\phi}_x \equiv \vec{\phi}(\mathbf{x})$. The two-point function will include a constant (independent of x) for a non-zero $\langle\delta t\rangle$. This can be reabsorbed into a shift in t_0, whose dependence we have suppressed here, and so we will ignore the constant in the following computation. This means that we will compute the *connected* part of the correlation functions.

We would like to form an expansion, but we do not have a classical trajectory about which to expand. Instead we use the following idea: we recognize that $\vec{\phi}\cdot\vec{\phi}$ should be centralized around its mean value of $\mathcal{N}\phi_{rms}^2$, plus relatively small fluctuations at

large $\mathcal{N}$. This means that it is convenient to write

$$\frac{\vec{\phi}\cdot\vec{\phi}}{\mathcal{N}\phi_{rms}^2} = 1 + \left(\frac{\vec{\phi}\cdot\vec{\phi}}{\mathcal{N}\phi_{rms}^2} - 1\right) \tag{3.29}$$

and treat the term in parenthesis on the right as small, as it represents the fluctuations from the mean. This allows us to Taylor expand the logarithm in powers of

$$\Phi \equiv \frac{\vec{\phi}\cdot\vec{\phi}}{\mathcal{N}\phi_{rms}^2} - 1, \tag{3.30}$$

with $\langle\Phi\rangle = 0$. Now recall that the series expansion of the logarithm for small Φ is

$$\ln(1+\Phi) = \Phi - \frac{\Phi^2}{2} + \frac{\Phi^3}{3} - \frac{\Phi^4}{4} + \ldots, \tag{3.31}$$

allowing us to expand to any desired order in Φ.

The leading non-zero order is quadratic $\sim \Phi^2$. It is

$$\begin{aligned}(2\lambda)^2\langle\delta t(\mathbf{x})\delta t(\mathbf{0})\rangle_2 &= \langle\Phi(\mathbf{x})\Phi(\mathbf{0})\rangle, \\ &= \frac{\langle\phi_i(\mathbf{x})\phi_i(\mathbf{x})\phi_j(\mathbf{0})\phi_j(\mathbf{0})\rangle}{(\mathcal{N}\phi_{rms}^2)^2} - 1,\end{aligned} \tag{3.32}$$

where we are implicitly summing over indices in the second line (for simplicity, we will place all component indices (i, j) downstairs). Using Wick's theorem to perform the four-point contraction, we find the result

$$(2\lambda)^2\langle\delta t(\mathbf{x})\delta t(\mathbf{0})\rangle_2 = \frac{2\Delta^2(x)}{\mathcal{N}}, \tag{3.33}$$

where $x \equiv |\mathbf{x}|$. This provides the leading approximation for large $\mathcal{N}$, or small Δ. This should be contrasted to the RSG approximation used in Refs. [16, 17] in which the correlation function is approximated as $\sim \Delta$, rather than $\sim \Delta^2$, at leading order.

For brevity, we shall not go through the result at each higher order here, but we report on results at higher order in Appendix 3.8.1. By summing those results to

different orders, we find

$$(2\lambda)^2\langle\delta t(\mathbf{x})\delta t(\mathbf{0})\rangle = \frac{2\Delta^2}{\mathcal{N}} + \frac{2\Delta^4}{\mathcal{N}^2} - \frac{4\Delta^4}{\mathcal{N}^3} + \frac{16\Delta^6}{3\mathcal{N}^3} + \frac{8\Delta^4}{\mathcal{N}^4} - \frac{32\Delta^6}{\mathcal{N}^4} + \frac{24\Delta^8}{\mathcal{N}^4} + \mathcal{O}\left(\frac{1}{\mathcal{N}^5}\right), \tag{3.34}$$

(where $\Delta = \Delta(x)$ here). We find that various cancellations have occurred. For example, the $-8\Delta^2/\mathcal{N}^2$ term that enters at cubic order (see Appendix 3.8.1) has canceled.

Note that at a given order in $1/\mathcal{N}$ there are various powers of Δ^2. However, by collecting all terms at a given power in Δ^2, we can identify a pattern in the value of its coefficients as functions of $\mathcal{N}$. We find

$$\begin{aligned}&(2\lambda)^2\langle\delta t(\mathbf{x})\delta t(\mathbf{0})\rangle \\ &= \frac{2\Delta^2(x)}{\mathcal{N}} + \frac{2\Delta^4(x)}{\mathcal{N}(\mathcal{N}+2)} + \frac{16\Delta^6(x)}{3\mathcal{N}(\mathcal{N}+2)(\mathcal{N}+4)} \\ &\quad + \frac{24\Delta^8(x)}{\mathcal{N}(\mathcal{N}+2)(\mathcal{N}+4)(\mathcal{N}+6)} + \dots\end{aligned} \tag{3.35}$$

We then identify the entire series as

$$(2\lambda)^2\langle\delta t(\mathbf{x})\delta t(\mathbf{0})\rangle = \sum_{n=1}^{\infty} C_n(\mathcal{N})\,\Delta^{2n}(x), \tag{3.36}$$

where the coefficients are

$$C_n(\mathcal{N}) = \frac{1}{n^2}\binom{\frac{\mathcal{N}}{2} - 1 + n}{n}^{-1}, \tag{3.37}$$

with $\binom{a}{b}$ the binomial coefficient. This series is convergent for any $\mathcal{N}$ and $\Delta \in (0, 1]$, and is one of our central results.

For the case of a single scalar or a doublet (complex field), the full series organizes

itself into known functions. For $\mathcal{N} = 1$ we find

$$\begin{aligned}(2\lambda)^2\langle\delta t(\mathbf{x})\delta t(\mathbf{0})\rangle &= 2\Delta^2(x) + \frac{2\Delta^4(x)}{3} + \frac{16\Delta^6(x)}{45} + \dots \\ &= 2\left(\sin^{-1}\Delta(x)\right)^2. \end{aligned} \tag{3.38}$$

For $\mathcal{N} = 2$ we find

$$\begin{aligned}(2\lambda)^2\langle\delta t(\mathbf{x})\delta t(\mathbf{0})\rangle &= \Delta^2(x) + \frac{\Delta^4(x)}{2^2} + \frac{\Delta^6(x)}{3^2} + \dots \\ &= \mathrm{Li}_2(\Delta^2(x)), \end{aligned} \tag{3.39}$$

where $\mathrm{Li}_s(z)$ is the polylogarithm function. We also find that for any even value of $\mathcal{N}$, the series is given by the polylogarithm function plus a polynomial in Δ; this is described in Appendix 3.8.2.

Using the power series, we can easily obtain plots of the two-point function for any $\mathcal{N}$. For convenience, we plot the re-scaled quantity $\mathcal{N}(2\lambda)^2\langle\delta t(\mathbf{x})\delta t(\mathbf{0})\rangle$ as a function of Δ in Figure 3-4 (top) for different $\mathcal{N}$. We see convergence of all curves as we increase $\mathcal{N}$, which confirms that the leading behavior of the (un-scaled) two-point function is $\sim 1/\mathcal{N}$. In Figure 3-4 (bottom) we plot $\mathcal{N}\langle\delta t(\mathbf{x})\delta t(\mathbf{0})\rangle$ as a function of x for different masses and two different $\mathcal{N}$.

3.4.2 Three-Point Function

The three-point function is given by a simple modification of eq. (3.28), namely

$$\begin{aligned}&-(2\lambda)^3\langle\delta t(\mathbf{x})\delta t(\mathbf{y})\delta t(\mathbf{0})\rangle \\ &= \left\langle \ln\left(\frac{\vec{\phi}_x\cdot\vec{\phi}_x}{\mathcal{N}\phi_{rms}^2}\right)\ln\left(\frac{\vec{\phi}_y\cdot\vec{\phi}_y}{\mathcal{N}\phi_{rms}^2}\right)\ln\left(\frac{\vec{\phi}_0\cdot\vec{\phi}_0}{\mathcal{N}\phi_{rms}^2}\right)\right\rangle. \end{aligned} \tag{3.40}$$

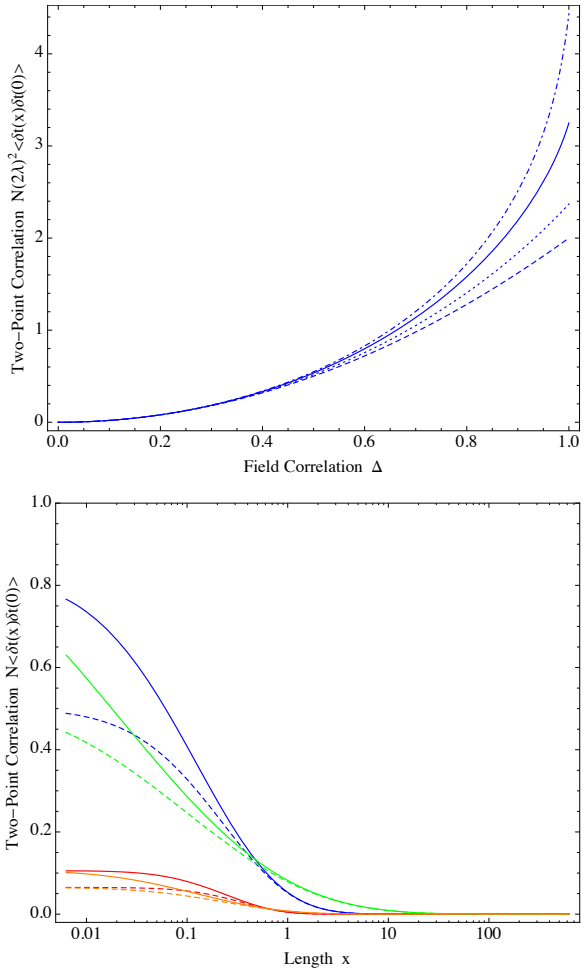

Figure 3-4: Top: a plot of the (re-scaled) two-point function of the time-delay $\mathcal{N}(2\lambda)^2\langle\delta t(\mathbf{x})\delta t(\mathbf{0})\rangle$ as a function of $\Delta \in [0,1]$ as we vary $\mathcal{N}$: dot-dashed is $\mathcal{N}=1$, solid is $\mathcal{N}=2$, dotted is $\mathcal{N}=6$, and dashed is $\mathcal{N}\to\infty$. Bottom: a plot of the (re-scaled) two-point function of the time-delay $\mathcal{N}\langle\delta t(\mathbf{x})\delta t(\mathbf{0})\rangle$ as a function of x for different masses: blue is $m_0=2$ and $m_\psi=1/2$, red is $m_0=4$ and $m_\psi=1/2$, green is $m_0=2$ and $m_\psi=1/4$, orange is $m_0=4$ and $m_\psi=1/4$, with solid for $\mathcal{N}=2$ and dashed for $\mathcal{N}\to\infty$.

Here we will work only to leading non-zero order, which in this case is cubic. We expand the logarithms as before to obtain

$$\begin{aligned}
&-(2\lambda)^3\langle\delta t(\mathbf{x})\delta t(\mathbf{y})\delta t(\mathbf{0})\rangle_3 \\
&= \langle\Phi(\mathbf{x})\Phi(\mathbf{y})\Phi(\mathbf{0})\rangle, \\
&= \frac{\langle\phi_i(\mathbf{x})\phi_i(\mathbf{x})\phi_j(\mathbf{y})\phi_j(\mathbf{y})\phi_k(\mathbf{0})\phi_k(\mathbf{0})\rangle}{(\mathcal{N}\phi_{rms}^2)^3} + 2 \\
&\quad - \left(\frac{\langle\phi_i(\mathbf{x})\phi_i(\mathbf{x})\phi_j(\mathbf{y})\phi_j(\mathbf{y})\rangle}{(\mathcal{N}\phi_{rms}^2)^2} + 2\,\text{perms}\right),
\end{aligned} \tag{3.41}$$

where "perms" is short for permutations under interchanging $\mathbf{x}$, $\mathbf{y}$, $\mathbf{0}$. Using Wick's theorem to perform the various contractions, we find the result

$$-(2\lambda)^3\langle\delta t(\mathbf{x})\delta t(\mathbf{y})\delta t(\mathbf{0})\rangle_3 = \frac{8\,\Delta(|\mathbf{x}-\mathbf{y}|)\,\Delta(x)\,\Delta(y)}{\mathcal{N}^2}. \tag{3.42}$$

We would now like to use the three-point function as a measure of non-Gaussianity. For a single random variable, a measure of non-Gaussianity is to compute a dimensionless ratio of the skewness to the 3/2 power of the variance. For a field theory, we symmetrize over variables, and define the following measure of non-Gaussianity in position space

$$S \equiv \frac{\langle\delta t(\mathbf{x})\delta t(\mathbf{y})\delta t(\mathbf{0})\rangle}{\sqrt{\langle\delta t(\mathbf{x})\delta t(\mathbf{y})\rangle\langle\delta t(\mathbf{x})\delta t(\mathbf{0})\rangle\langle\delta t(\mathbf{y})\delta t(\mathbf{0})\rangle}}. \tag{3.43}$$

(Recall that we are ignoring $\langle\delta t\rangle$, as it can be just re-absorbed into t_0, so the three-point and two-point functions are the connected pieces). Computing this at the leading order approximation using eqs. (3.33, 3.42) (valid for large $\mathcal{N}$, or small Δ), we find

$$S \approx -\sqrt{\frac{8}{\mathcal{N}}}\,. \tag{3.44}$$

Curiously, the dependence on $\mathbf{x}$, $\mathbf{y}$ has dropped out at this order. We see that for small $\mathcal{N}$ there is significant non-Gaussianity, while for large $\mathcal{N}$ the theory becomes Gaussian, as expected from the central limit theorem.

3.4.3 Momentum Space

Let us now present our results in k-space. We shall continue to analyze the results at high $\mathcal{N}$, or small Δ, which allows us to just include the leading order results.

For the two-point function, we define the power spectrum through

$$\langle \delta t(\mathbf{k}_1)\delta t(\mathbf{k}_2)\rangle = (2\pi)^3\delta(\mathbf{k}_1+\mathbf{k}_2)P_{\delta t}(k_1). \tag{3.45}$$

We use eq. (3.33) and Fourier transform to k-space using the convolution theorem. To do so it is convenient to introduce a dimensionless field $\tilde{\phi}_i \equiv \phi_i/\phi_{rms}$ and introduce the corresponding power spectrum $P_{\tilde{\phi}}(k) = P_\phi(k)/\phi_{rms}^2 = |u_k|^2/\phi_{rms}^2$, which is the Fourier transform of $\Delta(x)$. We then find the result

$$P_{\delta t}(k) \approx \frac{1}{2\lambda^2\mathcal{N}}\int \frac{d^3k'}{(2\pi)^3} P_{\bar{\phi}}(k')P_{\bar{\phi}}(|\mathbf{k}-\mathbf{k}'|). \tag{3.46}$$

A dimensionless measure of fluctuations is the following

$$\mathcal{P}_{\delta t}(k) \equiv \frac{k^3H^2P_{\delta t}(k)}{2\pi^2}, \tag{3.47}$$

The factor of $k^3/(2\pi^2)$ is appropriate as this gives the variance per log interval: $\langle (H\delta t)^2\rangle = \int d\ln k\ \mathcal{P}_{\delta t}(k)$. By studying eq. (3.46), one can show $P_{\delta t} \approx$const for small k and falls off for large k. This creates a spike in $\mathcal{P}_{\delta t}(k)$ at a finite k^* and its amplitude is rather large. (This is to be contrasted with the usual fluctuations in de Sitter space, $P_{\delta t}(k) \propto 1/k^3$, making $\mathcal{P}_{\delta t}(k)$ approximately scale invariant.) We see that the amplitude of the spike scales as $\sim 1/\mathcal{N}$, and so it is reduced for large $\mathcal{N}$. A plot of $\mathcal{P}_{\delta t}(k)$ is given in Figure 3-5.

For the three-point function, we define the bispectrum through

$$\langle \delta t(\mathbf{k}_1)\delta t(\mathbf{k}_2)\delta t(\mathbf{k}_3)\rangle = (2\pi)^3\delta(\mathbf{k}_1+\mathbf{k}_2+\mathbf{k}_3)B_{\delta t}(k_1,k_2,k_3) \tag{3.48}$$

where we have indicated that the bispectrum only depends on the magnitude of the 3 k-vectors, with the constraint that the vectors sum to zero. We use eq. (3.42) and

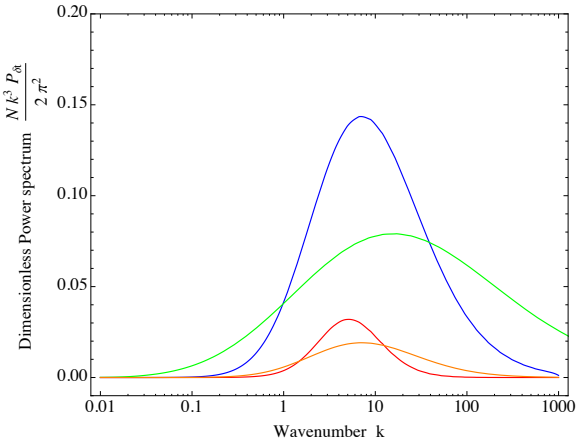

Figure 3-5: The dimensionless power spectrum $\mathcal{N}\mathcal{P}_{\delta t}(k)$ at large $\mathcal{N}$ as a function of k (in units of H) for different choices of masses: blue is $m_0 = 2$ and $m_\psi = 1/2$, red is $m_0 = 4$ and $m_\psi = 1/2$, green is $m_0 = 2$ and $m_\psi = 1/4$, orange is $m_0 = 4$ and $m_\psi = 1/4$.

Fourier transform to k-space, again using the convolution theorem. We find

$$B_{\delta t}(k_1, k_2, k_3) \approx -\frac{1}{3\lambda^3 \mathcal{N}^2} \times \left[\int \frac{d^3k}{(2\pi)^3} P_{\bar{\phi}}(k) P_{\bar{\phi}}(|\mathbf{k}_1 - \mathbf{k}|) P_{\bar{\phi}}(|\mathbf{k}_2 + \mathbf{k}|) + 2\,\text{perms}\right] \tag{3.49}$$

To measure non-Gaussianity in k-space, it is conventional to introduce the dimensionless f_{NL} parameter, defined as[1]

$$f_{NL}(k_1, k_2, k_3) \equiv \frac{B_{\delta t}(k_1, k_2, k_3)}{P_{\delta t}(k_1) P_{\delta t}(k_2) + 2\,\text{perms}}. \tag{3.50}$$

By substituting the above expressions for $P_{\delta t}$ and $B_{\delta t}$, we see that f_{NL} is independent of $\mathcal{N}$ at this leading order. However, this belies the true dependence of non-Gaussianity on the number of fields. This is because f_{NL} is a quantity that can be large even if the non-Gaussianity is relatively small (for example, on CMB scales, any f_{NL} smaller than $\mathcal{O}(10^5)$ is a small level of non-Gaussianity). Instead a more appropriate measure of non-Gaussianity in k-space is to compute some ratio of the bispectrum to the 3/2 power of the power spectrum, analogous to the position space

[1] A factor of 6/5 is often included when studying the gauge invariant quantity ζ that appears in cosmological perturbation theory, but it does not concern us here.

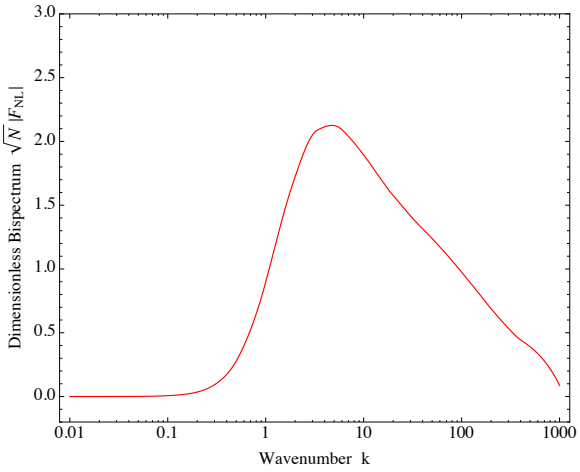

Figure 3-6: The dimensionless bispectrum $\sqrt{\mathcal{N}}\,\mathcal{F}_{NL}$ as a function of k (in units of H) at large $\mathcal{N}$ for $m_0 = 4$ and $m_\psi = 1/2$.

definition in eq. (3.43). For the simple equilateral case, $k_1 = k_2 = k_3$, we define

$$\mathcal{F}_{NL}(k) \equiv \frac{k^{3/2} B_{\delta t}(k)}{3\sqrt{2}\,\pi P_{\delta t}(k)^{3/2}}, \tag{3.51}$$

where we have inserted a factor of $k^{3/2}/(\sqrt{2}\,\pi)$ from measuring the fluctuations per log interval. Using eqs. (3.46, 3.49), we see that $\mathcal{F}_{NL} \propto 1/\sqrt{\mathcal{N}}$, as we found in position space. In Figure 3-6, we plot this function. We note that although the non-Gaussianity is large, the peak is on a length scale that is small compared to the CMB and so it evades recent bounds [6].

3.5 Constraints on Hybrid Models

Hybrid inflation models must satisfy several observational constraints. Here we discuss these constraints, including the role that $\mathcal{N}$ plays, and discuss the implications for the scale of the density spike.

3.5.1 Topological Defects

The first constraint on hybrid models concerns the possible formation of topological defects. Since the waterfall field starts at $\phi = 0$ and then falls to some vacuum, it

spontaneously breaks a symmetry. For a single field $\mathcal{N} = 1$, this breaks a $\mathbb{Z}_2$ symmetry; see Figure 3-1. For multiple fields $\mathcal{N} > 1$, this breaks an $SO(\mathcal{N})$ symmetry. $\mathcal{N} = 1$ leads to the formation of *domain walls*, which are clearly ruled out observationally, so these models are strongly disfavored; $\mathcal{N} = 2$ leads to the formation of *cosmic strings*, which have not been observed and if they exist are constrained to be small in number. This would require a very large number of e-foldings of the waterfall phase to make compatible with observations, and seems unrealistic; $\mathcal{N} = 3$ leads to the formation of *monopoles*, which are somewhat less constrained; $\mathcal{N} = 4$ leads to the formation of *textures*, which are relatively harmless; $\mathcal{N} > 4$ avoids topological defects altogether. So choosing several waterfall fields is preferred by current constraints on topological defects.

3.5.2 Inflationary Perturbations

Inflation generates fluctuations on large scales which are being increasingly constrained by data. An important constraint on any inflation model is the bound on the tensor-to-scalar ratio r. Recent CMB measurements from Planck places an upper bound on tensor modes of $r < 0.11$ (95% confidence) [6]. The amplitude of tensor modes is directly set by the energy density during inflation. Typical hybrid models are at relatively low energy scales, without the need for extreme fine tuning, and so they immediately satisfy this bound.

Although hybrid inflation passes the tensor mode constraint with flying colors, its ability to pass the scalar mode constraint is much less clear. The tilt of the scalar mode spectrum is characterized by the primordial spectral index n_s. WMAP [5] and recent Planck measurements [6] place the spectral index near

$$n_{s,obs} \approx 0.96, \tag{3.52}$$

giving a red spectrum. Here we examine the constraints imposed on hybrid models in order to obtain this value of n_s.

The tilt on large scales is determined by the timer field ψ. For low scale models

of inflation, such as hybrid inflation, the prediction for the spectral index is

$$n_s = 1 + 2\,\eta, \tag{3.53}$$

where

$$\eta \approx \frac{1}{8\pi G}\frac{V''_\psi}{V_0} = \frac{V''_\psi}{3\,H^2}. \tag{3.54}$$

This is to be evaluated N_e e-foldings from the end of inflation, where $N_e = 50 - 60$ in typical models. Combining the above equations, we need to satisfy $V''_\psi \approx -0.06\,H^2$. If we take $V_\psi = m_\psi^2\psi^2/2$, then $V''_\psi > 0$, and $n_s > 1$, which is ruled out. So we need higher order terms in the potential to cause it to become concave down at large values of ψ where η is evaluated, while leaving the quadratic approximation for V_ψ valid at small ψ. For most reasonable potential functions, such as potentials that flatten at large field values, we expect $|V''_\psi| \lesssim m_\psi^2$. So this suggests a bound

$$m_\psi^2 \gtrsim 0.06\,H^2, \tag{3.55}$$

which can only be avoided by significant fine tuning of the potential. Hence although the timer field is assumed light ($m_\psi < H$), it cannot be extremely light.

3.5.3 Implications for Scale of Spike

The length scale associated with the spike in the spectrum is set by the Hubble length during inflation H^{-1}, red-shifted by the number of e-foldings of the waterfall phase N_w. Since the Hubble scale during inflation is typically microscopic, we need the duration of the waterfall phase N_w to be significant (e.g., $N_w \sim 30 - 40$) to obtain a spike on astrophysically large scales. Here we examine if this is possible.

Since we have defined $t = 0$ to be when the transition occurs ($\psi = \psi_c$), then $N_w = Ht$ with final value at $t = t_{end}$. To determine the final value, we note that modes grow at the rate λ, derived earlier in eq. (3.21). For $m_\psi < H$, we can approximate the parameter p (eq. (3.18)) as $p \approx m_\psi^2/3H$. Using the above spectral index bound in eq. (3.55), we see that for significantly large N_w (e.g., $N_w \sim 30 - 40$) the exponential

factor

$$\exp(-2\,p\,t) \approx \exp\left(-\frac{2\,m_\psi^2 N_w}{3\,H^2}\right) \tag{3.56}$$

is somewhat small and we will ignore it here. In this regime, the dimensionless growth rate λ/H can be approximated as a constant

$$\frac{\lambda}{H} \approx -\frac{3}{2} + \sqrt{\frac{9}{4} + \frac{m_0^2}{H^2}}. \tag{3.57}$$

The typical starting value for ϕ is roughly of order H (de Sitter fluctuations) and the typical end value for ϕ is roughly of order M_{Pl} (Planck scale). For self consistency, ϕ must pass from its starting value to its end value in N_w e-foldings with rate set by λ/H. This gives the approximate value for N_w as[2]

$$N_w \approx \frac{H}{\lambda} \ln\left(\frac{M_{Pl}}{H}\right). \tag{3.58}$$

This has a clear consequence: If we choose $m_0 \gg H$, as is done in some models of hybrid inflation, then $H/\lambda \ll 1$. So unless we push H to be many, many orders of magnitude smaller then M_{Pl}, then N_w will be rather small. This will lead to a spike in the spectrum on rather small scales and possibly ignorable to astrophysics.

Note that if we had ignored the spectral index bound that leads to eq. (3.55), then we could have taken m_ψ arbitrarily small, leading to an arbitrarily small p value. In this (unrealistic) limit, it is simple to show

$$\frac{\lambda}{H} \approx \frac{2\,m_\psi^2\,m_0^2\,N_w}{9\,H^4}. \tag{3.59}$$

So by taking m_ψ arbitrarily small, λ could be made small, and N_w could easily be made large. However, the existence of the spectral index bound essentially forbids this, requiring us to go in a different direction.

The only way to increase N_w and satisfy the spectral index bound on m_ψ is to

[2]A better approximation comes from tracking the full time dependence of λ and integrating the argument of the exponential $\exp(\int^t dt'\lambda(t'))$, but this approximation suffices for the present discussion.

take m_0 somewhat close to H. This allows H/λ to be appreciable from eq. (3.57). For instance, if we set $m_0 = 1.3\,H$, then $H/\lambda \approx 2$. If we then take H just a few orders of magnitude below M_{Pl}, say $H \sim 10^{-6,7} M_{Pl}$, which is reasonable for inflation models, we can achieve a significant value for N_w. This will lead to a spike in the spectrum on astrophysically large scales, which is potentially quite interesting. It is possible that there will be distortions in the spectrum by taking m_0 close to H, but we will not explore those details here. However, there is an important consequence that we explore in the next subsection.

3.5.4 Eternal Inflation

Since we are being pushed towards a somewhat low value of m_0, near H, we need to check if the theory still makes sense. One potential problem is that the theory may enter a regime of eternal inflation. This could occur for the waterfall field at the hill-top. This would wipe out information of the timer field, which established the approximately scale invariant spectrum on cosmological scales.

The boundary for eternal inflation is roughly when the density fluctuations are $\mathcal{O}(1)$, and this occurs when the fluctuations in the time delay are $\langle (H\,\delta t)^2 \rangle = \mathcal{O}(1)$. To convert this into a lower bound on m_0, let us imagine that m_0 is even smaller than H. In this regime, the growth rate λ can be estimated using eq. (3.57) as $\lambda \sim m_0^2/H^2$. Using eq. (3.33) this gives $\langle (H\,\delta t)^2 \rangle \sim H^4/(\mathcal{N} m_0^4)$. This implies that eternal inflation occurs when the waterfall mass is below a critical value m_0^c, which is roughly

$$m_0^c \sim \frac{H}{\mathcal{N}^{1/4}}. \tag{3.60}$$

So when $\mathcal{N} \sim 1$ we cannot have m_0 near H, because we then enter eternal inflation. On the other hand, for large $\mathcal{N}$ we are allowed to have m_0 near H and avoid this problem. This makes sense intuitively, because for many fields it is statistically favorable for at least one of the fields to fall off the hill-top, causing inflation to end. Hence large $\mathcal{N}$ is more easily compatible with the above set of constraints than low $\mathcal{N}$.

3.6 Discussion and Conclusions

In this work we studied density perturbations in hybrid inflation caused by $\mathcal{N}$ waterfall fields, which contains a spike in the spectrum. We derived expressions for correlation functions of the time-delay and constrained parameters with observations.

Density Perturbations: We derived a convergent series expansion in powers of $1/\mathcal{N}$ and $\Delta(x)$, the dimensionless correlation function for the field, for the two-point function of the time-delay for any $\mathcal{N}$, and the leading order behavior of the three-point function of the time-delay for large $\mathcal{N}$. These correlation functions are well approximated by the first term in the series for large $\mathcal{N}$ (even for $\mathcal{N} = 2$ the leading term is moderately accurate to $\sim 30\%$, and much more accurate for higher $\mathcal{N}$). In this regime, the fluctuations are suppressed, with two-point and three-point functions given by

$$\begin{aligned} \langle \delta t(\mathbf{x})\, \delta t(\mathbf{0}) \rangle &\approx \frac{\Delta^2(x)}{2\lambda^2 \mathcal{N}}, \\ \langle \delta t(\mathbf{x})\, \delta t(\mathbf{y})\, \delta t(\mathbf{0}) \rangle &\approx -\frac{\Delta(|\mathbf{x}-\mathbf{y}|)\Delta(x)\Delta(y)}{\lambda^3 \mathcal{N}^2}. \end{aligned} \tag{3.61}$$

Although this reduces the spike in the spectrum, for any moderate value of $\mathcal{N}$, such as $\mathcal{N} = 3, 4, 5$, the amplitude of the spike is still quite large (orders of magnitude larger than the $\sim 10^{-5}$ level fluctuations on larger scales relevant to the CMB), and may have significant astrophysical consequences. Also, the relative size of the three-point function to the 3/2 power of the two-point function scales as $\sim 1/\sqrt{\mathcal{N}}$. In accordance with the central limit theorem, the fluctuations become more Gaussian at large $\mathcal{N}$. This will make the analysis of the subsequent cosmological evolution more manageable, as this provides a simple spectrum for initial conditions. We note that since we are considering small scales compared to the CMB, then this non-Gaussianity evades Planck bounds [6].

Constraints: We mentioned that hybrid models avoid topological defects for large $\mathcal{N}$ and satisfy constraints on tensor modes for any $\mathcal{N}$. A very serious constraint on hybrid models comes from the observed spectral index $n_s \approx 0.96$, which requires the

potential to flatten at large field values. One consequence of this is that the timer field mass m_ψ needs to be only a little smaller than the Hubble parameter during inflation H, or else the model is significantly fine tuned. For a large value of the waterfall field mass m_0, this would imply a large growth rate of fluctuations, a rapid termination of inflation, and in turn a density spike on very small scales. Otherwise, we need to make the waterfall field mass m_0 somewhat close to H, but this faces problems with eternal inflation. However, by using a large number of waterfall fields $\mathcal{N}$, it is safer to make the waterfall field mass m_0 somewhat close to H. This reduces the growth rate of fluctuations, prolonging the waterfall phase for many e-foldings.

> Thus large $\mathcal{N}$ presents a plausible setup to establish a spike in the density perturbations on astrophysically large length scales that is consistent with other constraints.

Outlook: It may be possible that these perturbations seed primordial black holes, which may be relevant to supermassive black holes, or an intriguing form of dark matter. An investigation into these topics is underway. It would be important to fully explore the eternal inflation bound and the effects on the spectrum for relatively light waterfall field masses. Finally, it would be of interest to try to embed these large $\mathcal{N}$ models into fundamental physics, such as string theory, and to explore reheating [36] and baryogenesis [37, 38] in this framework.

3.7 Acknowledgements

We would like to thank Victor Buza and Alexis Giguere for very helpful discussions. This work is supported by the U.S. Department of Energy under cooperative research agreement Contract Number DE-FG02-05ER41360 and in part by MIT's Undergraduate Research Opportunities Program.

3.8 Appendix

3.8.1 Series Expansion to Higher Orders

Earlier we computed the two-point correlation function for the time-delay at quadratic order, and then stating the results at all orders. Here we mention the results order by order.

a. Cubic Order

At cubic order $\sim \Phi^3$ we find

$$(2\lambda)^2\langle\delta t(\mathbf{x})\delta t(\mathbf{0})\rangle_3 \;=\; -\frac{8\Delta^2}{\mathcal{N}^2} \tag{3.62}$$

b. Quartic Order

At quartic order $\sim \Phi^4$ we find

$$(2\lambda)^2\langle\delta t(\mathbf{x})\delta t(\mathbf{0})\rangle_4 \;=\; \frac{8\Delta^2+2\Delta^4}{\mathcal{N}^2}+\frac{40\Delta^2+4\Delta^4}{\mathcal{N}^3} \tag{3.63}$$

c. Quintic Order

At quintic order $\sim \Phi^5$ we find

$$\begin{aligned}(2\lambda)^2\langle\delta t(\mathbf{x})\delta t(\mathbf{0})\rangle_5 \;=\; & -\frac{96\Delta^2+32\Delta^4}{\mathcal{N}^3} \\ & -\frac{256\Delta^2+64\Delta^4}{\mathcal{N}^4}\end{aligned} \tag{3.64}$$

d. Sextic Order

At sextic order $\sim \Phi^6$ we find

$$\begin{aligned}(2\lambda)^2\langle\delta t(\mathbf{x})\delta\tau(\mathbf{0})\rangle_6 &= \frac{168\Delta^2+72\Delta^4+16\Delta^6}{3\mathcal{N}^3} \\ &+\frac{1056\Delta^2+464\Delta^4+32\Delta^6}{\mathcal{N}^4} \\ &+\frac{6144\Delta^2+2496\Delta^4+128\Delta^6}{3\mathcal{N}^5}\end{aligned} \tag{3.65}$$

e. Septic Order

At septic order $\sim \Phi^7$ we find

$$\begin{aligned}(2\lambda)^2\langle\delta t(\mathbf{x})\delta t(\mathbf{0})\rangle_7 &= -\frac{32(43\Delta^2+22\Delta^4+6\Delta^6)}{\mathcal{N}^4} \\ &+\mathcal{O}\left(\frac{1}{\mathcal{N}^5}\right)\end{aligned} \tag{3.66}$$

f. Octic Order

At octic order $\sim \Phi^8$ we find

$$\begin{aligned}(2\lambda)^2\langle\delta t(\mathbf{x})\delta t(\mathbf{0})\rangle_8 &= \frac{8(72\Delta^2+39\Delta^4+16\Delta^6+3\Delta^8)}{\mathcal{N}^4} \\ &+\mathcal{O}\left(\frac{1}{\mathcal{N}^5}\right)\end{aligned} \tag{3.67}$$

3.8.2 Two-Point Function for Even Number of Fields

When $\mathcal{N}$ is even the expression always involves the polylog function that we found for $\mathcal{N}=2$, plus corrections that depend on $\mathcal{N}$. We find that the form of the answer is

$$\begin{aligned}(2\lambda)^2\langle\delta t(\mathbf{x})\delta t(\mathbf{0})\rangle &= \mathrm{Li}_2(\Delta^2)+\frac{P_{\mathcal{N}}(\Delta^2)}{\Delta^{\mathcal{N}-4}} \\ &+\frac{\bar{P}_{\mathcal{N}}(\Delta^2)\ln(1-\Delta^2)}{\Delta^{\mathcal{N}-2}},\end{aligned} \tag{3.68}$$

where

$$P_{\mathcal{N}}(\Delta^2) \text{ is a polynomial of degree } (\mathcal{N}-4)/2, \tag{3.69}$$

$$\bar{P}_{\mathcal{N}}(\Delta^2) \text{ is a polynomial of degree } (\mathcal{N}-2)/2. \tag{3.70}$$

For $\mathcal{N}=4$, we find

$$P_4(\Delta^2) = -1, \tag{3.71}$$

$$\bar{P}_4(\Delta^2) = -1+\Delta^2. \tag{3.72}$$

For $\mathcal{N}=6$, we find

$$P_6(\Delta^2) = \frac{1}{2}-\frac{7}{4}\Delta^2, \tag{3.73}$$

$$\bar{P}_6(\Delta^2) = \frac{1}{2}-2\Delta^2+\frac{3}{2}\Delta^4. \tag{3.74}$$

For $\mathcal{N}=8$, we find

$$P_8(\Delta^2) = -\frac{1}{3}+\frac{4}{3}\Delta^2-\frac{85}{36}\Delta^4, \tag{3.75}$$

$$\bar{P}_8(\Delta^2) = -\frac{1}{3}+\frac{3}{2}\Delta^2-3\Delta^4+\frac{11}{6}\Delta^6. \tag{3.76}$$

3.8.3 Alternative Derivation of Time-Delay Spectra

Here we write the two-point function as a multidimensional integral. It is convenient now to switch to a vector notation thus making the components of ϕ explicit.

$$\tilde{\phi}(\mathbf{0},t) \equiv \vec{\phi}_x \equiv (X_1, X_2, X_3, \ldots, X_{\mathcal{N}}), \tag{3.77}$$

$$\tilde{\phi}(\mathbf{x},t) \equiv \vec{\phi}_0 \equiv (X_{\mathcal{N}+1}, X_{\mathcal{N}+2}, X_{\mathcal{N}+3}, \ldots, X_{2\mathcal{N}}), \tag{3.78}$$

$$\vec{X} \equiv (X_1, X_2, X_3, \ldots, X_{2\mathcal{N}}). \tag{3.79}$$

The average value of a function F of a random variable $\vec{X}$ with probability distribution function $p(X)$ is given by

$$\langle F[X]\rangle = \int dX p(X) F[X]. \tag{3.80}$$

Since we are using a free field approximation, $\vec{X}$ follows a joint Gaussian distribution

$$p(X) = \frac{1}{(2\pi)^{\mathcal{N}}\sqrt{\det(\Sigma)}} \exp\left(-\frac{1}{2}X^T\Sigma^{-1}X\right), \tag{3.81}$$

where

$$\Sigma_{ij} = \langle X_i X_j\rangle, \tag{3.82}$$

is the correlation matrix. The components of Σ can be easily calculated using the commutation relations for the creation and annihilation operators in $\phi(\mathbf{x},t)$, from Eq. (3.11). Due to the high degree of symmetry the matrix itself has a very simple structure:

$$\Sigma_{ij} = \frac{1}{\mathcal{N}}(\delta_{i,j} + \delta_{i,(j\pm\mathcal{N})}\Delta). \tag{3.83}$$

Finally, we can write the two-point function as:

$$\begin{aligned}
&(2\lambda)^2\langle\delta t(\mathbf{x})\delta t(\mathbf{0})\rangle \\
&= \int \frac{\mathcal{N}^2 d\vec{X}}{(2\pi)^{\mathcal{N}}(1-\Delta^2)^{\frac{\mathcal{N}}{2}}} \log(|\vec{\phi}_0|^2)\log(|\vec{\phi}_x|^2)\times \\
&\quad \exp\{-\frac{\mathcal{N}}{2(1-\Delta^2)}[|\vec{\phi}_0|^2 + |\vec{\phi}_x|^2 - 2\mathcal{N}\Delta\vec{\phi}_0\cdot\vec{\phi}_x]\}.
\end{aligned} \tag{3.84}$$

Then we can Taylor expand the integrand in powers of Δ. We see that all odd powers of Δ vanish, leaving only even powers in the expansion. Performing these integrals term by term in the Taylor expansion, leads to the results reported earlier in eqs. (3.35, 3.36, 3.37).

Bibliography

[1] A. H. Guth, "The inflationary universe: a possible solution to the horizon and flatness problems," Phys. Rev. D **23**, 347 (1981).

[2] A. D. Linde, "A new inflationary universe scenario: a possible solution of the horizon, flatness, homogeneity, isotropy and primordial monopole problems," Phys. Lett. B **108**, 389 (1982).

[3] A. Albrecht and P. J. Steinhardt, "Cosmology for grand unified theories with radiatively induced symmetry breaking," Phys. Rev. Lett. **48**, 1220 (1982).

[4] A. H. Guth and D. I. Kaiser, "Inflationary cosmology: Exploring the universe from the smallest to the largest scales," Science **307**, 884 (2005) [arXiv:astro-ph/0502328].

[5] G. Hinshaw *et al.* [WMAP Collaboration], "Nine-Year Wilkinson Microwave Anisotropy Probe (WMAP) Observations: Cosmological Parameter Results," arXiv:1212.5226 [astro-ph.CO].

[6] P. A. R. Ade *et al.* [Planck Collaboration], "Planck 2013 results. XXII. Constraints on inflation," arXiv:1303.5082 [astro-ph.CO].

[7] A. D. Linde, "Particle Physics and Inflationary Cosmology," arXiv:hep-th/0503203.

[8] A. R. Liddle and D. H. Lyth, *Cosmological Inflation and Large-Scale Structure*, Cambridge University Press (2000).

[9] P. Binetruy and G. R. Dvali, "D-term inflation," Phys. Lett. B **388** (1996) 241 [arXiv:hep-ph/9606342].

[10] L. McAllister and E. Silverstein, "String Cosmology: A Review," Gen. Rel. Grav. **40** (2008) 565 [arXiv:0710.2951 [hep-th]].

[11] N. Arkani-Hamed, P. Creminelli, S. Mukohyama and M. Zaldarriaga, "Ghost Inflation," JCAP **0404** (2004) 001 [arXiv:hep-th/0312100].

[12] S. Kachru, R. Kallosh, A. Linde, J. M. Maldacena, L. P. McAllister and S. P. Trivedi, "Towards inflation in string theory," JCAP **0310** (2003) 013 [arXiv:hep-th/0308055].

[13] F. L. Bezrukov and M. E. Shaposhnikov, "The Standard Model Higgs boson as the inflaton," Phys. Lett. B **659**, 703 (2008) [arXiv:hep-th/0710.3755].

[14] M. P. Hertzberg, "Can Inflation be Connected to Low Energy Particle Physics?," JCAP **1208**, 008 (2012) [arXiv:1110.5650 [hep-ph]].

[15] A. Linde, "Hybrid Inflation," Phys. Rev. D **49**, 748-754 (1994) [arXiv:astro-ph/9307002].

[16] L. Randall, M. Soljacic, and A.H. Guth,"Supernatural Inflation," arXiv:hep-ph/9601296v1.

[17] L. Randall, M. Soljacic, and A.H. Guth,"Supernatural Inflation: Inflation from Supersymmetry with No (Very) Small Parameters," Nucl. Phys. B **472**, 377-408 (1996) [arXiv:hep-ph/9512439v3].

[18] J. G. Bellido, A. Linde, and D. Wands, "Density Perturbations and Black Hole Formation in Hybrid Inflation," Phys. Rev. D **54**, 6040-6058 (1996). [arXiv:astro-ph/9605094].

[19] B.J. Carr, "Primordial Black Holes as a Probe of Cosmology and High Energy Physics," Lect. Notes Phys. **631**, 301 (2003) [arXiv: astro-ph/0310838].

[20] B.J. Carr, "Primordial Black Holes–Recent Developments," 22nd Texas Symposium at Stanford, 12-17 December 2004, eConf C **041213**, 0204 (2004) [arXiv:astro-ph/0504034].

[21] B.J. Carr, "Primordial Black Holes: Do They Exist and Are They Useful?" to appear in Proceedings of "Inflating Horizon of Particle Astrophysics and Cosmology," Universal Academy Press Inc and Yamada Science Foundation (2005) [arXiv:astro-ph/0511743].

[22] B.J. Carr, "Primordial black hole formation and hybrid inflation," arXiv:1107.1681 [astro-ph.CO].

[23] K.M. Burgess, "Early Stages in Structure Formation," Ph.D. Thesis, Massachusetts Institute of Technology, 2004.

[24] N.T. Son, "Density Perturbations in Hybrid Inflation," Master's Thesis, Massachusetts Institute of Technology, 2009.

[25] D. Lyth, "Issues concerning the waterfall of hybrid inflation," Prog. Theor. Phys. Suppl. **190**, 107-119 (2011) [arXiv:1005.2461].

[26] D. Lyth, "The hybrid inflation waterfall and the primordial curvature perturbation," [arXiv:astro-ph/1201.4312].

[27] D. Lyth, "Contribution of the hybrid inflation waterfall to the primordial curvature perturbation," JCAP **1107**, 035 (2011) [arXiv:1012.4617].

[28] J. Martin, and V. Vennin, "Stochastic Effects in Hybrid Inflation," Phys. Rev. D **85**, 043525 (2012) [arXiv:1110.2070].

[29] A.A. Abolhasani, H. Firouzjahi, and M. Sasaki, "Curvature perturbation and waterfall dynamics in hybrid inflation," JCAP **1110**, 015 (2011) [arXiv:1106.6315].

[30] H. Kodama, K. Kohri, and K. Nakayama, "On the waterfall behavior in hybrid inflation" [arXiv:1102.5612].

[31] J. Fonseca, M. Sasaki, and D. Wands, "Large-scale Perturbations from the Waterfall Field in Hybrid Inflation," Prog. Theor. Phys. **126**, 331-350 (2011) [arXiv:1005.4053].

[32] A. H. Guth and E. I. Sfakianakis, "Density Perturbations in Hybrid Inflation Using a Free Field Theory Time-Delay Approach," arXiv:1210.8128 [astro-ph.CO].

[33] S.W. Hawking, "The development of irregularities in a single bubble inflationary universe," Phys. Lett. B **115**, 295 (1982).

[34] A.H. Guth and S.Y. Pi, "Fluctuations in the new inflationary universe," Phys. Rev. Lett. **49**, 1110 (1982).

[35] A.H. Guth, "Quantum fluctuations in cosmology and how they lead to a multiverse," to be published in the Proceedings of the 25th Solvay Conference in Physics, *The Theory of the Quantum World,* Brussels, October 2011.

[36] L. Kofman, A. D. Linde and A. A. Starobinsky, "Towards the theory of reheating after inflation," Phys. Rev. D **56**, 3258 (1997) [hep-ph/9704452].

[37] M. P. Hertzberg and J. Karouby, "Baryogenesis from the Inflaton Field," arXiv:1309.0007 [hep-ph].

[38] M. P. Hertzberg and J. Karouby, "Generating the Observed Baryon Asymmetry from the Inflaton Field," arXiv:1309.0010 [hep-ph].

Chapter 4

Primordial Bispectrum from Multifield Inflation with Nonminimal Couplings

Realistic models of high-energy physics include multiple scalar fields. Renormalization requires that the fields have nonminimal couplings to the spacetime Ricci curvature scalar, and the couplings can be large at the energy scales of early-universe inflation. The nonminimal couplings induce a nontrivial field-space manifold in the Einstein frame, and they also yield an effective potential in the Einstein frame with nontrivial curvature. The ridges or bumps in the Einstein-frame potential can lead to primordial non-Gaussianities of observable magnitude. We develop a covariant formalism to study perturbations in such models and calculate the primordial bispectrum. As in previous studies of non-Gaussianities in multifield models, our results for the bispectrum depend sensitively on the fields' initial conditions.

4.1 Introduction

Inflationary cosmology remains the leading account of the very early universe, consistent with high-precision measurements of the cosmic microwave background radiation (CMB) [1, 2, 3]. A longstanding challenge, however, has been to realize success-

ful early-universe inflation within a well-motivated model from high-energy particle physics.

Realistic models of high-energy physics routinely include multiple scalar fields [4, 5]. Unlike single-field models, multifield models generically produce entropy (or isocurvature) perturbations. The entropy perturbations, in turn, can cause the gauge-invariant curvature perturbation, ζ, to evolve even on the longest length-scales, after modes have been stretched beyond the Hubble radius during inflation [6, 7, 8, 9, 10, 11, 12, 13]. Understanding the coupling and evolution of entropy perturbations in multifield models is therefore critical for studying features in the predicted power spectrum, such as non-Gaussianities, that are absent in simple single-field models. (For reviews see [14, 12, 13, 15, 16, 17].)

Recent reviews of primordial non-Gaussianities have emphasized four criteria, at least one of which must be satisfied as a necessary (but not sufficient) condition for observable power spectra to deviate from predictions of single-field models. These criteria include [17, 15]: (1) multiple fields; (2) noncanonical kinetic terms; (3) violation of slow-roll; or (4) an initial quantum state for fluctuations different than the usual Bunch-Davies vacuum. As we demonstrate here, the first three of these criteria are *generically* satisfied by models that include multiple scalar fields with nonminimal couplings to the spacetime Ricci curvature scalar.

Nonminimal couplings arise in the action as necessary renormalization counterterms for scalar fields in curved spacetime [18, 19, 22, 23, 20, 21]. In many models the nonminimal coupling strength, ξ, grows without bound under renormalization-group flow [21]. In such models, if the nonminimal couplings are $\xi \sim \mathcal{O}(1)$ at low energies, they will rise to $\xi \gg 1$ at the energy scales of early-universe inflation. We therefore expect realistic models of inflation to incorporate multiple scalar fields, each with a large nonminimal coupling. (Non-Gaussianities in single-field models with nonminimal couplings have been studied in [24].)

Upon performing a conformal transformation to the Einstein frame — in which the gravitational portion of the action assumes canonical Einstein-Hilbert form — the nonminimal couplings induce a field-space manifold that is not conformal to

flat [25]. The curvature of the field-space manifold, in turn, can induce additional interactions among the matter fields, beyond those included in the Jordan-frame potential. Moreover, the scalar fields necessarily acquire noncanonical kinetic terms in the Einstein frame. These new features can have a dramatic impact on the behavior of the fields during inflation, and hence on the primordial power spectrum.

Chief among the multifield effects for producing new features in the primordial power spectrum is the ability of fields' trajectories to turn in field-space as the system evolves. Such turns are not possible in single-field models, which include only a single direction of field-space. In the case of multiple fields, special features in the effective potential, such as ridges or bumps, can focus the background fields' trajectories through field space or make them diverge. When neighboring trajectories diverge, primordial bispectra can be amplified to sufficient magnitude that they should be detectable in the CMB [26, 14, 30, 16, 15, 13, 32, 31, 27, 28, 29].

To date, features like ridges in the effective potential have been studied for the most part phenomenologically rather than being strongly motivated by fundamental physics. Here we demonstrate that ridges arise naturally in the Einstein-frame effective potential for models that incorporate multiple fields with nonminimal couplings. Likewise, as noted above, models with multiple nonminimally coupled scalar fields necessarily include noncanonical kinetic terms in the Einstein frame, stemming from the curvature of the field-space manifold. Both the bumpy features in the potential and the nonzero curvature of the field-space manifold routinely cause the fields' evolution to depart from slow-roll for some duration of their evolution during inflation.

Recent analyses of primordial non-Gaussianities have emphasized two distinct types of fine-tuning needed to produce observable bispectra: fine-tuning the shape of the effective potential to include features like ridges; and separately fine-tuning the fields' initial conditions so that the fields begin at or near the top of these ridges [30, 29, 32, 31]. Here we show that the first of these types of fine-tuning is obviated for multifield models with nonminimal couplings; such features of the potential are generic. The second type of fine-tuning, however, is still required: even in the presence of ridges and bumps, the fields' initial conditions must be fine-tuned in order to

produce measurable non-Gaussianities.

In Section II we examine the evolution of the fields in the Einstein frame and emphasize the ubiquity of features such as ridges that could make the fields' trajectories diverge in field space. Section III introduces our covariant, multifield formalism for studying the evolution of background fields and linearized perturbations on the curved field-space manifold. In Section IV we analyze adiabatic and entropy perturbations and quantify their coupling using a covariant version of the familiar transfer-function formalism [11, 13, 35]. In Section V we build on recent work [36, 37, 38] to calculate the primordial bispectrum for multifield models, applying it here to models with nonminimal couplings. We find that although the nonminimal couplings induce new interactions among the entropy perturbations compared to models in which all fields have minimal coupling, the dominant contribution to the bispectrum remains the familiar local form of f_{NL}, made suitably covariant to apply to the curved field-space manifold. Concluding remarks follow in Section VI. We collect quantities relating to the curvature of the field-space manifold in the Appendix.

4.2 Evolution in the Einstein Frame

We consider $\mathcal{N}$ scalar fields in $(3+1)$ spacetime dimensions, with spacetime metric signature $(-,+,+,+)$. We work in terms of the reduced Planck mass, $M_{\rm pl} \equiv (8\pi G)^{-1/2} = 2.43 \times 10^{18}$ GeV. Greek letters label spacetime indices, $\mu, \nu = 0, 1, 2, 3$; lower-case Latin letters label spatial indices, $i, j = 1, 2, 3$; and upper-case Latin letters label field-space indices, $I, J = 1, 2, ..., \mathcal{N}$.

In the Jordan frame, the scalar fields' nonminimal couplings to the spacetime Ricci curvature scalar remain explicit in the action. We denote quantities in the Jordan frame with a tilde, such as the spacetime metric, $\tilde{g}_{\mu\nu}(x)$. The action for $\mathcal{N}$ scalar fields in the Jordan frame may be written

$$S_{\rm Jordan} = \int d^4x \sqrt{-\tilde{g}} \left[f(\phi^I)\tilde{R} - \frac{1}{2}\tilde{\mathcal{G}}_{IJ}\tilde{g}^{\mu\nu}\partial_\mu\phi^I\partial_\nu\phi^J - \tilde{V}(\phi^I) \right], \tag{4.1}$$

where $f(\phi^I)$ is the nonminimal coupling function and $\tilde{V}(\phi^I)$ is the potential for the scalar fields in the Jordan frame. We have included the possibility that the scalar fields in the Jordan frame have noncanonical kinetic terms, parameterized by coefficients $\tilde{\mathcal{G}}_{IJ}(\phi^K)$. Canonical kinetic terms correspond to $\tilde{\mathcal{G}}_{IJ} = \delta_{IJ}$.

We next perform a conformal transformation to work in the Einstein frame, in which the gravitational portion of the action assumes Einstein-Hilbert form. We define a rescaled spacetime metric tensor, $g_{\mu\nu}(x)$, via the relation,

$$g_{\mu\nu}(x) = \Omega^2(x)\, \tilde{g}_{\mu\nu}(x), \tag{4.2}$$

where the conformal factor is related to the nonminimal coupling function as

$$\Omega^2(x) = \frac{2}{M_{\rm pl}^2} f(\phi^I(x)). \tag{4.3}$$

Eq. (4.1) then takes the form [25]

$$S_{\rm Einstein} = \int d^4x\sqrt{-g}\left[\frac{M_{\rm pl}^2}{2}R - \frac{1}{2}\mathcal{G}_{IJ}g^{\mu\nu}\partial_\mu\phi^I\partial_\nu\phi^J - V(\phi^I)\right]. \tag{4.4}$$

The potential in the Einstein frame is scaled by the conformal factor,

$$V(\phi^I) = \frac{1}{\Omega^4(x)}\tilde{V}(\phi^I) = \frac{M_{\rm pl}^4}{4f^2(\phi^I)}\tilde{V}(\phi^I). \tag{4.5}$$

The coefficients of the noncanonical kinetic terms in the Einstein frame depend on the nonminimal coupling function, $f(\phi^I)$, and its derivatives, and are given by [39, 25]

$$\mathcal{G}_{IJ}(\phi^K) = \frac{M_{\rm pl}^2}{2f(\phi^I)}\left[\tilde{\mathcal{G}}_{IJ}(\phi^K) + \frac{3}{f(\phi^I)}f_{,I}f_{,J}\right], \tag{4.6}$$

where $f_{,I} = \partial f/\partial\phi^I$.

As demonstrated in [21], the nonminimal couplings induce a field-space manifold in the Einstein frame, associated with the metric $\mathcal{G}_{IJ}(\phi^K)$ in Eq. (4.6), which is not conformal to flat for models in which multiple scalar fields have nonminimal cou-

plings in the Jordan frame. Thus there does not exist any combination of conformal transformation plus field-rescalings that can bring the induced metric into the form $\mathcal{G}_{IJ} = \delta_{IJ}$. In other words, multifield models with nonminimal couplings necessarily include noncanonical kinetic terms in the Einstein frame, even if the fields have canonical kinetic terms in the Jordan frame, $\tilde{\mathcal{G}}_{IJ} = \delta_{IJ}$. When analyzing multifield inflation with nonminimal couplings, we therefore must work either with a noncanonical gravitational sector or with noncanonical kinetic terms. Here we adopt the latter. Because there is no way to avoid noncanonical kinetic terms in the Einstein frame in such models, we do not rescale the fields. For the remainder of the chapter, we restrict attention to models with canonical kinetic terms in the Jordan frame, $\tilde{\mathcal{G}}_{IJ} = \delta_{IJ}$, in which the curvature of the field-space manifold in the Einstein frame depends solely upon $f(\phi^I)$ and its derivatives.

Varying the action of Eq. (4.4) with respect to $g_{\mu\nu}(x)$ yields the Einstein field equations,

$$R_{\mu\nu} - \frac{1}{2} g_{\mu\nu} R = \frac{1}{M_{\rm pl}^2} T_{\mu\nu}, \tag{4.7}$$

where

$$T_{\mu\nu} = \mathcal{G}_{IJ} \partial_\mu \phi^I \partial_\nu \phi^J - g_{\mu\nu} \left[\frac{1}{2} \mathcal{G}_{IJ} g^{\alpha\beta} \partial_\alpha \phi^I \partial_\beta \phi^J + V(\phi^I) \right]. \tag{4.8}$$

Varying Eq. (4.4) with respect to ϕ^I yields the equation of motion,

$$\Box \phi^I + g^{\mu\nu} \Gamma^I{}_{JK} \partial_\mu \phi^J \partial_\nu \phi^K - \mathcal{G}^{IK} V_{,K} = 0, \tag{4.9}$$

where $\Box \phi^I \equiv g^{\mu\nu} \phi^I_{;\mu;\nu}$ and $\Gamma^I{}_{JK}(\phi^L)$ is the Christoffel symbol for the field-space manifold, calculated in terms of $\mathcal{G}_{IJ}$.

We expand each scalar field to first order around its classical background value,

$$\phi^I(x^\mu) = \varphi^I(t) + \delta\phi^I(x^\mu), \tag{4.10}$$

and also expand the scalar degrees of freedom of the spacetime metric to first order, perturbing around a spatially flat Friedmann-Robertson-Walker (FRW) metric [40,

11, 12],

$$\begin{aligned} ds^2 &= g_{\mu\nu}(x)\, dx^\mu dx^\nu \\ &= -\left(1+2A\right) dt^2 + 2a\left(\partial_i B\right) dx^i dt + a^2\left[(1-2\psi)\delta_{ij} + 2\partial_i\partial_j E\right] dx^i dx^j, \end{aligned} \tag{4.11}$$

where $a(t)$ is the scale factor. To background order, the 00 and ij components of Eq. (4.7) may be combined to yield the usual dynamical equations,

$$\begin{aligned} H^2 &= \frac{1}{3M_{\rm pl}^2}\left[\frac{1}{2}\mathcal{G}_{IJ}\dot{\varphi}^I\dot{\varphi}^J + V(\varphi^I)\right], \\ \dot{H} &= -\frac{1}{2M_{\rm pl}^2}\mathcal{G}_{IJ}\dot{\varphi}^I\dot{\varphi}^J, \end{aligned} \tag{4.12}$$

where $H \equiv \dot{a}/a$ is the Hubble parameter, and the field-space metric is evaluated at background order, $\mathcal{G}_{IJ} = \mathcal{G}_{IJ}(\varphi^K)$.

Both the curvature of the field-space manifold and the form of the effective potential in the Einstein frame depend upon the nonminimal coupling function, $f(\phi^I)$. The requirement of renormalizability for scalar matter fields in a (classical) curved background spacetime dictates the form of $f(\phi^I)$ [18, 19, 20, 21]:

$$f(\phi^I) = \frac{1}{2}\left[M_0^2 + \sum_I \xi_I \left(\phi^I\right)^2\right], \tag{4.13}$$

where M_0 is some mass-scale that could be distinct from $M_{\rm pl}$, and the nonminimal couplings ξ_I are dimensionless constants that need not be equal to each other. If any of the fields develop nonzero vacuum expectation values, $\langle\phi^I\rangle = v^I$, then one may expect $M_{\rm pl}^2 = M_0^2 + \sum_I \xi_I (v^I)^2$. Here we will assume either that $v^I = 0$ for each field or that $\sqrt{\xi_I}\, v^I \ll M_{\rm pl}$, so that $M_0 \simeq M_{\rm pl}$.

The nonminimal couplings ξ_I could in principle take any "bare" value. (Conformal couplings correspond to $\xi_I = -1/6$; we only consider positive couplings here, $\xi_I > 0$.) Under renormalization-group flow the constants vary logarithmically with energy scale. The exact form of the β functions depends upon details of the matter sector, but for models whose content is akin to the Standard Model the β functions are

positive and the flow of ξ_I has no fixed point, rising with energy scale without bound [21]. Studies of the flow of ξ in the case of Higgs inflation [41] indicate growth of ξ by $\mathcal{O}(10^1 - 10^2)$ between the electroweak symmetry-break scale, $\Lambda \sim 10^2$ GeV, and typical inflationary scales, $\Lambda \sim 10^{16}$ GeV [42]. Hence we anticipate that realistic models will include nonminimal couplings $\xi_I \gg 1$ during inflation.

Renormalizable potentials in (3+1) spacetime dimensions can include terms up to quartic powers of the fields. A potential in the Jordan frame that assumes a generic renormalizable, polynomial form such as

$$\tilde{V}(\phi^I) = \frac{1}{2}\sum_I m_I^2 \left(\phi^I\right)^2 + \frac{1}{2}\sum_{I<J} g_{IJ} \left(\phi^I\right)^2 \left(\phi^J\right)^2 + \frac{1}{4}\sum_I \lambda_I \left(\phi^I\right)^4 \tag{4.14}$$

will yield an effective potential in the Einstein frame that is stretched by the conformal factor in accord with Eq. (4.5). As the Jth component of ϕ^I becomes arbitrarily large the potential in that direction will become asymptotically flat,

$$V(\phi^I) = \frac{M_{\rm pl}^4}{4}\frac{\tilde{V}(\phi^I)}{f^2(\phi^I)} \to \frac{M_{\rm pl}^4}{4}\frac{\lambda_J}{\xi_J^2} \tag{4.15}$$

(no sum on J), unlike the quartic behavior of the potential in the large-field limit in the Jordan frame. (The flatness of the effective potential for large field values was one inspiration for Higgs inflation [41].) Inflation in such models occurs in a regime of field values such that $\xi_J(\varphi^J)^2 \gg M_{\rm pl}^2$ for at least one component, J. As emphasized in [41], for large nonminimal couplings, $\xi_J \gg 1$, all of inflation therefore may occur for field values that satisfy $|\varphi^J| < M_{\rm pl}$, unlike the situation for ordinary chaotic inflation with polynomial potentials and minimal couplings.

Although the effective potential in the Einstein frame will asymptote to a constant value in any given direction of field space, the constants will not, in general, be equal to each other. Thus at finite values of the fields, the potential will generically develop features, such as ridges or bumps, that are absent from the Jordan-frame potential. Because the asymptotic values of $V(\phi^I)$ in any particular direction are proportional to $1/\xi_J^2$, the steepness of the ridges depends sharply on the ratios of the nonminimal

coupling constants. If some explicit symmetry, such as the $SU(2)$ electroweak gauge symmetry obeyed by the Higgs multiplet in Higgs inflation [41], forces all the couplings to be equal — $\xi_I = \xi$, $m_I^2 = m^2$, and $\lambda_I = g_{IJ} = \lambda$ for all I, J — then the ridges in the Einstein-frame potential disappear and the potential asymptotes to the same constant value in each direction of field space. We study the dynamics of such special cases in [43]. For the remainder of this chapter, we consider models in which the constants are of similar magnitude but not exactly equal to each other.

For definiteness, consider a two-field model with a potential in the Jordan frame of the form

$$\tilde{V}(\phi, \chi) = \frac{1}{2} m_\phi^2 \phi^2 + \frac{1}{2} m_\chi^2 \chi^2 + \frac{1}{2} g \phi^2 \chi^2 + \frac{\lambda_\phi}{4} \phi^4 + \frac{\lambda_\chi}{4} \chi^4 \tag{4.16}$$

and nonminimal coupling function given by

$$f(\phi, \chi) = \frac{1}{2} \left[M_{\rm pl}^2 + \xi_\phi \phi^2 + \xi_\chi \chi^2 \right]. \tag{4.17}$$

In the Einstein frame the potential becomes

$$V(\phi, \chi) = \frac{M_{\rm pl}^4}{4} \frac{\left(2 m_\phi^2 \phi^2 + 2 m_\chi^2 \chi^2 + 2 g \phi^2 \chi^2 + \lambda_\phi \phi^4 + \lambda_\chi \chi^4 \right)}{\left[M_{\rm pl}^2 + \xi_\phi \phi^2 + \xi_\chi \chi^2 \right]^2}. \tag{4.18}$$

See Fig. 4-1.

In addition to the ridges shown in Fig. 4-1, other features of the Einstein-frame potential can arise depending on the Jordan-frame couplings. For example, the tops of the ridges can develop small indentations, such that the top of a ridge along $\chi \sim 0$ becomes a local minimum rather than a local maximum. In that case, field trajectories that begin near the top of a ridge tend to focus rather than diverge, keeping the amplitude of non-Gaussianities very small. For the two-field potential of Eq. (4.18), we find [44]

$$\left(\partial_\chi^2 V \right)_{|\chi=0} = \frac{1}{\left[M_{\rm pl}^2 + \xi_\phi \phi^2 \right]^3} \left[\left(g \xi_\phi - \lambda_\phi \xi_\chi \right) \phi^4 + \left(\xi_\phi m_\chi^2 - 2 \xi_\chi m_\phi^2 + g M_{\rm pl}^2 \right) \phi^2 + m_\chi^2 M_{\rm pl}^2 \right]. \tag{4.19}$$

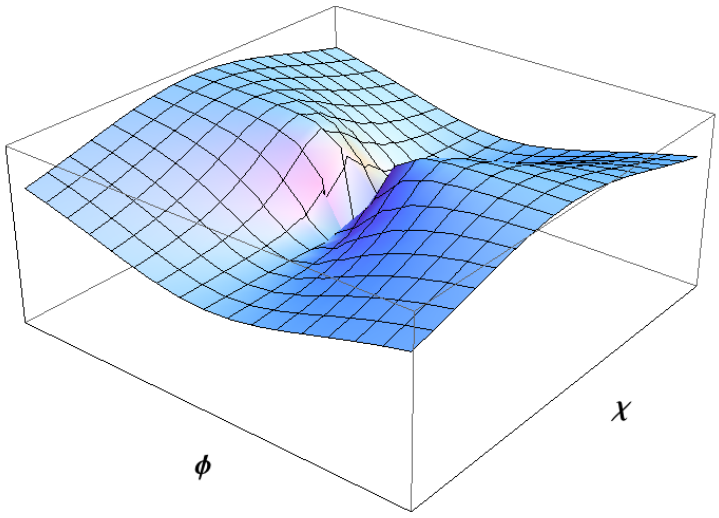

Figure 4-1: The Einstein-frame effective potential, Eq. (4.18), for a two-field model. The potential shown here corresponds to the couplings $\xi_\chi/\xi_\phi = 0.8$, $\lambda_\chi/\lambda_\phi = 0.3$, $g/\lambda_\phi = 0.1$, and $m_\phi^2 = m_\chi^2 = 10^{-2}\,\lambda_\phi M_{\rm pl}^2$.

For realistic values of the masses that satisfy $m_\phi^2, m_\chi^2 \ll M_{\rm pl}^2$, and at early times when $\xi_\phi \phi^2 \gg M_{\rm pl}^2$, the top of the ridge along the $\chi \sim 0$ direction will remain a local maximum if

$$g\xi_\phi < \lambda_\phi \xi_\chi. \tag{4.20}$$

When the couplings satisfy Eq. (4.20), the shape of the potential in the vicinity of its ridges is similar to that of the product potential, $V = m^2 e^{-\lambda\phi^2}\chi^2$, which has been studied in detail in [30, 32]. Trajectories of the fields that begin near each other close to the top of a ridge will diverge as the system evolves; that divergence in trajectories can produce a sizeable amplitude for the bispectrum, as we will see below.

Even potentials with modest ratios of the nonminimal couplings can produce trajectories that diverge sharply, as shown in Fig. 4-2. As we will see in Section V, trajectory 2 of Fig. 4-2 (solid red line) yields a sizeable amplitude for the bispectrum that is consistent with present bounds, whereas trajectories 1 and 3 produce negligible non-Gaussianities. We will return to the three trajectories of Fig. 2 throughout the chapter, as illustrations of the types of field dynamics that yield interesting possibilities for the power spectrum.

Unlike the product potential studied in [30, 32], the potential of Eq. (4.18) con-

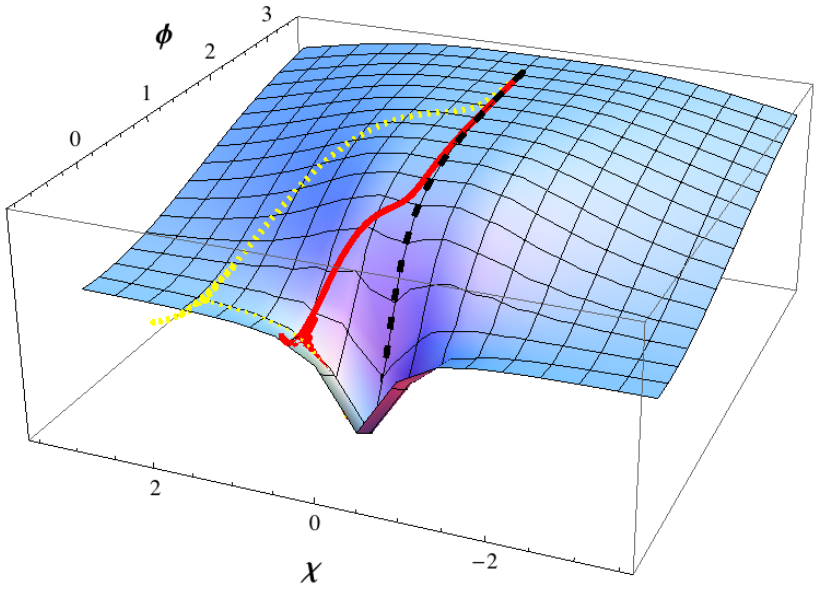

Figure 4-2: Parametric plot of the fields' evolution superimposed on the Einstein-frame potential. Trajectories for the fields ϕ and χ that begin near the top of a ridge will diverge. In this case, the couplings of the potential are $\xi_\phi = 10$, $\xi_\chi = 10.02$, $\lambda_\chi/\lambda_\phi = 0.5$, $g/\lambda_\phi = 1$, and $m_\phi = m_\chi = 0$. (We use a dimensionless time variable, $\tau \equiv \sqrt{\lambda_\phi}\, M_{\rm pl}\, t$, so that the Jordan-frame couplings are measured in units of λ_ϕ.) The trajectories shown here each have the initial condition $\phi(\tau_0) = 3.1$ (in units of $M_{\rm pl}$) and different values of $\chi(\tau_0)$: $\chi(\tau_0) = 1.1 \times 10^{-2}$ ("trajectory 1," yellow dotted line); $\chi(\tau_0) = 1.1 \times 10^{-3}$ ("trajectory 2," red solid line); and $\chi(\tau_0) = 1.1 \times 10^{-4}$ ("trajectory 3," black dashed line).

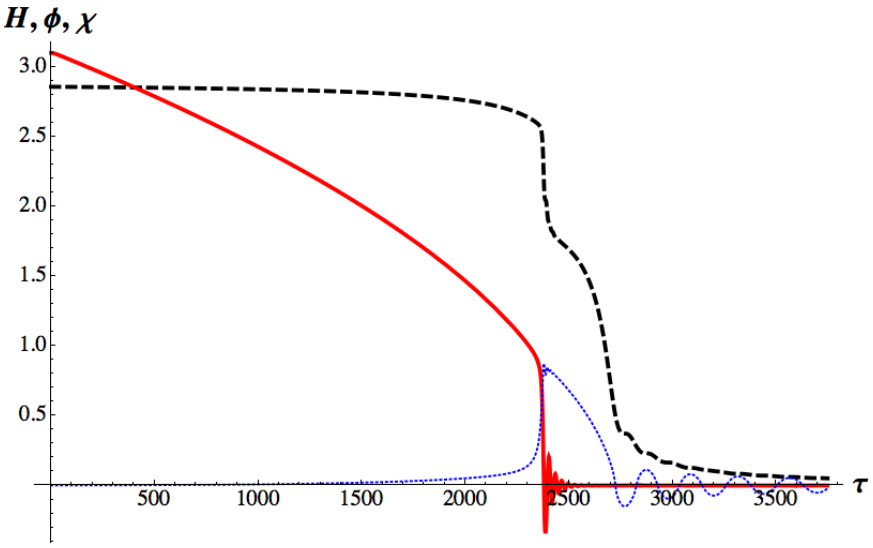

Figure 4-3: The evolution of the Hubble parameter (black dashed line) and the background fields, $\phi(\tau)$ (red solid line) and $\chi(\tau)$ (blue dotted line), for trajectory 2 of Fig. 2. (We use the same units as in Fig. 2, and have plotted $100H$ so its scale is commensurate with the magnitude of the fields.) For these couplings and initial conditions the fields fall off the ridge in the potential at $\tau = 2373$ or $N = 66.6$ efolds, after which the system inflates for another 4.9 efolds until $\tau_{\rm end} = 2676$, yielding $N_{\rm total} = 71.5$ efolds.

tains valleys in which the system will still inflate. For trajectories 1 (orange dotted line) and 2 (red solid line) in Fig. 4-2, for example, the system begins near $\chi \sim 0$ and rolls off the ridge; because $\lambda_\chi/\xi_\chi^2 \neq 0$, the valleys in the χ direction are also false vacua and hence the system continues to inflate as the fields relax toward the global minimum at $\phi = \chi = 0$. Near the end of inflation, when $\xi_\phi\phi^2 + \xi_\chi\chi^2 < M_{\rm pl}^2$, the fields oscillate around the global minimum of the potential, which can drive a period of preheating. See Fig. 4-3.

Evolution of the fields like that shown in Fig. 4-3 is generic for this class of models when the fields begin near the top of a ridge, and can produce interesting phenomenological features in addition to observable bispectra. For example, the oscillations of ϕ around $\phi = 0$ when the system first rolls off the ridge could produce an observable time-dependence of the scale factor during inflation, as analyzed in [45]. The added period of inflation from the false vacuum of the χ valley could lead to scale-dependent features in the power spectrum associated with double-inflation [46].

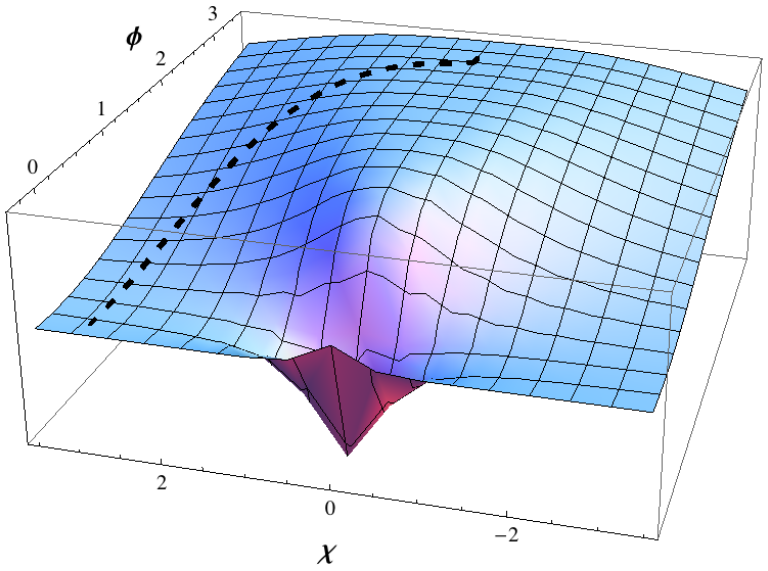

Figure 4-4: Models with nonzero masses include additional features in the Einstein-frame potential which can also cause neighboring field trajectories to diverge. In this case, we superimpose the evolution of the fields ϕ and χ on the Einstein-frame potential. The parameters shown here are identical to those in Fig. 4-2 but with $m_\phi^2 = 0.075\,\lambda_\phi\,M_{\rm pl}^2$ and $m_\chi^2 = 0.0025\,\lambda_\phi\,M_{\rm pl}^2$ rather than 0. The initial conditions match those of trajectory 3 of Fig. 4-2: $\phi(\tau_0) = 3.1$ and $\chi(\tau_0) = 1.1 \times 10^{-4}$ in units of $M_{\rm pl}$.

In the class of models we consider here, neighboring trajectories may also diverge if we include small but nonzero bare masses for the fields. For example, in Fig. 4-4 we show the evolution of the fields for the same initial conditions as trajectory 3 of Fig. 4-2 — the black, dashed curve that barely deviates from the middle of the ridge. The evolution shown in Fig. 4-2 was for the case $m_\phi = m_\chi = 0$. If, instead, we include nonzero masses, then the curvature of the effective potential at small field values becomes different from the zero-mass case. In particular, for positive, real values of the masses, the ridges develop features that push the fields off to one side, recreating behavior akin to what we found in trajectories 1 and 2 of Fig. 4-2.

Because the field-space manifold is curved, the fields' trajectories will turn even in the absence of tree-level couplings from the Jordan-frame potential: the fields' geodesic motion alone is nontrivial. The Ricci scalar for the field-space manifold in the two-field case is given in Eq. (4.115). In Fig. 4-5 we plot the fields' motion in the curved manifold for the case when $\tilde{V}(\phi, \chi) = V(\phi, \chi) = 0$. The curvature of the manifold is negligible at large field values but grows sharply near $\phi \sim \chi \sim 0$.

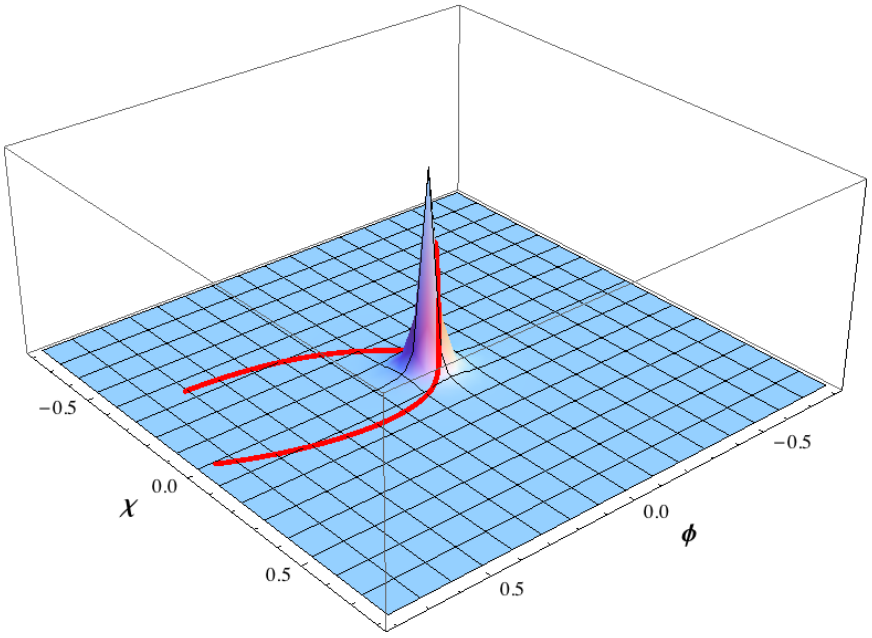

Figure 4-5: Parametric plot of the evolution of the fields ϕ and χ superimposed on the Ricci curvature scalar for the field-space manifold, $\mathcal{R}$, in the absence of a Jordan-frame potential. The fields' geodesic motion is nontrivial because of the nonvanishing curvature. Shown here is the case $\xi_\phi = 10$, $\xi_\chi = 10.02$, $\phi(\tau_0) = 0.75$, $\chi(\tau_0) = 0.01$, $\phi'(\tau_0) = -0.01$, and $\chi'(\tau_0) = 0.005$.

Given the nonvanishing curvature of the field-space manifold, we must study the evolution of the fields and their perturbations with a covariant formalism, to which we now turn.

4.3 Covariant Formalism

A gauge-invariant formalism for studying perturbations in multifield models in the Jordan frame was developed in [47, 48]. In this chapter we work in the Einstein frame, following the approach established in [7, 8, 9, 10, 27, 29, 30, 31, 28, 35, 33, 34, 32, 36, 37, 38]. Our approach is especially indebted to the geometric formulation of [32]. In [32], the authors introduce a particular tetrad construction with which to label the field-space manifold locally, which they dub the "kinematical basis." The adoption of the kinematical basis simplifies certain expressions and highlights features of physical interest in the primordial power spectrum, but it does so at the expense of obscuring the relationship between observable quantities and the fields that appear in the original Lagrangian, in terms of which any given model is specified. Rather than adopt the kinematical basis here, we develop a covariant approach in terms of a single coordinate chart that covers the entire field manifold. This offers greater insight into the global structure of the manifold, as illustrated in Fig. 4-5. We also keep coordinate labels explicit, which facilitates application of our formalism to the original basis of fields, ϕ^I, that appears in the governing Lagrangian. Also unlike [32], we work in terms of cosmic time, t, rather than the number of efolds during inflation, N, because we are interested in applying our formalism (in later work) to eras such as preheating, for which N is a poor dynamical parameter. Because of these formal distinctions from [32], we briefly introduce our general formalism in this section.

We expand each scalar field to first order around its classical background value, as in Eq. (4.10). The background fields, $\varphi^I(t)$, parameterize classical paths through the curved field-space manifold, and hence can be used as coordinate descriptions of the trajectories. Just like spacetime coordinates in general relativity, x^μ, the array φ^I is *not* a vector in the field-space manifold [49]. Infinitesimal displacements, $d\varphi^I$, do

behave as proper vectors, and hence so do derivatives of φ^I with respect to an affine parameter such as t.

For any vector in the field space, A^I, we define a covariant derivative with respect to the field-space metric as usual by

$$\mathcal{D}_J A^I = \partial_J A^I + \Gamma^I{}_{JK} A^K. \tag{4.21}$$

Following [**?**, **?**, 18], we also introduce a covariant derivative with respect to cosmic time via the relation

$$\mathcal{D}_t A^I \equiv \dot{\varphi}^J \mathcal{D}_J A^I = \dot{A}^I + \Gamma^I{}_{JK} A^J \dot{\varphi}^K, \tag{4.22}$$

where overdots denote derivatives with respect to t. The construction of Eq. (4.22) is essentially a directional derivative along the trajectory.

For models with nontrivial field-space manifolds, the tangent space to the manifold at one time will not coincide with the tangent space at some later time. Hence the authors of [36, 37] introduce a covariant means of handling field fluctuations, which we adopt here. As specified in Eq. (4.10), the value of the physical field at a given location in spacetime, $\phi^I(x^\mu)$, consists of the homogenous background value, $\varphi^I(t)$, and some gauge-dependent fluctuation, $\delta\phi^I(x^\mu)$. The fluctuation $\delta\phi^I$ represents a finite coordinate displacement from the classical trajectory, and hence does not transform covariantly. This motivates a construction of a vector $\mathcal{Q}^I$ to represent the field fluctuations in a covariant manner. The two field values, ϕ^I and φ^I, may be connected by a geodesic in the field-space manifold parameterized by some parameter λ, such that $\phi^I(\lambda = 0) = \varphi^I$ and $\phi^I(\lambda = 1) = \varphi^I + \delta\phi^I$. These boundary conditions allow us to identify a unique vector, $\mathcal{Q}^I$, that connects the two field values, such that $\mathcal{D}_\lambda \phi^I|_{\lambda=0} = \mathcal{Q}^I$. One may then expand $\delta\phi^I$ in a power series in $\mathcal{Q}^I$ [36, 37],

$$\delta\phi^I = \mathcal{Q}^I - \frac{1}{2!}\Gamma^I{}_{JK}\mathcal{Q}^J\mathcal{Q}^K + \frac{1}{3!}\left(\Gamma^I{}_{LM}\Gamma^M{}_{JK} - \Gamma^I{}_{JK,L}\right)\mathcal{Q}^J\mathcal{Q}^K\mathcal{Q}^L + ... \tag{4.23}$$

where the Christoffel symbols are evaluated at background order in the fields, $\Gamma^I{}_{JK} =$

$\Gamma^I{}_{JK}(\varphi^L)$. To first order in fluctuations $\delta\phi^I \to \mathcal{Q}^I$, and hence at linear order we may treat the two quantities interchangeably. When we consider higher-order combinations of the field fluctuations below, however, such as the contribution of the three-point function of field fluctuations to the bispectrum, we must work in terms of the vector $\mathcal{Q}^I$ rather than $\delta\phi^I$.

We introduce the gauge-invariant Mukhanov-Sasaki variables for the perturbations [40, 11, 12],

$$Q^I \equiv \mathcal{Q}^I + \frac{\dot{\varphi}^I}{H}\psi. \tag{4.24}$$

Because both $\mathcal{Q}^I$ and $\dot{\varphi}^I$ are vectors in the field-space manifold, Q^I is also a vector. The Mukhanov-Sasaki variables, Q^I, should not be confused with the vector of field fluctuations, $\mathcal{Q}^I$. The Q^I are gauge-invariant with respect to spacetime gauge transformations up to first order in the perturbations, and are constructed from a linear combination of field fluctuations and metric perturbations. The quantity $\mathcal{Q}^I$ does not incorporate metric perturbations; it is constructed from the (gauge-dependent) field fluctuations and background-order quantities such as the field-space Christoffel symbols. At lowest order in perturbations, $\mathcal{Q}^I \to Q^I$ in the spatially flat gauge.

Using Eq. (4.24), Eq. (4.9) separates into background and first-order expressions,

$$\mathcal{D}_t\dot{\varphi}^I + 3H\dot{\varphi}^I + \mathcal{G}^{IK}V_{,K} = 0, \tag{4.25}$$

and

$$\mathcal{D}_t^2 Q^I + 3H\mathcal{D}_t Q^I + \left[\frac{k^2}{a^2}\delta^I{}_J + \mathcal{M}^I{}_J - \frac{1}{M_{\rm pl}^2 a^3}\mathcal{D}_t\left(\frac{a^3}{H}\dot{\varphi}^I\dot{\varphi}_J\right)\right]Q^J = 0. \tag{4.26}$$

The mass-squared matrix appearing in Eq. (4.26) is given by

$$\mathcal{M}^I{}_J \equiv \mathcal{G}^{IK}\left(\mathcal{D}_J\mathcal{D}_K V\right) - \mathcal{R}^I{}_{LMJ}\dot{\varphi}^L\dot{\varphi}^M, \tag{4.27}$$

where $\mathcal{R}^I{}_{LMJ}$ is the Riemann tensor for the field-space manifold. All expressions in Eqs. (4.25), (4.26), and (4.27) involving $\mathcal{G}_{IJ}$, $\Gamma^I{}_{JK}$, $\mathcal{R}^I{}_{LMJ}$, and V are evaluated at

background order in the fields, φ^I.

The system simplifies further if we distinguish between the adiabatic and entropic directions in field space [7]. The length of the velocity vector for the background fields is given by

$$|\dot{\varphi}^I| \equiv \dot{\sigma} = \sqrt{\mathcal{G}_{IJ}\dot{\varphi}^I\dot{\varphi}^J}. \tag{4.28}$$

Introducing the unit vector,

$$\hat{\sigma}^I \equiv \frac{\dot{\varphi}^I}{\dot{\sigma}}, \tag{4.29}$$

the background equations, Eqs. (4.12) and (4.25), simplify to

$$\begin{aligned} H^2 &= \frac{1}{3M_{\rm pl}^2}\left[\frac{1}{2}\dot{\sigma}^2 + V\right], \\ \dot{H} &= -\frac{1}{2M_{\rm pl}^2}\dot{\sigma}^2 \end{aligned} \tag{4.30}$$

and

$$\ddot{\sigma} + 3H\dot{\sigma} + V_{,\sigma} = 0, \tag{4.31}$$

where we have defined

$$V_{,\sigma} \equiv \hat{\sigma}^I V_{,I}. \tag{4.32}$$

The background dynamics of Eqs. (4.30) and (4.31) take the form of a single-field model with canonical kinetic term, with the exception that $V(\varphi^I)$ in Eqs. (4.30) and (4.31) depends on all $\mathcal{N}$ independent fields, φ^I.

The directions in field space orthogonal to $\hat{\sigma}^I$ are spanned by

$$\hat{s}^{IJ} \equiv \mathcal{G}^{IJ} - \hat{\sigma}^I\hat{\sigma}^J. \tag{4.33}$$

The quantities $\hat{\sigma}^I$ and $\hat{s}^{IJ}$ obey the useful relations

$$\begin{aligned} \hat{\sigma}_I \hat{\sigma}^I &= 1, \\ \hat{s}^{IJ} \hat{s}_{IJ} &= \mathcal{N} - 1, \\ \hat{s}^I{}_A \hat{s}^A{}_J &= \hat{s}^I{}_J, \\ \hat{\sigma}_I \hat{s}^{IJ} &= 0 \text{ for all } J. \end{aligned} \tag{4.34}$$

Therefore we may use $\hat{\sigma}^I$ and $\hat{s}^{IJ}$ as projection operators to decompose any vector in field space into components along the direction $\hat{\sigma}^I$ and perpendicular to $\hat{\sigma}^I$ as

$$A^I = \hat{\sigma}^I \hat{\sigma}_J A^J + \hat{s}^I{}_J A^J. \tag{4.35}$$

In particular, $\dot{S}^I \equiv \hat{s}^I{}_J \dot{\varphi}^J$ vanishes identically, $\dot{S}^I = 0$. Thus all of the dynamics of the background fields are captured by the behavior of $\dot{\sigma}$ and $\hat{\sigma}^I$.

Given the simple structure of the background evolution, Eqs. (4.30) and (4.31), we introduce slow-roll parameters akin to the single-field case. We define

$$\epsilon \equiv -\frac{\dot{H}}{H^2} = \frac{3\dot{\sigma}^2}{(\dot{\sigma}^2 + 2V)} \tag{4.36}$$

and

$$\eta_{\sigma\sigma} \equiv M_{\rm pl}^2 \frac{\mathcal{M}_{\sigma\sigma}}{V}, \tag{4.37}$$

where we have defined

$$\begin{aligned} \mathcal{M}_{\sigma J} &\equiv \hat{\sigma}_I \mathcal{M}^I{}_J = \hat{\sigma}^K \left(\mathcal{D}_K \mathcal{D}_J V \right), \\ \mathcal{M}_{\sigma\sigma} &\equiv \hat{\sigma}_I \hat{\sigma}^J \mathcal{M}^I{}_J = \hat{\sigma}^K \hat{\sigma}^J \left(\mathcal{D}_K \mathcal{D}_J V \right). \end{aligned} \tag{4.38}$$

The term in $\mathcal{M}^I{}_J$ involving $\mathcal{R}^I{}_{LMJ}$ vanishes when contracted with $\hat{\sigma}_I$ or $\hat{\sigma}^J$ due to the first Bianchi identity (since the relevant term is already contracted with $\hat{\sigma}^L \hat{\sigma}^M$), and hence $\mathcal{M}_{\sigma\sigma}$ is independent of $\mathcal{R}^I{}_{LMJ}$. For trajectory 2 of Fig. 4-2 (solid red line), we see that slow-roll is temporarily violated when the fields roll off the ridge of the potential. See Fig. 4-6.

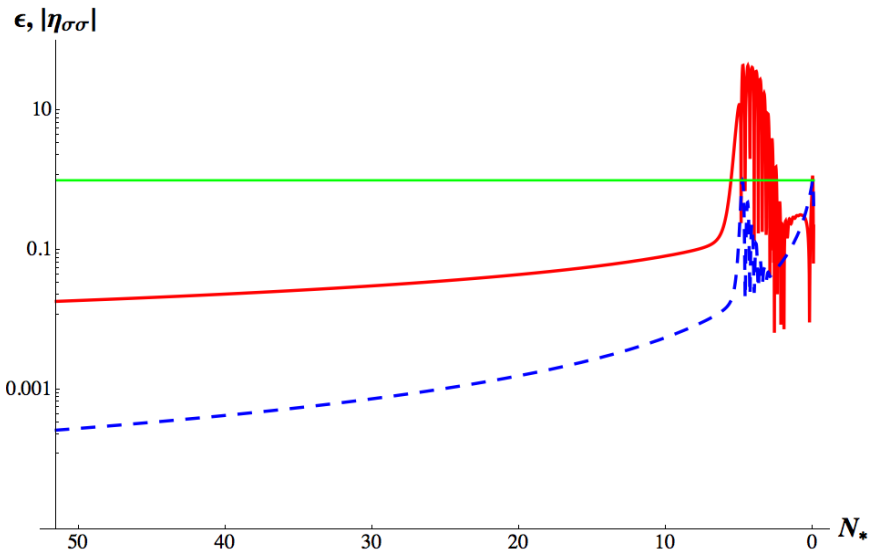

Figure 4-6: The slow-roll parameters ϵ (blue dashed line) and $|\eta_{\sigma\sigma}|$ (solid red line) versus N_* for trajectory 2 of Fig. 2, where N_* is the number of efolds before the end of inflation. Note that $|\eta_{\sigma\sigma}|$ temporarily grows significantly larger than 1 after the fields fall off the ridge in the potential at around $N_* \sim 5$.

A central quantity of interest is the *turn-rate* [32], which we denote ω^I. The turn-rate is given by the (covariant) rate of change of the unit vector, $\hat{\sigma}^I$,

$$\omega^I \equiv \mathcal{D}_t \hat{\sigma}^I = -\frac{1}{\dot{\sigma}} V_{,K} \hat{s}^{IK}, \tag{4.39}$$

where the last expression follows upon using the equations of motion, Eqs. (4.25) and (4.31). Because $\omega^I \propto \hat{s}^{IK}$, we have

$$\omega^I \hat{\sigma}_I = 0. \tag{4.40}$$

Using Eqs. (4.33) and (4.39), we also find

$$\mathcal{D}_t \hat{s}^{IJ} = -\hat{\sigma}^I \omega^J - \omega^I \hat{\sigma}^J. \tag{4.41}$$

For evolution of the fields like that shown in Fig. 4-2, the turn-rate peaks when the fields roll off the ridge; see Fig. 4-7.

We may decompose the perturbations along directions parallel to and perpendic-

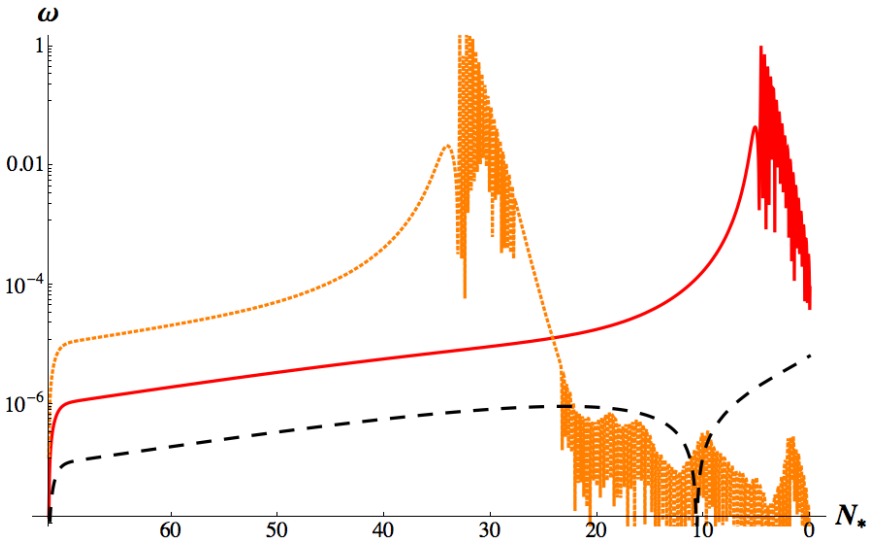

Figure 4-7: The turn-rate, $\omega = |\omega^I|$, for the three trajectories of Fig. 4-2: trajectory 1 (orange dotted line); trajectory 2 (red solid line); and trajectory 3 (black dashed line). The rapid oscillations in ω correspond to oscillations of ϕ in the lower false vacuum of the χ valley. For trajectory 1, ω peaks at $N_* = 34.5$ efolds before the end of inflation; for trajectory 2, ω peaks at $N_* = 4.9$ efolds before the end of inflation; and for trajectory 3, ω remains much smaller than 1 for the duration of inflation.

ular to $\hat{\sigma}^I$:

$$\begin{aligned} Q_\sigma &\equiv \hat{\sigma}_I Q^I, \\ \delta s^I &\equiv \hat{s}^I{}_J Q^J. \end{aligned} \tag{4.42}$$

Note that δs^I may be defined either in terms of the field fluctuations or the Mukhanov-Sasaki variables, since $\hat{s}^I{}_J \delta\phi^J = \hat{s}^I{}_J Q^J$. Though δs^I is a vector in field-space with $\mathcal{N}$ components, only $\mathcal{N} - 1$ of these components are linearly independent. We will isolate particular components of interest in Section IV.

Taking a Fourier transform, such that for any function $F(t, x^i)$ we have $a^2(t)\partial_i\partial^i F(t, x^i) = -k^2 F_k(t)$ where k is the comoving wavenumber, Eq. (4.26) separates into two equations of motion (we suppress the label k on Fourier modes),

$$\begin{aligned} \ddot{Q}_\sigma + 3H\dot{Q}_\sigma + \left[\frac{k^2}{a^2} + \mathcal{M}_{\sigma\sigma} - \omega^2 - \frac{1}{M_{\rm pl}^2 a^3}\frac{d}{dt}\left(\frac{a^3\dot{\sigma}^2}{H}\right)\right] Q_\sigma \\ = 2\frac{d}{dt}\left(\omega_J \delta s^J\right) - 2\left(\frac{V_{,\sigma}}{\dot{\sigma}} + \frac{\dot{H}}{H}\right)\left(\omega_J \delta s^J\right) \end{aligned} \tag{4.43}$$

and

$$\mathcal{D}_t^2\delta s^I + \left[3H\delta^I{}_J + 2\hat{\sigma}^I\omega_J\right]\mathcal{D}_t\delta s^I + \left[\frac{k^2}{a^2}\delta^I{}_J + \mathcal{M}^I{}_J - 2\hat{\sigma}^I\left(\mathcal{M}_{\sigma J} + \frac{\ddot{\sigma}}{\dot{\sigma}}\omega_J\right)\right]\delta s^J = -2\omega^I\left[\dot{Q}_\sigma + \frac{\dot{H}}{H}Q_\sigma - \frac{\ddot{\sigma}}{\dot{\sigma}}Q_\sigma\right]. \tag{4.44}$$

Although the effective mass of the adiabatic perturbations, $m_{\rm eff}^2 = \mathcal{M}_{\sigma\sigma} - \omega^2$, is independent of $\mathcal{R}^I{}_{LMJ}$, the curvature of the field-space manifold introduces couplings among components of the entropy perturbations, δs^I, by means of the $\mathcal{M}^I{}_J$ term in Eq. (4.44). The quantities Q_σ and $(\omega_J\delta s^J)$ are scalars in field space, so the covariant time derivatives in Eq. (4.43) reduce to ordinary time derivatives.

From Eqs. (4.43) and (4.44), it is clear that the adiabatic and entropy perturbations decouple if the turn-rate vanishes, $\omega^I = 0$. Moreover, Eq. (4.43) for Q_σ is identical in form to that of a single-field model (with $m_{\rm eff}^2 = \mathcal{M}_{\sigma\sigma} - \omega^2$), but with a nonzero source term that depends on the combination $\omega_J\delta s^J$. Even in the presence of significant entropy perturbations, δs^I, the power spectrum for adiabatic perturbations will be devoid of features such as non-Gaussianities unless the turn-rate is nonzero, $\omega^I \neq 0$.

4.4 Adiabatic and Entropy Perturbations

In Section III we identified the vector of entropy perturbations, δs^I, which includes $\mathcal{N}-1$ physically independent degrees of freedom. As we will see in this section, these $\mathcal{N}-1$ physical components may be further clarified by introducing a particular set of unit vectors and projection operators in addition to $\hat{\sigma}^I$ and $\hat{s}^{IJ}$. With them we may identify components of δs^I of particular physical interest.

We denote the gauge-invariant curvature perturbation as $\mathcal{R}_c$, not to be confused with the Ricci scalar for the field-space manifold, $\mathcal{R}$. The perturbation $\mathcal{R}_c$ is defined as [40, 11, 12]

$$\mathcal{R}_c \equiv \psi - \frac{H}{(\rho+p)}\delta q, \tag{4.45}$$

where ρ and p are the background-order energy density and pressure for the fluid filling the FRW spacetime, and δq is the energy-density flux of the perturbed fluid, $T^0_i \equiv \partial_i \delta q$. Given Eq. (4.8), we find

$$\begin{aligned} \rho &= \frac{1}{2}\dot{\sigma}^2 + V, \\ p &= \frac{1}{2}\dot{\sigma}^2 - V, \\ \delta q &= -\mathcal{G}_{IJ}\dot{\phi}^I \delta\phi^J = -\dot{\sigma}\hat{\sigma}_J \delta\phi^J, \end{aligned} \tag{4.46}$$

and hence, upon using Eqs. (4.24) and (4.42),

$$\mathcal{R}_c = \psi + \frac{H}{\dot{\sigma}}\hat{\sigma}_J \delta\phi^J = \frac{H}{\dot{\sigma}} Q_\sigma. \tag{4.47}$$

We thus find that $\mathcal{R}_c \propto Q_\sigma$, and that the righthand side of Eq. (4.44) is proportional to $\dot{\mathcal{R}}_c$. Recall that these expressions hold to first order in fluctuations, for which $\delta\phi^I \to \mathcal{Q}^I$.

In the presence of entropy perturbations, the gauge-invariant curvature perturbation need not remain conserved, $\dot{\mathcal{R}}_c \neq 0$. In particular, the nonadiabatic pressure perturbation is given by [11, 12]

$$\delta p_{\rm nad} \equiv \delta p - \frac{\dot{p}}{\dot{\rho}}\delta\rho = -\frac{2V_{,\sigma}}{3H\dot{\sigma}}\delta\rho_m + 2\dot{\sigma}\left(\omega_J \delta s^J\right), \tag{4.48}$$

where $\delta\rho_m \equiv \delta\rho - 3H\delta q$ is the gauge-invariant comoving density perturbation. The perturbed Einstein field equations (to linear order) require [11, 12]

$$\delta\rho_m = -2M_{\rm pl}^2 \frac{k^2}{a^2}\Psi, \tag{4.49}$$

where Ψ is the gauge-invariant Bardeen potential [40, 11, 12]

$$\Psi \equiv \psi + a^2 H\left(\dot{E} - \frac{B}{a}\right). \tag{4.50}$$

Therefore in the long-wavelength limit, for $k \ll aH$, the only source of nonadiabatic

pressure comes from the entropy perturbations, δs^I. Using the usual relations [11, 12] among the gauge-invariant quantities $\mathcal{R}_c$ and $\zeta \equiv -\psi + (H/\dot{\rho})\delta\rho$, we find

$$\dot{\mathcal{R}}_c = \frac{H}{\dot{H}}\frac{k^2}{a^2}\Psi + \frac{2H}{\dot{\sigma}}\left(\omega_J \delta s^J\right). \tag{4.51}$$

Thus even for modes with $k \ll aH$, $\mathcal{R}_c$ will not be conserved in the presence of entropy perturbations if the turn-rate is nonzero, $\omega^I \neq 0$.

Eqs. (4.43) and (4.51) indicate that a particular component of the vector δs^I is of special physical relevance: the combination $(\omega_J \delta s^J)$ serves as the source for Q_σ and hence for $\dot{\mathcal{R}}_c$. Akin to the "kinematical basis" of [32], we may therefore introduce a new unit vector that points in the direction of the turn-rate, ω^I, together with a new projection operator that picks out the subspace perpendicular to both $\hat{\sigma}^I$ and ω^I:

$$\begin{aligned} \hat{s}^I &\equiv \frac{\omega^I}{\omega}, \\ \gamma^{IJ} &\equiv \mathcal{G}^{IJ} - \hat{\sigma}^I\hat{\sigma}^J - \hat{s}^I\hat{s}^J, \end{aligned} \tag{4.52}$$

where $\omega = |\omega^I|$ is the magnitude of the turn-rate vector. Using the relations in Eq. (4.34), the definitions in Eq. (4.52) imply

$$\begin{aligned} \hat{s}^{IJ} &= \hat{s}^I\hat{s}^J + \gamma^{IJ}, \\ \gamma^{IJ}\gamma_{IJ} &= \mathcal{N} - 2, \\ \hat{s}^{IJ}\hat{s}_J &= \hat{s}^I, \\ \hat{\sigma}_I\hat{s}^I &= \hat{\sigma}_I\gamma^{IJ} = \hat{s}_I\gamma^{IJ} = 0 \text{ for all } J. \end{aligned} \tag{4.53}$$

We then find

$$\begin{aligned} \mathcal{D}_t\hat{s}^I &= -\omega\hat{\sigma}^I - \Pi^I, \\ \mathcal{D}_t\gamma^{IJ} &= \hat{s}^I\Pi^J + \Pi^I\hat{s}^J \end{aligned} \tag{4.54}$$

where

$$\Pi^I \equiv \frac{1}{\omega}\mathcal{M}_{\sigma K}\gamma^{IK}, \tag{4.55}$$

and hence, from Eq. (4.53),

$$\hat{\sigma}_I \Pi^I = \hat{s}_I \Pi^I = 0. \tag{4.56}$$

The vector of entropy perturbations, δs^I, may then be written as

$$\delta s^I = \hat{s}^I Q_s + B^I, \tag{4.57}$$

where

$$\begin{aligned} Q_s &\equiv \hat{s}_J Q^J, \\ B^I &\equiv \gamma^I{}_J Q^J. \end{aligned} \tag{4.58}$$

The quantity that sources Q_σ and $\mathcal{R}_c$ is now easily identified as the scalar, $\omega_J \delta s^J = \omega Q_s$, which corresponds to just one component of the vector δs^I.

Making use of Eqs. (4.30), (4.47), and (4.51), the equation of motion for δs^I in Eq. (4.44) separates into

$$\begin{aligned} \ddot{Q}_s + 3H\dot{Q}_s + \left[\frac{k^2}{a^2} + \mathcal{M}_{ss} + 3\omega^2 - \Pi^2\right] Q_s \\ = 4M_{\rm pl}^2 \frac{\omega}{\dot{\sigma}} \frac{k^2}{a^2} \Psi - \mathcal{D}_t \left(\Pi_J B^J\right) - \Pi_J \mathcal{D}_t B^J - \mathcal{M}_{sJ} B^J - 3H \left(\Pi_J B^J\right) \end{aligned} \tag{4.59}$$

and

$$\begin{aligned} \mathcal{D}_t^2 B^I + \left[3H\delta^I{}_J + 2\left(\hat{\sigma}^I \omega_J - \hat{s}^I \Pi_J\right)\right] \mathcal{D}_t B^J \\ + \left[\frac{k^2}{a^2}\delta^I{}_J + \gamma^{IA}\mathcal{M}_{AJ} - \hat{\sigma}^I \mathcal{M}_{\sigma J} - \hat{s}^I \left(3H\Pi_J + \mathcal{D}_t \Pi_J\right)\right] B^J \\ = 2\Pi^I \dot{Q}_s - \gamma^{IA}\mathcal{M}_{As} Q_s + \left(3H\Pi^I + \mathcal{D}_t \Pi^I\right) Q_s. \end{aligned} \tag{4.60}$$

In analogy to (4.38), we have introduced the projections

$$\begin{aligned} \mathcal{M}_{sJ} &\equiv \hat{s}_I \mathcal{M}^I{}_J, \\ \mathcal{M}_{ss} &\equiv \hat{s}_I \hat{s}^J \mathcal{M}^I{}_J. \end{aligned} \tag{4.61}$$

Note, however, that unlike $\mathcal{M}_{\sigma J}$, the term in $\mathcal{M}^I{}_J$ proportional to $\mathcal{R}^I{}_{LMJ}$ does not vanish upon contracting with $\hat{s}_I$ or $\hat{s}^J$. Hence the Riemann-tensor term in $\mathcal{M}^I{}_J$ induces interactions among the components of δs^I.

For models with $\mathcal{N} \geq 3$ scalar fields, we may introduce additional unit vectors and projection operators with which to characterize components of B^I. The next in the series are given by

$$\begin{aligned} \hat{u}^I &\equiv \frac{\Pi^I}{\Pi}, \\ q^{IJ} &\equiv \gamma^{IJ} - \hat{u}^I \hat{u}^J. \end{aligned} \tag{4.62}$$

Repeating steps as before, we find

$$\begin{aligned} \mathcal{D}_t \hat{u}^I &= \Pi \hat{s}^I + \tau^I, \\ \mathcal{D}_t q^{IJ} &= -\hat{u}^I \tau^J - \tau^I \hat{u}^J, \end{aligned} \tag{4.63}$$

where

$$\tau^I \equiv \frac{1}{\Pi} \left[\mathcal{M}_{sK} + \frac{\dot{\sigma}}{\omega} \hat{\sigma}^A \hat{\sigma}_L \left(\mathcal{D}_A \mathcal{M}^L{}_K \right) \right] q^{IK}. \tag{4.64}$$

We then have

$$B^I = \hat{u}^I Q_u + C^I \tag{4.65}$$

in terms of

$$\begin{aligned} Q_u &\equiv \hat{u}_J Q^J, \\ C^I &\equiv q^I{}_J Q^J. \end{aligned} \tag{4.66}$$

This decomposition reproduces the structure in the "kinematical basis" [32] but can be applied in any coordinate basis for the field-space manifold: Q_σ is sourced by Q_s; Q_s is sourced by Q_σ and Q_u (though we have used Eq. (4.51) to substitute the dependence on $\dot{Q}_\sigma$ for the $\nabla^2 \Psi$ term in Eq. (4.59)); Q_u is sourced by Q_s and $Q_v \equiv \tau_J Q^J / |\tau^I|$, and so on.

For our present purposes the two-field model will suffice. The perturbations then consist of two scalar degrees of freedom, Q_σ and Q_s, which obey Eqs. (4.43) and

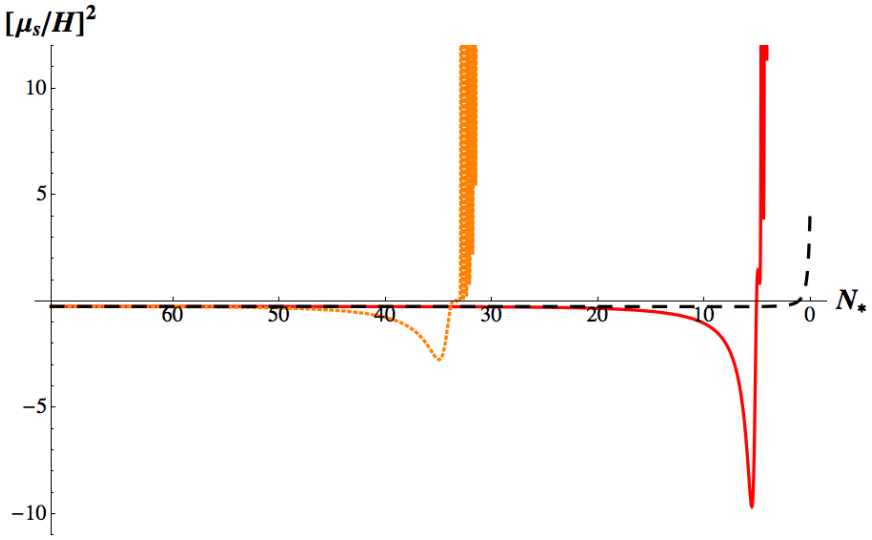

Figure 4-8: The effective mass-squared of the entropy perturbations relative to the Hubble scale, $(\mu_s/H)^2$, for the trajectories shown in Fig. 4-2: trajectory 1 (orange dotted line); trajectory 2 (red solid line); and trajectory 3 (black dashed line). For all three trajectories, $\mu_s^2 < 0$ while the fields remain near the top of the ridge, since μ_s^2 is related to the curvature of the potential in the direction orthogonal to the background fields' evolution. The effective mass grows much larger than H as soon as the fields roll off the ridge of the potential.

(4.59) (with $B^I = \Pi^I = 0$) respectively. The effective mass-squared of the entropy perturbations becomes

$$\mu_s^2 \equiv \mathcal{M}_{ss} + 3\omega^2. \tag{4.67}$$

If the entropy perturbations are heavy during slow-roll, with $\mu_s > 3H/2$, then the amplitude of long-wavelength modes, with $k \ll aH$, will fall exponentially: $Q_s \sim a^{-3/2}(t)$ during quasi-de Sitter expansion. For trajectories that begin near the top of a ridge, on the other hand, the entropy modes will remain light or even tachyonic at early times, since μ_s^2 is related to the curvature of the potential in the direction orthogonal to the background fields' trajectory. Once the background fields roll off the ridge, the entropy mass immediately grows very large, suppressing further growth in the amplitude of Q_s. See Fig. 4-8.

The perturbations in the adiabatic direction are proportional to the gauge-invariant curvature perturbation, as derived in Eq. (4.47). Following the usual convention [35],

we may define a normalized entropy perturbation as

$$\mathcal{S} \equiv \frac{H}{\dot{\sigma}} Q_s. \tag{4.68}$$

In the long-wavelength limit, the coupled perturbations obey general relations of the form [35]

$$\begin{aligned} \dot{\mathcal{R}}_c &= \alpha H \mathcal{S} + \mathcal{O}\left(\frac{k^2}{a^2 H^2}\right), \\ \dot{\mathcal{S}} &= \beta H \mathcal{S} + \mathcal{O}\left(\frac{k^2}{a^2 H^2}\right), \end{aligned} \tag{4.69}$$

in terms of which we may write the transfer functions as

$$\begin{aligned} T_{\mathcal{RS}}(t_*, t) &= \int_{t_*}^{t} dt' \, \alpha(t') H(t') T_{\mathcal{SS}}(t_*, t'), \\ T_{\mathcal{SS}}(t_*, t) &= \exp\left[\int_{t_*}^{t} dt' \, \beta(t') H(t')\right]. \end{aligned} \tag{4.70}$$

The transfer functions relate the gauge-invariant perturbations at one time, t_*, to their values at some later time, t. We take t_* to be the time when a fiducial scale of interest first crossed outside the Hubble radius during inflation, defined by $a^2(t_*)H^2(t_*) = k_*^2$. In the two-field case, both $\mathcal{R}_c$ and $\mathcal{S}$ are scalars in field space, and hence α, β, $T_{\mathcal{RS}}$, and $T_{\mathcal{SS}}$ are also scalars. Thus there is no time-ordering ambiguity in the integral for $T_{\mathcal{SS}}$ in Eq. (4.70).

In the two-field case, Eq. (4.51) becomes

$$\dot{\mathcal{R}} = 2\omega \mathcal{S} + \mathcal{O}\left(\frac{k^2}{a^2 H^2}\right). \tag{4.71}$$

Comparing with Eq. (4.69), we find

$$\alpha(t) = \frac{2\omega(t)}{H(t)}. \tag{4.72}$$

The variation of the gauge-invariant curvature perturbation is proportional to the

turn-rate. For $\dot{\mathcal{S}}$ we take the long-wavelength and slow-roll limits of Eq. (4.59):

$$\dot{Q}_s \simeq -\frac{\mu_s^2}{3H} Q_s. \tag{4.73}$$

Eq. (4.69) then yields

$$\beta = -\frac{\mu_s^2}{3H^2} - \epsilon + \frac{\ddot{\sigma}}{H\dot{\sigma}}. \tag{4.74}$$

Taking the slow-roll limit of Eq. (4.31) for $\dot{\sigma}$, we have

$$3H\dot{\sigma} \simeq -\hat{\sigma}^I V_{,I}. \tag{4.75}$$

Taking a covariant time derivative of both sides, using the definition of ω^I in Eq. (4.39), and introducing the slow-roll parameter

$$\eta_{ss} \equiv M_{\rm pl}^2 \frac{\mathcal{M}_{ss}}{V}, \tag{4.76}$$

we arrive at

$$\beta = -2\epsilon - \eta_{ss} + \eta_{\sigma\sigma} - \frac{4}{3}\frac{\omega^2}{H^2}, \tag{4.77}$$

where $\eta_{\sigma\sigma}$ is defined in Eq. (4.37). For trajectories that begin near the top of a ridge, η_{ss} will be negative at early times (like μ_s^2), which can yield $\beta > 0$. In that case, $T_{\mathcal{SS}}(t_*, t)$ will grow. If one also has a nonzero turn-rate, ω — and hence, from Eq. (4.72), a nonzero α within the integrand for $T_{\mathcal{RS}}(t_*, t)$ — then the growing entropy modes will source the adiabatic mode.

The power spectrum for the gauge-invariant curvature perturbation is defined by [11, 12]

$$\langle \mathcal{R}_c(\mathbf{k}_1)\mathcal{R}_c(\mathbf{k}_2)\rangle = (2\pi)^3 \delta^{(3)}(\mathbf{k}_1 + \mathbf{k}_2) P_{\mathcal{R}}(k_1), \tag{4.78}$$

where the angular brackets denote a spatial average and $P_{\mathcal{R}}(k) = |\mathcal{R}_c|^2$. The dimensionless power spectrum is then given by

$$\mathcal{P}_{\mathcal{R}}(k) = \frac{k^3}{2\pi^2} |\mathcal{R}_c|^2, \tag{4.79}$$

and the spectral index is defined as

$$n_s \equiv 1 + \frac{\partial \ln \mathcal{P}_\mathcal{R}}{\partial \ln k}. \tag{4.80}$$

Using the transfer functions, we may relate the power spectrum at time t_* to its value at some later time, t, as

$$\mathcal{P}_\mathcal{R}(k) = \mathcal{P}_\mathcal{R}(k_*) \left[1 + T^2_{\mathcal{RS}}(t_*, t)\right], \tag{4.81}$$

where k corresponds to a scale that crossed the Hubble radius at some time $t > t_*$. The scale-dependence of the transfer functions becomes [13, 12, 35, 32],

$$\begin{aligned} \frac{1}{H}\frac{\partial T_{\mathcal{RS}}}{\partial t_*} &= -\alpha - \beta T_{\mathcal{RS}}, \\ \frac{1}{H}\frac{\partial T_{\mathcal{SS}}}{\partial t_*} &= -\beta T_{\mathcal{SS}}, \end{aligned} \tag{4.82}$$

and hence the spectral index for the power spectrum of the adiabatic fluctuations becomes

$$n_s = n_s(t_*) + \frac{1}{H}\left(\frac{\partial T_{\mathcal{RS}}}{\partial t_*}\right) \sin(2\Delta) \tag{4.83}$$

where

$$\cos\Delta \equiv \frac{T_{\mathcal{RS}}}{\sqrt{1 + T^2_{\mathcal{RS}}}}. \tag{4.84}$$

Given Eq. (4.43) in the limit $\omega_J \delta s^J = \omega Q_s \ll 1$, the spectral index evaluated at t_* matches the usual single-field result to lowest order in slow-roll parameters [11, 12, 50]:

$$n_s(t_*) = 1 - 6\epsilon(t_*) + 2\eta_{\sigma\sigma}(t_*). \tag{4.85}$$

Scales of cosmological interest first crossed the Hubble radius between 40 and 60 efolds before the end of inflation. In each of the scenarios of Fig. 4-2 the fields remained near the top of the ridge in the potential until fewer than 40 efolds before the end of inflation. As indicated in Fig. 4-9, $T_{\mathcal{RS}}$ remains small between $N_* = 60$ and 40 for each of the three trajectories, with little sourcing of the adiabatic perturbations

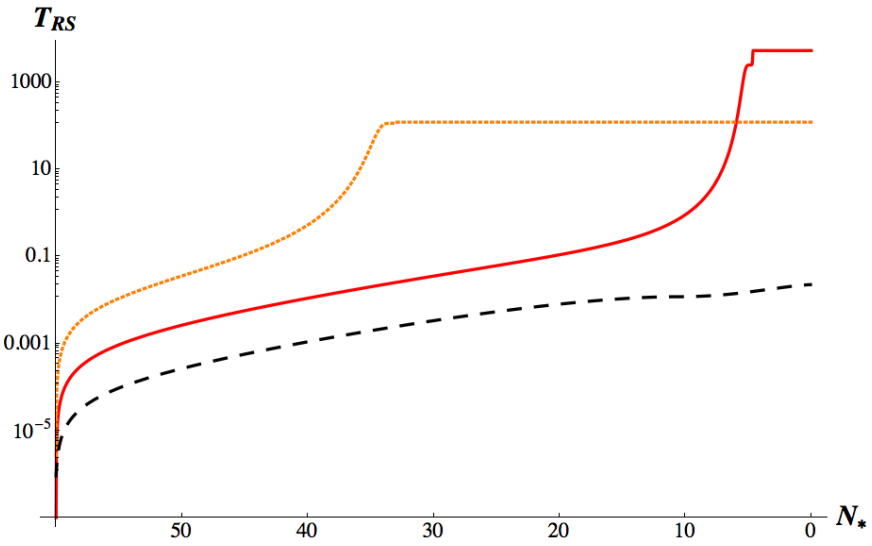

Figure 4-9: The transfer function $T_{\mathcal{RS}}$ for the three trajectories of Fig. 4-2: trajectory 1 (orange dotted line); trajectory 2 (red solid line); and trajectory 3 (black dashed line). Trajectories 2 and 3, which begin nearer the top of the ridge in the potential than trajectory 1, evolve as essentially single-field models during early times, before the fields roll off the ridge.

by the entropy perturbations. This behavior of $T_{\mathcal{RS}}$ is consistent with the behavior of $\omega = \alpha H/2$ as shown in Fig. 4-7: ω (and hence α) remains small until the fields roll off the ridge in the potential. Only in the case of trajectory 1, which began least high on the ridge among the trajectories and hence fell down the ridge soonest (at $N_* = 34.5$ efolds before the end of inflation), does $T_{\mathcal{RS}}$ become appreciable by $N_* = 40$. In particular, we find $T_{\mathcal{RS}}(N_{40}) = 0.530$ for trajectory 1; $T_{\mathcal{RS}}(N_{40}) = 0.011$ for trajectory 2; and $T_{\mathcal{RS}}(N_{40}) = 0.001$ for trajectory 3.

Fixing the fiducial scale k_* to be that which first crossed the Hubble radius $N_* = 60$ efolds before the end of inflation, we find $n_s(t_*) = 0.967$ for each of the three trajectories of Fig. 4-2, in excellent agreement with the observed value $n_s = 0.971 \pm 0.010$ [3]. Corrections to n_s from the scale-dependence of $T_{\mathcal{RS}}$ remain negligible as long as $T_{\mathcal{RS}}$ remains small between $N_* = 60$ and 40. Consequently, we find negligible tilt in the spectral index across the entire observational window for trajectories 2 and 3, whereas the spectral index for trajectory 1 departs appreciably from $n_s(t_*)$ for scales that crossed the Hubble radius near $N_* = 40$. See Fig. 4-10.

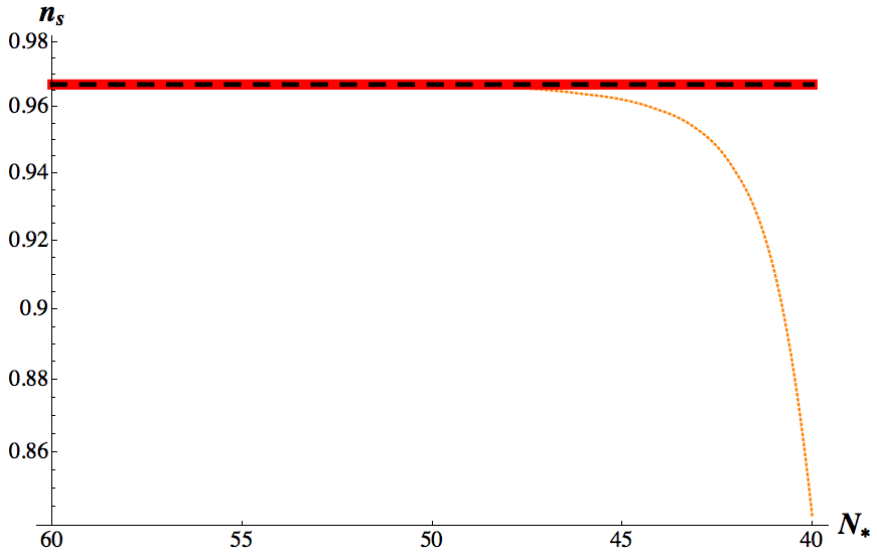

Figure 4-10: The spectral index, n_s, versus N_* for the three trajectories of Fig. 4-2: trajectory 1 (orange dotted line); trajectory 2 (red solid line); and trajectory 3 (black dashed line). The spectral indices for trajectories 2 and 3 coincide and show no tilt from the value $n_s(N_{60}) = 0.967$.

4.5 Primordial Bispectrum

In the usual calculation of primordial bispectra, one often assumes that the field fluctuations behave as nearly Gaussian around the time t_*, in which case the three-point function for the field fluctuations should be negligible. Using the $\mathcal{Q}^I$ construction of Eq. (4.23), the authors of [36, 37] calculated the action up to third order in perturbations and found several new contributions to the three-point function for field fluctuations, mediated by the Riemann tensor for the field space, $\mathcal{R}^I{}_{JKL}$. The presence of the new terms is not surprising; we have seen that $\mathcal{R}^I{}_{JKL}$ induces new interactions among the perturbations even at linear order, by means of the mass-squared matrix, $\mathcal{M}^I{}_J$ in Eq. (4.27). Evaluated at time t_*, the three-point function for $\mathcal{Q}^I$ calculated in [37] takes the form

$$\begin{aligned}\langle \mathcal{Q}^I(\mathbf{k}_1)\mathcal{Q}^J(\mathbf{k}_2)\mathcal{Q}^K(\mathbf{k}_3)\rangle_* = (2\pi)^3\delta^{(3)}(\mathbf{k}_1+\mathbf{k}_2+\mathbf{k}_3)\frac{H_*^4}{k_1^3k_2^3k_3^3} \\ \times\left[\mathcal{A}_*^{IJK}+\mathcal{B}_*^{IJK}+\mathcal{C}_*^{IJK}+\mathcal{D}_*^{IJK}\right].\end{aligned} \tag{4.86}$$

Upon using the definition of $\hat{\sigma}^I$ in Eq. (4.29), the background equation of Eq. (4.30) to relate $\dot{H}$ to $\dot{\sigma}^2$, and the definition of ϵ in Eq. (4.36), the terms on the righthand side of Eq. (4.86) may be written [37, 51]

$$\begin{aligned}
\mathcal{A}_*^{IJK} &= \frac{\sqrt{2\epsilon}}{M_{\rm pl}}\,\hat{\sigma}^I\mathcal{G}^{JK}f_{\mathcal{A}}(\mathbf{k}_1,\mathbf{k}_2,\mathbf{k}_3) + \text{cyclic permutations},\\
\mathcal{B}_*^{IJK} &= \frac{4M_{\rm pl}\sqrt{2\epsilon}}{3}\,\hat{\sigma}_A\mathcal{R}^{I(JK)A}f_{\mathcal{B}}(\mathbf{k}_1,\mathbf{k}_2,\mathbf{k}_3) + \text{cyclic permutations},\\
\mathcal{C}_*^{IJK} &= \frac{2M_{\rm pl}^2\,\epsilon}{3}\,\hat{\sigma}_A\hat{\sigma}_B\mathcal{R}^{(I|AB|J;K)}f_{\mathcal{C}}(\mathbf{k}_1,\mathbf{k}_2,\mathbf{k}_3) + \text{cyclic permutations},\\
\mathcal{D}_*^{IJK} &= -\frac{8M_{\rm pl}^2\,\epsilon}{3}\,\hat{\sigma}_A\hat{\sigma}_B\mathcal{R}^{I(JK)A;B}f_{\mathcal{D}}(\mathbf{k}_1,\mathbf{k}_2,\mathbf{k}_3) + \text{cyclic permutations},
\end{aligned} \tag{4.87}$$

where $\mathcal{R}^{IABJ;K} = \mathcal{G}^{KM}\mathcal{D}_M\mathcal{R}^{IABJ}$, and $f_{\mathcal{I}}(\mathbf{k}_i)$ are shape-functions in Fourier space that depend on the particular configuration of triangles formed by the wavevectors $\mathbf{k}_i$. Comparable to the findings in [28, 29], each of the contributions to the three-point function for the field fluctuations is suppressed by a power of the slow-roll parameter, $\epsilon \ll 1$.

The quantity of most interest to us is not the three-point function for the field fluctuations but the bispectrum for the gauge-invariant curvature perturbation, ζ, which may be parameterized as

$$\langle\zeta(\mathbf{k}_1)\zeta(\mathbf{k}_2)\zeta(\mathbf{k}_3)\rangle \equiv (2\pi)^3\delta^{(3)}\left(\mathbf{k}_1+\mathbf{k}_2+\mathbf{k}_3\right)B_\zeta(\mathbf{k}_1,\mathbf{k}_2,\mathbf{k}_3). \tag{4.88}$$

Recall that the two gauge-invariant curvature perturbations, $\mathcal{R}_c$ and ζ, coincide in the long-wavelength limit when working to first order in metric perturbations [11, 12]. In terms of $\mathcal{Q}^I$, the δN expansion [53, 54, 56, 55] for ζ on super-Hubble scales becomes [**?**]

$$\zeta(x^\mu) = \left(\mathcal{D}_I N\right)\mathcal{Q}^I(x^\mu) + \frac{1}{2}\left(\mathcal{D}_I\mathcal{D}_J N\right)\mathcal{Q}^I(x^\mu)\mathcal{Q}^J(x^\mu) + ... \tag{4.89}$$

where $N = \ln|a(t_{\rm end})H(t_{\rm end})/k_*|$ is the number of efolds after a given scale k_* first crossed the Hubble radius until the end of inflation. At t_*, Eqs. (4.86) and (4.89)

yield

$$\begin{aligned}\langle\zeta(\mathbf{k}_1)\zeta(\mathbf{k}_2)\zeta(\mathbf{k}_3)\rangle_* = N_{,I}N_{,J}N_{,K}\langle\mathcal{Q}^I(\mathbf{k}_1)\mathcal{Q}^J(\mathbf{k}_2)\mathcal{Q}^K(\mathbf{k}_3)\rangle_* \\ + \frac{1}{2}\left(\mathcal{D}_I\mathcal{D}_J N\right)N_{,K}N_{,L} \\ \times\int\frac{d^3q}{(2\pi)^3}\langle\mathcal{Q}^I(\mathbf{k}_1-\mathbf{q})\mathcal{Q}^K(\mathbf{k}_2)\rangle_*\langle\mathcal{Q}^J(\mathbf{q})\mathcal{Q}^L(\mathbf{k}_3)\rangle_* + \text{cyclic perms.}\end{aligned} \tag{4.90}$$

The bottom two lines on the righthand side give rise to the usual form of f_{NL}, made suitably covariant to reflect $\mathcal{G}_{IJ}\neq\delta_{IJ}$. Adopting the conventional normalization, this term contributes [13, 12, 14, 15, 16]:

$$\begin{aligned}\langle\zeta(\mathbf{k}_1)\zeta(\mathbf{k}_2)\zeta(\mathbf{k}_3)\rangle_{f_{NL}} = (2\pi)^3\delta^{(3)}\left(\mathbf{k}_1+\mathbf{k}_2+\mathbf{k}_3\right)\frac{H_*^4}{k_1^3k_2^3k_3^3} \\ \times\left[-\frac{6}{5}f_{NL}\left(N_{,I}N^{,I}\right)^2\right]\left[k_1^3+k_2^3+k_3^3\right]\end{aligned} \tag{4.91}$$

where

$$f_{NL} = -\frac{5}{6}\frac{N^{,A}N^{,B}\mathcal{D}_A\mathcal{D}_B N}{\left(N_{,I}N^{,I}\right)^2}. \tag{4.92}$$

The term on the first line of Eq. (4.90), proportional to the nonzero three-point function for the field fluctuations, yields new contributions to the bispectrum. However, the three-point function $\langle\mathcal{Q}^I\mathcal{Q}^J\mathcal{Q}^K\rangle_*$ is contracted with the symmetric object, $N_{,I}N_{,J}N_{,K}$. Hence we must consider each term within A^{IJK} with care.

In general, the field-space indices, I, J, K, and the momentum-space indices, $\mathbf{k}_i$, must be permuted as pairs: $(I,\mathbf{k}_1),(J,\mathbf{k}_2),(K,\mathbf{k}_3)$. This is because the combinations arise from contracting the external legs of the various propagators, such as $\langle\mathcal{Q}^I(\mathbf{k}_1)\mathcal{Q}^J(\mathbf{k}_2)\rangle$ and $\langle\mathcal{Q}^J(\mathbf{k}_2)\mathcal{Q}^K(\mathbf{k}_3)\rangle$, with the internal legs of each three-point vertex [37, 57]. Let us first consider the special case of an equilateral arrangement in momentum space, in which $k_1=k_2=k_3=k_*$. Then the term proportional to $\mathcal{A}^{IJK}$

contributes

$$\begin{aligned}\langle\zeta(\mathbf{k}_1)\zeta(\mathbf{k}_2)\zeta(\mathbf{k}_3)\rangle_{\mathcal{A}} &= (2\pi)^3\delta^{(3)}(\mathbf{k}_1+\mathbf{k}_2+\mathbf{k}_3)\frac{H_*^4}{4k_*^9} \\ &\qquad\times\frac{\sqrt{2\epsilon}}{M_{\rm pl}}\left(N_{,I}N_{,J}N_{,K}\right)\left[\hat{\sigma}^I\mathcal{G}^{JK}+\hat{\sigma}^J\mathcal{G}^{KI}+\hat{\sigma}^K\mathcal{G}^{IJ}\right]f_{\mathcal{A}}(k) \\ &= (2\pi)^3\delta^{(3)}(\mathbf{k}_1+\mathbf{k}_2+\mathbf{k}_3)\frac{H_*^4}{4k_*^9} \\ &\qquad\times\frac{3\sqrt{2\epsilon}}{M_{\rm pl}}\left[\left(\hat{\sigma}^I N_{,I}\right)\left(N_{,A}N^{,A}\right)\right]f_{\mathcal{A}}(k),\end{aligned} \tag{4.93}$$

where $f_{\mathcal{A}}(k)$ depends only on k. Taking the equilateral limit of the relevant expression in Eq. (3.17) of [37], we find $f_{\mathcal{A}}(k)\to -5k_*^3/4$. Using Eqs. (4.22), (4.29), (4.30), and (4.36), we also have

$$\hat{\sigma}^I N_{,I}=\frac{1}{\dot{\sigma}}\dot{\varphi}^I\mathcal{D}_I N=\frac{1}{\dot{\sigma}}\mathcal{D}_t N=\frac{H}{\dot{\sigma}}=\frac{1}{M_{\rm pl}H\sqrt{2\epsilon}}, \tag{4.94}$$

and hence

$$\langle\zeta(\mathbf{k}_1)\zeta(\mathbf{k}_2)\zeta(\mathbf{k}_3)\rangle_{\mathcal{A}}=(2\pi)^3\delta^{(3)}(\mathbf{k}_1+\mathbf{k}_2+\mathbf{k}_3)\frac{H_*^4}{4k_*^9}\left[\frac{3}{M_{\rm pl}^2}\left(N_{,A}N^{,A}\right)\right]f_{\mathcal{A}}(k). \tag{4.95}$$

The term arising from $\mathcal{B}^{IJK}$ contributes

$$\begin{aligned}\langle\zeta(\mathbf{k}_1)\zeta(\mathbf{k}_2)\zeta(\mathbf{k}_3)\rangle_{\mathcal{B}} &= (2\pi)^3\delta^{(3)}(\mathbf{k}_1+\mathbf{k}_2+\mathbf{k}_3)\frac{H_*^4}{4k_*^9} \\ &\qquad\times\frac{4M_{\rm pl}\sqrt{2\epsilon}}{3}\,\hat{\sigma}_A N_{,I}N_{,J}N_{,K}\left[\mathcal{R}^{IJKA}+\mathcal{R}^{IKJA}+\text{cyclic}\right]f_{\mathcal{B}}(k).\end{aligned} \tag{4.96}$$

But from the symmetry properties of the Riemann tensor we have $\mathcal{R}^{IJKA}=\mathcal{R}^{KAIJ}=-\mathcal{R}^{AKIJ}$, and from the first Bianchi identity,

$$\mathcal{R}_{A[KIJ]}=0. \tag{4.97}$$

The antisymmetry of the Riemann tensor in its last three indices means that any contraction of the form

$$\mathcal{O}_{IJK}\mathcal{R}^{AKIJ} = 0 \tag{4.98}$$

for objects $\mathcal{O}_{IJK}$ that are symmetric in the indices I, J, K. In our case, we have $\mathcal{O}_{IJK} = N_{,I}N_{,J}N_{,K}$ and thus every term in the square brackets of Eq. (4.96) including the cyclic permutations may be put in the form of Eq. (4.98). We therefore find

$$\langle\zeta(\mathbf{k}_1)\zeta(\mathbf{k}_2)\zeta(\mathbf{k}_3)\rangle_{\mathcal{B}} = 0 \tag{4.99}$$

identically in the equilateral limit.

The term arising from $\mathcal{C}^{IJK}$ contributes

$$\begin{aligned}\langle\zeta(\mathbf{k}_1)\zeta(\mathbf{k}_2)\zeta(\mathbf{k}_3)\rangle_{\mathcal{C}} = (2\pi)^3\delta^{(3)}(\mathbf{k}_1+\mathbf{k}_2+\mathbf{k}_3)\frac{H^4}{4k_*^9} \\ \times \frac{2M_{\rm pl}^2\,\epsilon}{3}\,\hat{\sigma}_A\hat{\sigma}_B N_{,I}N_{,J}N_{,K}\mathcal{R}^{(I|AB|J;K)}f_{\mathcal{C}}(k).\end{aligned} \tag{4.100}$$

In the equilateral limit, we find $f_{\mathcal{C}}(k_*) \simeq 15k_*^3$, based on the limit of the appropriate expression in Eq. (3.17) of [37]. We may identify the nonzero terms in Eq. (4.100) using the Bianchi identities. The first Bianchi identity is given in Eq. (4.97), and the second Bianchi identity may be written

$$\mathcal{R}_{AB[CD;E]} = 0. \tag{4.101}$$

Using the (anti)symmetry properties of the Riemann tensor and Eqs. (4.97) and (4.101), together with the fact that the combinations $\mathcal{O}_{IJK} \equiv N_{,I}N_{,J}N_{,K}$ and $\Omega_{AB} \equiv \hat{\sigma}_A\hat{\sigma}_B$ are symmetric in their indices, we find the only nonzero term within Eq. (4.100) to be

$$\begin{aligned}\langle\zeta(\mathbf{k}_1)\zeta(\mathbf{k}_2)\zeta(\mathbf{k}_3)\rangle_{\mathcal{C}} = (2\pi)^3\delta^{(3)}(\mathbf{k}_1+\mathbf{k}_2+\mathbf{k}_3)\frac{H^4}{4k_*^9} \\ \times \frac{2M_{\rm pl}^2\,\epsilon}{3}\,\hat{\sigma}_A\hat{\sigma}_B N_{,I}N_{,J}N_{,K}\mathcal{R}^{IABJ;K}f_{\mathcal{C}}(k).\end{aligned} \tag{4.102}$$

The final term to consider arises from $\mathcal{D}^{IJK}$. In particular, in the equilaterial limit we have

$$\langle\zeta(\mathbf{k}_1)\zeta(\mathbf{k}_2)\zeta(\mathbf{k}_3)\rangle_{\mathcal{D}} = (2\pi)^3\delta^{(3)}(\mathbf{k}_1+\mathbf{k}_2+\mathbf{k}_3)\frac{H^4}{4k_*^9} \times -\frac{4M_{\rm pl}^2\,\epsilon}{3}\,\hat{\sigma}_A\hat{\sigma}_B N_{,I}N_{,J}N_{,K}\left[\mathcal{R}^{IJKA;B}+\mathcal{R}^{IKJA;B}+\text{cyclic}\right]f_{\mathcal{D}}(k). \tag{4.103}$$

Again we may use $\mathcal{R}_{IJKA}=\mathcal{R}_{KAIJ}=-\mathcal{R}_{AKIJ}$ and Eq. (4.97) to put the first term in square brackets in Eq. (4.103) in the form

$$\mathcal{O}_{IJK}\mathcal{R}^{AKIJ;B}=0 \tag{4.104}$$

for $\mathcal{O}_{IJK}$ symmetric. The same occurs for the second term in square brackets in Eq. (4.103) and for all cyclic permutations of I,J,K. Hence we find

$$\langle\zeta(\mathbf{k}_1)\zeta(\mathbf{k}_2)\zeta(\mathbf{k}_3)\rangle_{\mathcal{D}}=0 \tag{4.105}$$

identically in the equilateral limit.

The new nonvanishing terms in Eqs. (4.95) and (4.102) remain considerably smaller than the f_{NL} term of Eq. (4.91) for the family of models of interest. The term stemming from $\mathcal{A}^{IJK}$ in Eq. (4.95) is proportional to $(N_{,A}N^{,A})$, whereas the f_{NL} term is multiplied to the square of that term. For models of interest here, in which the potential includes ridges, the gradient term is significant. For each of the three trajectories of Fig. 2, for example, $(N_{,A}N^{,A})=\mathcal{O}(10^3)$ across the full range $N_*=60$ to $N_*=40$. The gradient increases as the ratio of ξ_χ/ξ_ϕ increases, and hence the f_{NL} term will dominate the term coming from $\mathcal{A}^{IJK}$ whenever $|f_{NL}|>10^{-3}$.

For the term involving $\mathcal{R}^{IABJ;K}$ in Eq. (4.102), we may take advantage of the fact that for two-field models the Riemann tensor for the field space may be written

$$\mathcal{R}_{ABCD}=\mathcal{K}(\phi^I)\left[\mathcal{G}_{AC}\mathcal{G}_{BD}-\mathcal{G}_{AD}\mathcal{G}_{BC}\right], \tag{4.106}$$

where $\mathcal{K}(\phi^I)$ is the Gaussian curvature. In two dimensions, $\mathcal{K}(\phi^I) = \frac{1}{2}\mathcal{R}(\phi^I)$, where $\mathcal{R}$ is the Ricci scalar. Since $\mathcal{D}_K \mathcal{G}_{AB} = \mathcal{G}_{AB;K} = 0$ and $\mathcal{K}(\phi^I)$ is a scalar in the field space, the covariant derivative of the Riemann tensor is simply proportional to the ordinary (partial) derivative of the Gaussian curvature, $\mathcal{K}$. In particular, we find

$$\hat{\sigma}_A \hat{\sigma}_B N_{,I} N_{,J} N_{,K} \mathcal{R}^{IABJ;K} = -\left(\hat{s}^{IJ} N_{,I} N_{,J}\right)\left(N_{,K} \mathcal{K}^{,K}\right), \tag{4.107}$$

where $\hat{s}^{IJ} \equiv \mathcal{G}^{IJ} - \hat{\sigma}^I \hat{\sigma}^J$ is the projection operator for directions orthogonal to the adiabatic direction. We calculate $\mathcal{K}$ in Eq. (4.115). At early times, as the system undergoes slow-roll inflation, we have $\xi_\phi \phi^2 + \xi_\chi \chi^2 \gg M_{\rm pl}^2$. For the trajectories as in Fig. 2, moreover, the system evolves along a ridge such that $\xi_\phi \phi^2 \gg \xi_\chi \chi^2$. In that case, we find

$$\mathcal{K} \simeq \frac{1}{108 \xi_\phi^2 M_{\rm pl}^2}\left[1 + 6(\xi_\phi + \xi_\chi) + 36\xi_\phi(\xi_\chi - \xi_\phi)\right] \sim \phi^0,\ \chi^0, \tag{4.108}$$

and hence $\mathcal{K}^{,I} \sim 0$. Thus, in addition to being suppressed by the slow-roll factor, ϵ, the contribution to the primordial bispectrum from the $\mathcal{R}^{IABJ;K}$ term is negligible in typical scenarios of interest, because of the weak variation of the Gaussian curvature of the field-space manifold around the times $N_* = 60$ to $N_* = 40$ efolds before the end of inflation. This matches the behavior shown in Fig. 4-5: the field-space manifold is nearly flat until one reaches the vicinity of $\phi, \chi \sim 0$, near the end of inflation.

Though these results were derived in the equilateral limit, for which $k_1 = k_2 = k_3 = k_*$, we expect the same general pattern to apply more generally, for example, to the squeezed local configuration in which $k_1 \simeq k_2 = k_*$ and $k_3 \simeq 0$. As one departs from the equilateral limit the exact cancellations of Eqs. (4.99) and (4.105) no longer hold, though each of the components of the field-space Riemann tensor and its gradients remains small between $N_* = 60$ to $N_* = 40$ efolds before the end of inflation for models of the class we have been studying here. Meanwhile, the k-dependent functions, $f_{\mathcal{I}}(\mathbf{k}_i)$ in Eq. (4.87), remain of comparable magnitude to the k-dependent contribution in Eq. (4.91) [37] — each contributes as $[\mathcal{O}(1) - \mathcal{O}(10)] \times k^3$

— while the coefficients of the additional terms arising from $\mathcal{A}^{IJK}$, $\mathcal{B}^{IJK}$, $\mathcal{C}^{IJK}$, and $\mathcal{D}^{IJK}$ are further suppressed by factors of ϵ. For models of the class we have been studying here, we therefore expect the (covariant version of the) usual f_{NL} term to dominate the primordial bispectrum. Moreover, given the weak dependence of the Gaussian curvature $\mathcal{K}(\phi^I)$ with ϕ^I between $N_* = 60$ and $N_* = 40$, we do not expect any significant contributions to the running of f_{NL} with scale to come from the curvature of the field-space manifold, given the analysis in [38].

We calculate the magnitude of f_{NL} numerically, following the definition in Eq. (4.92). The discrete derivative of N along the ϕ direction is constructed as

$$N_{,\phi} = \frac{N(\phi + \Delta\phi, \chi) - N(\phi - \Delta\phi, \chi)}{2\Delta\phi}, \tag{4.109}$$

where $N(\phi, \chi)$ is the number of efolds between t_* and $t_{\rm end}$, where $t_{\rm end}$ is determined by the physical criterion that $\ddot{a} = 0$ (equivalent to $\epsilon = 1$). For each quantity, such as $N(\phi + \Delta\phi, \chi)$, we re-solve the exact background equations of motion numerically and measure how the small variation in field values at t_* affects the number of efolds of inflation between t_* and the time at which $\ddot{a} = 0$. The discrete derivatives along the other field directions and the second derivatives are constructed in a corresponding manner. Covariant derivatives are calculated using the discrete derivatives defined here and the field-space Christoffel symbols evaluated at background order. For the trajectories of interest, the fields violate slow-roll late in their evolution (after they have fallen off the ridge of the potential), but they remain slowly rolling around the time t_*; if they did not, as we saw in Section IV, then the predictions for the spectral index, $n_s(t_*)$ would no longer match observations. We therefore do not consider separate variations of the field velocities at the time t_*, since in the vicinity of t_* they are related to the field values. Because the second derivatives of N are very sensitive to the step sizes $\Delta\phi$ and $\Delta\chi$, we work with 32-digit accuracy, for which our numerical results converge for finite step-sizes in the range $\Delta\phi, \Delta\chi = \{10^{-6}, 10^{-5}\}$.

For the three trajectories of Fig. 4-2, we find the middle case, trajectory 2, yields a value of f_{NL} of particular interest: $|f_{NL}| = 43.3$ for fiducial scales k_* that first

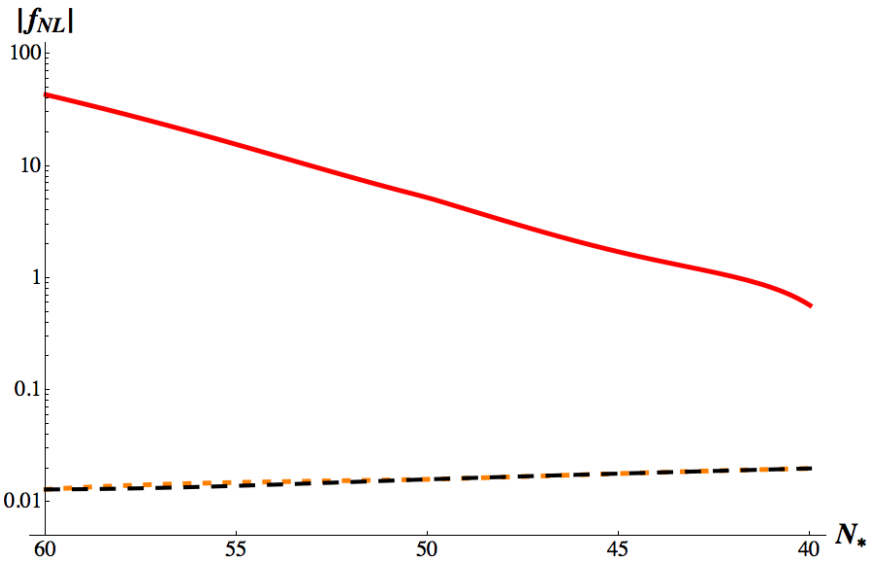

Figure 4-11: The non-Gaussianity parameter, $|f_{NL}|$, for the three trajectories of Fig. 4-2: trajectory 1 (orange dotted line); trajectory 2 (solid red line); and trajectory 3 (black dashed line). Changing the fields' initial conditions by a small amount leads to dramatic changes in the magnitude of the primordial bispectrum.

crossed the Hubble radius $N_* = 60$ efolds before the end of inflation. Note the strong sensitivity of f_{NL} to the fields' initial conditions: varying the initial value of $\chi(\tau_0)$ by just $|\Delta\chi(\tau_0)| = 10^{-3}$ changes the fields' evolution substantially — either causing the fields to roll off the hill too early (trajectory 1) or not to turn substantially in field space at all (trajectory 3) — both of which lead to negligible values for f_{NL}. See Fig. 4-11.

4.6 Conclusions

We have demonstrated that multifield models with nonminimal couplings generically produce the conditions required to generate primordial bispectra of observable magnitudes. Such models satisfy at least three of the four criteria identified in previous reviews of primordial non-Gaussianities [17, 15], namely, the presence of multiple fields with noncanonical kinetic terms whose dynamics temporarily violate slow-roll evolution.

Two distinct features are relevant in this class of models: the conformal stretching

of the effective potential in the Einstein frame, which introduces nontrivial curvature distinct from features in the Jordan-frame potential; and nontrivial curvature of the induced manifold for the field space in the Einstein frame. So long as the nonminimal couplings are not precisely equal to each other, the Einstein-frame potential will include bumps or ridges that will tend to cause neighboring trajectories of the fields to diverge over the course of inflation. Such features of the potential are generic to this class of models, and hence are strongly motivated by fundamental physics.

We have found that the curvature of the potential dominates the effects of interest at early and intermediate stages of inflation, whereas the curvature of the field-space manifold becomes important near the end of inflation (and hence during preheating). The generic nature of the ridges in the Einstein-frame potential removes one of the kinds of fine-tuning that have been emphasized in recent studies of non-Gaussianities in multifield models, namely, the need to introduce potentials of particular shapes [16, 29, 31, 32]. (We are presently performing an extensive sweep of parameter space to investigate how f_{NL} behaves as one varies the couplings ξ_I, λ_I, and m_I. This will help determine regions of parameter space consistent with current observations.) On the other hand, much as in [16, 29, 31, 32], we find a strong sensitivity of the magnitude of the bispectrum to the fields' initial conditions. Thus the production during inflation of bispectra with magnitude $|f_{NL}| \sim \mathcal{O}(50)$ requires fine-tuning of initial conditions such that the fields begin at or near the top of a ridge in the potential.

A subtle question that deserves further study is whether the formalism and results derived in this chapter show any dependence on frame. Although we have developed a formalism that is gauge-invariant with respect to spacetime gauge transformations, and covariant with respect to the curvature of the field-space manifold, we have applied the formalism only within the Einstein frame. The authors of [48] recently demonstrated that gauge-invariant quantities such as the curvature perturbation, ζ, can behave differently in the Jordan and Einstein frames for multifield models with nonminimal couplings. The question of possible frame-dependence of the analysis presented here remains under study. Whether quantities such as f_{NL} show significant evolution during reheating for this family of models, as has been emphasized for

related models [31, 58], likewise remains a subject of further research.

4.7 Acknowledgements

It is a great pleasure to thank Mustafa Amin, Bruce Bassett, Rhys Borchert, Xingang Chen, Joseph Elliston, Alan Guth, Carter Huffman, Francisco Peña, Katelin Schutz, and David Seery for helpful discussions. This work was supported in part by the U.S. Department of Energy (DoE) under contract No. DE-FG02-05ER41360 and in part by MIT's Undergraduate Research Opportunities Program.

4.8 Appendix

4.8.1 Field-Space Metric and Related Quantities

Given $f(\phi^I)$ in Eq. (4.17) for a two-field model, the field-space metric in the Einstein frame, Eq. (4.6), takes the form

$$\begin{aligned} \mathcal{G}_{\phi\phi} &= \left(\frac{M_{\rm pl}^2}{2f}\right)\left[1+\frac{3\xi_\phi^2\phi^2}{f}\right], \\ \mathcal{G}_{\phi\chi} = \mathcal{G}_{\chi\phi} &= \left(\frac{M_{\rm pl}^2}{2f}\right)\left[\frac{3\xi_\phi\xi_\chi\phi\chi}{f}\right], \\ \mathcal{G}_{\chi\chi} &= \left(\frac{M_{\rm pl}^2}{2f}\right)\left[1+\frac{3\xi_\chi^2\chi^2}{f}\right]. \end{aligned} \tag{4.110}$$

The components of the inverse metric are

$$\begin{aligned} \mathcal{G}^{\phi\phi} &= \left(\frac{2f}{M_{\rm pl}^2}\right)\left[\frac{2f+6\xi_\chi^2\chi^2}{C}\right], \\ \mathcal{G}^{\phi\chi} = \mathcal{G}^{\chi\phi} &= -\left(\frac{2f}{M_{\rm pl}^2}\right)\left[\frac{6\xi_\phi\xi_\chi\phi\chi}{C}\right], \\ \mathcal{G}^{\chi\chi} &= \left(\frac{2f}{M_{\rm pl}^2}\right)\left[\frac{2f+6\xi_\phi^2\phi^2}{C}\right], \end{aligned} \tag{4.111}$$

where we have defined the convenient combination

$$\begin{aligned} C(\phi,\chi) &\equiv M_{\rm pl}^2 + \xi_\phi(1+6\xi_\phi)\phi^2 + \xi_\chi(1+6\xi_\chi)\chi^2 \\ &= 2f + 6\xi_\phi^2\phi^2 + 6\xi_\chi^2\chi^2. \end{aligned} \tag{4.112}$$

The Christoffel symbols for our field space take the form

$$\begin{aligned} \Gamma^{\phi}_{\ \phi\phi} &= \frac{\xi_\phi(1+6\xi_\phi)\phi}{C} - \frac{\xi_\phi\phi}{f}, \\ \Gamma^{\phi}_{\ \chi\phi} = \Gamma^{\phi}_{\ \phi\chi} &= -\frac{\xi_\chi\chi}{2f}, \\ \Gamma^{\phi}_{\ \chi\chi} &= \frac{\xi_\phi(1+6\xi_\chi)\phi}{C}, \\ \Gamma^{\chi}_{\ \phi\phi} &= \frac{\xi_\chi(1+6\xi_\phi)\chi}{C}, \\ \Gamma^{\chi}_{\ \phi\chi} = \Gamma^{\chi}_{\ \chi\phi} &= -\frac{\xi_\phi\phi}{2f}, \\ \Gamma^{\chi}_{\ \chi\chi} &= \frac{\xi_\chi(1+6\xi_\chi)\chi}{C} - \frac{\xi_\chi\chi}{f} \end{aligned} \tag{4.113}$$

For two-dimensional manifolds we may always write the Riemann tensor in the form

$$\mathcal{R}_{ABCD} = \mathcal{K}(\phi^I)\left[\mathcal{G}_{AC}\mathcal{G}_{BD} - \mathcal{G}_{AD}\mathcal{G}_{BC}\right], \tag{4.114}$$

where $\mathcal{K}(\phi^I)$ is the Gaussian curvature. In two dimensions, $\mathcal{K}(\phi^I) = \frac{1}{2}\mathcal{R}(\phi^I)$, where $\mathcal{R}(\phi^I)$ is the Ricci scalar. Given the field-space metric of Eq. (4.110), we find

$$\mathcal{R}(\phi^I) = 2\mathcal{K}(\phi^I) = \frac{2}{3M_{\rm pl}^2C^2}\left[(1+6\xi_\phi)(1+6\xi_\chi)(4f^2) - C^2\right]. \tag{4.115}$$

Bibliography

[1] A. H. Guth and D. I. Kaiser, "Inflationary cosmology: Exporing the universe from the smallest to the largest scales," Science **307**,884 (2005) [arXiv:astro-ph/0502328].

[2] E. Komatsu et al. [WMAP collaboration], "Seven-year Wilkinson Microwave Anisotropy Probe (WMAP) observations: Cosmological interpretation," Astrophy. J. Suppl. **192**, 18 (2011) [arXiv:1001.4538 [astro-ph.CO]].

[3] G. Hinshaw et al. [WMAP collaboration], "Nine-year Wilkinson Microwave Anisotropy Probe (WMAP) observations: Cosmological parameter results," arXiv:1212.5226 [astro-ph.CO].

[4] D. H. Lyth and A. Riotto, "Particle physics models of inflation and the cosmological density perturbation," Phys. Rept. **314**, 1 (1999) [arXiv:hep-ph/9807278].

[5] A. Mazumdar and J. Rocher, "Particle physics models of inflation and curvaton scenarios," Phys. Rept. **497**, 85 (2011) [arXiv:1001.0993 [hep-ph]].

[6] Y. Nambu and A. Taruya, "Evolution of cosmological perturbation in reheating phase of the universe," Prog. Theor. Phys. 97 (1997): 83 [arXiv:gr-qc/9609029]; B. A. Bassett, D. I. Kaiser, and R. Maartens, "General relativistic effects in preheating," Phys. Lett. B455 (1999): 84 [arXiv:hep-ph/9808404]; F. Finelli and R. Brandenberger, "Parametric amplification of gravitational fluctuations during reheating," Phys. Rev. Lett. 82 (1999): 1362 [arXiv:hep-ph/9809490]; B. A. Bassett, F. Tamburini, D. I. Kaiser, and R. Maartens, "Metric preheating

and limitations of linearized gravity," Nucl. Phys. B561 (1999): 188 [arXiv:hep-ph/9901319]; B. A. Bassett, C. Gordon, R. Maartens, and D. I. Kaiser, "Restoring the sting to metric preheating," Phys. Rev. D61 (2000): 061302 [arXix:hep-ph/9909482]; S. Tsujikawa and B. A. Bassett, "A new twist to preheating," Phys. Rev. D62 (2000): 043510 [arXiv:hep-ph/0003068]; F. Finelli and R. Brandenberger, "Parametric amplification of metric fluctuations during reheating in two field models," Phys. Rev. D62 (2000): 0833502 [arXiv:hep-ph/0003172]; S. Tsujikawa and B. A. Bassett, "When can preheating affect the CMB?," Phys. Lett. B536 (2002): 9 [arXiv:astro-ph/0204031].

[7] C. Gordon, D. Wands, B. A. Bassett, and R. Maartens, "Adiabatic and entropy perturbations from inflation," Phys. Rev. **D63**, 023506 (2001) [arXiv:astro-ph/0009131].

[8] S. Groot Nibbelink and B. J. W. van Tent, "Density perturbations arising from multiple field slow-roll inflation," arXiv:hep-ph/0011325; "Scalar perturbations during multiple-field slow-roll inflation," Class. Quant. Grav. **19**, 613 (2002) [arXiv:hep-ph/0107272].

[9] R. Easther and J. T. Giblin, "The Hubble slow roll expansion for multi field inflation," Phys. Rev. D72 (2005): 103505 [arXiv:astro-ph/0505033].

[10] F. Di Marco, F. Finelli, and R. Brandenberger, "Adiabatic and isocurvature perturbations for multifield generalized Einstein models," Phys. Rev. **D67**, 063512 (2003) [arXiv:astro-ph/0211276].

[11] B. A. Bassett, S. Tsujikawa, and D. Wands, "Inflation dynamics and reheating," Rev. Mod. Phys. 78 (2006): 537 [arXiv:astro-ph/0507632].

[12] K. A. Malik and D. Wands, "Cosmological perturbations," Phys. Rept. **475**, 1 (2009) [arXiv:0809.4944 [astro-ph]].

[13] D. Wands, "Multiple field inflation," Lect. Notes. Phys. **738**, 275 (2008) [arXiv:astro-ph/0702187].

[14] N. Bartolo et al., "Non-Gaussianity from inflation: Theory and observations," Phys. Rept. **402**, 103 (2004) [arXiv:astro-ph/0406398].

[15] X. Chen, "Primordial non-Gaussianities from inflation models," Adv. Astron. **2010**, 638979 (2010) [arXiv:1002.1416 [astro-ph]].

[16] C. T. Byrnes and K.-Y. Choi, "Review of local non-Gaussianity from multi-field inflation," Adv. Astron. 2010, 724525 (2010) [arXiv:1002.3110 [astro-ph.CO]].

[17] E. Komatsu et al., "Non-Gaussianity as a probe of the physics of the primordial universe and the astrophysics of the low redshift universe," arXiv:0902:4759 [astro-ph.CO].

[18] C. G. Callan, Jr., S. R. Coleman, and R. Jackiw, "A new improved energy-momentum tensor," Annals Phys. 59 (1970): 42-73.

[19] T. S. Bunch, P. Panangaden, and L. Parker, "On renormalisation of $\lambda\phi^4$ field theory in curved space-time, I," J. Phys. A 13 (1980): 901-918; T. S. Bunch and P. Panangaden, "On renormalisation of $\lambda\phi^4$ field theory in curved space-time, II," J. Phys. A (1980): 919-932.

[20] N. D. Birrell and P. C. W. Davies, *Quantum Fields in Curved Space* (New York: Cambridge University Press, 1982).

[21] I. L. Buchbinder, S. D. Odintsov, and I. L. Shapiro, *Effective Action in Quantum Gravity* (New York: Taylor and Francis, 1992).

[22] Y. Fujii and K. Maeda, *The Scalar-Tensor Theory of Gravitation* (New York: Cambridge University Press, 2003).

[23] V. Faraoni, *Cosmology in Scalar-Tensor Gravity* (Boston: Kluwer, 2004).

[24] T. Qiu and K.-C. Yang, "Non-Gaussianities in single field inflation with non-minimal coupling," Phys. Rev. D83 (2011): 084022 [arXiv:1012.1697 [hep-th]].

[25] D. I. Kaiser, "Conformal transformations with multiple scalar fields," Phys. Rev. **D81**, 084044 (2010) [arXiv:1003.1159 [gr-qc]].

[26] F. Bernardeau and J-P. Uzan, "Non-Gaussianity in multi-field inflation," Phys. Rev. D66 (2002): 103506 [arXiv:hep-ph/0207295]; F. Bernardeau and J-P Uzan, "Inflationary models inducing non-Gaussian metric fluctuations," Phys. Rev. D67 (2003): 121301 [arXiv:astro-ph/0209330].

[27] D. Langlois and S. Renaux-Petel, "Perturbations in generalized multi-field inflation," JCAP **0804** (2008): 017 [arXiv:0801.1085 [hep-th]].

[28] D. Seery and J. E. Lidsey, "Primordial non-Gaussianities from multiple-field inflation," JCAP 0509 (2005): 011 [arXiv:astro-ph/0506056].

[29] S. Yokoyama, T. Suyama, and T. Tanaka, "Primordial non-Gaussianity in multi-scalar slow-roll inflation," JCAP 0707 (2007): 013 [arXiv:0705.3178 [astro-ph]; S. Yokoyama, T. Suyama, and T. Tanaka, "Primordial non-Gaussianity in multi-scalar inflation," Phys. Rev. D77 (2008): 083511 [arXiv:0711.2920 [astro-ph]].

[30] C. T. Byrnes, K-Y Choi, and L. M. H. Hall, "Conditions for large non-Gaussianity in two-field slow-roll inflation," JCAP 0810 (2008): 008 [arXiv:0807.1101 [astro-ph]].

[31] J. Ellison, D. J. Mulryne, D. Seery, and R. Tavakol, "Evolution of f_{NL} to the adiabatic limit," JCAP 1111 (2011): 005 [arXiv:1106.2153 [astro-ph.CO]]; D. Seery, D. J. Mulryne, J. Frazer, and R. H. Ribeiro, "Inflationary perturbation theory is geometrical optics in phase space," JCAP 09 (2012): 010 [arXiv:1203.2635 [astro-ph.CO]].

[32] C. M. Peterson and M. Tegmark, "Testing two-field inflation," Phys. Rev. **D83**, 023522 (2011) [arXiv:1005.4056 [astro-ph.CO]]; "Non-Gaussianity in two-field inflation," Phys. Rev. **D84**, 023520 (2011) [arXiv:1011.6675 [astro-ph.CO]]; "Testing multi-field inflation: A geometric approach," arXiv:1111.0927 [astro-ph.CO].

[33] J. O. Gong and H. M. Lee, "Large non-Gaussianity in non-minimal inflation," JCAP 1111 (2011): 040 [arXiv:1105.0073 [hep-ph]];

[34] A. Mazumdar and L. Wang, "Separable and non-separable multi-field inflation and large non-Gaussianity," JCAP 09 (2012): 005 [arXiv:1203.3558 [astro-ph]].

[35] D. Wands, K. A. Malik, D. H. Lyth, and A. R. Liddle, "A new approach to the evolution of cosmological perturbations on large scales," Phys. Rev. D62 (2000): 043527 [arXiv:astro-ph/0003278]; L. Amendola, C. Gordon, D. Wands, and M. Sasaki, "Correlated perturbations from inflation and the cosmic microwave background," Phys. Rev. Lett. 88 (2002): 211302 [arXiv:astro-ph/0107089]; D. Wands, N. Bartolo, S. Matarrese, and A. Riotto, "An observational test of two-field inflation," Phys. Rev. D66 (2002): 043520 [arXiv:astro-ph/0205253].

[36] J.-O. Gong and T. Tanaka, "A covariant approach to general field space metric in multi-field inflation," JCAP 1103 (2011): 015 [arXiv:1101.4809 [astro-ph.CO]].

[37] J. Elliston, D. Seery, and R. Tavakol, "The inflationary bispectrum with curved field-space," arXiv:1208.6011 [astro-ph.CO].

[38] C. T. Byrnes and J.-O. Gong, "General formula for the running of f_{NL}," arXiv:1210.1851 [astro-ph.CO].

[39] D. S. Salopek, J. R. Bond, and J. M. Bardeen, "Designing density fluctuation spectra in inflation," Phys. Rev. **D40**, 1753 (1989).

[40] V. F. Mukhanov, H. A. Feldman, and R. H. Brandenberger, "Theory of cosmological perturbations," Phys. Rept. **215**, 203 (1992).

[41] F. L. Bezrukov and M. E. Shaposhnikov, "The Standard Model Higgs boson as the inflaton," Phys. Lett. **B659**, 703 (2008) [arXiv:0710.3755 [hep-th]].

[42] A. de Simone, M. P. Hertzberg, and F. Wilczek, "Running inflation in the Standard Model," Phys. Lett. B678 (2009): 1-8 [arXiv:0812.4946 [hep-ph]]; F. L.

Bezrukov, A. Magnin, and M. E. Shaposhnikov, "Standard Model Higgs boson mass from inflation," Phys. Lett. B675 (2009): 88-92 [arXiv:0812.4950 [hep-ph]]; F. L. Bezrukov and M. E. Shaposhnikov, "Standard Model Higgs boson mass from inflation: two loop analysis," JHEP 0907 (2009): 089 [arXiv:0904.1537 [hep-ph]]; A. O. Barvinsky, A. Yu. Kamenshchik, C. Kiefer, A. A. Starobinsky, C. Steinwachs, "Asymptotic freedom in inflationary cosmology with a non-minimally coupled Higgs field," JCAP 0912 (2009): 003 [arXiv:0904.1698 [hep-ph]].

[43] R. N. Greenwood, D. I. Kaiser, and E. I. Sfakianakis, "Multifield dynamics of Higgs inflation," arXiv:1210.8190 [hep-ph].

[44] The leading behavior of Eq. (4.19) in the limit $\xi_\phi \phi^2 \gg M_{\rm pl}^2$ is unchanged if we calculate the curvature of the potential using the covariant derivative for the field-space, $(\mathcal{D}_\chi^2 V)_{|\chi=0}$, where $\mathcal{D}_I$ is defined in Eq. (4.21).

[45] X. Chen, "Primordial features as evidence for inflation," arXiv:1104.1323 [hep-th]; X. Chen, "Fingerprints of primordial universe paradigms as features in density perturbations," arXiv:1106.1635 [astro-ph.CO].

[46] J. Silk and M. S. Turner, "Double inflation," Phys. Rev. D 35 (1987): 419-428; M. S. Turner, J. V. Villumsen, N. Vittorio, J. Sil, and R. Juszkiewicz, "Double inflation: A possible resolution of the large scale structure problem," Astrophys. J. 323 (1987): 423-432; D. Polarski and A. A. Starobinsky, "Spectra of perturbations produced by double inflation with an intermediate matter dominated stage," Nucl. Phys. B385 (1992): 623; D. Polarski and A. A. Starobinsky, "Structure of primordial gravitational waves spectrum in a double inflationary model," Phys. Lett. B356 (1995): 196 [arXiv:astro-ph/9505125].

[47] D. I. Kaiser and A. T. Todhunter, "Primordial perturbations from multi-field inflation with nonminimal couplings," Phys. Rev. **D81**, 124037 (2010) [arXiv:1004.3805 [astro-ph.CO]].

[48] J. White, M. Minamitsuji, and M. Sasaki, "Cosmological perturbation in multi-field inflation with non-minimal coupling," arXiv:1205.0656 [astro-ph.CO].

[49] R. W. Wald, *General Relativity* (Chicago: University of Chicago Press, 1984).

[50] D. I. Kaiser, "Primordial spectral indices from generalized Einstein theories," Phys. Rev. D52 (1995): 4295 [arXiv:astro-ph/9408044].

[51] Because the field fluctuations at time t_1 live in a different tangent space to the field-space manifold than do the fluctuations at time t_2, the authors of [37] introduce propagators and related transport functions to translate between quantities in the two distinct tangent spaces, building on previous work in [52]. Since the two tangent spaces coincide in the limit $t_2 \to t_1$, the propagators reduce to the identity matrix in that limit. What matters in our discussion is the symmetry structure of the various terms in Eq. (4.86), which should hold at any time, hence we evaluate the three-point function at time t_*.

[52] G. J. Anderson, D. J. Mulryne, and D. Seery, "Transport equations for the inflationary trispectrum," arXiv:1205.0024 [astro-ph.CO].

[53] M. Sasaki and E. D. Stewart, "A general analytic formula for the spectral index of the density perturbations produced during inflation," Prog. Theo. Phys. **95**, 71 (1996) [arXiv:astro-ph/9507001].

[54] D. H. Lyth, K. A. Malik, and M. Sasaki, "A general proof of the conservation of the curvature perturbation," JCAP 0505 (2005): 004 [arXiv:astro-ph/0411220].

[55] H.-C. Lee, M. Sasaki, E. D. Stewart, T. Tanaka, and S. Yokoyama, "A new delta N formalism for multi-component inflation," JCAP 0510 (2005): 004 [arXiv:astro-ph/0506262].

[56] D. H. Lyth and Y. Rodriguez, "The inflationary prediction for primordial non-Gaussianity," Phys. Rev. Lett. 95 (2005): 121302 [arXiv:astro-ph/0504045].

[57] We are especially indebted to Joseph Elliston for helpful discussions on this point.

[58] G. Leung, E. R. M. Tarrant, C. T. Byrnes, and E. J. Copeland, "Reheating, multifield inflation and the fate of primordial observables," JCAP 09 (2012): 008 [arXiv:1206.5196 [astro-ph.CO]].

Chapter 5

Multifield Dynamics of Higgs Inflation

Higgs inflation is a simple and elegant model in which early-universe inflation is driven by the Higgs sector of the Standard Model. The Higgs sector can support early-universe inflation if it has a large nonminimal coupling to the Ricci spacetime curvature scalar. At energies relevant to such an inflationary epoch, the Goldstone modes of the Higgs sector remain in the spectrum in renormalizable gauges, and hence their effects should be included in the model's dynamics. We analyze the multifield dynamics of Higgs inflation and find that the multifield effects damp out rapidly after the onset of inflation, because of the gauge symmetry among the scalar fields in this model. Predictions from Higgs inflation for observable quantities, such as the spectral index of the power spectrum of primordial perturbations, therefore revert to their familiar single-field form, in excellent agreement with recent measurements. The methods we develop here may be applied to any multifield model with nonminimal couplings in which the $\mathcal{N}$ fields obey an $SO(\mathcal{N})$ symmetry in field space.

5.1 Introduction

The recent discovery at CERN of a scalar boson with Higgs-like properties [1] heightens the question of whether the Standard Model Higgs sector could have played inter-

esting roles in the early universe, at energies well above the electroweak symmetry-breaking scale. In particular, the suggestive evidence for the Higgs boson raises the possibility to return to an original motivation for cosmological inflation, namely, to realize a phase of early-universe acceleration driven by a scalar field that is part of a well-motivated model from high-energy particle physics [2, 3, 4].

Higgs inflation [5] represents an elegant approach to building a workable inflationary model based on realistic ingredients from particle physics. In this model, a large nonminimal coupling of the Standard Model electroweak Higgs sector drives a phase of early-universe inflation. Such nonminimal couplings are generic: they arise as necessary renormalization counterterms for scalar fields in curved spacetime [6, 7, 8, 9]. Moreover, renormalization-group analyses indicate that for models with matter akin to the Standard Model, the nonminimal coupling, ξ, should grow without bound with increasing energy scale [9]. Previous analyses of Higgs inflation have found that ξ typically grows by at least an order of magnitude between the electroweak symmetry-breaking scale and the inflationary scale [10, 11, 12].

The Standard Model Higgs sector includes four scalar degrees of freedom: the (real) Higgs scalar and three Goldstone modes. In renormalizable gauges, all four scalar fields remain in the spectrum at high energies [13, 14, 12, 16, 17]. Thus the dynamics of Higgs inflation should be studied as a multifield model with nonminimal couplings. An important feature of multifield models, which is absent in single-field models, is that the fields' trajectories can turn within field space as the system evolves. Such turns are a necessary (but not sufficient) condition for multifield models to depart from the empirical predictions of simple single-field models [18, 19, 20, 21, 22, 23, 24].

In this chapter we analyze the background dynamics of Higgs inflation, in which all four scalar fields of the Standard Model electroweak Higgs sector have nonminimal couplings. We find that multifield dynamics damp out quickly after the onset of inflation, before perturbations on cosmologically relevant length scales first cross the Hubble radius. As regards observable quantities like the power spectrum of primordial perturbations, the model therefore behaves effectively as a single-field model. The

multifield dynamics remain subdominant in Higgs inflation because of the particular symmetries of the Higgs sector. Closely related models, which lack those symmetries, can produce conspicuous departures from the single-field case [24].

We are principally interested here in the behavior of classical background fields and long-wavelength perturbations, which behave essentially classically. Therefore we bracket, for this analysis, the question of the unitarity of Higgs inflation. Conflicting conclusions have been advanced regarding whether the appropriate renormalization cut-off scale for this model should be $M_{\rm pl}$, $M_{\rm pl}/\sqrt{\xi}$, or $M_{\rm pl}/\xi$, where $M_{\rm pl} \equiv (8\pi G)^{-1/2}$ is the reduced Planck mass [14, 15, 12, 16, 25]. Even if Higgs inflation might conclusively be shown to violate unitarity, the techniques developed here for the analysis of multifield dynamics will be relevant for related models that incorporate multiple scalar fields with nonminimal couplings and symmetries (such as gauge symmetries) that enforce specific relations among the couplings of the model. In particular, we expect that multifield effects in models with $\mathcal{N}$ scalar fields, in which the scalar fields obey an $SO(\mathcal{N})$ symmetry, should damp out rapidly.

In Section II, we briefly introduce the multifield formalism and establish notation. We apply the formalism to Higgs inflation in Section III, and in Section IV we analyze the behavior of the turn-rate, which quantifies the rate at which the background trajectory of the system deviates from a single-field case. We study how quickly the turn-rate damps to zero, both analytically and numerically, confirming that for Higgs inflation the turn-rate becomes negligible within a few efolds after the start of inflation. In Section V we turn to implications for observable features of the primordial power spectrum, confirming that multifield Higgs inflation reproduces the empirical predictions of previous single-field studies. Concluding remarks follow in Section VI.

5.2 Multifield Dynamics

Following the approach established in [24], we consider models with $\mathcal{N}$ scalar fields in $(3 + 1)$ spacetime dimensions. We use Greek letters to label spacetime indices,

$\mu, \nu = 0, 1, 2, 3$; lower-case Latin letters to label spatial indices, $i, j = 1, 2, 3$; and upper-case Latin letters to label field-space indices, $I, J = 1, 2, ..., \mathcal{N}$. We also work in terms of the reduced Planck mass, $M_{\rm pl} \equiv (8\pi G)^{-1/2}$. In the Jordan frame, the action takes the form

$$S_{\rm Jordan} = \int d^4x\sqrt{-\tilde{g}}\left[f(\phi^I)\tilde{R} - \frac{1}{2}\delta_{IJ}\tilde{g}^{\mu\nu}\partial_\mu\phi^I\partial_\nu\phi^J - \tilde{V}(\phi^I)\right]. \tag{5.1}$$

Here $f(\phi^I)$ is the nonminimal coupling function, and we use tildes for quantities in the Jordan frame. We perform a conformal transformation to the Einstein frame by rescaling the spacetime metric tensor,

$$g_{\mu\nu}(x) = \frac{2}{M_{\rm pl}^2} f(\phi^I(x))\, \tilde{g}_{\mu\nu}(x), \tag{5.2}$$

so that the action in the Einstein frame becomes [26]

$$S_{\rm Einstein} = \int d^4x\sqrt{-g}\left[\frac{M_{\rm pl}^2}{2}R - \frac{1}{2}\mathcal{G}_{IJ}g^{\mu\nu}\partial_\mu\phi^I\partial_\nu\phi^J - V(\phi^I)\right]. \tag{5.3}$$

The potential in the Einstein frame, V, is related to the Jordan-frame potential, $\tilde{V}$, as

$$V(\phi^I) = \frac{M_{\rm pl}^4}{4f^2(\phi^I)}\tilde{V}(\phi^I), \tag{5.4}$$

and the coefficients of the noncanonical kinetic terms are [27, 26]

$$\mathcal{G}_{IJ}(\phi^K) = \frac{M_{\rm pl}^2}{2f(\phi^I)}\left[\delta_{IJ} + \frac{3}{f(\phi^I)}f_{,I}f_{,J}\right], \tag{5.5}$$

where $f_{,I} = \partial f/\partial\phi^I$. The nonminimal couplings induce a field-space manifold in the Einstein frame that is not conformal to flat; $\mathcal{G}_{IJ}$ serves as a metric on the curved manifold [26]. Therefore we adopt the covariant approach of [24], which respects the curvature of the field-space manifold.

Varying Eq. (5.3) with respect to ϕ^I yields the equation of motion,

$$\Box\phi^I + g^{\mu\nu}\Gamma^I_{\ JK}\partial_\mu\phi^J\partial_\nu\phi^K - \mathcal{G}^{IK}V_{,K} = 0, \tag{5.6}$$

where $\Box\phi^I \equiv g^{\mu\nu}\phi^I{}_{;\mu;\nu}$ and $\Gamma^I{}_{JK}(\phi^L)$ is the Christoffel symbold for the field-space manifold, calculated in terms of $\mathcal{G}_{IJ}$. We expand each scalar field to first order around its classical background value,

$$\phi^I(x^\mu) = \varphi^I(t) + \delta\phi^I(x^\mu), \tag{5.7}$$

and also expand the scalar degrees of freedom of the spacetime metric to first order around a spatially flat Friedmann-Robertson-Walker (FRW) metric [28, 29, 30]

$$ds^2 = -(1+2A)dt^2 + 2a(\partial_i B)dx^i dt + a^2\left[(1-2\psi)\delta_{ij} + 2\partial_i\partial_j E\right]dx^i dx^j, \tag{5.8}$$

where $a(t)$ is the scale factor. We further introduce a covariant derivative with respect to the field-space metric and a directional derivative along the background fields' trajectory, such that for any vector A^I in the field-space manifold we have

$$\begin{aligned} \mathcal{D}_J A^I &= \partial_J A^I + \Gamma^I{}_{JK}A^K, \\ \mathcal{D}_t A^I &\equiv \dot\varphi^J \mathcal{D}_J A^I = \dot A^I + \Gamma^I{}_{JK}A^J\dot\varphi^K, \end{aligned} \tag{5.9}$$

where overdots denote derivatives with respect to cosmic time, t.

To background order, Eq. (5.6) becomes

$$\mathcal{D}_t\dot\varphi^I + 3H\dot\varphi^I + \mathcal{G}^{IK}V_{,K} = 0, \tag{5.10}$$

where all quantities involving $\mathcal{G}_{IJ}(\phi^K)$, $V(\phi^I)$, and their derivatives are evaluated at background order in the fields: $\mathcal{G}_{IJ} \to \mathcal{G}_{IJ}(\varphi^K)$ and $V \to V(\varphi^I)$. Following [18] we distinguish between adiabatic and entropic directions in field space by introducing a unit vector

$$\hat\sigma^I \equiv \frac{\dot\varphi^I}{\dot\sigma}, \tag{5.11}$$

where

$$\dot\sigma \equiv |\dot\varphi^I| = \sqrt{\mathcal{G}_{IJ}\dot\varphi^I\dot\varphi^J}. \tag{5.12}$$

The operator

$$\hat{s}^{IJ} \equiv \mathcal{G}^{IJ} - \hat{\sigma}^I \hat{\sigma}^J \tag{5.13}$$

projects onto the subspace orthogonal to $\hat{\sigma}^I$. Eq. (5.10) then simplifies to

$$\ddot{\sigma} + 3H\dot{\sigma} + V_{,\sigma} = 0 \tag{5.14}$$

where

$$V_{,\sigma} \equiv \hat{\sigma}^I V_{,I}. \tag{5.15}$$

The background dynamics likewise take the simple form

$$\begin{aligned} H^2 &= \frac{1}{3M_{\rm pl}^2}\left[\frac{1}{2}\dot{\sigma}^2 + V\right], \\ \dot{H} &= -\frac{1}{2M_{\rm pl}^2}\dot{\sigma}^2, \end{aligned} \tag{5.16}$$

where $H \equiv \dot{a}/a$ is the Hubble parameter.

We may also separate the perturbations into adiabatic and entropic directions. Working to first order in perturbations, we introduce the gauge-invariant Mukhanov-Sasaki variables [28, 29, 30, 31]

$$Q^I \equiv \delta\phi^I + \frac{\dot{\varphi}^I}{H}\psi \tag{5.17}$$

and the projections

$$\begin{aligned} Q_\sigma &\equiv \hat{\sigma}_I Q^I, \\ \delta s^I &\equiv \hat{s}^I{}_J Q^J. \end{aligned} \tag{5.18}$$

The gauge-invariant curvature perturbation may be defined as $\mathcal{R}_c \equiv \psi - [H/(\rho+p)]\delta q$, where the perturbed energy-momentum flux is given by $T^0_i = \partial_i \delta q$ [29, 30]. We then find that $\mathcal{R}_c$ is proportional to Q_σ [24]

$$\mathcal{R}_c = \frac{H}{\dot{\sigma}} Q_\sigma. \tag{5.19}$$

Expanding Eq. (5.6) to first order and using the projections of Eq. (5.18), the perturbations Q_σ and δs^I obey [24]

$$\begin{aligned}\ddot{Q}_\sigma + 3H\dot{Q}_\sigma + \left[\frac{k^2}{a^2} + \mathcal{M}_{\sigma\sigma} - \omega^2 - \frac{1}{M_{\rm pl}^2 a^3}\frac{d}{dt}\left(\frac{a^3\dot{\sigma}^2}{H}\right)\right] Q_\sigma \\ = 2\frac{d}{dt}\left(\omega_J \delta s^J\right) - 2\left(\frac{V_{,\sigma}}{\dot{\sigma}} + \frac{\dot{H}}{H}\right)\left(\omega_J \delta s^J\right)\end{aligned} \tag{5.20}$$

and

$$\begin{aligned}\mathcal{D}_t^2 \delta s^I + \left[3H\delta^I{}_J + 2\hat{\sigma}^I \omega_J\right]\mathcal{D}_t \delta s^I + \left[\frac{k^2}{a^2}\delta^I{}_J + \mathcal{M}^I{}_J - 2\hat{\sigma}^I\left(\mathcal{M}_{\sigma J} + \frac{\ddot{\sigma}}{\dot{\sigma}}\omega_J\right)\right]\delta s^J \\ = -2\omega^I\left[\dot{Q}_\sigma + \frac{\dot{H}}{H}Q_\sigma - \frac{\ddot{\sigma}}{\dot{\sigma}}Q_\sigma\right],\end{aligned} \tag{5.21}$$

where the mass-squared matrix is

$$\begin{aligned}\mathcal{M}^I{}_J &\equiv \mathcal{G}^{IK}\left(\mathcal{D}_J\mathcal{D}_K V\right) - \mathcal{R}^I{}_{LMJ}\dot{\varphi}^L\dot{\varphi}^M, \\ \mathcal{M}_{\sigma J} &\equiv \hat{\sigma}_I \mathcal{M}^I{}_J, \;\; \mathcal{M}_{\sigma\sigma} \equiv \hat{\sigma}_I\hat{\sigma}^J\mathcal{M}^I{}_J.\end{aligned} \tag{5.22}$$

The turn-rate [23, 24] is given by

$$\omega^I \equiv \mathcal{D}_t\hat{\sigma}^I = -\frac{1}{\dot{\sigma}}V_{,K}\hat{s}^{IK}, \tag{5.23}$$

and $\omega \equiv |\omega^I|$. Eqs. (5.20) and (5.21) decouple if the turn-rate vanishes, $\omega^I = 0$. In that case, Q_σ evolves just as in the single-field case [28, 29, 30, 23, 24]. Given Eq. (5.19), that means that the power spectrum of primordial perturbations, $\mathcal{P}_\mathcal{R}$, would also evolve as in single-field models. Thus a necessary (but not sufficient) condition for multifield models of this form to deviate from the empirical predictions of simple single-field models is for the turn-rate to be nonnegligible for some duration of the fields' evolution, $\omega^I \neq 0$.

5.3 Application to Higgs Inflation

The matter contribution to Higgs inflation [5] consists of the Standard Model electroweak Higgs sector, which may be written as a doublet of complex scalar fields,

$$h = \begin{pmatrix} h^+ \\ h^0 \end{pmatrix}. \tag{5.24}$$

The complex fields h^+ and h^0 may be further decomposed into (real) scalar degrees of freedom,

$$\begin{aligned} h^+ &= \frac{1}{\sqrt{2}}\left(\chi^1 + i\chi^2\right), \\ h^0 &= \frac{1}{\sqrt{2}}\left(\phi + i\chi^3\right), \end{aligned} \tag{5.25}$$

where ϕ is the Higgs scalar and χ^a (with $a = 1, 2, 3$) are the Goldstone modes. In the Jordan frame, the potential $\tilde{V}(\phi^I)$ depends only on the combination

$$h^\dagger h = \frac{1}{2}\left[\phi^2 + \boldsymbol{\chi}^2\right], \tag{5.26}$$

where $\boldsymbol{\chi} = (\chi^1, \chi^2, \chi^3)$ is a 3-vector of the Goldstone fields. In particular, the symmetry-breaking potential may be written

$$\tilde{V}(\phi^I) = \frac{\lambda}{4}\left(\phi^2 + \boldsymbol{\chi}^2 - v^2\right)^2, \tag{5.27}$$

in terms of the vacuum expectation value, v. For the Standard Model, $v = 246$ GeV $\ll M_{\rm pl}$. For Higgs inflation, the nonminimal coupling function is given by

$$f(\phi^I) = \frac{M_0^2}{2} + \xi h^\dagger h = \frac{1}{2}\left[M_0^2 + \xi\left(\phi^2 + \boldsymbol{\chi}^2\right)\right], \tag{5.28}$$

where $M_0^2 \equiv M_{\rm pl}^2 - \xi v^2$ and $\xi > 0$ is the dimensionless nonminimal coupling constant. In Higgs inflation, we take $\xi \sim \mathcal{O}(10^4)$ [5], and therefore we may safely set $M_0^2 = M_{\rm pl}^2$. In the Einstein frame, the potential gets stretched by the nonminimcal coupling

function $f(\phi^I)$ according to Eq. (5.4). Given Eqs. (5.27) and (5.28), this yields

$$V(\phi^I) = \frac{\lambda M_{\rm pl}^4 \left(\phi^2 + \boldsymbol{\chi}^2 - v^2\right)^2}{4\left[M_{\rm pl}^2 + \xi\left(\phi^2 + \boldsymbol{\chi}^2\right)\right]^2}. \tag{5.29}$$

The model is thus symmetric under rotations among ϕ and χ^a that preserve the magnitude $\sqrt{\phi^2 + \boldsymbol{\chi}^2}$. When written in the "Cartesian" field-space basis of Eq. (5.25), in other words, the $SU(2)$ electroweak gauge symmetry manifests as an $SO(4)$ spherical symmetry in field space.

For any model with $\mathcal{N}$ real-valued scalar fields that respects an $SO(\mathcal{N})$ symmetry, the background dynamics depend on just three initial conditions: the initial magnitude and initial velocity along the radial direction in field space, and the initial velocity perpendicular to the radial direction. Without loss of generality, therefore, we may analyze the background dynamics of Higgs inflation in terms of just two real-valued scalar fields, ϕ and χ, and we may set $\chi(0) = 0$, specifying only initial values for $\phi(0)$, $\dot{\phi}(0)$, and $\dot{\chi}(0)$. This reduction in the effective number of degrees of freedom stems entirely from the gauge symmetry of the Standard Model electroweak sector. The remaining dependence on $\dot{\chi}$, meanwhile, distinguishes the background dynamics from a genuinely single-field model, in which one neglects the Goldstone fields altogether. For the remainder of this chapter, we exploit the gauge symmetry to consider only a single Goldstone mode, $\boldsymbol{\chi} \to \chi$, reducing the problem to that of a two-field model. Then $f(\phi^I)$ and $V(\phi^I)$ depend on the background fields only in the combination

$$r \equiv \sqrt{\phi^2 + \chi^2}. \tag{5.30}$$

Previous analyses [5, 27, 32, 33, 34] which considered single-field versions of this model (neglecting the Goldstone modes) found successful inflation for field values $\xi\phi^2 \gg M_{\rm pl}^2$. We confirm this below for the multifield case including the Goldstone modes. The reason is easy to see from Eq. (5.29). In the limit $\xi(\phi^2+\chi^2) = \xi r^2 \gg M_{\rm pl}^2$,

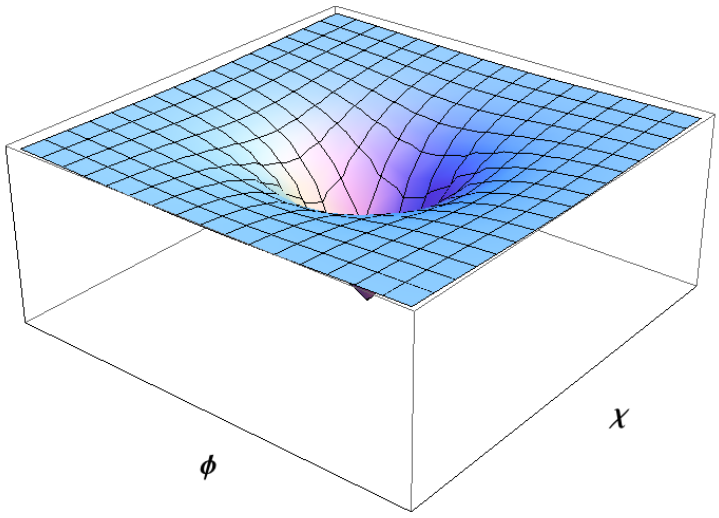

Figure 5-1: The potential for Higgs inflation in the Einstein frame, $V(\phi, \chi)$. Note the flattening of the potential for large field values, which is quite distinct from the behavior of the Jordan-frame potential, $\tilde{V}(\phi, \chi)$ in Eq. (5.27).

the potential in the Einstein frame becomes very flat, approaching

$$V(\phi^I) \to \frac{\lambda M_{\rm pl}^4}{4\xi^2}\left[1 + \mathcal{O}\left(\frac{M_{\rm pl}^2}{\xi r^2}\right)\right]. \tag{5.31}$$

See Fig. 5-1.

Given $\xi \sim 10^4$, the initial energy density for this model lies well below the Planck scale, $\rho \simeq V \simeq \lambda M_{\rm pl}^4/\xi^2 \sim 10^{-9} M_{\rm pl}^4$. In fact, as we will see, successful slow-roll inflation (producing at least 70 efolds of inflation) occurs for initial values of the fields below the Planck scale, unlike in models of chaotic inflation with polynomial potentials that lack nonminimal couplings. Moreover, as emphasized in [5], the flattening of the potential in the Einstein frame at large field values makes Higgs inflation easily compatible with the latest observations of the spectral index, n_s. Ordinary chaotic inflation with a $\lambda\phi^4$ potential and minimal coupling, on the other hand, yields a spectral index outside the 95% confidence interval for the best-fit value of n_s [35, 36]. Below we confirm this behavior for Higgs inflation even when the Goldstone degrees of freedom are included.

The field-space metric $\mathcal{G}_{IJ}$ is determined by the nonminimal coupling function, $f(\phi^I)$, and its derivatives. Explicit expressions for the components of $\mathcal{G}_{IJ}$ for a two-

field model with arbitrary couplings, ξ_ϕ and ξ_χ, are given in the Appendix of [24]. In the case of Higgs inflation, the $SU(2)$ gauge symmetry enforces $\xi_\phi = \xi_\chi = \xi$. Given this symmetry, the convenient combination, $C(\phi^I)$, introduced in the Appendix of [24] becomes

$$C(\phi^I) = 2f + 6\xi^2\left(\phi^2 + \chi^2\right) = M_{\rm pl}^2 + \xi(1+6\xi)r^2. \tag{5.32}$$

For $\xi_\phi = \xi_\chi = \xi$, the Ricci curvature scalar for the field-space manifold, as calculated in [24], takes the form

$$\mathcal{R} = \frac{4\xi}{C^2}\left[C + 3\xi M_{\rm pl}^2\right]. \tag{5.33}$$

During inflation, when $\xi r^2 \gg M_{\rm pl}^2$, this reduces to

$$\mathcal{R} \to \frac{2}{3\xi r^2} \ll M_{\rm pl}^{-2}, \tag{5.34}$$

indicating that the field-space manifold has a spherical symmetry with radius of curvature $r_c \sim \sqrt{\xi}\, r$. As shown in [24], the curvature of the field-space manifold remains negligible in such models until the fields satisfy $\xi r^2 \ll M_{\rm pl}^2$, near the end of inflation.

From Eq. (5.10), and using the expressions for $\mathcal{G}^{IJ}$ and $\Gamma^I{}_{JK}$ in the Appendix of [24], the equation of motion for the background field $\phi(t)$ takes the form

$$\ddot{\phi} + 3H\dot{\phi} + \frac{\xi(1+6\xi)}{C}\phi\left(\dot{\phi}^2 + \dot{\chi}^2\right) - \frac{\dot{f}}{f}\dot{\phi} + \lambda M_{\rm pl}^4\frac{\phi(\phi^2+\chi^2)}{2fC} = 0. \tag{5.35}$$

The equation for χ follows upon replacing $\phi \longleftrightarrow \chi$. Using Eq. (5.12), the square of the fields' velocity vector becomes

$$\dot{\sigma}^2 = \left(\frac{M_{\rm pl}^2}{2f}\right)\left[\left(\dot{\phi}^2 + \dot{\chi}^2\right) + \frac{3\dot{f}^2}{f}\right], \tag{5.36}$$

and the gradient of the potential in the direction $\hat{\sigma}^I$ becomes

$$\hat{\sigma}^I V_{,I} = V_{,\sigma} = \frac{\lambda M_{\rm pl}^6\left(\phi^2+\chi^2\right)}{\xi(2f)^3}\frac{\dot{f}}{\dot{\sigma}}. \tag{5.37}$$

We may verify that multifield Higgs inflation exhibits slow-roll behavior for typical choices of couplings and initial conditions. First consider the single-field case, in which we set $\chi = \dot{\chi} = 0$. Near the start of inflation (with $\xi\phi^2 \gg M_{\rm pl}^2$), the terms in Eq. (5.35) that stem from the field's noncanonical kinetic term take the form

$$\frac{\xi(1+6\xi)}{C}\phi\dot{\phi}^2 - \frac{\dot{f}}{f}\dot{\phi} \to -\frac{\dot{\phi}^2}{\phi}. \tag{5.38}$$

The usual slow-roll requirement for single-field models, $|\dot{\phi}| \ll |H\phi|$, ensures that the terms in Eq. (5.38) remain much less than the $3H\dot{\phi}$ term in Eq. (5.35). Neglecting $\ddot{\phi}$, the single-field, slow-roll limit of Eq. (5.35) becomes

$$3H\dot{\phi} \simeq -\frac{\lambda M_{\rm pl}^4}{6\xi^3\phi}, \tag{5.39}$$

or, upon using $H^2 \simeq V/(3M_{\rm pl}^2)$,

$$\dot{\phi} \simeq -\frac{\sqrt{\lambda}\, M_{\rm pl}^3}{3\sqrt{3}\,\xi^2\phi}. \tag{5.40}$$

Setting $\xi = 10^4$ and fixing the initial field velocity by Eq. (5.40) requires $\phi(0) \geq 0.1M_{\rm pl}$ to yield $N \geq 70$ efolds of inflation in the single-field case.

A much broader range of initial conditions yields $N \geq 70$ efolds in the two-field case. From Eq. (5.16) we see that inflation (with $\ddot{a} > 0$) requires $\dot{\sigma}^2 \ll V$. Given the $SO(\mathcal{N})$ symmetry of the model, we may set $\chi(0) = 0$ without loss of generality, and parameterize the fields' initial velocities as

$$\begin{aligned} \dot{\phi}(0) &= \frac{\sqrt{\lambda}\, M_{\rm pl}^3}{3\sqrt{3}\,\xi^2\phi(0)}\, x, \\ \dot{\chi}(0) &= \frac{\sqrt{\lambda}\, M_{\rm pl}^3}{3\sqrt{3}\,\xi^2\phi(0)}\, y \end{aligned} \tag{5.41}$$

in terms of dimensionless constants x and y. (The single-field case corresponds to $x = -1, y = 0$.) Near the start of inflation, when $\xi r^2 = \xi\phi^2 \gg M_{\rm pl}^2$, Eq. (5.36)

becomes

$$\dot{\sigma}^2|_{\chi(0)=0} \to \left(\frac{\lambda M_{\rm pl}^4}{4\xi^2}\right)\left(\frac{M_{\rm pl}^2}{\xi\phi^2(0)}\right)^2 \frac{4}{27\xi}\left[(1+6\xi)x^2+y^2\right]. \tag{5.42}$$

The first term in parentheses is just the value of the potential, V, near the start of inflation, as given in Eq. (5.31). The second term in parentheses is small near the beginning of inflation, given $\xi r^2 \gg M_{\rm pl}^2$. Hence the initial values for $\dot{\phi}$ and $\dot{\chi}$, parameterized by the coefficients x and y, may be substantially larger than in the single-field case while still keeping $\dot{\sigma}^2 \ll V$.

Fig. 5-2 shows $H(t)$, $\phi(t)$, and $\chi(t)$ for a scenario in which $\dot{\phi}(0)$ and $\dot{\chi}(0)$ greatly exceed the single-field relation of Eq. (5.40): $|x| = 10^2$ and $|y| = 10^6$. As is evident in the figure, the large initial velocities cause the fields to oscillate rapidly. The extra kinetic energy makes the initial value of $H(t)$ larger than in the corresponding single-field case. The increase in H, in turn, causes the fields' velocities to damp out even more quickly, due to the $3H\dot{\phi}$ and $3H\dot{\chi}$ Hubble-drag terms in each field's equation of motion. Thus the system rapidly settles into a slow-roll regime that continues for 70 efolds. As shown in Fig. 3, we may achieve $N \geq 70$ efolds with even smaller initial field values by making the initial field velocities correspondingly larger.

5.4 Turn Rate

The components of the turn-rate, ω^I in Eq. (5.23), take the form

$$\omega^\phi = -\frac{\lambda M_{\rm pl}^4}{\dot{\sigma}}\frac{r^2}{2f}\left[\frac{\phi}{C} - \frac{M_{\rm pl}^2}{4f^2}\frac{\dot{\phi}}{\dot{\sigma}^2}\left(\phi\dot{\phi}+\chi\dot{\chi}\right)\right]. \tag{5.43}$$

The other component, ω^χ, follows upon replacing $\phi \longleftrightarrow \chi$. The length of the turn-rate vector is given by

$$\omega = |\omega^I| = \sqrt{\mathcal{G}_{IJ}\omega^I\omega^J} = \frac{1}{\dot{\sigma}}\sqrt{\hat{s}^{KM}V_{,K}V_{,M}}\,, \tag{5.44}$$

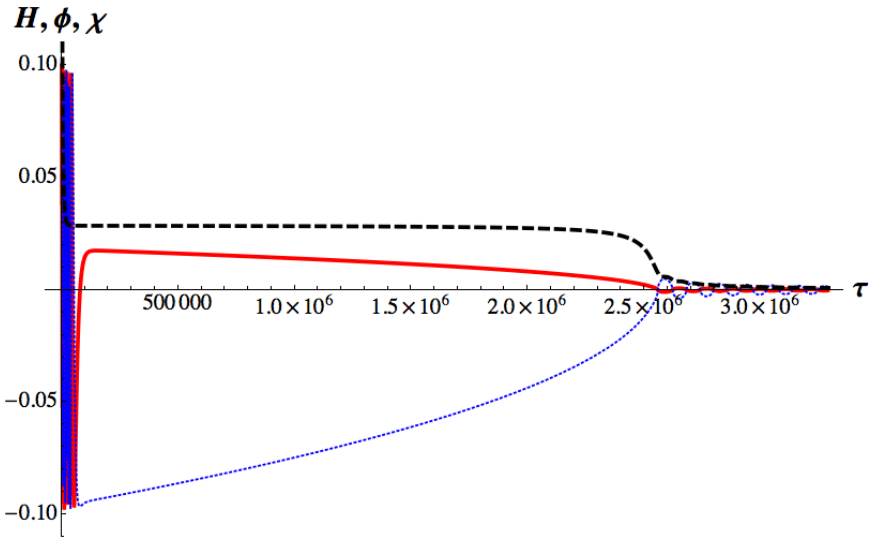

Figure 5-2: The evolution of $H(t)$ (black dashed line) and the fields $\phi(t)$ (red solid line) and $\chi(t)$ (blue dotted line). The fields are measured in units of $M_{\rm pl}$ and we use the dimensionless time variable $\tau = \sqrt{\lambda}\, M_{\rm pl} t$. We have plotted $10^3 H$ so that its scale is commensurate with the magnitude of the fields. The Hubble parameter begins large, $H(0) = 8.1 \times 10^{-4}$, but quickly falls by a factor of 30 as it settles to its slow-roll value of $H = 2.8 \times 10^{-5}$. Inflation proceeds for $\Delta\tau = 2.5 \times 10^6$ to yield $N = 70.7$ efolds of inflation. The solutions shown here correspond to $\xi = 10^4$, $\phi(0) = 0.1$, $\chi(0) = 0$, $\dot{\phi}(0) = -2 \times 10^{-6}$, and $\dot{\chi}(0) = 2 \times 10^{-2}$. For the same value of $\phi(0)$, Eq. (5.40) corresponds to $\dot{\phi}(0) = -2 \times 10^{-8}$ for the single-field case.

where the final expression follows upon using the definition of ω^I in Eq. (5.23) and the identity $\hat{s}^{KM} = \hat{s}^K{}_A \hat{s}^{MA}$, which follows from Eq. (5.13). We find

$$\dot{\sigma}^2 \omega^2 = \hat{s}^{KM} V_{,K} V_{,M} = \frac{\lambda^2 M_{\rm pl}^{10}}{(2f)^5 C} r^6 \left[C - \xi^2 r^2\right] - (V_{,\sigma})^2 \,. \tag{5.45}$$

The evolution of the turn rate for typical initial conditions is shown in Fig. 5-4.

In order to analyze the evolution of the background fields, it is easier to move from Cartesian to polar coordinates, in which the angular velocity and turn rate have more intuitive behavior. In addition to the radius, $r^2 = \phi^2 + \chi^2$, we also define the angle

$$\gamma \equiv \arctan\left(\frac{\chi}{\phi}\right) . \tag{5.46}$$

Single-field trajectories correspond to constant $\gamma(t)$. In the polar coordinate system,

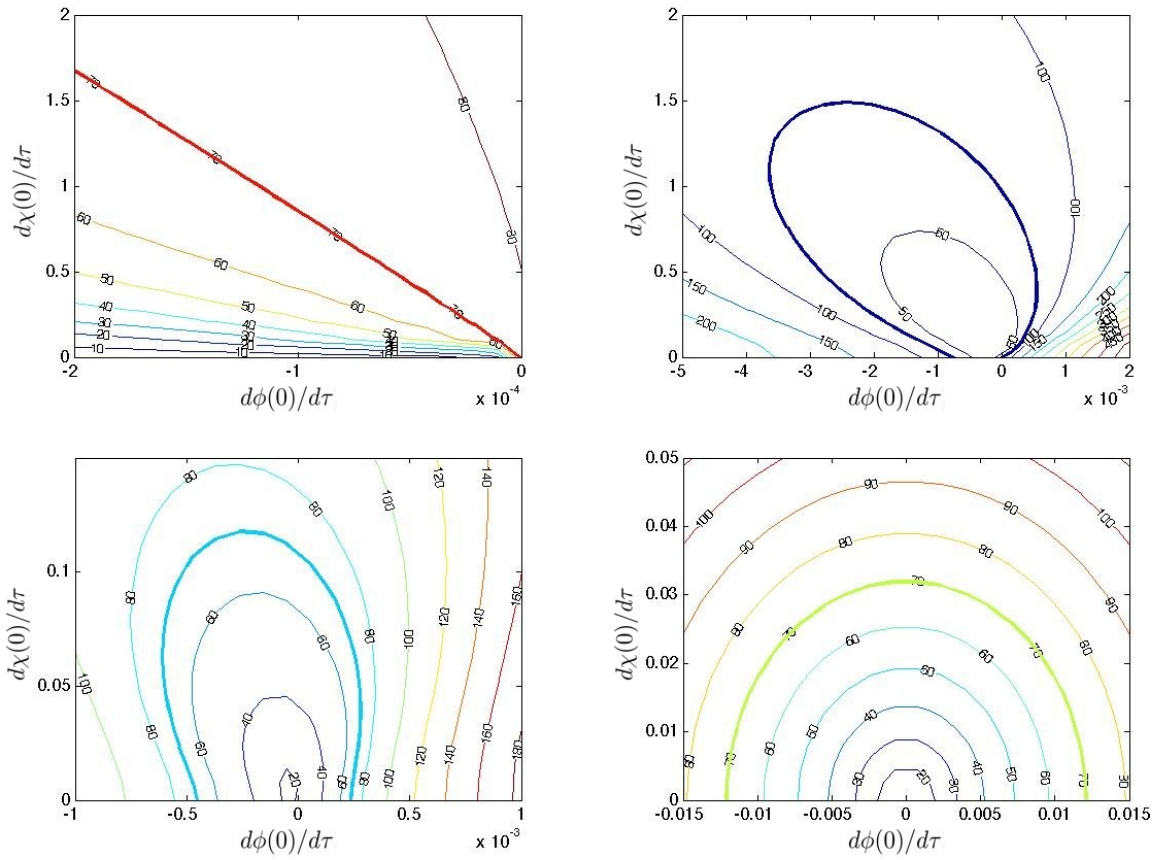

Figure 5-3: Contour plots showing the number of efolds of inflation as one varies the fields' initial conditions, keeping $\xi = 10^4$ fixed. In each panel, the vertical axis is $\dot{\chi}(0)$ and the horizontal axis is $\dot{\phi}(0)$. The panels correspond to $\phi(0) = 10^{-1}\ M_{\rm pl}$ (top left), $10^{-2}\ M_{\rm pl}$ (top right), $5 \times 10^{-3}\ M_{\rm pl}$ (bottom left) and $10^{-4}\ M_{\rm pl}$ (bottom right), and we again use dimensionless time $\tau = \sqrt{\lambda}\, M_{\rm pl} t$. In each panel, the line for $N = 70$ efolds is shown in bold. Note how large these initial velocities are compared to the single-field expectation of Eq. (5.40).

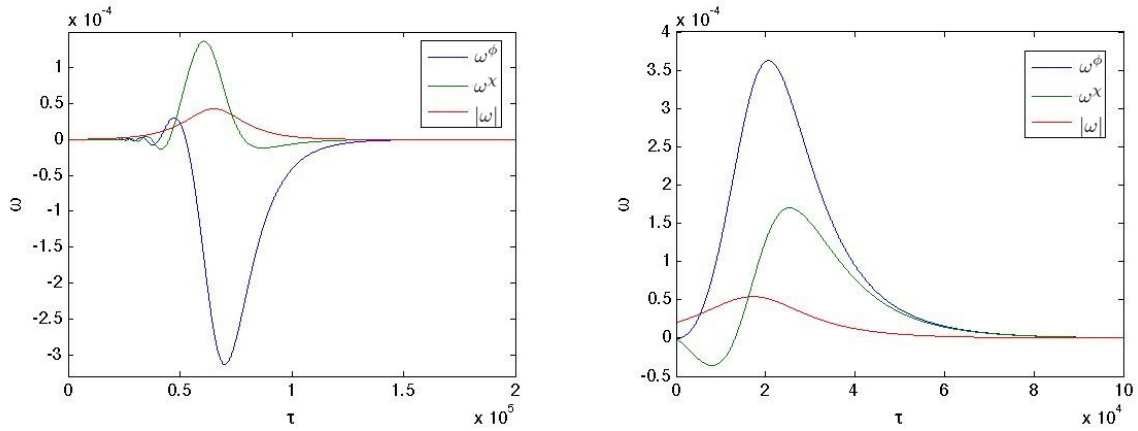

Figure 5-4: Evolution of the turn rate. The left picture shows the evolution with initial conditions as in Fig. 5-2. The right figure has initial conditions $\phi(0) = 0.1$, $\chi(0) = \dot{\phi}(0) = 0$, and $\dot{\chi}(0) = 2 \times 10^{-5}$ in units of $M_{\rm pl}$ and $\tau = \sqrt{\lambda}\, M_{\rm pl} t$. In both cases we set $\xi = 10^4$. Recall from Fig. 5-2 that inflation lasts until $\tau_{\rm end} \sim \mathcal{O}(10^6)$ for these initial conditions; hence we find that ω damps out within a few efolds after the start of inflation.

the background dynamics of Eq. (5.16) may be written

$$\begin{aligned} H^2 &= \frac{1}{12f}\left[\dot{r}^2 + r^2\dot{\gamma}^2 + \frac{3\xi^2}{f} r^2\dot{r}^2 + \frac{\lambda M_{\rm pl}^2}{2}\frac{r^4}{(M_{\rm pl}^2 + \xi r^2)}\right], \\ \dot{H} &= -\frac{1}{4f}\left[\dot{r}^2 + r^2\dot{\gamma}^2 + \frac{3\xi^2}{f} r^2\dot{r}^2\right]. \end{aligned} \tag{5.47}$$

The equations of motion become

$$\ddot{r} + 3H\dot{r} - r\dot{\gamma}^2 + \frac{\xi(1+6\xi)}{C} r\left(\dot{r}^2 + r^2\dot{\gamma}^2\right) - \frac{\xi}{f}\dot{r}^2 r + \lambda M_{\rm pl}^4 \frac{r^3}{2fC} = 0 \tag{5.48}$$

and

$$\ddot{\gamma} + \left(3H + 2\frac{\dot{r}}{r}\frac{M_{\rm pl}^2}{(M_{\rm pl}^2 + \xi r^2)}\right)\dot{\gamma} = 0. \tag{5.49}$$

In this new basis the turn rate may be written compactly as

$$\omega^2 = \frac{\lambda^2 M_{\rm pl}^8}{2fC}\left(\frac{r^4\dot{\gamma}}{r^2\dot{\gamma}^2(M_{\rm pl}^2 + \xi r^2) + \dot{r}^2 C}\right)^2 \tag{5.50}$$

This expression vanishes in both the limits $|\dot{\gamma}| \to 0$ and $|\dot{\gamma}| \to \infty$: if the angular velocity is either too large or too small, the fields' evolution reverts to effectively

single-field behavior (either purely radial motion or purely angular motion). Of the two limits, however, only pure-radial motion is stable. It is ultimately the evolution of $\gamma(t)$ that will determine the fate of the turn rate.

It is obvious from Eq. (5.49) that the line $\dot{\gamma} = 0$ is the fixed point of the angular motion. The character of the fixed point is defined by the sign of the $\dot{\gamma}$ term, which is less trivial. It can be negative close to $r = 0$ due to the high curvature of the field manifold and the small value of the Hubble parameter, but in the slow-roll regime of the radial field, with $\xi r^2 \gg M_{\rm pl}^2$, the sign of $\dot{\gamma}$ is safely positive. That means that we can treat the angular motion as damped throughout inflation.

For large nonminimal coupling and/or slow rolling of the radial field the last term in Eq. (5.49) may be neglected, which yields

$$\ddot{\gamma} + 3H\dot{\gamma} = 0. \tag{5.51}$$

The only complicated object in Eq. (5.51) is the Hubble parameter, which may be simplified in the limit of a slow rolling radial field and large nonminimal coupling upon making use of Eq. (5.47):

$$H \simeq \frac{1}{\sqrt{6\xi}}\sqrt{\dot{\gamma}^2 + \frac{\lambda M_{\rm pl}^2}{2\xi}}. \tag{5.52}$$

Then Eq. (5.51) becomes

$$\ddot{\gamma} + \frac{3}{\sqrt{6\xi}}\sqrt{\dot{\gamma}^2 + \frac{\lambda M_{\rm pl}^2}{2\xi}}\,\dot{\gamma} \simeq 0. \tag{5.53}$$

Although Eq. (5.53) can be solved exactly (see the Appendix), it is instructive to examine the two limits of large and small $\dot{\gamma}$, which provide most of the relevant information.

For small angular velocity, $\dot{\gamma} \ll \sqrt{\lambda M_{\rm pl}^2/2\xi}$, we recover the linear limit

$$\ddot{\gamma} + \frac{3}{\xi}\sqrt{\frac{\lambda M_{\rm pl}^2}{12}}\,\dot{\gamma} \simeq 0 \tag{5.54}$$

with the solution

$$\dot{\gamma} = \dot{\gamma}_0 \, \exp\left[-\frac{\sqrt{3\lambda}}{2\xi} M_{\rm pl}\, t\right] \propto e^{-3N}, \tag{5.55}$$

where $N = Ht$. It is very easy to measure time in efolds in this limit, since the Hubble parameter is nearly constant. Eq. (5.55) illustrates that any small, initial angular velocity will be suppressed within a couple of efolds, or equivalently within a time of the order of $\xi/(\sqrt{\lambda}\, M_{\rm pl})$.

In the opposite limit, $\dot{\gamma} \gg \sqrt{\lambda M_{\rm pl}^2/2\xi}$, which we call the nonlinear regime, Eq. (5.53) becomes

$$\ddot{\gamma} + 3\frac{1}{\sqrt{6\xi}}\dot{\gamma}^2 \simeq 0 \tag{5.56}$$

with the solution

$$\dot{\gamma} = \left[\frac{1}{\dot{\gamma}_0} + \frac{3t}{\sqrt{6\xi}}\right]^{-1}. \tag{5.57}$$

Given Eqs. (5.55) and (5.57), we may follow the evolution of any initial angular velocity. If $\dot{\gamma}$ begins large enough it will start in the nonlinear regime, where it will stay until it becomes of order $\sqrt{\lambda M_{\rm pl}^2/2\xi}$. We parameterize the cross-over regime as

$$\dot{\gamma} = \sqrt{\lambda} M_{\rm pl}\, \frac{z}{\sqrt{2\xi}} \tag{5.58}$$

where z is some constant of order one. The cross-over time may then be estimated by inverting Eq. (5.57) to find

$$t_{\rm nl} = \frac{\sqrt{6\xi}}{3}\left[\sqrt{\frac{2\xi}{\lambda}}\frac{1}{M_{\rm pl}\, z} - \frac{1}{\dot{\gamma}_0}\right]. \tag{5.59}$$

There exists an upper limit on the time it takes for the angular velocity to decay, namely

$$\sqrt{\lambda} M_{\rm pl}\, t_{\rm nl,max} = \frac{2}{\sqrt{3}}\frac{\xi}{z}. \tag{5.60}$$

We have verified all of these analytic predictions using numerical calculations of the exact equations for the coupled two-field system in an expanding universe. In Fig. 5-5 we plot the number of efolds from the beginning of inflation at which the

turn rate reaches its maximum value, as we vary the fields' initial velocities. Note that for any combination of initial conditions that yields at least $N_{\rm tot} = 70$ efolds, ω reaches its maximum value between $N(\omega_{\rm max}) = 3.5$ and 5 efolds from the start of the fields' evolution (for the range of initial conditions considered there). In Fig. 5-6 we plot ω as a function of time as we vary the initial angular velocity, $\dot{\gamma}(0)$. The curves in red correspond to initial conditions in the linear regime, while the curves in blue start in the nonlinear regime. Note that the curves starting in the nonlinear regime have the same amplitude. The existence of a maximum time, $t_{\rm nl,max}$, is evident from the bunching of the blue curves. We find $\sqrt{\lambda} M_{\rm pl}\, t_{\rm nl,max} = \tau_{\rm nl,max} \sim \text{few} \times \xi \sim 10^4$, as expected from Eq. (5.60). In these units and for the initial conditions used in Fig. 5-6, inflation lasts until $\tau_{\rm end} \sim \mathcal{O}(10^6)$, so $\tau_{\rm nl,max}$ occurs very early after the onset of inflation.

Eq. (5.55) shows that the linear region lasts at most a few efolds, so the duration of the nonlinear region is what will ultimately determine whether or not multifield effects will persist until observationally relevant length scales first cross the Hubble radius. In the nonlinear regime, Eq. (5.52) yields $H \simeq \dot{\gamma}/\sqrt{6\xi}$ with $\dot{\gamma}$ given by Eq. (5.57). The number of efolds for which the nonlinear regime persists is given by

$$N_{\rm nl} = \int_0^{t_{\rm nl}} H dt \simeq \frac{1}{\sqrt{6\xi}} \int_0^{t_{\rm nl}} \dot{\gamma} dt = \frac{1}{3} \ln \left(\sqrt{\frac{2\xi}{\lambda}} \frac{\dot{\gamma}_0}{M_{\rm pl}\, z} \right). \tag{5.61}$$

We examine Eq. (5.61) numerically by fixing $\xi = 10^4$ and $\phi(0) = 0.1 M_{\rm pl}$ and choosing pairs of initial velocities, $\dot{\phi}(0)$ and $\dot{\chi}(0)$, that yield 70 efolds (see Fig. 5-7, left); and also by setting $\dot{\phi}(0)$ to various constant values and varying $\dot{\chi}(0)$ (Fig. 5-7, right). The results fall neatly along a least-squares logarithmic fit, as expected from Eq. (5.61). The function $N_{\rm nl}$ grows slowly. In order for multifield effects to remain important more than a few efolds after the start of inflation, the initial angular velocity would need to be enormous: at least ten orders of magnitude larger than typical values of the initial field velocity for single-field inflation, as given in Eq. (5.40). We do not know of any realistic mechanism that could generate initial field velocities so large. Moreover, for many combinations of initial conditions shown in the righthand side of

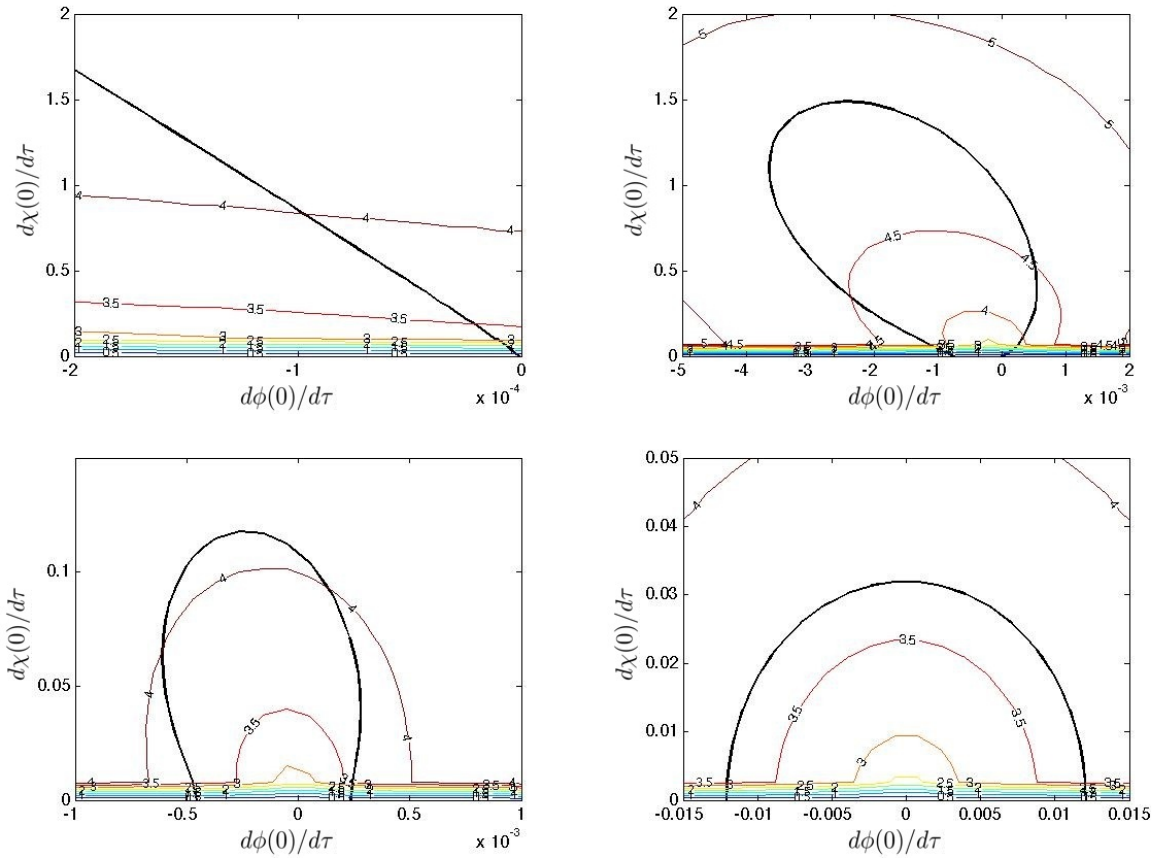

Figure 5-5: Contour plots showing the number of efolds at which the maximum of the turn rate occurs, as one varies the fields' initial conditions. In each panel, the vertical axis is $\dot{\chi}(0)$ and the horizontal axis is $\dot{\phi}(0)$. The panels correspond to $\phi(0) = 10^{-1}\, M_{\rm pl}$ (top left), $10^{-2}\, M_{\rm pl}$ (top right), $5 \times 10^{-3}\, M_{\rm pl}$ (bottom left) and $10^{-4}\, M_{\rm pl}$ (bottom right). We set $\xi = 10^4$ and use the dimensionless time-variable $\tau = \sqrt{\lambda}\, M_{\rm pl} t$. The thick black curve is the contour line of initial conditions that yield $N = 70$ efolds.

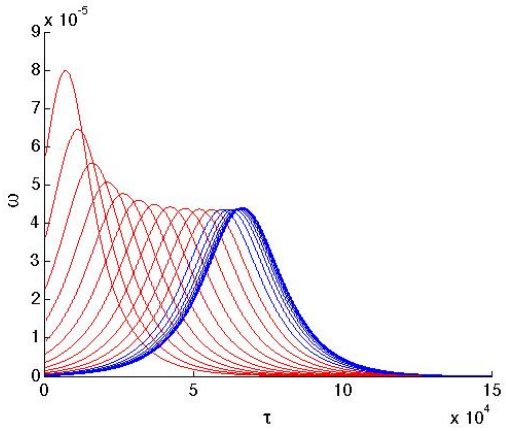

Figure 5-6: The turn rate as a function of time for different values of the initial angular velocity. The parameters used are $\xi = 10^4$, $\phi(0) = 0.1M_{\rm pl}$, $\dot{\phi}(0) = \chi(0) = 0$, and $\frac{0.01}{\sqrt{2\xi}} \leq \dot{\gamma}(0) \leq \frac{100}{\sqrt{2\xi}}$, in terms of dimensionless time, $\tau = \sqrt{\lambda}\, M_{\rm pl} t$. In these units and for $\phi(0) = 0.1M_{\rm pl}$, inflation lasts until $\tau_{\rm end} \sim \mathcal{O}(10^6)$.

Fig. 5-7, $N_{\rm tot} > 70$ efolds (several sets of initial conditions yield $N_{\rm tot} \sim 90$ efolds). For those scenarios, the turn rate reaches its maximum value deep within the early phase of the system's evolution, long before observationally relevant perturbations first cross the Hubble radius. The multifield dynamics for this model thus behave similarly to those in related multifield models of inflation that involve the Higgs sector, such as [37].

We may consider the behavior of $a(t)$ and $H(t)$ in the two different regimes more closely. From the definition of H and $\dot{H}$ in Eq. (5.47) and neglecting the terms proportional to $\dot{r}$ (which is equivalent to requiring the field to be slow rolling along the radial direction), we find

$$\frac{\ddot{a}}{a} = \dot{H} + H^2 = \frac{1}{12f}\left(-2r^2\dot{\gamma}^2 + \frac{\lambda M_{\rm pl}^2}{2}\frac{r^4}{M_{\rm pl}^2 + \xi r^2}\right). \tag{5.62}$$

When the potential dominates we recover what we called the linear regime in the analysis of the decay of ω. In that regime

$$\frac{\ddot{a}}{a} > 0, \tag{5.63}$$

which is an accelerated expansion or cosmological inflation. However, in the nonlinear

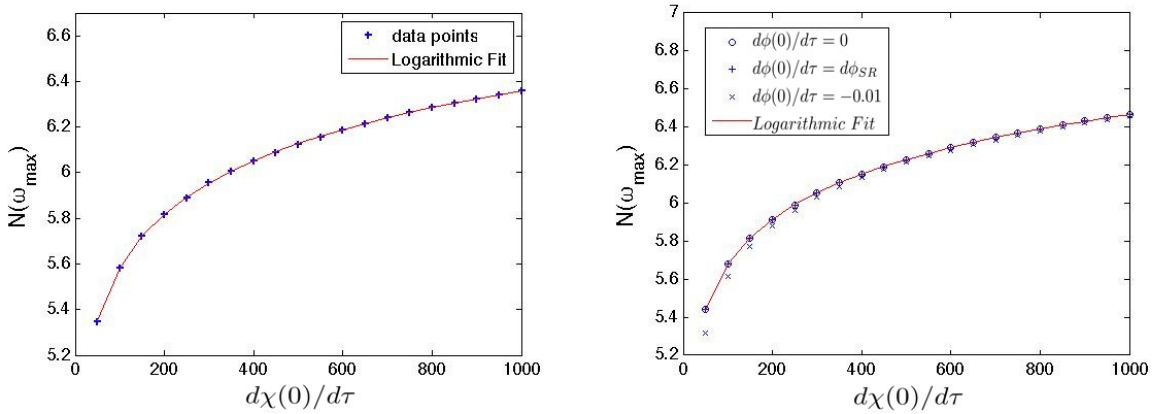

Figure 5-7: Number of efolds until the maximum value of the turn rate is reached, as a function of $\dot{\chi}(0)$. On the left we plot $N(\omega_{\rm max})$ for initial conditions that yield $N_{\rm tot} = 70$ efolds; on the right we plot the same quantity for various values of $\dot{\phi}(0)$. The logarithmic fit is an excellent match to our analytic result, Eq. (5.61).

regime, when $\dot{\gamma}$ dominates, the situation reverses and we find

$$\frac{\ddot{a}}{a} = -\frac{1}{6f} r^2 \dot{\gamma}^2 < 0, \tag{5.64}$$

which is an expansion and a very rapid one (because of the large value of H), but it is not inflation. Regardless of whether we have true inflation or simply rapid expansion at early times, we may always define the number of efolds as

$$N = \int_{t_{\rm in}}^{t_{\rm end}} H dt. \tag{5.65}$$

Thus we may use N as our clock and measure time in efolds from the beginning of the system's evolution, regardless of whether it is in the inflationary phase or not. The fact that in the nonlinear regime the universe is not inflating only makes our results stronger: all multifield effects decay before the observable scales exit the horizon in a model that produces enough inflation to solve the standard cosmological problems.

As a final test of our analysis we set $\xi = 10^2$ instead of $\xi = 10^4$. The smaller value of the nonminimal coupling does not lead to a viable model of Higgs inflation — the WMAP normalization of the power spectrum requires a larger value of ξ [5] — but we may nonetheless study the dynamics of such a model. We collect the important

information about the dynamics of this model in Fig. 5-8. As expected, the model can provide 70 or more efolds of inflation for a wide range of parameters, and the corresponding turn rate peaks well before observationally relevant length scales first crossed the Hubble radius, even when we increase $\dot{\chi}(0)$ to a few hundred in units of $\tau = \sqrt{\lambda} M_{\rm pl} t$. The excellent logarithmic fit of the time at which the turn rate is maximum versus $\dot{\chi}(0)$ is again evident. Finally the curves of the turn rate versus time show the same qualitative and quantitative characteristics as Fig. 5-6 for $\xi = 10^4$. Specifically, if one rescales time and the turn rate appropriately by ξ, the two sets of curves would be hardly distinguishable.

5.5 Implications for the Primordial Spectrum

We have found that in models with an $SO(\mathcal{N})$ symmetry among the scalar fields, the turn rate quickly damps to negligible magnitude within a few efolds after the start of inflation. In this section we confirm that such behavior yields empirical predictions for observable quantities like the primordial power spectrum of perturbations that reproduce expectations from corresponding single-field models.

For models that behave effectively as two-field models, which includes the class of $SO(\mathcal{N})$-symmetric models we investigate here, we may distinguish two scalar perturbations: the perturbations in the adiabatic direction, Q_σ defined in Eq. (5.18), and a scalar entropic perturbation [24],

$$Q_s \equiv \frac{\omega_I}{\omega} \delta s^I. \tag{5.66}$$

We noted in Eq. (5.19) that Q_σ is proportional to the gauge-invariant curvature perturbation, $\mathcal{R}_c$. We adopt a similar normalization for the entropy perturbation,

$$\mathcal{S} \equiv \frac{H}{\dot{\sigma}} Q_s. \tag{5.67}$$

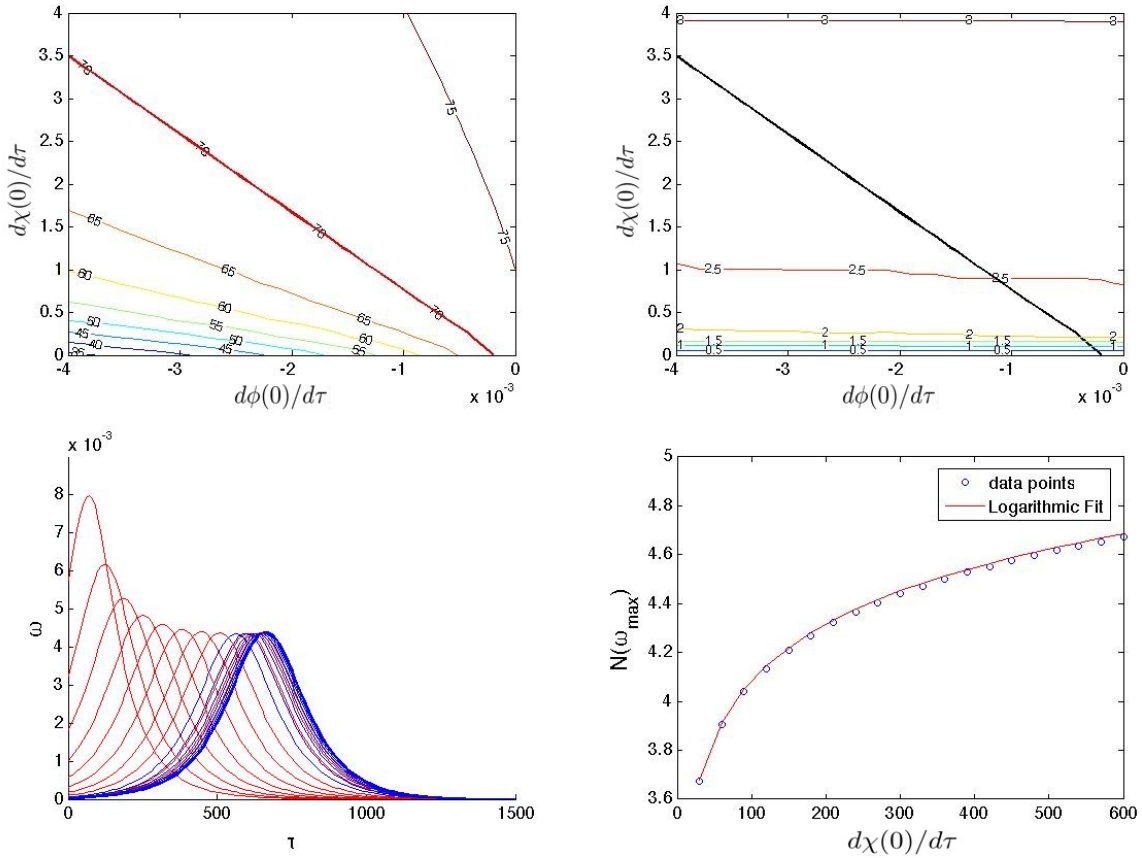

Figure 5-8: Dynamics of our two-field model with $\xi = 10^2$, $\phi(0) = 1M_{\rm pl}$, and $\chi(0) = 0$. Clockwise from top left: (1) Contour plot showing the number of efolds as one varies the fields' initial conditions. The thick curve corresponds to 70 efolds. (2) Contour plot showing the number of efolds at which the maximum of the turn rate occurs, as one varies the fields' initial conditions. The thick curve corresponds to $N_{\rm tot} = 70$ efolds. (3) Number of efolds until the maximum value of the turn rate is reached for initial conditions giving $N_{\rm tot} = 70$ efolds, along with a logarithmic fit. (4) The turn rate as a function of time for different values of the initial angular velocity, with $\dot{\phi}(0) = 0$ and $\frac{0.01}{\sqrt{2\xi}} \leq \dot{\gamma}(0) \leq \frac{100}{\sqrt{2\xi}}$, in units of $\tau = \sqrt{\lambda}\, M_{\rm pl} t$.

In the long-wavelength limit, the adiabatic and entropic perturbations obey [38, 24]

$$\begin{aligned}\dot{\mathcal{R}}_c &= \alpha H \mathcal{S} + \mathcal{O}\left(\frac{k^2}{a^2 H^2}\right), \\ \dot{\mathcal{S}} &= \beta H \mathcal{S} + \mathcal{O}\left(\frac{k^2}{a^2 H^2}\right),\end{aligned} \tag{5.68}$$

so that we may define the transfer functions

$$\begin{aligned}T_{\mathcal{RS}}(t_*, t) &= \int_{t_*}^{t} dt'\, \alpha(t') H(t') T_{\mathcal{SS}}(t_*, t'), \\ T_{\mathcal{SS}}(t_*, t) &= \exp\left[\int_{t_*}^{t} dt'\, \beta(t') H(t')\right].\end{aligned} \tag{5.69}$$

We take t_* to be the time when a fiducial scale of interest first crossed the Hubble radius during inflation, defined by $a^2(t_*)H^2(t_*) = k_*^2$. In [24], we calculated

$$\alpha(t) = \frac{2\omega(t)}{H(t)} \tag{5.70}$$

and

$$\beta(t) = -2\epsilon - \eta_{ss} + \eta_{\sigma\sigma} - \frac{4}{3}\frac{\omega^2}{H^2}, \tag{5.71}$$

where $\epsilon \equiv -\dot{H}/H^2$ and the other slow-roll parameters are defined as

$$\begin{aligned}\eta_{\sigma\sigma} &\equiv M_{\rm pl}^2 \frac{\mathcal{M}_{\sigma\sigma}}{V}, \\ \eta_{ss} &\equiv M_{\rm pl}^2 \frac{\omega_I \omega^J \mathcal{M}^I{}_J}{\omega^2 V}.\end{aligned} \tag{5.72}$$

The dimensionless power spectrum is given by

$$\mathcal{P}_{\mathcal{R}} = \frac{k^3}{2\pi^2} |\mathcal{R}_c|^2 \tag{5.73}$$

and hence, from Eqs. (5.68) and (5.69),

$$\mathcal{P}_{\mathcal{R}}(k) = \mathcal{P}_{\mathcal{R}}(k_*) \left[1 + T_{\mathcal{RS}}^2(t_*, t)\right], \tag{5.74}$$

where k corresponds to a length scale that crossed the Hubble radius at some time $t > t_*$. The spectral index is then given by

$$n_s(t) = n_s(t_*) - [\alpha(t) + \beta(t) T_{\mathcal{RS}}(t, t_*)] \sin(2\Delta), \tag{5.75}$$

where

$$\cos\Delta \equiv \frac{T_{\mathcal{RS}}}{\sqrt{1 + T_{\mathcal{RS}}^2}}. \tag{5.76}$$

In the limit $(\omega/H) \ll \eta_{\sigma\sigma}$, the spectral index evaluated at N_* assumes the single-field form [29, 30, 34],

$$n_s(t_*) = 1 - 6\epsilon(t_*) + 2\eta_{\sigma\sigma}(t_*). \tag{5.77}$$

Crucial to note is that the turn rate, ω, serves as a window function within $T_{\mathcal{RS}}(t, t_*)$: once the coefficient $\alpha = 2\omega/H$ becomes negligible, there will effectively be no transfer of power from the entropic to the adiabatic perturbations, much as we had found by examining the source terms on the righthand sides of Eqs. (5.20) and (5.21). The question then becomes whether $\omega(t)$, and hence $T_{\mathcal{RS}}(t_*, t)$, can depart appreciably from zero at times when perturbations on length scales of observational interest first cross the Hubble radius.

The longest length scales of interest are often taken to be those that first crossed the Hubble radius $N_* = 55 \pm 5$ efolds before the end of inflation [28, 29, 30]. Closer analysis suggests that length scales that first crossed the Hubble radius $N_* = 62 - 63$ efolds before the end of inflation correspond to the size of the present horizon [39]. Meanwhile, we follow [29] in assuming that successful inflation requires $N_{\rm tot} \geq 70$ efolds to solve the horizon and flatness problems. The question then becomes whether $\omega(t)$, and hence $T_{\mathcal{RS}}(t_*, t)$, can differ appreciably from zero for $N_* \leq 63$. Given the analysis in Section IV, the best chance for this to occur is for initial conditions that produce the minimum amount of inflation, $N_{\rm tot} = 70$.

In Table I, we present numerical results for key measures of multifield dynamics. In each case we set $\xi = 10^4$, $\phi(0) = 0.1 M_{\rm pl}$, and $\chi(0) = 0$. We vary $\dot{\chi}(0)$ as shown and adjust $\dot{\phi}(0)$ in each case so as to produce exactly $N_{\rm tot} = 70$ efolds of inflation.

$\dot{\chi}(0)$	$\omega(N_* = 63)$	$T_{\mathcal{RS}}(\max)$	$n_s(N_* = 63)$	$n_s(N_* = 60)$
10^{-2}	1.16×10^{-10}	2.68×10^{-6}	0.969	0.967
10^{-1}	1.20×10^{-9}	2.76×10^{-5}	0.969	0.967
1	9.41×10^{-9}	2.18×10^{-4}	0.969	0.967
10^{1}	1.18×10^{-7}	2.72×10^{-3}	0.969	0.967
10^{2}	1.12×10^{-6}	2.59×10^{-2}	0.973	0.967

Table 5.1: Numerical results for measures of multifield dynamics for Higgs inflation with $\xi = 10^4$. We use dimensionless time $\tau = \sqrt{\lambda} M_{\rm pl} t$.

Because $T_{\mathcal{RS}}$ remains so small in each of these cases, there is no discernible running of the spectral index within the window $N_* = 63$ to $N_* = 40$ efolds before the end of inflation. If we consider a fiducial scale k_* that first crosses the Hubble radius at $N_* = 63$ efolds before the end of inflation, then we find $n_s = 0.97$ across the whole range of initial conditions, in excellent agreement with the measured value of $n_s = 0.971 \pm 0.010$ [36]. If instead we set k_* as the scale that first crossed the Hubble radius $N_* = 60$ efolds before the end of inflation, we find $n_s = 0.967$ across the entire range of initial conditions, again in excellent agreement with the latest measurements.

5.6 Conclusions

In this chapter we have analyzed Higgs inflation as a multifield model with nonminimal couplings. Because the Goldstone modes of the Standard Model electroweak Higgs sector remain in the spectrum at high energies in renormalizable gauges, we have incorporated their effects in the dynamics of the model. Because of the high symmetry of the Higgs sector — guaranteed by the $SU(2)$ electroweak gauge symmetry, which manifests as an $SO(4)$ symmetry among the scalar fields of the Higgs sector — the nonmiminal couplings for the various scalar fields take precisely the same value ($\xi_\phi = \xi_\chi = \xi$), as do the tree-level couplings in the Jordan-frame potential ($\lambda_\phi = \lambda_\chi = \lambda$, and so on). The effective potential in the Einstein frame therefore contains none of the irregular features, such as bumps or ridges, that were highlighted in [24] for the case of multiple fields with arbitrary couplings. With no features such as ridges off of which the fields may fall during their evolution, Hubble drag will always

cause any initial angular motion within field space to damp out rapidly. Increasing the initial angular velocity to arbitrarily large values — well into what we call the nonlinear regime — only increases the value of H at early times, which makes the Hubble drag even more effective and hence hastens the damping out of the multifield effects.

The rapidity with which the turn-rate damps to zero combined with the requirement of $N_{\rm tot} \geq 70$ efolds for successful inflation means that the multifield dynamics become negligible before perturbations on scales of observational relevance first cross the Hubble radius. Even if we push the observational window of interest back to $N_* = 63$ efolds before the end of inflation, rather than the usual assumption of $N_* = 55 \pm 5$, we find that the model relaxes to effectively single-field dynamics prior to N_*. Hence the predictions from Higgs inflation for observable quantities, such as the spectral index of the power spectrum of primordial perturbations, reduce to their usual single-field form. Moreover, the absence of multifield effects for times later than N_* means that this model should produce negligible non-Gaussianities during inflation, in contrast to the broader family of models studied in [24].

The methods we introduce here may be applied to any multifield model with nonminimal couplings and an $SO(\mathcal{N})$ symmetry among the fields in field space. The conclusion therefore appears robust that such highly symmetric models should behave effectively as single-field models, at least within the observational window of interest between $N_* = 63$ and $N_* = 40$ efolds before the end of inflation. Of course, multfield effects could become important in such models at the end of inflation, during epochs such as preheating [40]. Such processes remain under study.

5.7 Acknowledgements

It is a pleasure to thank Alan Guth, Mustafa Amin, and Leo Stein for helpful discussions. This work was supported in part by the U.S. Department of Energy (DoE) under contract No. DE-FG02-05ER41360.

5.8 Appendix

5.8.1 Angular Evolution of the Field

For completeness, let us integrate the angular equation of motion, Eq. (5.53), for all values of $\dot{\gamma}$ (in the slow roll regime of the radial field). This yields

$$\frac{\dot{\gamma}(t)\left(\sqrt{\lambda}M_{\rm pl}+\sqrt{2\xi\dot{\gamma}_0^2+\lambda M_{\rm pl}^2}\right)}{\dot{\gamma}_0\left(\sqrt{\lambda}M_{\rm pl}+\sqrt{2\xi\dot{\gamma}^2(t)+\lambda M_{\rm pl}^2}\right)}=\exp\left[-\frac{\sqrt{3\lambda}\,M_{\rm pl}t}{2\xi}\right]. \tag{5.78}$$

In the two limits, $\dot{\gamma}_0 \ll \sqrt{\lambda}M_{\rm pl}/\sqrt{2\xi}$ and $\dot{\gamma}_0 \gg \sqrt{\lambda}M_{\rm pl}/\sqrt{2\xi}$, we may solve Eq. (5.78) and recover the forms of $\gamma(t)$ presented in Eqs. (5.55) and (5.57).

Bibliography

[1] ATLAS Collaboration, "Observation of a new particle in the search for the Standard Model Higgs boson with the ATLAS detector at the LHC," Phys Lett. B716 (2012): 1-29 [arXiv:1207.7214 [hep-ex]]; CMS Collaboration, "Observation of a new boson at a mass of 125 GeV with the CMS experiment at the LHC," Phys. Lett. B716 (2012): 30 [arXiv:1207.7235 [hep-ex]].

[2] D. H. Lyth and A. Riotto, "Particle physics models of inflation and the cosmological density perturbation," Phys. Rept. **314**, 1 (1999) [arXiv:hep-ph/9807278].

[3] A. H. Guth and D. I. Kaiser, "Inflationary cosmology: Exporing the universe from the smallest to the largest scales," Science **307**,884 (2005) [arXiv:astro-ph/0502328].

[4] A. Mazumdar and J. Rocher, "Particle physics models of inflation and curvaton scenarios," Phys. Rept. **497**, 85 (2011) [arXiv:1001.0993 [hep-ph]].

[5] F. L. Bezrukov and M. E. Shaposhnikov, "The Standard Model Higgs boson as the inflaton," Phys. Lett. **B659**, 703 (2008) [arXiv:0710.3755 [hep-th]].

[6] Y. Fujii and K. Maeda, *The Scalar-Tensor Theory of Gravitation* (New York: Cambridge University Press, 2003).

[7] V. Faraoni, *Cosmology in Scalar-Tensor Gravity* (Boston: Kluwer, 2004).

[8] N. D. Birrell and P. C. W. Davies, *Quantum Fields in Curved Space* (New York: Cambridge University Press, 1982).

[9] I. L. Buchbinder, S. D. Odintsov, and I. L. Shapiro, *Effective Action in Quantum Gravity* (New York: Taylor and Francis, 1992).

[10] A. de Simone, M. P. Hertzberg, and F. Wilczek, "Running inflation in the Standard Model," Phys. Lett. B678 (2009): 1 [arXiv:0812.4946 [hep-ph]].

[11] F. L. Bezrukov, A. Magnin, and M. E. Shaposhnikov, "Standard Model Higgs boson mass from inflation," Phys. Lett. B675 (2009): 88 [arXiv:0812.4950 [hep-ph]]; F. L. Bezrukov and M. E. Shaposhnikov, "Standard Model Higgs boson mass from inflation: two loop analysis," JHEP 0907 (2009): 089 [arXiv:0904.1537 [hep-ph]].

[12] A. O. Barvinsky, A. Yu. Kamenshchik, C. Kiefer, A. A. Starobinsky, and C. F. Steinwachs, "Asymptotic freedom in inflationary cosmology with a non-minimally coupled Higgs field," JCAP **0912** (2009): 003 [arXiv:0904.1698 [hep-ph]]; "Higgs boson, renormalization group, and naturalness in cosmology," arXiv:0910.1041v2 [hep-ph].

[13] S. Weinberg, *The Quantum Theory of Fields*, vol. 2, *Modern Applications* (New York: Cambridge University Press, 1996).

[14] C. P. Burgess, H. M. Lee, and M. Trott, "Power-counting and the validity of the classical approximation during inflation," JHEP **0909** (2009): 103 [arXiv:0902.4465 [hep-ph]]; C. P. Burgess, H. M. Lee, and M. Trott, "Comment on Higgs inflation and naturalness," JHEP **1007** (2010): 007 [arXiv:1002.2730 [hep-ph]].

[15] J. L. F. Barbon and J. R. Espinosa, "On the naturalness of Higgs inflation," Phys. Rev. D79 (2009): 081302 [arXiv:0903.0355 [hep-ph]].

[16] M. P. Hertzberg, "On inflation with non-minimal coupling," JHEP **1011** (2010): 023 [arXiv:1002.2995 [hep-ph]].

[17] S. Mooij and M. Postma, "Goldstone bosons and a dynamical Higgs field," JCAP **1109** (2011): 006 [arXiv:1104.4897 [hep-ph]].

[18] C. Gordon, D. Wands, B. A. Bassett, and R. Maartens, "Adiabatic and entropy perturbations from inflation," Phys. Rev. **D63**, 023506 (2001) [arXiv:astro-ph/0009131].

[19] S. Groot Nibbelink and B. J. W. van Tent, "Density perturbations arising from multiple field slow-roll inflation," arXiv:hep-ph/0011325; "Scalar perturbations during multiple-field slow-roll inflation," Class. Quant. Grav. **19**, 613 (2002) [arXiv:hep-ph/0107272].

[20] R. Easther and J. T. Giblin, "The Hubble slow roll expansion for multi field inflation," Phys. Rev. D72 (2005): 103505 [arXiv:astro-ph/0505033].

[21] D. Wands, "Multiple field inflation," Lect. Notes. Phys. **738**, 275 (2008) [arXiv:astro-ph/0702187].

[22] D. Langlois and S. Renaux-Petel, "Perturbations in generalized multi-field inflation," JCAP **0804** (2008): 017 [arXiv:0801.1085 [hep-th]].

[23] C. M. Peterson and M. Tegmark, "Testing two-field inflation," Phys. Rev. **D83**, 023522 (2011) [arXiv:1005.4056 [astro-ph.CO]]; "Non-Gaussianity in two-field inflation," Phys. Rev. **D84**, 023520 (2011) [arXiv:1011.6675 [astro-ph.CO]]; "Testing multi-field inflation: A geometric approach," arXiv:1111.0927 [astro-ph.CO].

[24] D. I. Kaiser, E. A. Mazenc, and E. I. Sfakianakis, "Primordial bispectrum from multifield inflation with nonminimal couplings," arXiv:1210.7487 [astro-ph.CO].

[25] R. N. Lerner and J. McDonald, "A unitarity-conserving Higgs inflation model," Phys. Rev. D82 (2010): 103525 [arXiv:1005.2978 [hep-ph]]; S. Ferrara, R. Kallosh, A. Linde, A. Marrani, and A. Van Proeyen, "Superconformal symmetry, NMSSM, and inflation," Phys. Rev. D83 (2011): 025008 [arXiv:1008.2942 [hep-th]]; F. Bezrukov, A. Magnin, M. Shaposhnikov, and S. Sibiryakov, "Higgs inflation: Consistency and generalizations," JHEP 1101

(2011): 016 [arXiv:1008.5157 [hep-ph]]; G. F. Giudice and H. M. Lee, "Unitarizing Higgs inflation," Phys. Lett. B694 (2011): 294 [arXiv:1010.1417 [hep-ph]]; F. Bezrukov, D. Gorbunov, and M. Shaposhnikov, "Late and early time phenomenology of Higgs-dependent cutoff," arXiv:1106.5019 [hep-ph]]; R. N. Lerner and J. McDonald, "Unitarity-violation in generalized Higgs inflation models," arXiv:1112.0954 [hep-ph]; D. A. Demir, "Gravi-Natural Higgs and Conformal New Physics," arXiv:1207.4584 [hep-ph].

[26] D. I. Kaiser, "Conformal transformations with multiple scalar fields," Phys. Rev. **D81**, 084044 (2010) [arXiv:1003.1159 [gr-qc]].

[27] D. S. Salopek, J. R. Bond, and J. M. Bardeen, "Designing density fluctuation spectra in inflation," Phys. Rev. **D40**, 1753 (1989).

[28] V. F. Mukhanov, H. A. Feldman, and R. H. Brandenberger, "Theory of cosmological perturbations," Phys. Rept. **215**, 203 (1992).

[29] B. A. Bassett, S. Tsujikawa, and D. Wands, "Inflation dynamics and reheating," Rev. Mod. Phys. **78**, 537 (2006) [arXiv:astro-ph/0507632].

[30] K. A. Malik and D. Wands, "Cosmological perturbations," Phys. Rept. **475**, 1 (2009) [arXiv:0809.4944 [astro-ph]].

[31] Because we are working only to first order in perturbations, we define Q^I in Eq. (5.17) in terms of $\delta\phi^I$ rather than the field-space vector $\mathcal{Q}^I$ that is introduced in [24], since, as shown there, $\delta\phi^I \rightarrow \mathcal{Q}^I + \mathcal{O}(\mathcal{Q}^2)$.

[32] R. Fakir and W. G. Unruh, "Improvement on cosmological chaotic inflation through nonminimal coupling," Phys. Rev. **D41**, 1783 (1990).

[33] N. Makino and M. Sasaki, "The density perturbation in the chaotic inflation with non-minimal coupling," Prog. Theo. Phys. **86**, 103 (1991).

[34] D. I. Kaiser, "Primordial spectral indices from generalized Einstein theories," Phys. Rev. **D52**, 4295 (1995) [arXiv:astro-ph/9408044].

[35] E. Komatsu et al. [WMAP collaboration], "Seven-year Wilkinson Microwave Anisotropy Probe (WMAP) observations: Cosmological interpretation," Astrophy. J. Suppl. **192**, 18 (2011) [arXiv:1001.4538 [astro-ph.CO]].

[36] G. Hinshaw et al. [WMAP collaboration], "Nine-year Wilkinson Microwave Anistropy Probe (WMAP) observations: Cosmological parameter results," arXiv:1212.5226 [astro-ph.CO].

[37] J. García-Bellido, J. Rubio, M. Shaposhnikov, and D. Zenhäusern, "Higgs-dilaton cosmology: From the early to the late universe," arXiv:1107.2163 [hep-ph].

[38] D. Wands, K. A. Malik, D. H. Lyth, and A. R. Liddle, "A new approach to the evolution of cosmological perturbations on large scales," Phys. Rev. D62 (2000): 043527 [arXiv:astro-ph/0003278]; L. Amendola, C. Gordon, D. Wands, and M. Sasaki, "Correlated perturbations from inflation and the cosmic microwave background," Phys. Rev. Lett. 88 (2002): 211302 [arXiv:astro-ph/0107089]; D. Wands, N. Bartolo, S. Matarrese, and A. Riotto, "An observational test of two-field inflation," Phys. Rev. D66 (2002): 043520 [arXiv:astro-ph/0205253].

[39] S. Dodelson and L. Hui, "A horizon ratio bound for inflationary fluctuations," Phys. Rev. Lett. 91 (2003): 131301 [arXiv:astro-ph/0305113]; A. R. Liddle and S. M. Leach, "How long before the end of inflation were observable perturbations produced?," Phys. Rev. D68 (2003): 103503 [arXiv:astro-ph/0305263]; M. Tegmark, "What does inflation really predict?," JCAP 0504 (2005): 001 [arXiv:astro-ph/0410281].

[40] F. Bezrukov, D. Gorbunov, and M. Shaposhnikov, "On initial conditions for the hot big bang," JCAP 0906 (2009): 029 [arXiv:0812.3622 [hep-ph]]; J. García-Bellido, D. G. Figueroa, and J. Rubio, "Preheating in the Standard Model with the Higgs-inflaton coupled to gravity," Phys. Rev. D79 (2009): 063531 [arXiv:0812.4624 [hep-ph]]; J.-F. Dufaux, D. G. Figueroa, and J. García-Bellido,

"Gravitational waves from Abelian gauge fields and cosmic strings at preheating," Phys. Rev. D82 (2010): 083518 [arXiv:1006.0217 [astro-ph.CO]].

Chapter 6

Multifield Inflation after *Planck*: The Case for Nonminimal Couplings

Multifield models of inflation with nonminimal couplings are in excellent agreement with the recent results from *Planck*. Across a broad range of couplings and initial conditions, such models evolve along an effectively single-field attractor solution and predict values of the primordial spectral index and its running, the tensor-to-scalar ratio, and non-Gaussianities squarely in the observationally most-favored region. Such models also can amplify isocurvature perturbations, which could account for the low power recently observed in the CMB power spectrum at low multipoles. Future measurements of primordial isocurvature perturbations could distinguish between the currently viable possibilities.

6.1 Introduction

Early-universe inflation remains the leading framework for understanding a variety of features of our observable universe [1, 2]. Most impressive has been the prediction of primordial quantum fluctuations that could seed large-scale structure. Recent measurements of the spectral tilt of primordial (scalar) perturbations, n_s, find a

decisive departure from a scale-invariant spectrum [3, 4]. The *Planck* collaboration's value, $n_s = 0.9603 \pm 0.0073$, differs from $n_s = 1$ by more than 5σ. At the same time, observations with *Planck* constrain the ratio of tensor-to-scalar perturbations to $r < 0.11$ (95% CL), and are consistent with the absence of primordial non-Gaussianities, $f_{\rm NL} \sim 0$ [4, 5].

The *Planck* team also observes less power in the angular power spectrum of temperature anisotropies in the cosmic microwave background radiation (CMB) at low multipoles, $\ell \sim 20 - 40$, compared to best-fit ΛCDM cosmology: a $2.5 - 3\sigma$ departure on large angular scales, $\theta > 5^\circ$ [6]. Many physical processes might ultimately account for the deviation, but a primordial source seems likely given the long length-scales affected. One plausible possibility is that the discrepancy arises from the amplification of isocurvature modes during inflation [4].

In this brief chapter we demonstrate that simple, well-motivated multifield models with nonminimal couplings match the latest observations particularly well, with no fine-tuning. This class of models (i) generically includes potentials that are concave rather than convex at large field values, (ii) generically predicts values of r and n_s in the most-favored region of the recent observations. (iii) generically predicts $f_{\rm NL} \sim 0$ except for exponentially fine-tuned initial field values, (iv) generically predicts ample entropy production at the end of inflation, with an effective equation of state $w_{\rm eff} \sim [0, 1/3]$, and (v) generically includes isocurvature perturbations as well as adiabatic perturbations, which might account for the low power in the CMB power spectrum at low multipoles.

We consider this class of models to be well-motivated for several reasons. Realistic models of particle physics include multiple scalar fields at high energies. In any such model, nonminimal couplings are *required* for self-consistency, since they arise as renormalization counterterms when quantizing scalar fields in curved spacetime [7]. Moreover, the nonminimal coupling constants generically rise with energy under renormalization-group flow with no UV fixed-point [8], and hence one expects $|\xi| \gg 1$ at inflationary energy scales. In such models inflation occurs for field values and energy densities well below the Planck scale (see [9, 10, 11] and references therein).

Higgs inflation [11] is an elegant example: in renormalizable gauges (appropriate for high energies) the Goldstone modes remain in the spectrum, yielding a multifield model [10, 12, 13].

We demonstrate here for the first time that models of this broad class exhibit an attractor behavior: over a wide range of couplings and fields' initial conditions, the fields evolve along an effectively single-field trajectory for most of inflation. Although attractor behavior is common for single-field models of inflation [14], the dynamics of multifield models generally show strong sensitivity to couplings and initial conditions (see, e.g., [15] and references therein). Not so for the class of multifield models examined here, thanks to the shape of the effective potential in the Einstein frame. The multifield attractor behavior demonstrated here means that for most regions of phase space and parameter space, this general class of models yields values of n_s, r, the running of the spectral index $\alpha = dn_s/d\ln k$, and $f_{\rm NL}$ in excellent agreement with recent observations. The well-known empirical success of single-field models with nonminimal couplings [16, 11] is thus preserved for more realistic models involving multiple fields. Whereas the attractor behavior creates a large observational degeneracy in the r vs. n_s plane, the isocurvature spectra from these models depend sensitively upon couplings and initial conditions. Future measurements of primordial isocurvature spectra could therefore distinguish among models in this class.

6.2 Multifield Dynamics

In the Jordan frame, the fields' nonminimal couplings remain explicit in the action,

$$S_{\rm J} = \int d^4x\sqrt{-\tilde{g}}\left[f(\phi^I)\tilde{R} - \frac{1}{2}\delta_{IJ}\tilde{g}^{\mu\nu}\partial_\mu\phi^I\partial_\nu\phi^J - \tilde{V}(\phi^I)\right], \tag{6.1}$$

where quantities in the Jordan frame are marked by a tilde. Performing the usual conformal transformation, $\tilde{g}_{\mu\nu}(x) \rightarrow g_{\mu\nu}(x) = 2M_{\rm pl}^{-2}f(\phi^I(x))\,\tilde{g}_{\mu\nu}(x)$, where $M_{\rm pl} \equiv (8\pi G)^{-1/2} = 2.43\times10^{18}$ GeV is the reduced Planck mass, we may write the action in

the Einstein frame as [9]

$$S_{\rm E} = \int d^4x\sqrt{-g}\left[\frac{M_{\rm pl}^2}{2}R - \frac{1}{2}\mathcal{G}_{IJ}g^{\mu\nu}\partial_\mu\phi^I\partial_\nu\phi^J - V(\phi^I)\right]. \tag{6.2}$$

The potential in the Einstein frame, $V(\phi^I)$, is stretched by the conformal factor compared to the Jordan-frame potential:

$$V(\phi^I) = \frac{M_{\rm pl}^4}{4f^2(\phi^I)}\tilde{V}(\phi^I). \tag{6.3}$$

The nonminimal couplings induce a curved field-space manifold in the Einstein frame with metric $\mathcal{G}_{IJ}(\phi^K) = (M_{\rm pl}^2/(2f))[\delta_{IJ}+3f_{,I}f_{,J}/f]$, where $f_{,I} = \partial f/\partial\phi^I$ [9]. We adopt the form for $f(\phi^I)$ required for renormalization [7],

$$f(\phi^I) = \frac{1}{2}\left[M_{\rm pl}^2 + \sum_I \xi_I(\phi^I)^2\right]. \tag{6.4}$$

Here we consider two-field models, $I, J = \phi, \chi$.

As emphasized in [11, 10, 9], the conformal stretching of the Einstein-frame potential, Eq. (6.3), generically leads to concave potentials at large field values, even for Jordan-frame potentials that are convex. In particular, for a Jordan-frame potential of the simple form $\tilde{V}(\phi^I) = \frac{\lambda_\phi}{4}\phi^4 + \frac{g}{2}\phi^2\chi^2 + \frac{\lambda_\chi}{4}\chi^4$, Eqs. (6.3) and (6.4) yield a potential in the Einstein frame that is nearly flat for large field values, $V(\phi^I) \to \lambda_J M_{\rm pl}^4/(4\xi_J^2)$ (no sum on J), as the Jth component of ϕ^I becomes arbitrarily large. This basic feature leads to "extra"-slow-roll evolution of the fields during inflation. If the couplings λ_J and ξ_J are not equal to each other, $V(\phi^I)$ develops ridges separated by valleys [9]. Inflation occurs in the valleys as well as along the ridges, since both are regions of false vacuum with $V \neq 0$. See Fig. 1.

Constraints on r constrain the energy scale of inflation, $H(t_*)/M_{\rm pl} < 3.7 \times 10^{-5}$ [4]. For Higgs inflation, with $\lambda_I = g = \lambda_\phi$ and $\xi_I = \xi_\phi$, the Hubble parameter during slow roll is given by $H/M_{\rm pl} \simeq \sqrt{\lambda_\phi/(12\xi_\phi^2)}$. Measurements of the Higgs mass near the electroweak symmetry-breaking scale require $\lambda_\phi \simeq 0.13$. Under renormalization-group flow, λ_ϕ will fall to the range $0 < \lambda_\phi < 0.01$ at the inflationary energy scale;

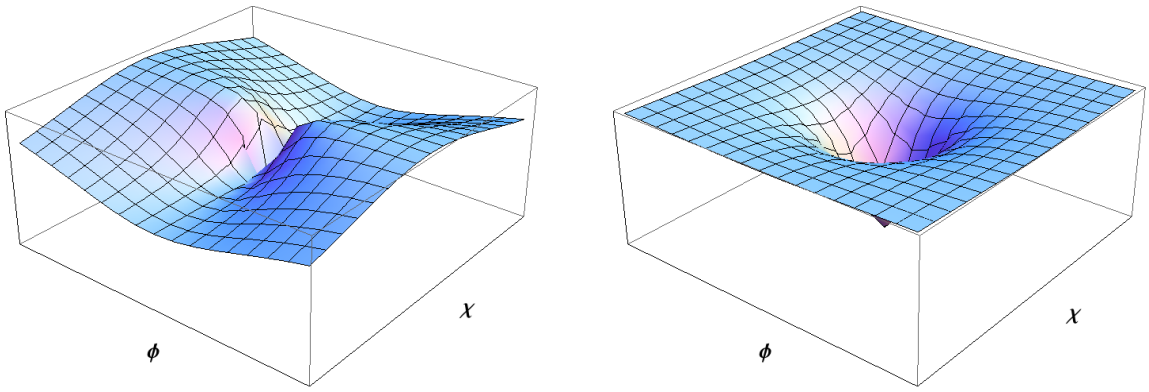

Figure 6-1: Potential in the Einstein frame, $V(\phi^I)$. *Left*: $\lambda_\chi = 0.75\,\lambda_\phi$, $g = \lambda_\phi$, $\xi_\chi = 1.2\,\xi_\phi$. *Right*: $\lambda_\chi = g = \lambda_\phi$, $\xi_\phi = \xi_\chi$. In both cases, $\xi_I \gg 1$ and $0 < \lambda_I, g < 1$.

$\lambda_\phi = 0.01$ requires $\xi_\phi \geq 780$ to satisfy the constraint on $H(t_*)/M_{\rm pl}$, which in turn requires $\xi_\phi \sim \mathcal{O}(10^1 - 10^2)$ at low energies [17]. For our general class of models, we therefore consider couplings at the inflationary energy scale of order $\lambda_I, g \sim \mathcal{O}(10^{-2})$ and $\xi_I \sim \mathcal{O}(10^3)$ [18].

Expanding the scalar fields to first order, $\phi^I(x^\mu) = \varphi^I(t) + \delta\phi^I(x^\mu)$, we find [9, 10]

$$\dot\sigma^2 = \mathcal{G}_{IJ}\dot\varphi^I\dot\varphi^J = \left(\frac{M_{\rm pl}^2}{2f}\right)\left[\dot\phi^2 + \dot\chi^2 + \frac{3\dot f^2}{f}\right]. \tag{6.5}$$

We also expand the spacetime metric to first order around a spatially flat Friedmann-Robertson-Walker metric. Then the background dynamics are given by [9]

$$\begin{gathered} H^2 = \frac{1}{3M_{\rm pl}^2}\left[\frac{1}{2}\dot\sigma^2 + V\right], \quad \dot H = -\frac{1}{2M_{\rm pl}^2}\dot\sigma^2, \\ \mathcal{D}_t\dot\varphi^I + 3H\dot\varphi^I + \mathcal{G}^{IK}V_{,K} = 0, \end{gathered} \tag{6.6}$$

where $\mathcal{D}_t$ is the (covariant) directional derivative, $\mathcal{D}_t A^I \equiv \dot\varphi^J\mathcal{D}_J A^I = \dot A^I + \Gamma^I{}_{JK}A^J\dot\varphi^K$ [19, 9]. The gauge-invariant Mukhanov-Sasaki variables for the linearized perturbations, Q^I, obey an equation of motion with a mass-squared matrix given by [19, 9]

$$\mathcal{M}^I{}_J \equiv \mathcal{G}^{IJ}\left(\mathcal{D}_J\mathcal{D}_K V\right) - \mathcal{R}^I{}_{LMJ}\dot\varphi^L\dot\varphi^M, \tag{6.7}$$

where $\mathcal{R}^I{}_{LMJ}$ is the Riemann tensor for the field-space manifold.

To analyze inflationary dynamics, we use a multifield formalism (see [2, 20] for reviews) made covariant with respect to the nontrivial field-space curvature (see [9, 19] and references therein). We define adiabatic and isocurvature directions in the curved field space via the unit vectors $\hat{\sigma}^I \equiv \dot{\varphi}^I/\dot{\sigma}$ and $\hat{s}^I \equiv \omega^I/\omega$, where the turn-rate vector is given by $\omega^I \equiv \mathcal{D}_t\hat{\sigma}^I$, and $\omega = |\omega^I|$. We also define slow-roll parameters [9, 19]:

$$\epsilon \equiv -\frac{\dot{H}}{H^2},\ \ \eta_{\sigma\sigma} \equiv M_{\rm pl}^2 \frac{\hat{\sigma}_I \hat{\sigma}^J \mathcal{M}^I{}_J}{V},\ \ \eta_{ss} \equiv M_{\rm pl}^2 \frac{\hat{s}_I \hat{s}^J \mathcal{M}^I{}_J}{V}. \tag{6.8}$$

Using Eq. (6.6), we have the exact relation, $\epsilon = 3\dot{\sigma}^2/(\dot{\sigma}^2 + 2V)$. The adiabatic and isocurvature perturbations may be parameterized as $\mathcal{R}_c = (H/\dot{\sigma})\hat{\sigma}_I Q^I$ and $\mathcal{S} = (H/\dot{\sigma})\hat{s}_I Q^I$, where $\mathcal{R}_c$ is the gauge-invariant curvature perturbation. Perturbations of pivot-scale $k_* = 0.002\,\mathrm{Mpc}^{-1}$ first crossed outside the Hubble radius during inflation at time t_*. In the long-wavelength limit, the evolution of $\mathcal{R}_c$ and $\mathcal{S}$ for $t > t_*$ is given by the transfer functions [9, 19]

$$\begin{aligned} T_{\mathcal{RS}}(t_*, t) &= \int_{t_*}^{t} dt'\, 2\omega(t') T_{\mathcal{SS}}(t_*, t'), \\ T_{\mathcal{SS}}(t_*, t) &= \exp\left[\int_{t_*}^{t} dt'\, \beta(t') H(t')\right], \end{aligned} \tag{6.9}$$

with $\beta(t) = -2\epsilon - \eta_{ss} + \eta_{\sigma\sigma} - \frac{4}{3}\frac{\omega^2}{H^2}$. Given the form of $T_{\mathcal{RS}}$, the perturbations $\mathcal{R}_c$ and $\mathcal{S}$ decouple if $\omega^I = 0$.

The dimensionless power spectrum for the adiabatic perturbations is defined as $\mathcal{P}_\mathcal{R}(k) = (2\pi)^{-2}k^3|\mathcal{R}_c|^2$ and the spectral index is defined as $n_s - 1 \equiv \partial \ln \mathcal{P}_\mathcal{R}/\partial \ln k$. Around t_* the spectral index is given by [9, 2, 20, 19]

$$n_s(t_*) = 1 - 6\epsilon(t_*) + 2\eta_{\sigma\sigma}(t_*). \tag{6.10}$$

At late times and in the long-wavelength limit, the power spectrum becomes $\mathcal{P}_\mathcal{R} = \mathcal{P}_\mathcal{R}(k_*)\,[1 + T_{\mathcal{RS}}^2]$, and hence the spectral index may be affected by the transfer of power from isocurvature to adiabatic modes: $n_s(t) = n_s(t_*) + H_*^{-1}(\partial T_{\mathcal{RS}}/\partial t_*)\sin(2\Delta)$, with $\cos\Delta \equiv T_{\mathcal{RS}}(1 + T_{\mathcal{RS}}^2)^{-1/2}$.

The mass of the isocurvature perturbations is $\mu_s^2 = 3H^2(\eta_{ss} + \omega^2/H^2)$ [9]. For $\mu_s < 3H/2$ we have $\mathcal{P}_\mathcal{S}(k_*) \simeq \mathcal{P}_\mathcal{R}(k_*)$ and hence $\mathcal{P}_S \simeq \mathcal{P}_\mathcal{R}(t_*)T^2_{\mathcal{SS}}$ at late times. In the Einstein frame the anisotropic pressure $\Pi^i{}_j \propto T^i{}_j$ for $i \neq j$ vanishes to linear order, so the tensor perturbations h_{ij} evolve just as in single-field models with $\mathcal{P}_T \simeq 128\,[H(t_*)/M_{\rm pl}]^2(k/k_*)^{-2\epsilon}$, and therefore $r \equiv \mathcal{P}_T/\mathcal{P}_\mathcal{R} = 16\epsilon/[1 + T^2_{\mathcal{RS}}]$ [2, 20, 19].

6.3 The Single-Field Attractor

To study the single-field attractor behavior, we first consider the case in which the system inflates in a valley along the $\chi = 0$ direction, perhaps after first rolling off a ridge. In the slow-roll limit and with $\chi \sim \dot\chi \sim 0$, Eq. (6.6) reduces to [10]

$$\dot\phi_{\rm SR} \simeq -\frac{\sqrt{\lambda_\phi}\,M_{\rm pl}^3}{3\sqrt{3}\,\xi_\phi^2\phi}. \tag{6.11}$$

Using $H/M_{\rm pl} \simeq \sqrt{\lambda_\phi/(12\xi_\phi^2)}$ we may integrate Eq. (6.11),

$$\frac{\xi_\phi\phi_*^2}{M_{\rm pl}^2} \simeq \frac{4}{3}N_*, \tag{6.12}$$

where N_* is the number of efolds before the end of inflation, and we have used $\phi(t_*) \gg \phi(t_{\rm end})$. (We arrive at comparable expressions if the system falls into a valley along some angle in field space, $\theta \equiv \arctan(\phi/\chi)$.) Eq. (6.5) becomes $\dot\sigma^2|_{\chi=0} \simeq 6M_{\rm pl}^2\dot\phi^2/\phi^2$ upon using $\xi_\phi \gg 1$. Using $V \simeq \lambda_\phi M_{\rm pl}^4/(4\xi_\phi^2)$ and Eqs. (6.11), (6.12) in Eq. (6.8) we find

$$\epsilon \simeq \frac{3}{4N_*^2}. \tag{6.13}$$

To estimate $\eta_{\sigma\sigma}$ we use $\eta_{\sigma\sigma} = \epsilon - \ddot\sigma/(H\dot\sigma) + \mathcal{O}(\epsilon^2)$ [2], and find

$$\eta_{\sigma\sigma} \simeq -\frac{1}{N_*}\left(1 - \frac{3}{4N_*}\right). \tag{6.14}$$

All dependence on λ_I and ξ_I has dropped out of these expressions for ϵ and $\eta_{\sigma\sigma}$ in Eqs. (6.13) and (6.14). For a broad range of initial field values and velocities —

and *independent* of the couplings — this entire class of models should quickly relax into an attractor solution in which the fields evolve along an effectively single-field trajectory with vanishing turn-rate, $\omega^I \sim 0$. Within this attractor solution we find analytically $\epsilon_* = 2.08 \times 10^{-4}$ and $\eta_{\sigma\sigma *} = -0.0165$ for $N_* = 60$; and $\epsilon_* = 3.00 \times 10^{-4}$ and $\eta_{\sigma\sigma *} = -0.0197$ for $N_* = 50$. To test this attractor behavior, we performed numerical simulations with a sampling of couplings and initial conditions. We fixed $\lambda_\phi = 0.01$ and $\xi_\phi = 10^3$ and looped over $\lambda_\chi = \{0.5, 0.75, 1\}\,\lambda_\phi$, $g = \{0.5, 0.75, 1\}\,\lambda_\phi$, and $\xi_\chi = \{0.8, 1, 1.2\}\,\xi_\phi$. These parameters gave a variety of potentials with combinations of ridges and valleys along different directions in field space. We set the initial amplitude of the fields to be $\sqrt{\phi_0^2 + \chi_0^2} = 10 \times \max[\xi_\phi^{-1/2}, \xi_\chi^{-1/2}]$ (in units of $M_{\rm pl}$), which generically produced 70 or more efolds of inflation. We varied the initial angle in field space, $\theta_0 = \arctan(\phi_0/\chi_0)$, among the values $\theta_0 = \{0, \pi/6, \pi/3, \pi/2\}$, and allowed for a relatively wide range of initial fields velocities: $\dot\phi_0, \dot\chi_0 = \{-10\,|\dot\phi_{\rm SR}|, 0, +10\,|\dot\phi_{\rm SR}|\}$, where $\dot\phi_{\rm SR}$ is given by Eq. (6.11).

Typical trajectories are shown in Fig. 6-2a. In each case, the fields quickly rolled into a valley and, after a brief, transient period of oscillation, evolved along a straight trajectory in field-space for the remainder of inflation with $\omega^I = 0$. Across this entire range of couplings and initial conditions, the analytic expressions for ϵ and $\eta_{\sigma\sigma}$ in Eqs. (6.13)-(6.14) provide close agreement with the exact numerical simulations. See Fig. 2b.

We confirmed numerically that for much larger initial field velocities, up to $\dot\phi_0, \dot\chi_0 \sim 10^6 |\dot\phi_{\rm SR}|$, such that the initial kinetic energy is larger than the difference between ridge-height and valley in the potential, the system exhibits a very brief, transient period of rapid angular motion (akin to [10]). The fields' kinetic energy rapidly redshifts away so that the fields land in a valley of the potential within a few efolds, after which slow-roll inflation continues along a single-field attractor trajectory just like the ones shown in Fig. 6-2a. Moreover, the attractor behavior is unchanged if one considers bare masses $m_\phi, m_\chi \ll M_{\rm pl}$ or a negative coupling $g < 0$, so long as one imposes the fairly minimal constraint that $V \geq 0$ and hence $g > -\sqrt{\lambda_\phi \lambda_\chi}$. (Each of these features could affect preheating dynamics but not the attractor be-

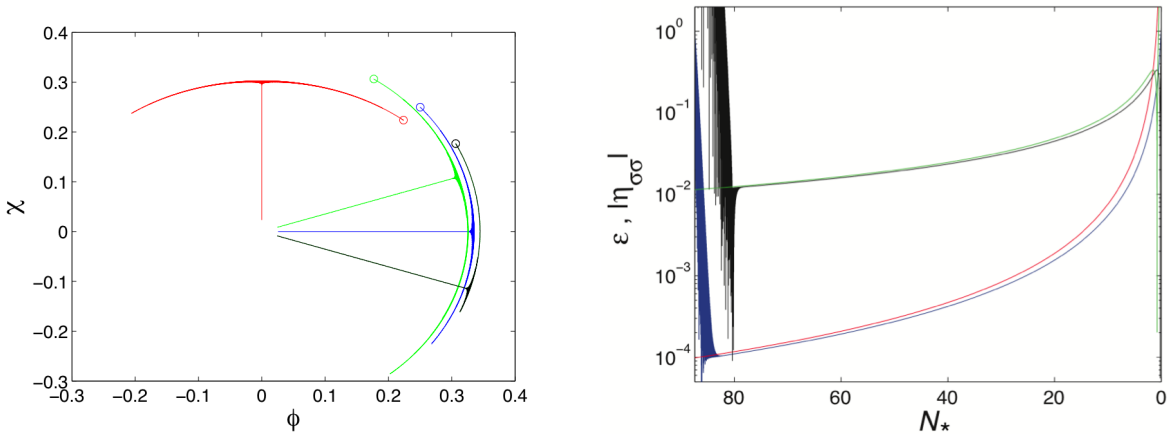

Figure 6-2: *Left*: Field trajectories for different couplings and initial conditions (here for $\dot{\phi}_0, \dot{\chi}_0 = 0$). Open circles indicate fields' initial values. The parameters $\{\lambda_\chi, g, \xi_\chi, \theta_0\}$ are given by: $\{0.75\lambda_\phi, \lambda_\phi, 1.2\xi_\phi, \pi/4\}$ (red), $\{\lambda_\phi, \lambda_\phi, 0.8\xi_\phi, \pi/4\}$ (blue), $\{\lambda_\phi, 0.75\lambda_\phi, 0.8\xi_\phi, \pi/6\}$ (green), $\{\lambda_\phi, 0.75\ \lambda_\phi, 0.8\xi_\phi, \pi/3\}$ (black). *Right*: Numerical vs. analytic evaluation of the slow-roll parameters, ϵ (numerical = blue, analytic = red) and $\eta_{\sigma\sigma}$ (numerical = black, analytic = green), for $\lambda_\phi = 0.01$, $\lambda_\chi = 0.75\ \lambda_\phi$, $g = \lambda_\phi$, $\xi_\phi = 10^3$, and $\xi_\chi = 1.2\ \xi_\phi$, with $\theta_0 = \pi/4$ and $\dot{\phi}_0 = \dot{\chi}_0 = +10\ |\dot{\phi}_{\rm SR}|$.

havior during inflation.) Lastly, we performed numerical simulations for the case of three fields rather than two, and again found that the dynamics quickly relax to the single-field attractor since the effective potential contains ridges and valleys, so the fields generically wind up within a valley.

6.4 Observables and the Attractor Solution

As we have confirmed numerically, trajectories in the single-field attractor solution generically have $\omega^I \sim 0$ between t_* and $t_{\rm end}$ (which we define as $\epsilon(t_{\rm end}) = 1$, or $\ddot{a}(t_{\rm end}) = 0$); hence $T_{\mathcal{RS}} \sim 0$ for these trajectories. The spectral index $n_s(t)$ therefore reduces to $n_s(t_*)$ of Eq. (6.10), and r reduces to $r = 16\epsilon\,[1 + \mathcal{O}(T^2_{\mathcal{RS}})] \simeq 16\epsilon$. Using Eqs. (6.13) and (6.14), we then find

$$n_s \simeq 1 - \frac{2}{N_*} - \frac{3}{N_*^2},\ \ r \simeq \frac{12}{N_*^2}, \tag{6.15}$$

and hence $n_s = 0.966$ and $r = 0.0033$ for $N_* = 60$; and $n_s = 0.959$ and $r = 0.0048$ for $N_* = 50$. We also calculated n_s and r numerically for each of the trajectories

described above, and found $n_s = 0.967$ and $r = 0.0031$ for $N_* = 60$, and $n_s = 0.960$ and $r = 0.0044$ for $N_* = 50$. These values sit right in the most-favored region of the latest observations. (See Fig. 1 in [4].) Even for a low reheat temperature, we find n_s within 2σ of the *Planck* value for $N_* \geq 38$. The predicted value $r \sim 10^{-3}$ could be tested by upcoming CMB polarization experiments.

For the running of the spectral index, $\alpha \equiv dn_s/d\ln k$, we use Eq. (6.15), the general relationship $(dx/d\ln k)\,|_* \simeq (\dot{x}/H)\,|_*$ [2], and $N_* = N_{\rm tot} - \int_{t_i}^{t_*} H dt$ to find

$$\alpha = \frac{dn_s}{d\ln k} \simeq -\frac{2}{N_*^2}\left(1 + \frac{3}{N_*}\right), \tag{6.16}$$

which yields $\alpha = -5.83 \times 10^{-4}$ for $N_* = 60$ and $\alpha = -8.48 \times 10^{-4}$ for $N_* = 50$, fully consistent with the result from *Planck*, $\alpha = -0.0134 \pm 0.0090$, indicating no observable running of the spectral index [4].

Meanwhile, for every trajectory in our large sample we numerically computed $f_{\rm NL}$ following the methods of [9]. Across the whole range of couplings and initial conditions considered here, we found $|f_{\rm NL}| < 0.1$, consistent with the latest observations [5]. In these models $f_{\rm NL}$ is exponentially sensitive to the fields' initial conditions, requiring a fine-tuning of $\mathcal{O}(10^{-4})$ to produce $|f_{\rm NL}| > 1$ [9]. In the absence of such fine-tuning these models generically predict $|f_{\rm NL}| \ll \mathcal{O}(1)$.

Unlike several models with concave potentials analyzed in [4], multifield models with nonminimal couplings should produce entropy efficiently at the end of inflation, when $\xi_I(\phi^I)^2 < M_{\rm pl}^2$. The energy density and pressure are given by $\rho = \frac{1}{2}\dot{\sigma}^2 + V(\phi^I)$ and $p = \frac{1}{2}\dot{\sigma}^2 - V(\phi^I)$ [9]. We confirmed numerically that for every trajectory in our large sample, the effective equation of state $w = p/\rho$ averaged to 0 beginning at $t_{\rm end}$ (when $\epsilon = 1$) and asymptoted to 1/3 within a few oscillations. This behavior may be understood analytically from the virial theorem, which acquires corrections proportional to gradients of the field-space metric coefficients, just like applications in curved spacetime [21]. We find $\langle \dot{\sigma}^2 \rangle = \langle V_{,J}\varphi^J \rangle + \langle \mathcal{C} \rangle = \langle 2M_{\rm pl}^4 V/f \rangle + \langle \mathcal{C} \rangle$, where $\mathcal{C} \equiv -\frac{1}{2}(\partial_J \mathcal{G}_{KL})\dot{\varphi}^K\dot{\varphi}^L\varphi^J$. More generally, inflation in these models ends with one or both fields oscillating quasi-periodically around the minimum of the potential, and

hence preheating should be efficient [2, 22, 23].

6.5 Isocurvature Perturbations

The models in this class predict three basic possibilities for isocurvature perturbations, depending on whether inflation occurs while the fields are in a valley, on top of a ridge, or in a symmetric potential with $\lambda_I = g = \lambda$ and $\xi_I = \xi$ and hence no ridges (like Higgs inflation). The fraction $\beta_{\rm iso}(k) \equiv \mathcal{P}_{\mathcal{S}}(k)/[\mathcal{P}_{\mathcal{R}}(k)+\mathcal{P}_{\mathcal{S}}(k)] = T^2_{\mathcal{SS}}/[1+T^2_{\mathcal{RS}}+T^2_{\mathcal{SS}}]$ [4] may distinguish between the various situations. In each of these scenarios, $\omega^I \sim 0$ and hence $T_{\mathcal{RS}} \sim 0$. Inflating in a valley, $\eta_{ss} > 1$ so $\mu_s^2/H^2 > 9/4$ and the (heavy) isocurvature modes are suppressed, $T_{\mathcal{SS}} \to 0$ and hence $\beta_{\rm iso} \sim 0$ for scales k corresponding to $N_* = 60 - 50$. Inflating on top of a ridge, $\eta_{ss} < 0$ so $\mu_s^2/H^2 < 0$ and the isocurvature modes grow via tachyonic instability, $T_{\mathcal{SS}} \gg 1$, and hence $\beta_{\rm iso} \sim 1$ across the same scales k. Scenarios in which the fields begin on top of a ridge and roll off at intermediate times can give any value $0 \leq \beta_{\rm iso} \leq 1$ depending sensitively upon initial conditions [24]. In the case of symmetric couplings, $\mu_s^2/H^2 \simeq 0$ [10], yielding $T_{\mathcal{SS}} \sim \mathcal{O}(10^{-3})$ and $\beta_{\rm iso} = 2.23 \times 10^{-5}$ for $N_* = 60$ and $\beta_{\rm iso} = 3.20 \times 10^{-5}$ for $N_* = 50$ [25].

6.6 Conclusions

Multifield models of inflation with nonminimal couplings possess a strong single-field attractor solution, such that they share common predictions for n_s, r, α, $f_{\rm NL}$, and for efficient entropy production across a broad range of couplings and initial conditions. The predicted spectral observables provide excellent agreement with the latest observations. These models differ, however, in their predicted isocurvature perturbation spectra, which might help break the observational degeneracy among members of this class.

Note. While the paper, which the present chapter is based on, was under review, similar results regarding attractor behavior in models with nonminimal couplings

were presented in [26].

6.7 Acknowledgements

It is a pleasure to thank Bruce Bassett, Rhys Borchert, Xingang Chen, Joanne Cohn, Alan Guth, Carter Huffman, Edward Mazenc, and Katelin Schutz for helpful discussions. This work was supported in part by the U.S. Department of Energy (DoE) under contract No. DE-FG02-05ER41360.

Bibliography

[1] A. H. Guth and D. I. Kaiser, "Inflationary cosmology: Exploring the universe from the smallest to the largest scales," Science **307**, 884 (2005) [arXiv:astro-ph/0502328].

[2] B. A. Bassett, S. Tsujikawa, and D. Wands, "Inflation dynamics and reheating," Rev. Mod. Phys. **78**, 537 (2006) [arXiv:astro-ph/0507632].

[3] WMAP collaboration, "Nine-year Wilkinson Microwave Anisotropy Probe (WMAP) observations: Cosmological parameter results," arXiv:1212.5226 [astro-ph.CO].

[4] Planck collaboration, "*Planck* 2013 results, XXII. Constraints on inflation," arXiv:1303.5082 [astro-ph.CO].

[5] Planck collaboration, "*Planck* 2013 results, XXIV. Constraints on primordial non-Gaussianity," arXiv:1303.5084 [astro-ph.CO].

[6] Planck collaboration, "*Planck* 2013 results, XV. CMB power spectra and likelihood," arXiv:1303.5075 [astro-ph.CO].

[7] N. D. Birrell and P. C. W. Davies, *Quantum Fields in Curved Space* (New York: Cambridge University Press, 1982).

[8] I. L. Buchbinder, S. D. Odintsov, and I. L. Shapiro, *Effective Action in Quantum Gravity* (New York: Taylor and Francis, 1992).

[9] D. I. Kaiser, E. A. Mazenc, and E. I. Sfakianakis, "Primordial bispectrum from multifield inflation with nonminimal couplings," Phys. Rev. D87 (2013): 064004 [arXiv:1210.7487 [astro-ph.CO]].

[10] R. N. Greenwood, D. I. Kaiser, and E. I. Sfakianakis, "Multifield dynamics of Higgs inflation," Phys. Rev. D87 (2013): 064021 [arXiv:1210.8190 [hep-ph]].

[11] F. L. Bezrukov and M. E. Shaposhnikov, "The Standard Model Higgs boson as the inflaton," Phys. Lett. **B659**, 703 (2008) [arXiv:0710.3755 [hep-th]].

[12] C. P. Burgess, H. M. Lee, and M. Trott, "On Higgs inflation and naturalness," JHEP 1007 (2010): 007 [arXiv:1002.2730 [hep-ph]]; M. P. Hertzberg, "On inflation with non-minimal coupling," JHEP 1011 (2010): 023 [arXiv: 1002.2995 [hep-ph]].

[13] S. Mooij and M. Postma, "Goldstone bosons and a dynamical Higgs field," JCAP 1109 (2011): 006 [arXiv:1104.4897 [hep-ph]].

[14] D. S. Salopek and J. R. Bond, "Nonlinear evolution of long-wavelength metric fluctuations in inflationary models," Phys. Rev. D 42 (1990): 3936; A. R. Liddle, P. Parsons, and J. D. Barrow, "Formalising the slow-roll approximation in inflation," Phys. Rev. D 50 (1994): 7222 [arXiv:astro-ph/9408015].

[15] R. Easther and L. C. Price, "Initial conditions and sampling for multifield inflation," arXiv:1304.4244 [astro-ph.CO].

[16] R. Fakir and W. G. Unruh, "Improvement on cosmological chaotic inflation through nonminimal coupling," Phys. Rev. D 41 (1990): 1792; D. S. Salopek, J. R. Bond, and J. M. Bardeen, "Designing density fluctuation spectra in inflation," Phys. Rev. D 40 (1989): 1753; N. Makino and M. Sasaki, "The density perturbation in the chaotic inflation with non-minimal coupling," Prog. Theo. Phys. 86 (1991): 103; D. I. Kaiser, "Primordial spectral indices from generalized Einstein theories," Phys. Rev. D 52 (1995): 4295 [arXiv:astro-ph/9408044];

E. Komatsu and T. Futamase, "Complete constraints on a nonminimally coupled chaotic inflationary scenario from the cosmic microwave background," Phys. Rev. D 59 (1999): 064029 [arXiv:astro-ph/9901127]; S. Tsujikawa and B. Gumjudpai, "Density perturbations in generalized Einstein scenarios and constraints on nonminimal couplings from the cosmic microwave background," Phys. Rev. D 69 (2004): 123523 [arXiv:astro-ph/0402185]; A. Linde, M. Noorbala, and A. Westphal, "Observational consequences of chaotic inflation with nonminimal coupling to gravity," JCAP 1103 (2011): 013 [arXiv:1101.2652 [hep-th]].

[17] F. Bezrukov, M. Yu. Kalmykov, B. A. Kniehl, and M. Shaposhnikov, "Higgs boson mass and new physics," arXiv:1205.2893 [hep-ph]. See also A. O. Barvinsky, A. Yu. Kamenschchik, C. Kiefer, A. A. Starobinsky, and C. F. Steinwachs, "Asymptotic freedom in inflationary cosmology with a nonminimally coupled Higgs field," JCAP 0912 (2009): 003 [arXiv:0904.1698 [hep-ph]]; A. De Simone, M. P. Hertzberg, and F. Wilczek, "Running inflation in the Standard Model," Phys. Lett. B 678 (2009): 1-8 [arXiv:0812.4946 [hep-ph]]; K. Allison, "Higgs ξ-inflation for the $125-126$ GeV Higgs: A two-loop analysis," arXiv:1306.6931 [hep-ph].

[18] There has been vigorous debate over whether such models with $\xi_I \gg 1$ violate unitarity (see Refs. 12, 14, 15, 24, and 25 of [10]). However, the constraint $H(t_*)/M_{\rm pl} < 10^{-5}$ means that the unitarity cutoff scale $\Lambda \gg H$ during inflation, and hence for the domain of interest we may rely on the classical background dynamics as analyzed here.

[19] D. Langlois and S. Renaux-Petel, "Perturbations in generalized multi-field inflation," JCAP 0804 (2008): 017 [arXiv:0801.1085 [hep-th]]; C. M. Peterson and M. Tegmark, "Testing multi-field inflation: A geometric approach," arXiv:1111.0927 [astro-ph.CO].

[20] D. Wands, "Multiple field inflation," Lect. Notes. Phys. **738**, 275 (2008) [arXiv:astro-ph/0702187].

[21] E. Gourgoulhon and S. Bonazzola, "A formulation of the virial theorem in general relativity," Class. Quantum Grav. 11 (1994): 443.

[22] B. A. Bassett and S. Liberati, "Geometric reheating after inflation," Phys. Rev. D 58 (1998): 021302 [arXiv:hep-ph/9709417]; S. Tsujikawa and B. A. Bassett, "When can preheating affect the CMB?," Phys. Lett. B 536 (2002): 9 [arXiv:astro-ph/0204031].

[23] F. Bezrukov, D. Gorbunov, and M. Shaposhnikov, "On initial conditions for the hot big bang," JCAP 0906 (2009): 029 [arXiv:0812.3622 [hep-ph]]; J. García-Bellido, D. G. Figueroa, and J. Rubio, "Preheating in the Standard Model with the Higgs-inflaton coupled to gravity," Phys. Rev. D 79 (2009): 063531 [arXiv:0812.4624 [hep-ph]]; J.-F. Dufaux, D. G. Figueroa, and J. García-Bellido, "Gravitational waves from Abelian gauge fields and cosmic strings at preheating," Phys. Rev. D 82 (2010): 083518 [arXiv:1006.0217 [astro-ph.CO]].

[24] K. Schutz, E. I. Sfakianakis, and D. I. Kaiser, "Multifield inflation after *Planck*: Isocurvature modes from nonminimal couplings," arXiv:1310.8285 [astro-ph.CO].

[25] In the case of Higgs inflation, in which the inflaton has no couplings other than to Standard Model particles, some as-yet unknown mechanism would be required to preserve primordial isocurvature perturbations through reheating. Primordial isocurvature perturbations could more readily survive reheating in symmetric-coupling models if the inflaton coupled to some non-Standard Model particles, such as cold dark matter particles.

[26] R. Kallosh and A. Linde, "Non-minimal inflationary attractors," arXiv:1307.7938 [hep-th]; R. Kallosh and A. Linde, "Multi-field conformal cosmological attractors," arXiv:1309.2015 [hep-th]; R. Kallosh, A. Linde,

and D. Roest, "A universal attractor for inflation at strong coupling," arXiv:1310.3950 [hep-th]; R. Kallosh, A. Linde, and D. Roest, "Superconformal inflationary α-attractors," arXiv:1311.0472 [hep-th].

[27] S. Ferrara, R. Kallosh, A. Linde, A. Marrani, and A. Van Proeyen, "Superconformal symmetry, NMSSM, and inflation," Phys. Rev. D83 (2011): 025008 [arXiv:1008.2942 [hep-th]]; F. Bezrukov, A. Magnin, M. Shaposhnikov, and S. Sibiryakov, "Higgs inflation: Consistency and generalizations," JHEP 1101 (2011): 016 [arXiv:1008.5157 [hep-ph]].

Chapter 7

Multifield Inflation after *Planck*: Isocurvature Modes from Nonminimal Couplings

Recent measurements by the *Planck* experiment of the power spectrum of temperature anisotropies in the cosmic microwave background radiation (CMB) reveal a deficit of power in low multipoles compared to the predictions from best-fit ΛCDM cosmology. If the low-ℓ anomaly persists after additional observations and analysis, it might be explained by the presence of primordial isocurvature perturbations in addition to the usual adiabatic spectrum, and hence may provide the first robust evidence that early-universe inflation involved more than one scalar field. In this chapter we explore the production of isocurvature perturbations in nonminimally coupled two-field inflation. We find that this class of models readily produces enough power in the isocurvature modes to account for the *Planck* low-ℓ anomaly, while also providing excellent agreement with the other *Planck* results.

7.1 Introduction

Inflation is a leading cosmological paradigm for the early universe, consistent with the myriad of observable quantities that have been measured in the era of precision

cosmology [1, 2, 3]. However, a persistent challenge has been to reconcile successful inflationary scenarios with well-motivated models of high-energy physics. Realistic models of high-energy physics, such as those inspired by supersymmetry or string theory, routinely include multiple scalar fields at high energies [4]. Generically, each scalar field should include a nonminimal coupling to the spacetime Ricci curvature scalar, since nonminimal couplings arise as renormalization counterterms when quantizing scalar fields in curved spacetime [5, 6, 7, 8]. The nonminimal couplings typically increase with energy-scale under renormalization-group flow [7], and hence should be large at the energy-scales of interest for inflation. We therefore study a class of inflationary models that includes multiple scalar fields with large nonminimal couplings.

It is well known that the predicted perturbation spectra from single-field models with nonminimal couplings produce a close fit to observations. Following conformal transformation to the Einstein frame, in which the gravitational portion of the action assumes canonical Einstein-Hilbert form, the effective potential for the scalar field is stretched by the conformal factor to be concave rather than convex [9, 10], precisely the form of inflationary potential most favored by the latest results from the *Planck* experiment [11].

The most pronounced difference between multifield inflation and single-field inflation is the presence of more than one type of primordial quantum fluctuation that can evolve and grow. The added degrees of freedom may lead to observable departures from the predictions of single-field models, including the production and amplification of isocurvature modes during inflation [12, 13, 14, 15, 16, 17, 18, 19].

Unlike adiabatic perturbations, which are fluctuations in the energy density, isocurvature perturbations arise from spatially varying fluctuations in the local equation of state, or from relative velocities between various species of matter. When isocurvature modes are produced primordially and stretched beyond the Hubble radius, causality prevents the redistribution of energy density on super-horizon scales. When the perturbations later cross back within the Hubble radius, isocurvature modes create pressure gradients that can push energy density around, sourcing curvature perturbations that contribute to large-scale anisotropies in the cosmic microwave background

radiation (CMB). (See, e.g., [20, 11].)

The recent measurements of CMB anisotropies by *Planck* favor a combination of adiabatic and isocurvature perturbations in order to improve the fit at low multipoles ($\ell \sim 20 - 40$) compared to the predictions from the simple, best-fit ΛCDM model in which primordial perturbations are exclusively adiabatic. The best fit to the present data arises from models with a modest contribution from isocurvature modes, whose primordial power spectrum $\mathcal{P}_{\mathcal{S}}(k)$ is either scale-invariant or slightly blue-tilted, while the dominant adiabatic contribution, $\mathcal{P}_{\mathcal{R}}(k)$, is slightly red-tilted [11]. The low-ℓ anomaly thus might provide the first robust empirical evidence that early-universe inflation involved more than one scalar field.

Well-known multifield models that produce isocurvature perturbations, such as axion and curvaton models, are constrained by the *Planck* results and do not improve the fit compared to the purely adiabatic ΛCDM model [11]. As we demonstrate here, on the other hand, the general class of multifield models with nonminimal couplings can readily produce isocurvature perturbations of the sort that could account for the low-ℓ anomaly in the *Planck* data, while also producing excellent agreement with the other spectral observables measured or constrained by the *Planck* results, such as the spectral index n_s, the tensor-to-scalar ratio r, the running of the spectral index α, and the amplitude of primordial non-Gaussianity $f_{\rm NL}$.

Nonminimal couplings in multifield models induce a curved field-space manifold in the Einstein frame [21], and hence one must employ a covariant formalism for this class of models. Here we make use of the covariant formalism developed in [22], which builds on pioneering work in [13, 18]. In Section 7.2 we review the most relevant features of our class of models, including the formal machinery required to study the evolution of primordial isocurvature perturbations. In Section 7.3 we focus on a regime of parameter space that is promising in the light of the *Planck* data, and for which analytic approxmations are both tractable and in close agreement with numerical simulations. In Section 7.4 we compare the predictions from this class of models to the recent *Planck* findings. Concluding remarks follow in Section 7.5.

7.2 Model

We consider two nonminimally coupled scalar fields $\phi^I \, \epsilon \, \{\phi, \, \chi\}$. We work in 3+1 spacetime dimensions with the spacetime metric signature $(-, \, +, \, +, \, +)$. We express our results in terms of the reduced Planck mass, $M_{\rm pl} \equiv (8\pi G)^{-1/2} = 2.43 \times 10^{18}$ GeV. Greek letters (μ, ν) denote spacetime 4-vector indices, lower-case Roman letters (i, j) denote spacetime 3-vector indices, and capital Roman letters (I, J) denote field-space indices. We indicate Jordan-frame quantities with a tilde, while Einstein-frame quantities will be *sans* tilde. Subscripted commas indicate ordinary partial derivatives and subscripted semicolons denote covariant derivatives with respect to the spacetime coordinates.

We begin with the action in the Jordan frame, in which the fields' nonminimal couplings remain explicit:

$$\tilde{S} = \int d^4x \sqrt{-\tilde{g}} \left[f(\phi^I) \tilde{R} - \frac{1}{2} \tilde{\mathcal{G}}_{IJ} \tilde{g}^{\mu\nu} \partial_\mu \phi^I \partial_\nu \phi^J - \tilde{V}(\phi^I) \right], \tag{7.1}$$

where $\tilde{R}$ is the spacetime Ricci scalar, $f(\phi^I)$ is the nonminimal coupling function, and $\tilde{\mathcal{G}}_{IJ}$ is the Jordan-frame field space metric. We set $\tilde{\mathcal{G}}_{IJ} = \delta_{IJ}$, which gives canonical kinetic terms in the Jordan frame. We take the Jordan-frame potential, $\tilde{V}(\phi^I)$, to have a generic, renormalizable polynomial form with an interaction term:

$$\tilde{V}(\phi, \chi) = \frac{\lambda_\phi}{4} \phi^4 + \frac{g}{2} \phi^2 \chi^2 + \frac{\lambda_\chi}{4} \chi^4, \tag{7.2}$$

with dimensionless coupling constants λ_I and g. As discussed in [22], the inflationary dynamics in this class of models are relatively insensitive to the presence of mass terms, $m_\phi^2 \phi^2$ or $m_\chi^2 \chi^2$, for realistic values of the masses that satisfy $m_\phi, m_\chi \ll M_{\rm pl}$. Hence we will neglect such terms here.

7.2.1 Einstein-Frame Potential

We perform a conformal transformation to the Einstein frame by rescaling the space-time metric tensor,

$$\tilde{g}_{\mu\nu}(x) = \Omega^2(x)\, g_{\mu\nu}(x), \tag{7.3}$$

where the conformal factor $\Omega^2(x)$ is related to the nonminimal coupling function via the relation

$$\Omega^2(x) = \frac{2}{M_{\rm pl}^2} f\left(\phi^I(x)\right). \tag{7.4}$$

This transformation yields the action in the Einstein frame,

$$S = \int d^4x\sqrt{-g}\left[\frac{M_{\rm pl}^2}{2}R - \frac{1}{2}\mathcal{G}_{IJ}g^{\mu\nu}\partial_\mu\phi^I\partial_\nu\phi^J - V(\phi^I)\right], \tag{7.5}$$

where all the terms *sans* tilde are stretched by the conformal factor. For instance, the conformal transformation to the Einstein frame induces a nontrivial field-space metric [21]

$$\mathcal{G}_{IJ} = \frac{M_{\rm pl}^2}{2f}\left[\delta_{IJ} + \frac{3}{f}\, f_{,I}f_{,J}\right], \tag{7.6}$$

and the potential is also stretched so that it becomes

$$\begin{aligned} V(\phi,\chi) &= \frac{M_{\rm pl}^4}{(2f)^2}\tilde{V}(\phi,\chi) \\ &= \frac{M_{\rm pl}^4}{(2f)^2}\left[\frac{\lambda_\phi}{4}\phi^4 + \frac{g}{2}\phi^2\chi^2 + \frac{\lambda_\chi}{4}\chi^4\right]. \end{aligned} \tag{7.7}$$

The form of the nonminimal coupling function is set by the requirements of renormalization [5, 6],

$$f(\phi,\chi) = \frac{1}{2}[M^2 + \xi_\phi\phi^2 + \xi_\chi\chi^2], \tag{7.8}$$

where ξ_ϕ and ξ_χ are dimensionless couplings and M is some mass scale such that when the fields settle into their vacuum expectation values, $f \to M_{\rm pl}^2/2$. Here we assume that any nonzero vacuum expectation values for ϕ and χ are much smaller than the Planck scale, and hence we may take $M = M_{\rm pl}$.

The conformal stretching of the potential in the Einstein frame makes it concave

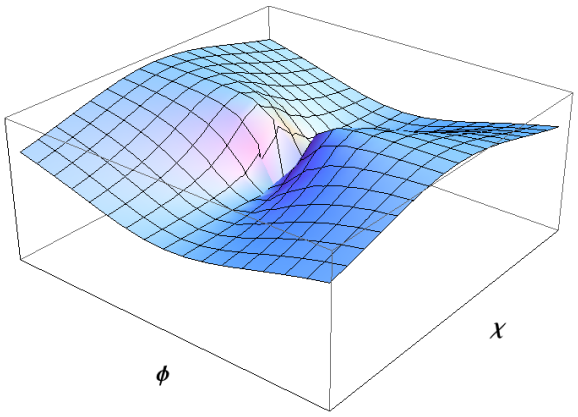

Figure 7-1: Potential in the Einstein frame, $V(\phi^I)$ in Eq. (7.7). The parameters shown here are $\lambda_\chi = 0.75\,\lambda_\phi$, $g = \lambda_\phi$, $\xi_\chi = 1.2\,\xi_\phi$, with $\xi_\phi \gg 1$ and $\lambda_\phi > 0$.

and asymptotically flat along either direction in field space, $I = \phi, \chi$,

$$V(\phi^I) \to \frac{M_{\rm pl}^4}{4}\frac{\lambda_I}{\xi_I^2}\left[1 + \mathcal{O}\left(\frac{M_{\rm pl}^2}{\xi_J(\phi^I)^2}\right)\right] \tag{7.9}$$

(no sum on I). For non-symmetric couplings, in which $\lambda_\phi \neq \lambda_\chi$ and/or $\xi_\phi \neq \xi_\chi$, the potential in the Einstein frame will develop ridges and valleys, as shown in Fig. 7-1. Crucially, $V > 0$ even in the valleys (for $g > -\sqrt{\lambda_\phi \lambda_\chi}$), and hence the system will inflate (albeit at varying rates) whether the fields ride along a ridge or roll within a valley, until the fields reach the global minimum of the potential at $\phi = \chi = 0$.

Across a wide range of couplings and initial conditions, the models in this class obey a single-field attractor [19]. If the fields happen to begin evolving along the top of a ridge, they will eventually fall into a neighboring valley. Motion in field space transverse to the valley will quickly damp away (thanks to Hubble drag), and the fields' evolution will include almost no further turning in field space. Within that single-field attractor, predictions for n_s, r, α, and $f_{\rm NL}$ all fall squarely within the most-favored regions of the latest *Planck* measurements [19].

The fields' approach to the attractor behavior — essentially, how quickly the fields roll off a ridge and into a valley — depends on the local curvature of the potential near the top of a ridge. Consider, for example, the case in which the direction $\chi = 0$ corresponds to a ridge. To first order, the curvature of the potential in the vicinity

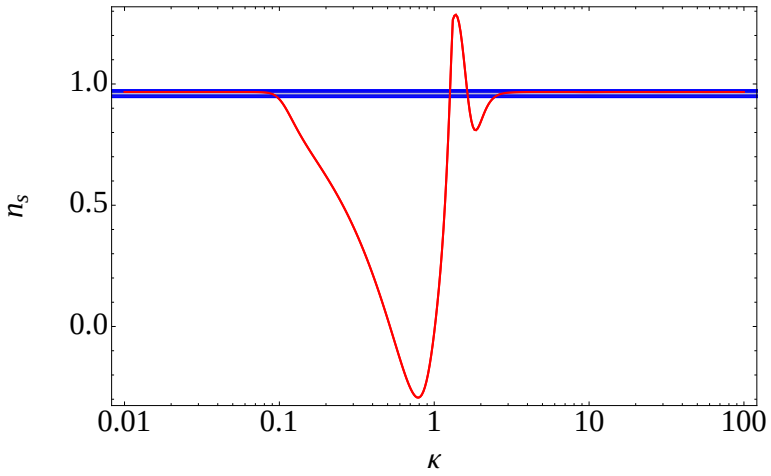

Figure 7-2: The spectral index n_s (red), as given in Eq. (7.61), for different values of κ, which characterizes the local curvature of the potential near the top of a ridge. Also shown are the 1σ (thin, light blue) and 2σ (thick, dark blue) bounds on n_s from the *Planck* measurements. The couplings shown here correspond to $\xi_\phi = \xi_\chi = 10^3$, $\lambda_\phi = 10^{-2}$, and $\lambda_\chi = g$, fixed for a given value of κ from Eq. (7.10). The fields' initial conditions are $\phi = 0.3$, $\dot{\phi}_0 = 0$, $\chi_0 = 10^{-3}$, $\dot{\chi}_0 = 0$, in units of $M_{\rm pl}$.

of $\chi = 0$ is proportional to $(g\xi_\phi - \lambda_\phi \xi_\chi)$ [22]. As we develop in detail below, a convenient combination with which to characterize the local curvature near the top of such a ridge is

$$\kappa \equiv \frac{4(\lambda_\phi \xi_\chi - g\xi_\phi)}{\lambda_\phi}. \tag{7.10}$$

As shown in Fig. 7-2, models in this class produce excellent agreement with the latest measurements of n_s from *Planck* across a wide range of parameters, where $n_s \equiv 1 + d\ln\mathcal{P}_\mathcal{R}/d\ln k$. Strong curvature near the top of the ridge corresponds to $\kappa \gg 1$: in that regime, the fields quickly roll off the ridge, settle into a valley of the potential, and evolve along the single-field attractor for the duration of inflation, as analyzed in [19]. More complicated field dynamics occur for intermediate values, $0.1 < \kappa < 4$, for which multifield dynamics pull n_s far out of agreement with empirical observations. The models again produce excellent agreement with the *Planck* measurements of n_s in the regime of weak curvature, $0 \leq \kappa \leq 0.1$.

As we develop below, other observables of interest, such as r, α, and $f_{\rm NL}$, likewise show excellent fit with the latest observations. In addition, the regime of weak

curvature, $\kappa \ll 1$, is particularly promising for producing primordial isocurvature perturbations with characteristics that could explain the low-ℓ anomaly in the recent *Planck* measurements. Hence for the remainder of this chapter we focus on the regime $\kappa \ll 1$, a region that is amenable to analytic as well as numerical analysis.

7.2.2 Coupling Constants

The dynamics of this class of models depend upon combinations of dimensionless coupling constants like κ defined in Eq. (7.10) and others that we introduce below. The phenomena analyzed here would therefore hold for various values of λ_I and ξ_I, such that combinations like κ were unchanged. Nonetheless, it is helpful to consider reasonable ranges for the couplings on their own.

The present upper bound on the tensor-to-scalar ratio, $r < 0.12$, constrains the energy-scale during inflation to satisfy $H(t_{\rm hc})/M_{\rm pl} \leq 3.7 \times 10^{-5}$ [11], where $H(t_{\rm hc})$ is the Hubble parameter at the time during inflation when observationally relevant perturbations first crossed outside the Hubble radius. During inflation the dominant contribution to H will come from the value of the potential along the direction in which the fields slowly evolve. Thus we may use the results from *Planck* and Eq. (7.9) to set a basic scale for the ratios of couplings, λ_I/ξ_I^2. For example, if the fields evolve predominantly along the direction $\chi \sim 0$, then during slow roll the Hubble parameter will be

$$H \simeq \sqrt{\frac{\lambda_\phi}{12\xi_\phi^2}}\, M_{\rm pl}, \tag{7.11}$$

and hence the constraint from *Planck* requires $\lambda_\phi/\xi_\phi^2 \leq 1.6 \times 10^{-8}$.

We adopt a scale for the self-couplings λ_I by considering a particularly elegant member of this class of models. In Higgs inflation [10], the self-coupling λ_ϕ is fixed by measurements of the Higgs mass near the electroweak symmetry-breaking scale, $\lambda_\phi \simeq 0.1$, corresponding to $m_H \simeq 125$ GeV [23, 24]. Under renormalization-group flow, λ_ϕ will fall to the range $0 < \lambda_\phi < 0.01$ at the inflationary energy scale [28]. Eq. (7.11) with $\lambda = 0.01$ requires $\xi_\phi \geq 780$ at inflationary energy scales to give the correct amplitude of density perturbations. For our general class of models, we therefore

consider couplings at the inflationary energy scale of order $\lambda_I, g \sim \mathcal{O}(10^{-2})$ and $\xi_I \sim \mathcal{O}(10^3)$. Taking into account the running of both λ_I and ξ_I under renormalization-group flow, these values correspond to $\lambda_I \sim \mathcal{O}(10^{-1})$ and $\xi_I \sim \mathcal{O}(10^2)$ at low energies [28].

We consider these to be reasonable ranges for the couplings. Though one might prefer dimensionless coupling constants to be $\mathcal{O}(1)$ in any "natural" scenario, the ranges chosen here correspond to low-energy couplings that are no more fine-tuned than the fine-structure constant, $\alpha_{\rm EM} \simeq 1/137$. Indeed, our choices are relatively conservative. For the case of Higgs inflation, the running of λ_ϕ is particularly sensitive to the mass of the top quark. Assuming a value for $m_{\rm top}$ at the low end of the present 2σ bound yields $\lambda_\phi \simeq 10^{-4}$ rather than 10^{-2} at high energies, which in turn requires $\xi_\phi \geq 80$ at the inflationary energy scale rather than $\xi_\phi \geq 780$ [29]. Nonetheless, for illustrative purposes, we use $\lambda_I, g \sim 10^{-2}$ and $\xi_I \sim 10^3$ for the remainder of our analysis.

We further note that despite such large nonminimal couplings, $\xi_I \sim 10^3$, our analysis is unhindered by any potential breakdown of unitarity. The energy scale at which unitarity might be violated for Higgs inflation has occasioned a great deal of heated debate in the literature, with conflicting claims that the renormalization cut-off scale should be in the vicinity of $M_{\rm pl}$, $M_{\rm pl}/\sqrt{\xi_\phi}$, or $M_{\rm pl}/\xi_\phi$ [30]. Even if one adopted the most stringent of these suggested cut-off scales, $M_{\rm pl}/\xi_\phi \sim 10^{-3}\, M_{\rm pl}$, the relevant dynamics for our analysis would still occur at energy scales well below the cut-off, given the constraint $H(t_{\rm hc}) \leq 3.7 \times 10^{-5}\, M_{\rm pl}$. (The unitarity cut-off scale in multifield models in which the nonminimal couplings ξ_I are not all equal to each other has been considered in [31], which likewise identify regimes of parameter space in which $\Lambda_{\rm eff}$ remains well above the energy scales and field values relevant to inflation.) Moreover, models like Higgs inflation can easily be "unitarized" with the addition of a single heavy scalar field [32], and hence all of the following analysis could be considered the low-energy dynamics of a self-consistent effective field theory. The methods developed here may be applied to a wide class of models, including those studied in [39, 40, 41, 42].

Finally, we note that for couplings $\lambda_I, g \sim 10^{-2}$ and $\xi_I \sim 10^3$ at high energies, the regime of weak curvature for the potential, $\kappa < 0.1$, requires that the couplings be close but not identical to each other. In particular, $\kappa \sim 0.1$ requires $g/\lambda_\phi \sim \xi_\chi/\xi_\phi \sim 1 \pm \mathcal{O}(10^{-5})$. Such small differences are exactly what one would expect if the effective couplings at high energies arose from some softly broken symmetry. For example, the field χ could couple to some scalar cold dark matter (CDM) candidate (perhaps a supersymmetric partner) or to a neutrino, precisely the kinds of couplings that would be required if the primordial isocurvature perturbations were to survive to late times and get imprinted in the CMB [20]. In that case, corrections to the β functions for the renormalization-group flow of the couplings λ_χ and ξ_χ would appear of the form $g_X^2/16\pi^2$ [7, 33], where g_X is the coupling of χ to the new field. For reasonable values of $g_X \sim 10^{-1} - 10^{-2}$, such additional terms could easily account for the small but non-zero differences among couplings at the inflationary energy scale.

7.2.3 Dynamics and Transfer Functions

When we vary the Einstein-frame action with respect to the fields ϕ^I, we get the equations of motion, which may be written

$$\Box\phi^I + \Gamma^I_{JK}\partial_\mu\phi^J\partial^\mu\phi^K - \mathcal{G}^{IJ}V_{,K} = 0, \tag{7.12}$$

where $\Box\phi^I \equiv g^{\mu\nu}\phi^I_{;\mu;\nu}$ and Γ^I_{JK} is the field-space Christoffel symbol.

We further expand each scalar field to first order in perturbations about its classical background value,

$$\phi^I(x^\mu) = \varphi^I(t) + \delta\phi^I(x^\mu) \tag{7.13}$$

and we consider scalar perturbations to the spacetime metric (which we assume to be a spatially flat Friedmann-Robertson-Walker metric) to first order:

$$\begin{aligned} ds^2 = &-(1+2A)dt^2 + 2a(t)(\partial_i B)dx^i dt + \\ &a(t)^2[(1-2\psi)\delta_{ij} + 2\partial_i\partial_j E]dx^i dx^j, \end{aligned} \tag{7.14}$$

where $a(t)$ is the scale factor and A, B, ψ and E are the scalar gauge degrees of freedom.

Under this expansion, the full equations of motion separate into background and first-order equations. The background equations are given by

$$\mathcal{D}_t\dot{\varphi}^I + 3H\dot{\varphi}^I + \mathcal{G}^{IJ}V_{,J} = 0, \tag{7.15}$$

where $\mathcal{D}_J A^I \equiv \partial_J A^I + \Gamma^I_{\ JK}A^K$ for an arbitrary vector, A^I, on the field-space manifold; $\mathcal{D}_t A^I \equiv \dot{\varphi}^J \mathcal{D}_J A^I$ is a directional derivative; and $H \equiv \dot{a}/a$ is the Hubble parameter. The 00 and $0i$ components of the background-order Einstein equations yield:

$$\begin{aligned} H^2 &= \frac{1}{3M_{\rm pl}^2}\left[\frac{1}{2}\mathcal{G}_{IJ}\dot{\varphi}^I\dot{\varphi}^J + V(\varphi^I)\right] \\ \dot{H} &= -\frac{1}{2M_{\rm pl}^2}\mathcal{G}_{IJ}\dot{\varphi}^I\dot{\varphi}^J. \end{aligned} \tag{7.16}$$

Using the covariant formalism of [22], we find the equations of motion for the perturbations,

$$\begin{aligned} &\mathcal{D}_t^2 Q^I + 3H\mathcal{D}_t Q^I + \\ &\quad\left[\frac{k^2}{a^2}\delta^I_J + \mathcal{M}^I_{\ J} - \frac{1}{M_{\rm pl}^2 a^3}\mathcal{D}_t\left(\frac{a^3}{H}\dot{\varphi}^I\dot{\varphi}_J\right)\right]Q^J = 0, \end{aligned} \tag{7.17}$$

where Q^I is the gauge-invariant Mukhanov-Sasaki variable

$$Q^I = \mathcal{Q}^I + \frac{\dot{\varphi}^I}{H}\psi, \tag{7.18}$$

and $\mathcal{Q}^I$ is a covariant fluctuation vector that reduces to $\delta\phi^I$ to first order in the fluctuations. Additionally, $\mathcal{M}^I_{\ J}$ is the effective mass-squared matrix given by

$$\mathcal{M}^I_{\ J} \equiv \mathcal{G}^{IK}\mathcal{D}_J\mathcal{D}_K V - \mathcal{R}^I_{\ LMJ}\dot{\varphi}^L\dot{\varphi}^M, \tag{7.19}$$

where $\mathcal{R}^I_{\ LMJ}$ is the field-space Riemann tensor.

The degrees of freedom of the system may be decomposed into adiabatic and

entropic (or isocurvature) by introducing the magnitude of the background fields' velocity vector,

$$\dot{\sigma} \equiv |\dot{\varphi}^I| = \sqrt{\mathcal{G}_{IJ}\dot{\varphi}^I\dot{\varphi}^J}, \tag{7.20}$$

with which we may define the unit vector

$$\hat{\sigma}^I \equiv \frac{\dot{\varphi}^I}{\dot{\sigma}} \tag{7.21}$$

which points along the fields' motion. Another important dynamical quantity is the turn-rate of the background fields, given by

$$\omega^I = \mathcal{D}_t\hat{\sigma}^I, \tag{7.22}$$

with which we may construct another important unit vector,

$$\hat{s}^I \equiv \frac{\omega^I}{\omega}, \tag{7.23}$$

where $\omega = |\omega^I|$. The vector $\hat{s}^I$ points perpendicular to the fields' motion, $\hat{s}^I\hat{\sigma}_I = 0$. The unit vectors $\hat{\sigma}^I$ and $\hat{s}^I$ effectively act like projection vectors, with which we may decompose any vector into adiabatic and entropic components. In particular, we may decompose the vector of fluctuations Q^I,

$$\begin{aligned} Q_\sigma &\equiv \hat{\sigma}_I Q^I \\ Q_s &\equiv \hat{s}_I Q^I, \end{aligned} \tag{7.24}$$

in terms of which Eq. (7.17) separates into two equations of motion:

$$\begin{aligned} &\ddot{Q}_\sigma + 3H\dot{Q}_\sigma + \left[\frac{k^2}{a^2} + \mathcal{M}_{\sigma\sigma} - \omega^2 - \frac{1}{M_{\rm pl}^2 a^3}\frac{d}{dt}\left(\frac{a^3\dot{\sigma}^2}{H}\right)\right] Q_\sigma \\ &\quad = 2\,\frac{d}{dt}\left(\omega\, Q_s\right) - 2\left(\frac{V_{,\sigma}}{\dot{\sigma}} + \frac{\dot{H}}{H}\right)\omega\, Q_s, \end{aligned} \tag{7.25}$$

$$\ddot{Q}_s + 3H\dot{Q}_s + \left[\frac{k^2}{a^2} + \mathcal{M}_{ss} + 3\omega^2\right] Q_s = 4M_{\rm pl}^2\,\frac{\omega}{\dot{\sigma}}\frac{k^2}{a^2}\Psi, \tag{7.26}$$

where Ψ is the gauge-invariant Bardeen potential [3],

$$\Psi \equiv \psi + a^2 H \left(\dot{E} - \frac{B}{a} \right), \tag{7.27}$$

and where $\mathcal{M}_{\sigma\sigma}$ and $\mathcal{M}_{ss}$ are the adiabatic and entropic projections of the mass-squared matrix, $\mathcal{M}^I{}_J$ from (7.19). More explicitly,

$$\begin{aligned} \mathcal{M}_{\sigma\sigma} &= \hat{\sigma}_I \hat{\sigma}^J \mathcal{M}^I{}_J \\ \mathcal{M}_{ss} &= \hat{s}_I \hat{s}^J \mathcal{M}^I{}_J. \end{aligned} \tag{7.28}$$

As Eqs. (7.25) and (7.26) make clear, the entropy perturbations will source the adiabatic perturbations but not the other way around, contingent on the turn-rate ω being nonzero. We also note that the entropy perturbations have an effective mass-squared of

$$\mu_s^2 = \mathcal{M}_{ss} + 3\omega^2. \tag{7.29}$$

In the usual fashion [3], we may construct the gauge-invariant curvature perturbation,

$$\mathcal{R}_c \equiv \psi - \frac{H}{(\rho + p)} \delta q \tag{7.30}$$

where ρ and p are the background-order density and pressure and δq is the energy-density flux of the perturbed fluid. In terms of our projected perturbations, we find [22]

$$\mathcal{R}_c = \frac{H}{\dot{\sigma}} Q_\sigma. \tag{7.31}$$

Analogously, we may define a normalized entropy (or isocurvature) perturbation as [3, 13, 14, 16, 18, 22]

$$\mathcal{S} \equiv \frac{H}{\dot{\sigma}} Q_s. \tag{7.32}$$

In the long-wavelength limit, the coupled perturbations obey relations of the form [3, 13, 14, 16, 18, 22]:

$$\begin{aligned} \dot{\mathcal{R}}_c &\simeq \alpha H \mathcal{S} \\ \dot{\mathcal{S}} &\simeq \beta H \mathcal{S}, \end{aligned} \tag{7.33}$$

which allows us to write the transfer functions as

$$\begin{aligned} T_{\mathcal{RS}}(t_{\rm hc}, t) &= \int_{t_{\rm hc}}^{t} dt'\, \alpha(t')\, H(t')\, T_{\mathcal{SS}}(t_{\rm hc}, t') \\ T_{\mathcal{SS}}(t_{\rm hc}, t) &= \exp\left[\int_{t_{\rm hc}}^{t} dt'\ \beta(t')\, H(t')\right], \end{aligned} \tag{7.34}$$

where $t_{\rm hc}$ is the time when a fiducial scale of interest first crosses the Hubble radius during inflation, $k_{\rm hc} = a(t_{\rm hc})H(t_{\rm hc})$. We find [22]

$$\begin{aligned} \alpha &= \frac{2\omega}{H} \\ \beta &= -2\epsilon - \eta_{ss} + \eta_{\sigma\sigma} - \frac{4\omega^2}{3H^2}, \end{aligned} \tag{7.35}$$

where ϵ, $\eta_{\sigma\sigma}$, and η_{ss} are given by

$$\begin{aligned} \epsilon &\equiv -\frac{\dot{H}}{H^2} \\ \eta_{\sigma\sigma} &\equiv \frac{M_{\rm pl}^2\, \mathcal{M}_{\sigma\sigma}}{V} \\ \eta_{ss} &\equiv \frac{M_{\rm pl}^2\, \mathcal{M}_{ss}}{V}. \end{aligned} \tag{7.36}$$

The first two quantities function like the familiar slow-roll parameters from single-field inflation: $\eta_{\sigma\sigma} = 1$ marks the end of the fields' slow-roll evolution, after which $\ddot{\sigma} \sim H\dot{\sigma}$, while $\epsilon = 1$ marks the end of inflation ($\ddot{a} = 0$ for $\epsilon = 1$). The third quantity, η_{ss}, is related to the effective mass of the isocurvature perturbations, and need not remain small during inflation.

Using the transfer functions, we may relate the power spectra at $t_{\rm hc}$ to spectra at later times. In the regime of interest, for late times and long wavelengths, we have

$$\begin{aligned} \mathcal{P}_{\mathcal{R}}(k) &= \mathcal{P}_{\mathcal{R}}(k_{\rm hc})\left[1 + T_{\mathcal{RS}}^2(t_{\rm hc}, t)\right] \\ \mathcal{P}_{\mathcal{S}}(k) &= \mathcal{P}_{\mathcal{R}}(k_{\rm hc})\, T_{\mathcal{SS}}^2(t_{\rm hc}, t). \end{aligned} \tag{7.37}$$

Ultimately, we may use $T_{\mathcal{RS}}$ and $T_{\mathcal{SS}}$ to calculate the isocurvature fraction,

$$\beta_{\rm iso} \equiv \frac{\mathcal{P}_{\mathcal{S}}}{\mathcal{P}_{\mathcal{S}} + \mathcal{P}_{\mathcal{R}}} = \frac{T_{\mathcal{SS}}^2}{T_{\mathcal{SS}}^2 + T_{\mathcal{RS}}^2 + 1}, \tag{7.38}$$

which may be compared to recent observables reported by the *Planck* collaboration.

An example of the fields' trajectory of interest is shown in Fig. 7-3. As shown in Fig. 7-4, while the fields evolve near the top of the ridge, the isocurvature modes are tachyonic, $\mu_s^2 < 0$, leading to the rapid amplification of isocurvature modes. When the turn-rate is nonzero, $\omega \neq 0$, the growth of Q_s can transfer power to the adiabatic perturbations, Q_σ. If $T_{\mathcal{RS}}$ grows too large from this transfer, then predictions for observable quantities such as n_s can get pulled out of agreement with present observations, as shown in the intermediate region of Fig. 7-2 and developed in more detail in Section 7.4. On the other hand, growth of Q_s is strongly suppressed when fields evolve in a valley, since $\mu_s^2/H^2 \gg 1$. In order to produce an appropriate fraction of isocurvature perturbations while also keeping observables such as n_s close to their measured values, one therefore needs field trajectories that stay on a ridge for a significant number of e-folds and have only a modest turn-rate so as not to transfer too much power to the adiabatic modes. This may be accomplished in the regime of weak curvature, $\kappa \ll 1$.

7.3 Trajectories of Interest

7.3.1 Geometry of the Potential

As just noted, significant growth of isocurvature perturbations occurs when $\mu_s^2 < 0$, when the fields begin near the top of a ridge. If the fields start in a valley, or if the curvature near the top of the ridge is large enough ($\kappa \gg 1$) so that the fields rapidly fall into a valley, then the system quickly relaxes to the single-field attractor found in [19], for which $\beta_{\rm iso} \to 0$. To understand the implications for quantities such as $\beta_{\rm iso}$, it is therefore important to understand the geomtery of the potential. This may be

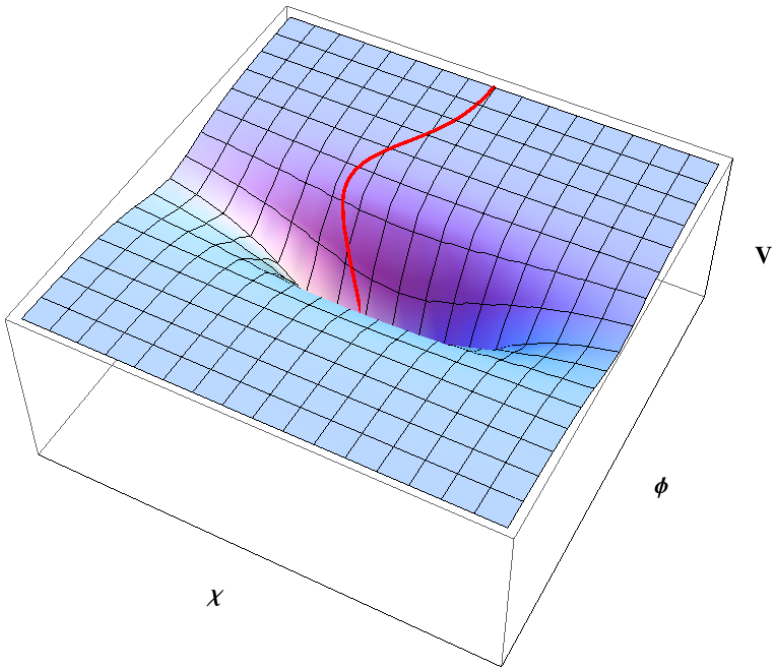

Figure 7-3: The fields' trajectory (red) superimposed upon the effective potential in the Einstein frame, V, with couplings $\xi_\phi = 1000$, $\xi_\chi = 1000.015$, $\lambda_\phi = \lambda_\chi = g = 0.01$, and initial conditions $\phi_0 = 0.35$, $\chi_0 = 8.1 \times 10^{-4}$, $\dot{\phi}_0 = \dot{\chi}_0 = 0$, in units of $M_{\rm pl}$.

accomplished by working with the field-space coordinates r and θ, defined via

$$\phi = r\cos\theta \ , \ \ \chi = r\sin\theta. \tag{7.39}$$

(The parameter θ was labeled γ in [27].) Inflation in these models occurs for $\xi_\phi\phi^2 + \xi_\chi\chi^2 \gg M_{\rm pl}^2$ [22]. That limit corresponds to taking $r \to \infty$, for which the potential becomes

$$V_{r\to\infty}(\theta) = \frac{M_{\rm pl}^4}{4}\,\frac{2g\cos^2\theta\sin^2\theta + \lambda_\phi\cos^4\theta + \lambda_\chi\sin^4\theta}{\left(\xi_\phi\cos^2\theta + \xi_\chi\sin^2\theta\right)^2}. \tag{7.40}$$

We further note that for our choice of potential in Eq. (7.7), $V(\phi,\chi)$ has two discrete symmetries, $\phi \to -\phi$ and $\chi \to -\chi$. This means that we may restrict our attention to only one quarter of the $\phi - \chi$ plane. We choose $\phi > 0$ and $\chi > 0$ without loss of generality.

The extrema (ridges and valleys) are those places where $V_{,\theta} = 0$, which formally

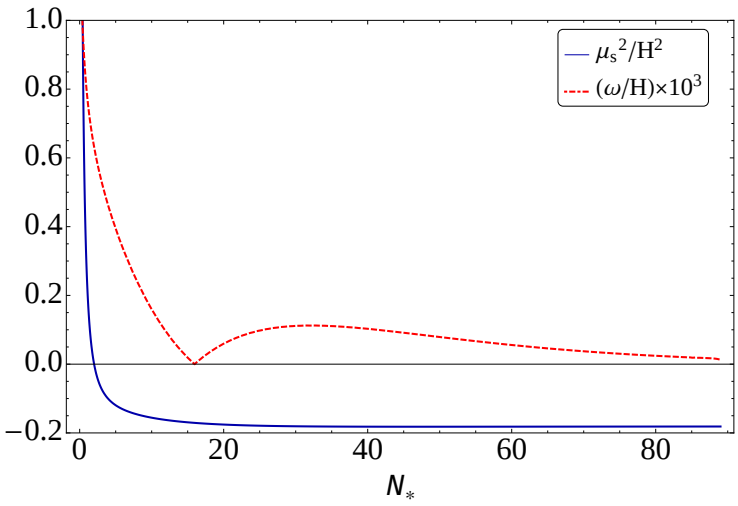

Figure 7-4: The mass of the isocurvature modes, μ_s^2/H^2 (blue, solid), and the turn rate, $(\omega/H) \times 10^3$ (red, dotted), versus e-folds from the end of inflation, N_*, for the trajectory shown in Fig. 7-3. Note that while the fields ride along the ridge, the isocurvature modes are tachyonic, $\mu_s^2 < 0$, leading to an amplification of isocurvature perturbations. The mass μ_s^2 becomes large and positive once the fields roll off the ridge, suppressing further growth of isocurvature modes.

has three solutions for $0 < \theta < \pi/2$ and $r \to \infty$:

$$\theta_1 = 0, \;\; \theta_2 = \frac{\pi}{2}, \;\; \theta_3 = \cos^{-1}\left[\frac{\sqrt{\Lambda_\chi}}{\sqrt{\Lambda_\phi + \Lambda_\chi}}\right], \tag{7.41}$$

where we have defined the convenient combinations

$$\begin{aligned} \Lambda_\phi &\equiv \lambda_\phi \xi_\chi - g\xi_\phi \\ \Lambda_\chi &\equiv \lambda_\chi \xi_\phi - g\xi_\chi. \end{aligned} \tag{7.42}$$

In order for θ_3 to be a real angle (between 0 and $\pi/2$), the argument of the inverse cosine in Eq. (7.41) must be real and bounded by 0 and 1. If Λ_χ and Λ_ϕ have the same sign, both conditions are automatically satisfied. If Λ_χ and Λ_ϕ have different signs then the argument may be either imaginary or larger than 1, in which case there is no real solution θ_3. If both Λ_χ and Λ_ϕ have the same sign, the limiting cases are: for $\Lambda_\chi \gg \Lambda_\phi$, then $\theta_3 \to 0$, and for $\Lambda_\chi \ll \Lambda_\phi$ then $\theta_3 \to \pi/2$.

In each quarter of the $\phi-\chi$ plane, we therefore have either two or three extrema, as shown in Fig. 7-5. Because of the mean-value theorem, two ridges must be separated

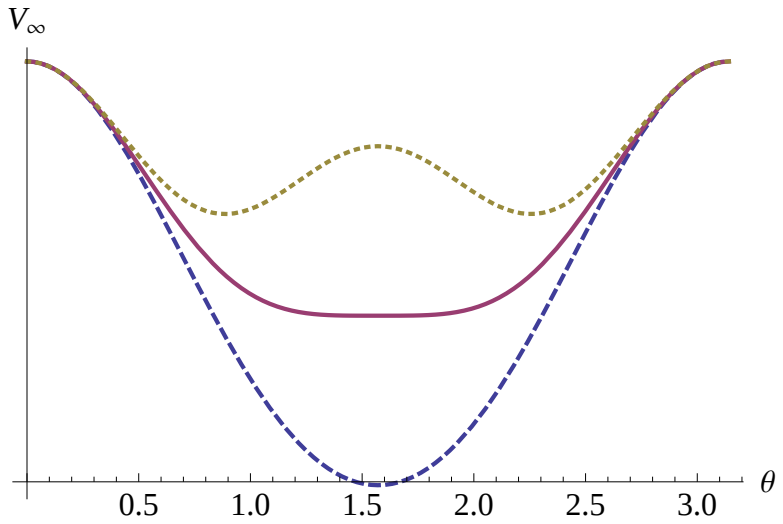

Figure 7-5: The asymptotic value $r \to \infty$ for three potentials with $\Lambda_\chi = -0.001$ (blue dashed), $\Lambda_\chi = 0$ (red solid), and $\Lambda_\chi = 0.001$ (yellow dotted), as a function of the angle $\theta = \arctan(\chi/\phi)$. For all three cases, $\Lambda_\phi = 0.0015$, $\xi_\phi = \xi_\chi = 1000$, and $\lambda_\phi = 0.01$.

by a valley and vice versa. If Λ_χ and Λ_ϕ have opposite signs, there are only two extrema, one valley and one ridge. This was the case for the parameters studied in [22]. If Λ_ϕ and Λ_χ have the same sign, then there is a third extremum (either two ridges and one valley or two valleys and one ridge) within each quarter plane. In the case of two ridges, their asymptotic heights are

$$\begin{aligned} V_{r\to\infty}(\theta_1) &= \frac{\lambda_\phi M_{\rm pl}^4}{4\xi_\phi^2}, \\ V_{r\to\infty}(\theta_2) &= \frac{\lambda_\chi M_{\rm pl}^4}{4\xi_\chi^2}, \end{aligned} \tag{7.43}$$

and the valley lies along the direction θ_3. In the limit $r \to \infty$, the curvature of the potential at each of these extrema is given by

$$\begin{aligned} V_{,\theta\theta}|_{\theta=0} &= -\frac{\Lambda_\phi M_{\rm pl}^4}{\xi_\phi^3}, \quad V_{,\theta\theta}|_{\theta=\pi/2} = -\frac{\Lambda_\chi M_{\rm pl}^4}{\xi_\chi^3}, \\ V_{,\theta\theta}|_{\theta=\theta_3} &= \frac{2\Lambda_\chi\Lambda_\phi(\Lambda_\phi+\Lambda_\chi)^2 M_{\rm pl}^4}{(\xi_\chi\Lambda_\phi+\xi_\chi\Lambda_\chi)^3}. \end{aligned} \tag{7.44}$$

In this section we have ignored the curvature of the field-space manifold, since for

large field values the manifold is close to flat [22], and hence ordinary and covariant derivatives nearly coincide. We demonstrate in Appendix B that the classification of local curvature introduced here holds generally for the dynamics relevant to inflation, even when one takes into account the nontrivial field-space manifold.

7.3.2 Linearized Dynamics

In this section we will examine trajectories for which ω is small but nonzero: small enough so that the isocurvature perturbations do no transfer all their energy away to the adiabatic modes, but large enough so that genuine multifield effects (such as $\beta_{\rm iso} \neq 0$) persist rather than relaxing to effectively single-field evolution.

We focus on situations in which inflation begins near the top of a ridge of the potential, with ϕ_0 large and both χ_0 and $\dot{\chi}_0$ small. Trajectories for which the fields remain near the top of the ridge for a substantial number of e-folds will produce a significant amplification of isocurvature modes, since $\mu_s^2 < 0$ near the top of the ridge and hence the isocurvature perturbations grow via tachyonic instability. From a model-building perspective it is easy to motivate such initial conditions by postulating a waterfall transition, similar to hybrid inflation scenarios [38], that pins the χ field exactly on the ridge. Anything from a small tilt of the potential to quantum fluctuations would then nudge the field off-center.

With χ_0 small, sufficient inflation requires $\xi_\phi \phi_0^2 \gg M_{\rm pl}^2$, which is easily accomplished with sub-Planckian field values given $\xi_\phi \gg 1$. We set the scale for χ_0 by imagining that χ begins exactly on top of the ridge. In the regime of weak curvature, $\kappa \ll 1$, quantum fluctuations will be of order

$$\left\langle \chi^2 \right\rangle = \frac{H^2}{2\pi} \Rightarrow \chi_{\rm rms} = \frac{H}{\sqrt{2\pi}} \tag{7.45}$$

where we take $\chi_{\rm rms} \equiv \sqrt{\langle \chi^2 \rangle}$ to be a classical estimator of the excursion of the field away from the ridge. The constraint from *Planck* that $H/M_{\rm pl} \leq 3.7 \times 10^{-5}$ during inflation then allows us to estimate $\chi_{\rm rms} \sim 10^{-5}\, M_{\rm pl}$ at the start of inflation. (A Gaussian wavepacket for χ will then spread as $\sqrt{N}$, where N is the number of e-folds

of inflation.) This sets a reasonable scale for χ_0; we examine the dynamics of the system as we vary χ_0 around $\chi_{\rm rms}$.

We may now expand the full background dynamics in the limit of small κ, χ, and $\dot{\chi}$. The equation of motion for ϕ, given by Eq. (7.15), does not include any terms linear in χ or $\dot{\chi}$, so the evolution of ϕ in this limit reduces to the single-field equation of motion, which reduces to

$$\dot{\phi}_{\rm SR} \simeq -\frac{\sqrt{\lambda_\phi}\, M_{\rm pl}^3}{3\sqrt{3}\xi_\phi^2 \phi} \tag{7.46}$$

in the slow-roll limit [27]. To first approximation, the ϕ field rolls slowly along the top of the ridge. Upon using Eq. (7.11), we may integrate Eq. (7.46) to yield

$$\frac{\xi_\phi \phi_*^2}{M_{\rm pl}^2} \simeq \frac{4}{3} N_*, \tag{7.47}$$

where N_* is the number of e-folds from the end of inflation, and we have used $\phi(t_*) \gg \phi(t_{\rm end})$. The slow-roll parameters may then be evaluated to lowest order in χ and $\dot{\chi}$ and take the form [19]

$$\begin{aligned} \epsilon &\simeq \frac{3}{4N_*^2} \\ \eta_{\sigma\sigma} &\simeq -\frac{1}{N_*}\left(1 - \frac{3}{4N_*}\right). \end{aligned} \tag{7.48}$$

Expanding the equation of motion for the χ field and considering $\xi_\phi, \xi_\chi \gg 1$ we find the linearized equation of motion

$$\ddot{\chi} + 3H\dot{\chi} - \frac{\Lambda_\phi M_{\rm pl}^2}{\xi_\phi^2}\chi \simeq 0, \tag{7.49}$$

which has the simple solution

$$\chi(t) \simeq \chi_0 \exp\left[\left(-\frac{3H}{2} \pm \sqrt{\frac{9H^2}{2} + \frac{\Lambda_\phi M_{\rm pl}^2}{\xi_\phi^2}}\right) N(t)\right], \tag{7.50}$$

where we again used Eq. (7.11) for H, and $N(t) \equiv \int_{t_0}^{t} H dt'$ is the number of e-folds

since the start of inflation. If we assume that $\Lambda_\phi M_{\rm pl}^2/\xi_\phi^2 \ll 9H^2/4$, which is equivalent to $\Lambda_\phi/\lambda_\phi \ll 3/16$, then we may Taylor expand the square root in the exponent of $\chi(t)$. This is equivalent to dropping the $\ddot{\chi}$ term from the equation of motion. In this limit the solution becomes

$$\chi(t) \simeq \chi_0 e^{\kappa N(t)}, \tag{7.51}$$

where κ is defined in Eq. (7.10). Upon using the definition of Λ_ϕ in Eq. (7.42), we now recognize $\kappa = 4\Lambda_\phi/\lambda_\phi$. Our approximation of neglecting $\ddot{\chi}$ thus corresponds to the limit $\kappa \ll 3/4$.

When applying our set of approximations to the isocurvature mass in Eq. (7.29), we find that the $\mathcal{M}_{ss}$ term dominates ω^2/H^2, and the behavior of $\mathcal{M}_{ss}$ in turn is dominated by $\mathcal{D}_J\mathcal{D}_K V$ rather than the term involving $\mathcal{R}^I_{JKL}$. Since we are projecting the mass-squared matrix orthogonal to the fields' motion, and since we are starting on a ridge along the ϕ direction, the derivative of V that matters most to the dynamics of the system in this limit is $\mathcal{D}_{\chi\chi}V$ evaluated at small χ. To second order in χ, we find

$$\begin{aligned}
\mathcal{D}_{\chi\chi}V = &-\frac{\Lambda_\phi M_{\rm pl}^4}{\xi_\phi^3\phi^2} \\
&+ \frac{M_{\rm pl}^6}{\xi_\phi^3(1+6\xi_\phi)\phi^4}\left[2\Lambda_\phi\frac{(1+6\xi_\phi)}{\xi_\phi} - \lambda_\phi\varepsilon\right] \\
&+ \frac{M_{\rm pl}^4\,\chi^2}{\xi_\phi^3(1+6\xi_\phi)\phi^4}\Big[3(1+6\xi_\phi)\Lambda_\chi + \\
&\qquad\qquad + (1-\varepsilon)(1+6\xi_\chi)\Lambda_\phi \\
&\qquad\qquad + 6(1-\varepsilon)(1+6\xi_\phi)\Lambda_\phi - \Lambda_\phi\varepsilon\Big],
\end{aligned} \tag{7.52}$$

where we have used Λ_ϕ and Λ_χ as given in Eq. (7.42) and also introduced

$$\varepsilon \equiv \frac{\xi_\phi - \xi_\chi}{\xi_\phi} = 1 - \frac{\xi_\chi}{\xi_\phi}. \tag{7.53}$$

These terms each illuminate an aspect of the geometry of the potential: as we found in Eq. (7.44), Λ_ϕ and Λ_χ are proportional to the curvature of the potential along the

ϕ and χ axes respectively, and ε is the ellipticity of the potential for large field values. Intuition coming from these geometric quantities motivates us to use them as a basis for determining the dynamics in our simulations. The approximations hold well for the first several e-folds of inflation, before the fields fall off the ridge of the potential.

Based on our linearized approximation we may expand all kinematical quantities in power series of χ_0 and $1/N_*$. We refer to the intermediate quantities in Appendix B and report here the important quantities that characterize the generation and transfer of isocurvature perturbations. To lowest order in χ and $\dot{\chi}$, the parameter η_{ss} defined in Eq. (7.36) takes the form

$$\eta_{ss} \simeq -\kappa - \frac{3}{4N_*}\left(\kappa + \frac{2\varepsilon}{3}\right) + \frac{3}{8N_*^2}\left(1-\varepsilon\right), \tag{7.54}$$

showing that to lowest order in $1/N_*$, $\eta_{ss} \sim -\kappa < 0$ and hence the isocurvature modes begin with a tachyonic mass. The quantities α and β from Eq. (7.35) to first order are

$$\begin{aligned} \alpha &\simeq \frac{\kappa\,\chi_0 \exp\left[\kappa(N_{\rm tot}-N_*)\right]}{\sqrt{2}\,\xi_\phi M_{\rm pl}}\sqrt{N_*}, \\ \beta &\simeq \kappa + \frac{1}{N_*}\left[\frac{3\kappa}{4}+\frac{\varepsilon}{2}-1\right] + \frac{1}{N_*^2}\left[\frac{3\varepsilon}{8}-\frac{9}{8}\right], \end{aligned} \tag{7.55}$$

where $N_{\rm tot}$ is the total number of e-folds of inflation. These expansions allow us to approximate the transfer function $T_{\mathcal{SS}}$ of Eq. (7.34),

$$\begin{aligned} T_{\mathcal{SS}} \simeq &\left(\frac{N_*}{N_{\rm hc}}\right)^{1-\frac{3\kappa}{4}-\frac{\varepsilon}{2}} \\ &\times \exp\left[\kappa\left(N_{\rm hc}-N_*\right) - \frac{3}{8}\left(3-\varepsilon\right)\left(\frac{1}{N_*}-\frac{1}{N_{\rm hc}}\right)\right], \end{aligned} \tag{7.56}$$

where $N_{\rm hc}$ is the number of e-folds before the end of inflation at which Hubble crossing occurs for the fiducial scale of interest. We may then use a semi-analytic form for $T_{\mathcal{RS}}$ by putting Eq. (7.56) into Eq. (7.34). This approximation is depicted in Fig. 7-6.

Our analytic approximation for $T_{\mathcal{SS}}$ vanishes identically in the limit $N_* \to 0$ (at

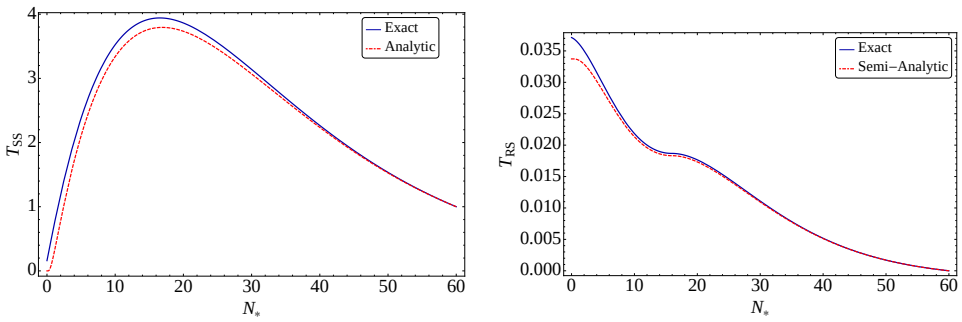

Figure 7-6: The evolution of $T_{\mathcal{SS}}$ (top) and $T_{\mathcal{RS}}$ (bottom) using the exact and approximated expressions, for $\kappa \equiv 4\Lambda_\phi/\lambda_\phi = 0.06$, $4\Lambda_\chi/\lambda_\chi = -0.06$ and $\varepsilon = -1.5 \times 10^{-5}$, with $\phi_0 = 0.35\ M_{\rm pl}$, $\chi_0 = 8.1 \times 10^{-4}\ M_{\rm pl}$, and $\dot{\phi}_0 = \dot{\chi}_0 = 0$. We take $N_{\rm hc} = 60$ and plot $T_{\mathcal{SS}}$ and $T_{\mathcal{RS}}$ against N_*, the number of e-folds before the end of inflation. The approximation works particularly well at early times and matches the qualitative behavior of the exact numerical solution at late times.

the end of inflation), though it gives an excellent indication of the general shape of $T_{\mathcal{SS}}$ for the duration of inflation. We further note that $T_{\mathcal{SS}}$ is independent of χ_0 to lowest order, while $T_{\mathcal{RS}} \propto \alpha \propto \kappa\chi_0$ and hence remains small in the limit we are considering. Thus for small κ, we expect $\beta_{\rm iso}$ to be fairly insensitive to changes in χ_0.

7.4 Results

We want to examine how the isocurvature fraction $\beta_{\rm iso}$ varies as we change the shape of the potential. We are particularly interested in the dependence of $\beta_{\rm iso}$ on κ, since the leading-order contribution to the isocurvature fraction from the shape of the potential is proportional to κ. Guided by our approximations, we simulated trajectories across 1400 potentials and we show the results in Figures 7-7 - 7-10. The simulations were done using zero initial velocities for ϕ and χ, and were performed using both Matlab and Mathematica, as a consistency check. We compare analytical approximations in certain regimes with our numerical findings.

As expected, we find that there is an interesting competition between the degree to which the isocurvature mass is tachyonic and the propensity of the fields to fall off the ridge. More explicitly, for small κ we expect the fields to stay on the ridge for most of inflation with a small turn rate that transfers little power to the adiabatic

modes. Therefore, in the small-κ limit, $T_{\mathcal{RS}}$ remains small while $T_{\mathcal{SS}}$ (and hence $\beta_{\rm iso}$) increases exponentially with increasing κ. Indeed, all the numerical simulations show that $\beta_{\rm iso}$ vs. κ increases linearly on a semilog scale for small κ. However, in the small-κ limit, the tachyonic isocurvature mass is also small, so $\beta_{\rm iso}$ remains fairly small in that regime. Meanwhile, for large κ we expect the fields to have a larger tachyonic mass while near the top of the ridge, but to roll off the ridge (and transfer significant power to the adiabatic modes) earlier in the evolution of the system. There should be an intermediate regime of κ in which the isocurvature mass is fairly large (and tachyonic) and the fields do not fall off the ridge too early. Indeed, a ubiquitous feature of our numerical simulations is that $\beta_{\rm iso}$ is always maximized around $\kappa \lesssim 0.1$, regardless of the other parameters of the potential.

7.4.1 Local curvature of the potential

In Fig. 7-7, we examine the variation of $\beta_{\rm iso}$ as we change χ_0 and κ. As expected, $\beta_{\rm iso}$ has no dependence on χ_0 for small κ. Increasing κ breaks the χ_0 degeneracy: the closer the fields start to the top of the ridge, the more time the fields remain near the top before rolling off the ridge and transferring power to the adiabatic modes. Just as expected, for the smallest value of χ_0, we see the largest isocurvature fraction. Even for relatively large χ_0, there is still a nontrivial contribution of isocurvature modes to the perturbation spectrum. Therefore, our model generically yields a large isocurvature fraction with little fine-tuning of the initial field values in the regime $\kappa \ll 1$.

We may calculate $\beta_{\rm iso}$ for the limiting case of zero curvature, $\kappa \to 0$, the vicinity in which the curves in Fig. 7-7 become degenerate. Taking the limit $\kappa \to 0$ means essentially reverting to a Higgs-like case, a fully $SO(2)$ symmetric potential with no turning of the trajectory in field space [27]. As expected, our approximate expression in Eq. (7.56) for $T_{\mathcal{RS}} \to 0$ in the limit $\kappa \to 0$, and hence we need only consider $T_{\mathcal{SS}}$.

As noted above, our approximate expression for $T_{\mathcal{SS}}$ in Eq. (7.56) vanishes in the limit $N_* \to 0$. Eq. (7.56) was derived for the regime in which our approximate expressions for the slow-roll parameters ϵ and $\eta_{\sigma\sigma}$ in Eq. (7.48) are reasonably ac-

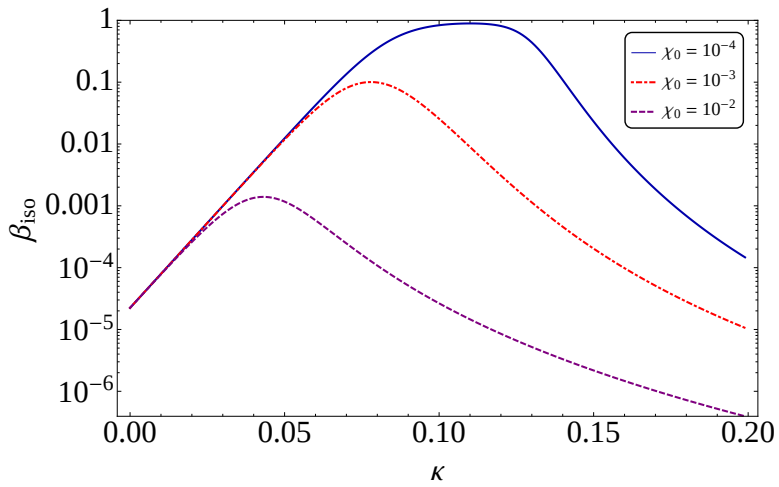

Figure 7-7: The isocurvature fraction for different values of χ_0 (in units of $M_{\rm pl}$) as a function of the curvature of the ridge, κ. All of the trajectories began at $\phi_0 = 0.3\,M_{\rm pl}$, which yields $N_{\rm tot} = 65.7$. For these potentials, $\xi_\phi = 1000$, $\lambda_\phi = 0.01$, $\varepsilon = 0$, and $\Lambda_\chi = 0$. The trajectories that begin closest to the top of the ridge have the largest values of $\beta_{\rm iso}$, with some regions of parameter space nearly saturating $\beta_{\rm iso} = 1$.

curate. Clearly the expressions in Eq. (7.48) will cease to be accurate near the end of inflation. Indeed, taking the expressions at face value, we would expect slow roll to end ($|\eta_{\sigma\sigma}| = 1$) at $N_* = 1/2$, and inflation to end ($\epsilon = 1$) at $N_* = 2/\sqrt{3}$, rather than at $N_* = 0$. Thus we might expect Eq. (7.48) to be reliable until around $N_* \simeq 1$, which matches the behavior we found in a previous numerical study [19]. Hence we will evaluate our analytic approximation for $T_{\mathcal{SS}}$ in Eq. (7.56) between $N_{\rm hc} = 60$ and $N_* \simeq 1$, rather than all the way to $N_* \to 0$. In the limit $\kappa \to 0$ and $\varepsilon \to 0$ and using $N_* = 1$, Eq. (7.56) yields

$$T_{\mathcal{SS}} \simeq \frac{1}{N_{\rm hc}} \exp\left[-9/8\right], \tag{7.57}$$

upon taking $N_{\rm hc} \gg N_*$. For $N_{\rm hc} = 60$, we therefore find $T_{\mathcal{SS}} \simeq 5.4 \times 10^{-3}$, and hence $\beta_{\rm iso} \simeq 2.9 \times 10^{-5}$. This value may be compared with the exact numerical value, $\beta_{\rm iso} = 2.3 \times 10^{-5}$. Despite the severity of our approximations, our analytic expression provides an excellent guide to the behavior of the system in the limit of small κ.

As we increase κ, the fields roll off the ridge correspondingly earlier in their evolution. The nonzero turn-rate causes a significant transfer of power from the isocurvature modes to the adiabatic modes. As $T_{\mathcal{RS}}$ grows larger, it lowers the overall value

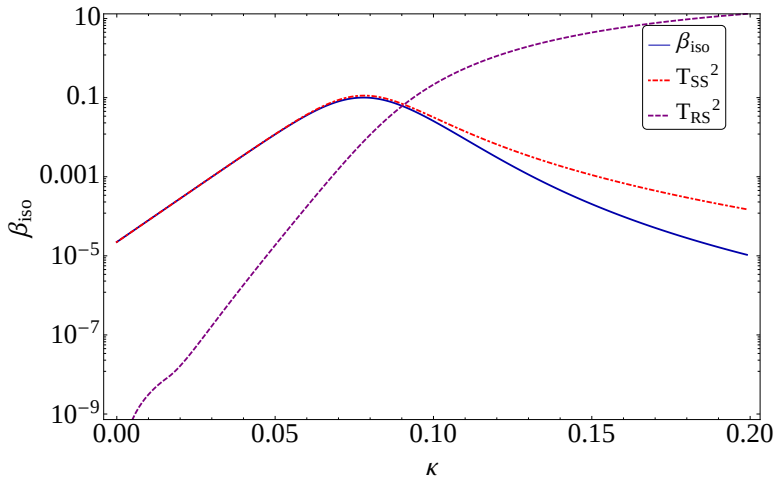

Figure 7-8: Contributions of $T_{\mathcal{RS}}$ and $T_{\mathcal{SS}}$ to $\beta_{\rm iso}$. The parameters used are $\phi_0 = 0.3\ M_{\rm pl}$, $\chi_0 = 10^{-3}\ M_{\rm pl}$, $\xi_\phi = 10^3$, $\lambda_\phi = 0.01$, $\varepsilon = 0$ and $\Lambda_\chi = 0$. For small κ, $\beta_{\rm iso}$ is dominated by $T_{\mathcal{SS}}$; for larger κ, $T_{\mathcal{RS}}$ becomes more important and ultimately reduces $\beta_{\rm iso}$.

of $\beta_{\rm iso}$. See Fig. 7-8.

7.4.2 Global structure of the potential

The previous discussion considered the behavior for $\Lambda_\chi = 0$. As shown in Fig. 7-5, the global structure of the potential will change if $\Lambda_\chi \neq 0$. In the limit $\kappa \ll 1$, the fields never roll far from the top of the ridge along the $\chi = 0$ direction, and therefore the shape of the potential along the χ direction has no bearing on $\beta_{\rm iso}$. However, large κ breaks the degeneracy in Λ_χ because the fields will roll off the original ridge and probe features of the potential along the χ direction. See Fig. 7-9.

In the case $\Lambda_\chi = 0$, the fields roll off the ridge and eventually land on a plain, where the isocurvature perturbations are minimally suppressed, since $\mu_s^2 \sim 0$. For $\Lambda_\chi > 0$, there is a ridge along the χ direction as well as along $\chi = 0$, which means that there must be a valley at some intermediate angle in field space. When the fields roll off the original ridge, they reach the valley in which $\mu_s^2 > 0$, and hence the isocurvature modes are more strongly suppressed than in the $\Lambda_\chi = 0$ case.

Interesting behavior may occur for the case $\Lambda_\chi < 0$. There exists a range of κ for which the isocurvature perturbations are more strongly amplified than a naive

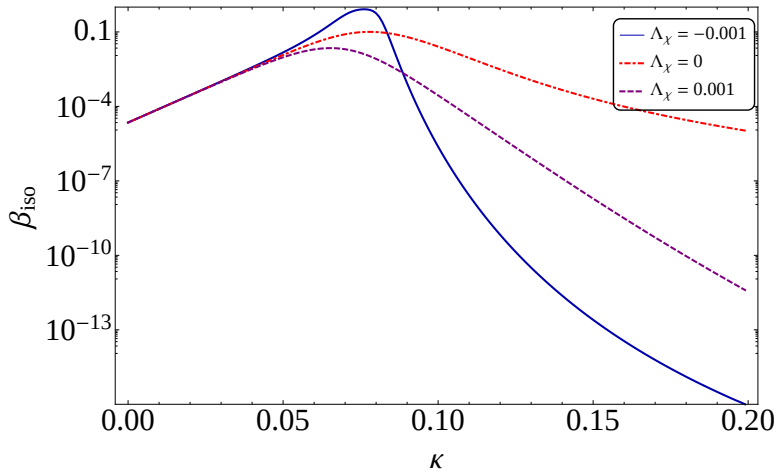

Figure 7-9: The isocurvature fraction for different values of Λ_χ as a function of the curvature of the ridge, κ. All of the trajectories began at $\phi_0 = 0.3\,M_{\rm pl}$ and $\chi_0 = 10^{-4}\,M_{\rm pl}$, yielding $N_{\rm tot} = 65.7$. For these potentials, $\xi_\phi = 1000$, $\lambda_\phi = 0.01$, and $\varepsilon = 0$. Potentials with $\Lambda_\chi < 0$ yield the largest $\beta_{\rm iso}$ peaks, though in those cases $\beta_{\rm iso}$ falls fastest in the large-κ limit due to sensitive changes in curvature along the trajectory. Meanwhile, potentials with positive Λ_χ suppress the maximum value of $\beta_{\rm iso}$ once $\kappa \gtrsim 0.1$ and local curvature becomes important.

estimate would suggest, thanks to the late-time behavior of $\eta_{ss} \sim (\mathcal{D}_{\chi\chi}V)/V$. If the second derivative decreases more slowly than the potential itself, then the isocurvature modes may be amplified for a short time as the fields roll down the ridge. This added contribution is sufficient to increase $\beta_{\rm iso}$ compared to the cases in which $\Lambda_\chi \geq 0$. However, the effect becomes subdominant as the curvature of the original ridge, κ, is increased. For larger κ, the fields spend more time in the valley, in which the isocurvature modes are strongly suppressed.

In Figure 7-10, we isolate effects of ε and κ on $\beta_{\rm iso}$. From Eq. (7.52), when Λ_ϕ is small (which implies that κ is small), ε sets the scale of the isocurvature mass. Positive ε makes the isocurvature mass-squared more negative near $\kappa = 0$, which increases the power in isocurvature modes. Conversely, negative ε makes the isocurvature mass-squared less negative near $\kappa = 0$, which decreases the power in isocurvature modes. In geometrical terms, in the limit $\Lambda_\phi = \Lambda_\chi = 0$, equipotential surfaces are ellipses with eccenticity $\sqrt{\varepsilon}$ for $\varepsilon > 0$ and $\sqrt{\varepsilon/(\varepsilon - 1)}$ for $\varepsilon < 0$. In this limit we may calculate $\beta_{\rm iso}$ exactly as we did for the case of $\varepsilon = 0$.

The other effect of changing ε is that it elongates the potential in either the ϕ

or χ direction. This deformation of the potential either enhances or decreases the degree to which the fields can turn, which in turn will affect the large-κ behavior. In particular, for $\varepsilon > 0$ the potential is elongated along the ϕ direction, which means that when the fields roll off the ridge, they immediately start turning and transferring power to the adiabatic modes. Conversely, for $\varepsilon < 0$ the potential is elongated along the χ direction, so once the fields fall off the ridge, they travel farther before they start turning. Therefore, in the large-κ limit, $\beta_{\rm iso}$ falls off more quickly for $\varepsilon > 0$ than for $\varepsilon < 0$.

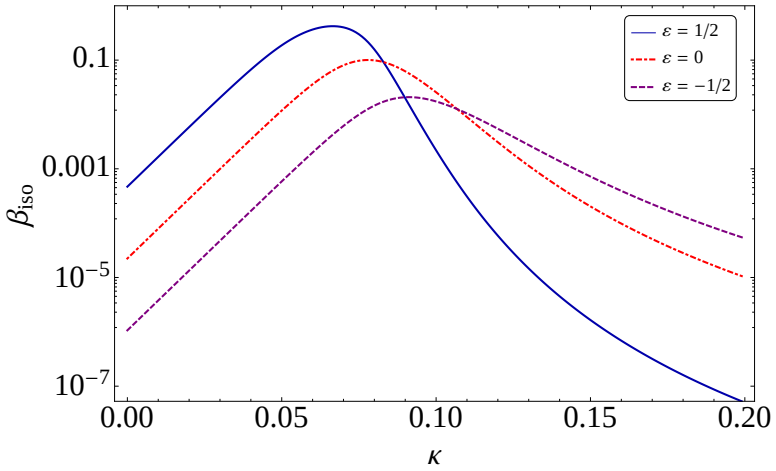

Figure 7-10: The isocurvature fraction for different values of ε as a function of the curvature of the ridge, κ. All of the trajectories began at $\chi_0 = 10^{-3}\ M_{\rm pl}$ and $\phi_0 = 0.3\ M_{\rm pl}$, with $N_{\rm tot} = 65.7$. For these potentials, $\xi_\phi = 1000$, $\lambda_\phi = 0.01$, and $\Lambda_\chi = 0$. Here we see the competition between ε setting the scale of the isocurvature mass and affecting the amount of turning in field-space.

We may use our analytic expression for $T_{\mathcal{SS}}$ in Eq. (7.56) for the case in which $\kappa \to 0$ with $\varepsilon \neq 0$. We find the value of $\beta_{\rm iso} \simeq T_{\mathcal{SS}}^2$ changes by a factor of 11 when we vary $\varepsilon \pm 1/2$, while our numerical solutions in Fig. 7-10 vary by a factor of 21. Given the severity of some of our analytic approximations, this close match again seems reassuring.

7.4.3 Initial Conditions

The quantity $\beta_{\rm iso}$ varies with the fields' initial conditions as well as with the parameters of the potential. Given the form of $T_{\mathcal{RS}}$ and $T_{\mathcal{SS}}$ in Eq. (7.34), we see that the

value of $\beta_{\rm iso}$ depends only on the behavior of the fields between $N_{\rm hc}$ and the end of inflation. This means that if we were to change ϕ_0 and χ_0 in such a way that the fields followed the same trajectory following $N_{\rm hc}$, the resulting values for $\beta_{\rm iso}$ would be identical.

We have seen in Eq. (7.47) that we may use ϕ as our inflationary clock, $\xi_\phi \phi_*^2/M_{\rm pl}^2 \simeq 4N_*/3$, where $N_* = N_{\rm tot} - N(t)$ is the number of e-folds before the end of inflation. We have also seen, in Eq. (7.51), that for small κ we may approximate $\chi(t) \simeq \chi_0 \exp[\kappa N(t)]$. If we impose that two such trajectories cross $N_{\rm hc}$ with the same value of χ, then we find

$$\Delta(\log \chi_0) = \kappa \Delta N = -\frac{3}{4}\xi_\phi \kappa \, \Delta \left(\frac{\phi_0^2}{M_{\rm pl}^2} \right). \tag{7.58}$$

We tested the approximation in Eq. (7.58) by numerically simulating over 15,000 trajectories in the same potential with different initial conditions. The numerical results are shown in Fig. 7-11, along with our analytic predictions, from Eq. (7.58), that contours of constant $\beta_{\rm iso}$ should appear parabolic in the semilog graph. As shown in Fig. 7-11, our analytic approximation matches the full numerical results remarkably well. We also note from Fig. 7-11 that for a given value of χ_0, if we increase ϕ_0 (thereby increasing the total duration of inflation, $N_{\rm tot}$), we will decrease $\beta_{\rm iso}$, behavior that is consistent with our approximate expressions for $T_{\mathcal{RS}}$ and $T_{\mathcal{SS}}$ in Eq. (7.56).

7.4.4 CMB observables

Recent analyses of the *Planck* data for low multipoles suggests an improvement of fit between data and underlying model if one includes a substantial fraction of primordial isocurvature modes, $\beta_{\rm iso} \sim \mathcal{O}(0.1)$. The best fits are obtained for isocurvature perturbations with a slightly blue spectral tilt, $n_I \equiv 1 + d\ln \mathcal{P}_{\mathcal{S}}/d\ln k \geq 1.0$ [11]. In the previous sections we have demonstrated that our general class of models readily produces $\beta_{\rm iso} \sim \mathcal{O}(0.1)$ in the regime $\kappa \lesssim 0.1$. The spectral tilt, n_I, for these

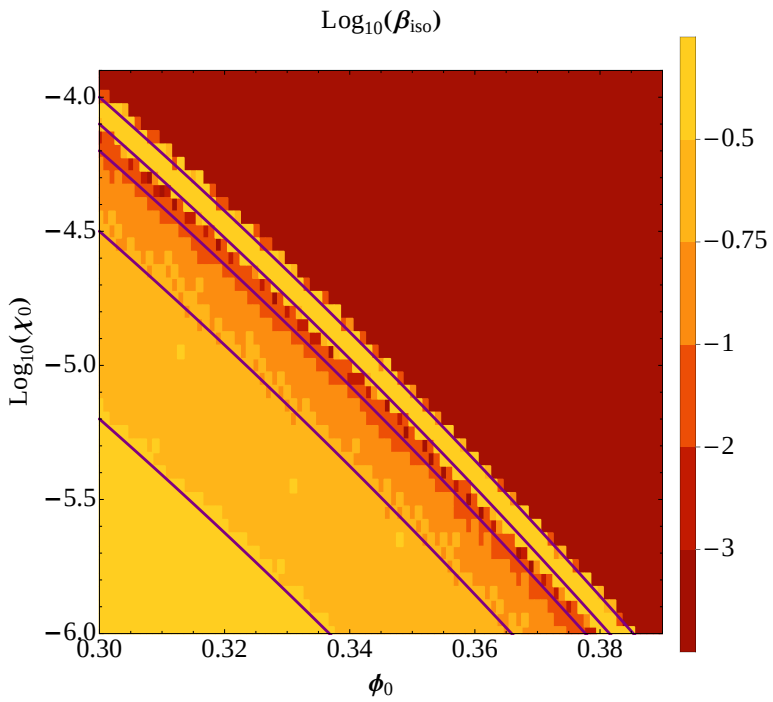

Figure 7-11: Numerical simulations of $\beta_{\rm iso}$ for various initial conditions (in units of $M_{\rm pl}$). All trajectories shown here were for a potential with $\kappa = 4\Lambda_\phi/\lambda_\phi = 0.116$, $4\Lambda_\chi/\lambda_\chi = -160.12$, and $\varepsilon = -2.9 \times 10^{-5}$. Also shown are our analytic predictions for contours of constant $\beta_{\rm iso}$, derived from Eq. (7.58) and represented by dark, solid lines. From top right to bottom left, the contours have $\beta_{\rm iso} = 0.071$, 0.307, 0.054, 0.183, and 0.355.

perturbations goes as [14, 18]

$$n_I = 1 - 2\epsilon + 2\eta_{ss}, \tag{7.59}$$

where ϵ and η_{ss} are evaluated at Hubble-crossing, $N_{\rm hc}$. Given our expressions in Eqs. (7.48) and (7.54), we then find

$$n_I \simeq 1 - 2\kappa - \frac{3}{2N_*}\left(\kappa + \frac{2\varepsilon}{3}\right) - \frac{3}{4N_*^2}\left(1 + \varepsilon\right). \tag{7.60}$$

For trajectories that produce a nonzero fraction of isocurvature modes, the isocurvature perturbations are tachyonic at the time of Hubble-crossing, with $\eta_{ss} \propto \mathcal{M}_{ss} \sim \mu_s^2 < 0$. Hence in general we find n_I will be slightly red-tilted, $n_I \leq 1$. However, in the regime of weak curvature, $\kappa \ll 1$, we may find $n_I \sim 1$. In particular, in the limit $\kappa \to 0$ and $\varepsilon \to 0$, then $n_I \to 1 - 3/(4N_*^2) \sim 1 - \mathcal{O}(10^{-4})$, effectively indistinguishable

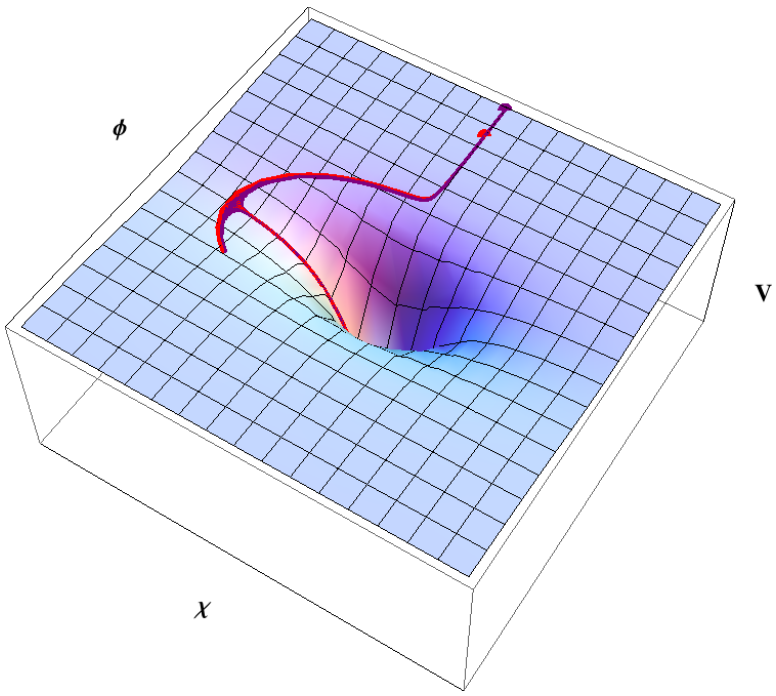

Figure 7-12: Two trajectories from Fig. 7-11 that lie along the $\beta_{\rm iso} = 0.183$ line, for $\phi_0 = 0.3\ M_{\rm pl}$ and $\phi_0 = 0.365\ M_{\rm pl}$. The dots mark the fields' initial values. The two trajectories eventually become indistinguishable, and hence produce identical values of $\beta_{\rm iso}$.

from a flat, scale-invariant spectrum. In general for $\kappa < 0.02$, we therefore expect $n_I > n_s$, where $n_s \sim 0.96$ is the spectral index for adiabatic perturbations. In that regime, the isocurvature perturbations would have a bluer spectrum than the adiabatic modes, albeit not a genuinely blue spectrum. An important test of our models will therefore be if future observations and analysis require $n_I > 1$ in order to address the present low-ℓ anomaly in the *Planck* measurements of the CMB temperature anisotropies.

Beyond $\beta_{\rm iso}$ and n_I, there are other important quantities that we need to address, and that can be used to distinguish between similar models: the spectral index for the adiabatic modes, n_s, and its running, $\alpha \equiv dn_s/d\ln k$; the tensor-to-scalar ratio, r; and the amplitude of primordial non-Gaussianity, $f_{\rm NL}$. As shown in [19], in the limit of large curvature, $\kappa \gg 1$, the system quickly relaxes to the single-field attractor for which $0.960 \leq n_s \leq 0.967$, $\alpha \sim \mathcal{O}(10^{-4})$, $0.0033 \leq r \leq 0.0048$, and $|f_{\rm NL}| \ll 1$. (The ranges for n_s and r come from considering $N_{\rm hc} = 50 - 60$.) Because the single-field

attractor evolution occurs when the fields rapidly roll off a ridge and remain in a valley, in which $\mu_s^2 > 0$, the models generically predict $\beta_{\rm iso} \ll 1$ in the limit $\kappa \gg 1$ as well. Here we examine how these observables evolve in the limit of weak curvature, $\kappa \ll 1$, for which, as we have seen, the models may produce substantial $\beta_{\rm iso} \sim \mathcal{O}(0.1)$.

Let us start with the spectral index, n_s. If isocurvature modes grow and transfer substantial power to the adiabatic modes before the end of inflation, then they may affect the value of n_s. In particular, we have [14, 18, 22]

$$n_s = n_s(t_{\rm hc}) + \frac{1}{H}\left[-\alpha(t_{\rm hc}) - \beta(t_{\rm hc})T_{\mathcal{RS}}\right]\sin(2\Delta), \tag{7.61}$$

where

$$n_s(t_{\rm hc}) = 1 - 6\epsilon + 2\eta_{\sigma\sigma} \tag{7.62}$$

and α and β are given in Eq. (7.35). The angle Δ is defined via

$$\cos\Delta \equiv \frac{T_{\mathcal{RS}}}{\sqrt{1+T_{\mathcal{RS}}^2}}. \tag{7.63}$$

The turn rate $\alpha = 2\omega/H$ is small at the moment when perturbations exit the Hubble radius, and the trigonometric factor obeys $-1 \leq \sin(2\Delta) \leq 1$. We also have $\beta \simeq \kappa + \mathcal{O}(N_*^{-1})$ at early times, from Eq. (7.55). Hence we see that $T_{\mathcal{RS}}$ must be significant in order to cause a substantial change in n_s compared to the value at Hubble crossing, $n_s(t_{\rm hc})$. Yet we found in Fig. 7-8 that $T_{\mathcal{RS}}$ grows large after $\beta_{\rm iso}$ has reached its maximum value. We therefore expect n_s to be equal to its value in the single-field attractor for $\kappa \lesssim 0.1$.

This is indeed what we find when we study the exact numerical evolution of n_s over a wide range of κ, as in Fig. 7-2, as well as in the regime of weak curvature, $\kappa \ll 1$, as shown in Fig. 7-13. For $\kappa \lesssim 0.1$ and using $N_{\rm hc} = 60$, we find n_s well within the present bounds from the *Planck* measurements: $n_s = 0.9603 \pm 0.0073$ [11]. Moreover, because the regime $\kappa \lesssim 0.1$ corresponds to $T_{\mathcal{RS}} \ll 1$, the analysis of the running of the spectral index, α, remains unchanged from [19], and we again find $\alpha \sim -2/N_*^2 \sim \mathcal{O}(10^{-4})$, easily consistent with the constraints from *Planck*,

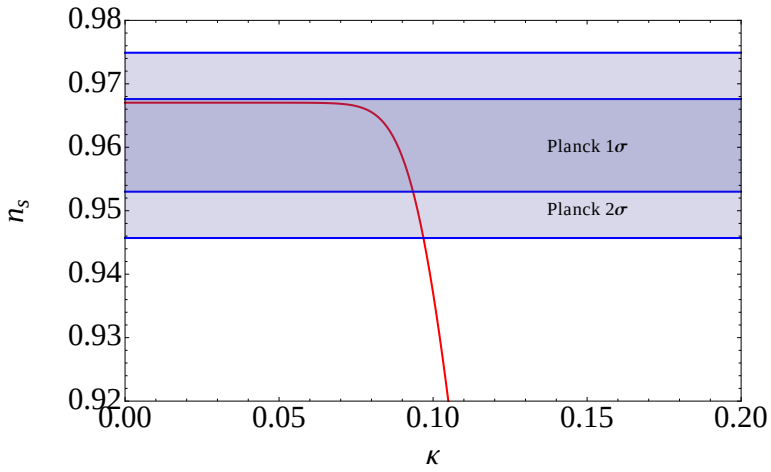

Figure 7-13: The spectral index n_s for different values of the local curvature κ. The parameters used are $\phi_0 = 0.3\, M_{\rm pl}$, $\chi_0 = 10^{-3}\, M_{\rm pl}$, $\xi_\phi = 1000$, $\lambda_\phi = 0.01$, $\varepsilon = 0$ and $\Lambda_\chi = 0$. Comparing this with Fig. 7-7 we see that the peak in the $\beta_{\rm iso}$ curve occurs within the *Planck* allowed region.

$\alpha = -0.0134 \pm 0.0090$ [11].

Another important observational tool for distinguishing between inflation models is the value of the tensor-to-scalar ratio, r. Although the current constraints are at the 10^{-1} level, future experiments may be able to lower the sensitivity by one or two orders of magnitude, making exact predictions potentially testable. For our models the value of r is given by [19]

$$r = \frac{16\epsilon}{1 + T_{\mathcal{RS}}^2}. \tag{7.64}$$

We see that once $T_{\mathcal{RS}} \sim \mathcal{O}(1)$, the value of r decreases, as is depicted in Fig. 7-14. One possible means to break the degeneracy between this family of models, apart from $\beta_{\rm iso}$, is the correlation between r and n_s. In the limit of vanishing $T_{\mathcal{RS}}$, both n_s and r revert to their single-field values, though they both vary in calculable ways as $T_{\mathcal{RS}}$ grows to be $\mathcal{O}(1)$. See Fig. 7-15.

We studied the behavior of $f_{\rm NL}$ in our family of models in detail in [22]. There we found that substantial $f_{\rm NL}$ required a large value of $T_{\mathcal{RS}}$ by the end of inflation. In this chapter we have found that $T_{\mathcal{RS}}$ remains small in the regime of weak curvature, $\kappa \lesssim 0.1$. Using the methods described in detail in [22], we have evaluated $f_{\rm NL}$ numerically for the broad class of potentials and trajectories described above, in the

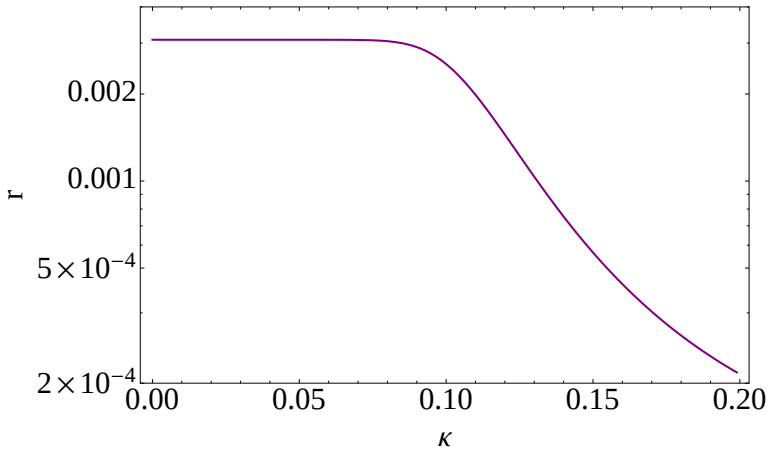

Figure 7-14: The tensor-to-scalar ratio as a function of the local curvature parameter κ. The parameters used are $\phi_0 = 0.3\,M_{\rm pl}$, $\chi_0 = 10^{-3}\,M_{\rm pl}$, $\xi_\phi = 1000$, $\lambda_\phi = 0.01$, $\varepsilon = 0$ and $\Lambda_\chi = 0$.

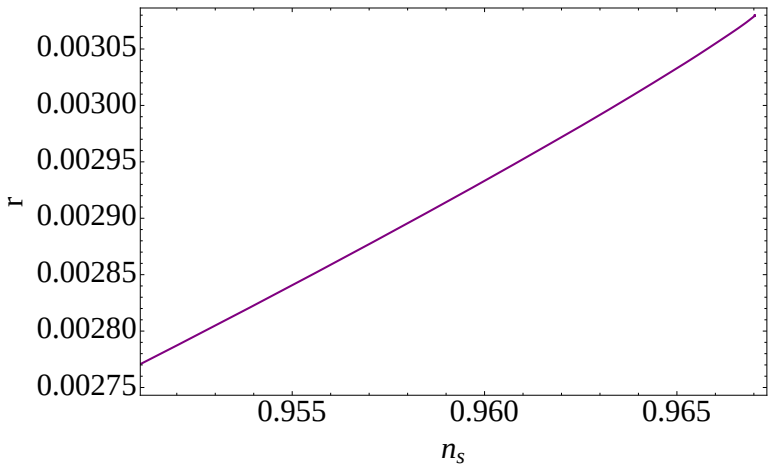

Figure 7-15: The correlation between r and n_s could theoretically break the degeneracy between our models. The parameters used for this plot are $\phi_0 = 0.3\,M_{\rm pl}$, $\chi_0 = 10^{-3}\,M_{\rm pl}$, $\xi_\phi = 1000$, $\lambda_\phi = 0.01$, $\varepsilon = 0$ and $\Lambda_\chi = 0$, with $0 \leq \kappa \leq 0.1$.

limit of weak curvature ($\kappa \ll 1$), and we find $|f_{\rm NL}| \ll \mathcal{O}(1)$ for the entire range of parameters and initial conditions, fully consistent with the latest bounds from *Planck* [35].

Thus we have found that there exists a range of parameter space in which multi-field dynamics remain nontrivial, producing $\beta_{\rm iso} \sim \mathcal{O}(0.1)$, even as the other important observable quantities remain well within the most-favored region of the latest observations from *Planck*.

7.5 Conclusions

Previous work has demonstrated that multifield inflation with nonminimal couplings provides close agreement with a number of spectral observables measured by the *Planck* collaboration [19] (see also [40]). In the limit of strong curvature of the effective potential in the Einstein frame, $\kappa \gg 1$, the single-field attractor for this class of models pins the predicted value of the spectral index, n_s, to within 1σ of the present best-fit observational value, while also keeping the tensor-to-scalar ratio, r, well below the present upper bounds. In the limit of $\kappa \gg 1$, these models also generically predict no observable running of the spectral index, and (in the absence of severe fine-tuning of initial conditions [22]) no observable non-Gaussianity, $|\alpha|, |f_{\rm NL}| \ll 1$. In the limit of the single-field attractor, however, these models also predict no observable multifield effects, such as amplification of primordial isocurvature modes, hence $\beta_{\rm iso} \sim 0$ in the limit $\kappa \gg 1$.

In this chapter, we have demonstrated that the same class of models can produce significant isocurvature modes, $\beta_{\rm iso} \sim \mathcal{O}(0.1)$, in the limit of weak curvature of the Einstein-frame potential, $\kappa \leq 0.1$. In that limit, these models again predict values for n_s, α, r, and $f_{\rm NL}$ squarely within the present best-fit bounds, while also providing a plausible explanation for the observed anomaly at low multipoles in recent measurements of CMB temperature anisotropies [11]. These models predict non-negligible isocurvature fractions across a wide range of initial field values, with a dependence of $\beta_{\rm iso}$ on couplings that admits an analytic, intuitive, geometric interpretation. Our

geometric approach provides an analytically tractable method in excellent agreement with numerical simulations, which could be applied to other multifield models in which the effective potential is "lumpy."

The mechanism for generating $\beta_{\rm iso} \sim 0.1$ that we have investigated in this chapter is based on the idea that a symmetry among the fields' bare couplings λ_I, g, and ξ_I is softly broken. Such soft breaking would result from a coupling of one of the fields (say, χ) to either a CDM scalar field or to a neutrino species; some such coupling would be required in order for the primordial isocurvature perturbations to survive to the era of photon decoupling, so that the primordial perturbations could be impressed in the CMB [20]. Hence whatever couplings might have enabled primordial isocurvature modes to modify the usual predictions from the simple, purely adiabatic ΛCDM model might also have generated weak but nonzero curvature in the effective potential, $\kappa \ll 1$. If the couplings λ_I, g, and ξ_I were not subject to a (softly broken) symmetry, or if the fields' initial conditions were not such that the fields began near the top of a ridge in the potential, then the predictions from this class of models would revert to the single-field attractor results analyzed in detail in [19].

Inflation in this class of models ends with the fields oscillating around the global minimum of the potential. Preheating in such models offers additional interesting phenomena [37], and further analysis is required to understand how the primordial perturbations analyzed here might be affected by preheating dynamics. In particular, preheating in multifield models — under certain conditions — can amplify perturbations on cosmologically interesting length scales [43]. Thus the behavior of isocurvature modes during preheating [44] requires careful study, to confirm whether preheating effects in the family of models considered here could affect any of the predictions for observable quantities calculated in this chapter. We are presently studying effects of preheating in this family of models.

Finally, expected improvements in observable constraints on the tensor-to-scalar ratio, as well as additional data on the low-ℓ portion of the CMB power spectrum, could further test this general class of models and perhaps distinguish among members of the class.

7.6 Acknowledgments

It is a pleasure to thank Bruce Bassett, Rhys Borchert, Xingang Chen, Alan Guth, Carter Huffman, Scott Hughes, Adrian Liu, and Edward Mazenc for helpful discussions. This work was supported in part by the U.S. Department of Energy (DOE) under Contract DE-FG02-05ER41360 and in part by MIT's Undergraduate Research Opportunities Program.

7.7 Appendix

7.7.1 Approximated Dynamical Quantities

In this appendix, we present results for dynamical quantities under our approximations that $\xi_\phi, \xi_\chi \gg 1$, $\xi_\phi \phi^2 \gg M_{\rm pl}^2$, and $\chi_0 \ll M_{\rm pl}$.

First we expand quantities associated with field-space curvature, starting with the field-space metric, $\mathcal{G}_{IJ}$, using the definition from Eq. (7.6). We arrive at the following expressions:

$$\begin{aligned} \mathcal{G}_{\phi\phi} &\simeq \frac{6M_{\rm pl}^2}{\phi^2} \\ \mathcal{G}_{\phi\chi} = \mathcal{G}_{\chi\phi} &\simeq \frac{6M_{\rm pl}^2 \xi_\chi \chi}{\xi_\phi \phi^3} \\ \mathcal{G}_{\chi\chi} &\simeq \frac{M_{\rm pl}^2}{\xi_\phi \phi^2}. \end{aligned} \tag{7.65}$$

We also find

$$\begin{aligned} \mathcal{G}^{\phi\phi} &\simeq \frac{\phi^2}{6M_{\rm pl}^2} \\ \mathcal{G}^{\phi\chi} = \mathcal{G}^{\chi\phi} &\simeq -\frac{\xi_\chi \phi \chi}{M_{\rm pl}^2} \\ \mathcal{G}^{\chi\chi} &\simeq \frac{\xi_\phi \phi^2}{M_{\rm pl}^2}. \end{aligned} \tag{7.66}$$

Next we expand the field-space Christoffel symbols, Γ^I_{JK}, and find

$$\begin{aligned}
\Gamma^\phi_{\phi\phi} &\simeq -\frac{1}{\phi} \\
\Gamma^\phi_{\chi\phi} = \Gamma^\phi_{\phi\chi} &\simeq -\frac{\xi_\chi \chi}{\xi_\phi \phi^2} \\
\Gamma^\phi_{\chi\chi} &\simeq \frac{\xi_\chi}{\xi_\phi \phi} \\
\Gamma^\chi_{\phi\phi} &\simeq \frac{\xi_\chi \chi}{\xi_\phi \phi^2} \\
\Gamma^\chi_{\chi\phi} = \Gamma^\chi_{\phi\chi} &\simeq -\frac{1}{\phi} \\
\Gamma^\chi_{\chi\chi} &\simeq -\frac{\xi_\chi \chi \left(2\xi_\phi - \xi_\chi\right)}{\xi_\phi^2 \phi^2}.
\end{aligned} \tag{7.67}$$

The nonzero components of the field-space Riemann curvature tensor become

$$\begin{aligned}
\mathcal{R}^\phi_{\phi\phi\chi} = -\mathcal{R}^\phi_{\phi\chi\phi} &\simeq \varepsilon(\varepsilon - 1)\frac{\chi}{\phi^3} \\
\mathcal{R}^\phi_{\chi\phi\chi} = -\mathcal{R}^\phi_{\chi\chi\phi} &\simeq -\frac{\varepsilon}{6\xi_\phi \phi^2} \\
\mathcal{R}^\chi_{\phi\chi\phi} = -\mathcal{R}^\chi_{\phi\phi\chi} &\simeq -\frac{\varepsilon}{\phi^2} \\
\mathcal{R}^\chi_{\chi\phi\chi} = -\mathcal{R}^\chi_{\chi\chi\phi} &\simeq \varepsilon(1 - \varepsilon)\frac{\chi}{\phi^3}.
\end{aligned} \tag{7.68}$$

We also expand dynamical quantities, beginning with the fields' velocity:

$$\dot\sigma \simeq \frac{\sqrt{2\lambda_\phi} M_{\rm pl}^4}{3\xi_\phi^2 \phi^2}, \tag{7.69}$$

and the turn rate ω in the ϕ and χ directions:

$$\begin{aligned}
\omega^\phi &\simeq 0 \\
\omega^\chi &\simeq \frac{3\phi^2\left(2M_{\rm pl}\Lambda_\phi \chi - \sqrt{3\lambda_\phi}\xi_\phi \dot\chi\right)}{2\sqrt{2\lambda_\phi} M_{\rm pl}^3}.
\end{aligned} \tag{7.70}$$

7.7.2 Covariant formalism and potential topography

We have defined the character of the maxima and minima of the potential using the (normal) partial derivative at asymptotically large field values, where the manifold is asymptotically flat, hence the normal and covariant derivatives asymptote to the same value. By keeping the next to leading order term in the series expansion, we can test the validity of this approach for characterizing the nature of the extrema.

We take as an example the potential parameters used in Fig. 7-3, specifically $\xi_\phi = 1000,\ \xi_\chi = 999.985,\ \lambda_\phi = 0.01,\ \lambda_\chi = 0.01,\ g = 0.01$. The ridge of the potential occurs at $\chi = 0$.

The asymptotic value of the second partial derivative is

$$V_{,\chi\chi}|_{\chi=0} \to \frac{-M_{\rm pl}^4 \Lambda_\phi}{\xi_\phi^3 \phi^2} = \frac{-M_{\rm pl}^4 \times 1.5 \cdot 10^{-5}}{\xi_\phi \phi^2} \tag{7.71}$$

Let us look at the partial second derivative for $\chi = 0$ and finite ϕ:

$$\begin{aligned} V_{,\chi\chi}|_{\chi=0} &= M_{\rm pl}^4 \phi^2 \frac{\left[-\Lambda_\phi \xi_\phi \phi^2 + g \xi_\phi M_{\rm pl}^2\right]}{\xi_\phi (M_{\rm pl}^2 + \xi_\phi \phi^2)^3} \\ &\propto \left[-0.015\ \xi_\phi \phi^2 + 10 M_{\rm pl}^2\right]. \end{aligned} \tag{7.72}$$

We see that the two terms can be comparable. In particular, the second derivative changes sign at

$$V_{,\chi\chi}|_{\chi=0} = 0 \Rightarrow \xi_\phi \phi_{tr}^2 \approx 667 M_{\rm pl}^2 \tag{7.73}$$

which is a field value larger than the one we used for our calculation. In order to get 70 efolds of inflation, $\xi_\phi \phi^2 \sim 100 M_{\rm pl}^2$, significantly smaller than the transition value. For $\phi < \phi_{tr}$ the second derivative is positive, meaning there is a transition where the local maximum becomes a local minimum. This means that if one was to take our Einstein frame potential as a phenomenological model without considering the field space metric, even at large field values, where slow roll inflation occurs, the results would be qualitatively different.

Let us now focus our attention on the covariant derivative, keeping in mind that

in a curved manifold it is a much more accurate indicator of the underlying dynamics.

$$\mathcal{D}_{\chi\chi}V = V_{,\chi\chi} - \Gamma^{\phi}_{\chi\chi}V_{,\phi} - \Gamma^{\chi}_{\chi\chi}V_{,\chi}. \tag{7.74}$$

Looking at the extra terms and keeping the lowest order terms we have $V_{,\chi} = 0$ by symmetry, $V_{,\phi} \approx \lambda_\phi/(\xi_\phi^3\phi^3)$, and $\Gamma^{\phi}_{\chi\chi} = \xi_\phi(1+6\xi_\chi)\phi/C \approx \xi_\chi/(\xi_\phi\phi)$.

We will now expand the covariant derivative term in $1/\phi$ and also in ξ_ϕ and ξ_χ. This way we will make sure that there is no transition in the behavior of the extremum for varying field values, that is to say the character of the extremum will be conserved term by term in the expansion (we only show this for the first couple of terms, but the trend is evident). We find

$$\begin{aligned}
\mathcal{D}_{\chi\chi}V = &\frac{-\Lambda_\phi M_{\rm pl}^4}{\xi_\phi^3\phi^2} \\
&+ \frac{M_{\rm pl}^6}{\xi_\phi^3\phi^2(\xi_\phi\phi^2)}\left[2\Lambda_\phi - \frac{\lambda_\phi\varepsilon}{6}\left(1-\frac{1}{6\xi_\phi}\right) + ...\right] \\
&+ \frac{M_{\rm pl}^8}{\xi_\phi^3\phi^2(\xi_\phi\phi^2)^2}\times \\
&\qquad\left[-3\Lambda_\phi + \frac{\lambda_\phi}{6}(1+2\varepsilon) - \frac{\lambda_\phi}{36\xi_\phi}(1+\varepsilon) + ...\right] \\
&+ ...
\end{aligned} \tag{7.75}$$

We have written the covariant derivative using the geometrically intuitive combinations of parameters, which was done in the main text in a more general setting ($\chi \neq 0$). It is worthwhile to note that we did not write the closed form solution for $\mathcal{D}_{\chi\chi}V$ (which is straightforward to calculate using the Christoffel symbols, given explicitly in [22]), since this power series expansion is both more useful and more geometrically transparent, since it is easy to see the order at which each effect is first introduced.

We see that once we take out the $(1/\xi_\phi^3\phi^2)$ behavior there remains a multiple series expansion as follows

- Series in $(1/\xi_\phi\phi^2)$

- Each term of the above series is expanded in inverse powers of ξ_ϕ.

For the example of Fig. 7-3 the relevant quantity that defines to lowest order in ξ_ϕ and ξ_χ all terms of the series is $\Lambda_\phi = 0.015$.

By inspection of the terms, we can see that for our choice of parameters the first term defines the behavior of the covariant derivative, which is also the asymptotic value of the normal second derivative that we used to characterize the character of the extremum. In the case when $\Lambda_\phi = 0$ the ellipticity term e is dominant. Even if $\lambda_\phi = \varepsilon = 0$ then the dominant term comes at an even higher order and is proportional to λ_ϕ.

In other words, the character of the extremum is conserved if one considers the covariant derivatives. For asymptotically large field values the two coincide, since the curvature vanishes. It is thus not only quantitatively but also qualitatively essential to use our covariant formalism for the study of these models, even at large field values where the curvature of the manifold is small.

Now that the character of the maximum is clear we can proceed to calculating all η_{ss}. We neglect the term in $\mathcal{M}_{ss}$ that is proportional to $\mathcal{R}^I_{JKL}$, since the curvature of the field-space manifold is subdominant for $\xi_\phi \phi_0^2 \gg M_{\rm pl}^2$ and the $\mathcal{R}^I_{JKL}$ term is multiplied by two factors of the fields' velocity. If in addition we take $\chi = \dot{\chi} = 0$, then $\mathcal{M}_{ss}$ becomes

$$\mathcal{M}_{ss} \simeq \hat{s}^\chi \hat{s}^\chi \mathcal{D}_{\chi\chi} V = \frac{\xi_\phi \phi^2}{M_{\rm pl}^2} \left(1 + \frac{M_{\rm pl}^2}{\xi_\phi \phi^2}\right) \mathcal{D}_{\chi\chi} V. \tag{7.76}$$

Using the double series expansion of Eq. (7.75) the entropic mass-squared becomes

$$\begin{aligned} \mathcal{M}_{ss} V = & \frac{-\Lambda_\phi M_{\rm pl}^2}{\xi_\phi^2} \\ & + \frac{M_{\rm pl}^4}{\xi_\phi^2 (\xi_\phi \phi^2)} \left[\Lambda_\phi - \frac{\lambda_\phi \varepsilon}{6}\left(1 - \frac{1}{6\xi_\phi}\right) + ...\right] \\ & + \frac{M_{\rm pl}^6}{\xi_\phi^2 (\xi_\phi \phi^2)^2} \left[-\Lambda_\phi + \frac{\lambda_\phi}{6}(1+\varepsilon) + ...\right] + ... \end{aligned} \tag{7.77}$$

To find the generalized slow roll parameter η_{ss} we need to divide by the potential,

which again can be expanded in a power series for $\chi \to 0$ as

$$V = M_{\rm pl}^4 \frac{\lambda_\phi}{4\xi_\phi^2} - M_{\rm pl}^6 \frac{\lambda_\phi}{2\xi_\phi^3 \phi^2} + M_{\rm pl}^8 \frac{3\lambda_\phi}{4\xi_\phi^4 \phi^4} + ... \tag{7.78}$$

The calculation of η_{ss} is now a straightforward exercise giving

$$\begin{aligned} \eta_{ss} \approx \frac{M_{\rm pl}^2 \mathcal{M}_{ss}}{V} &= \frac{-4\Lambda_\phi}{\lambda_\phi} \\ &+ \frac{M_{\rm pl}^2}{\xi_\phi \phi^2}\left[\frac{-4\Lambda_\phi}{\lambda_\phi} - \frac{2\varepsilon}{3} + \mathcal{O}\left(\frac{1}{\xi_\phi}\right)\right] \\ &+ \frac{M_{\rm pl}^4}{(\xi_\phi \phi^2)^2}\left[\frac{2}{3}(1-\varepsilon) + \mathcal{O}\left(\frac{1}{\xi_\phi}\right)\right] \\ &+ \mathcal{O}\left(\frac{1}{(\xi_\phi \phi^2)^3}\right) \\ \approx -\kappa + \frac{3}{4N_*}\left[-\kappa - \frac{2\varepsilon}{3}\right] &+ \frac{9}{16N_*^2}\left[\frac{2}{3}(1-\varepsilon)\right] \end{aligned} \tag{7.79}$$

where we used the slow-roll solution for ϕ from Eq. (7.47), identifying it as the inflationary clock and the definition $\kappa = 4\Lambda_\phi/\lambda_\phi$. By setting $\kappa = \varepsilon = 0$ we see that even in the fully symmetric case the isocurvature mass is small but positive.

In the limit of $\chi \to 0$ there is no turning ($\omega = 0$), and hence $T_{\mathcal{RS}} = 0$. In order to calculate T_{SS} we need

$$\begin{aligned} \beta &= -2\epsilon - \eta_{ss} + \eta_{\sigma\sigma} \\ &\simeq \kappa + \frac{1}{N_*}\left[\frac{3\kappa}{4} + \frac{\varepsilon}{2} - 1\right] + \frac{1}{N_*^2}\left[\frac{3\varepsilon}{8} - \frac{9}{8}\right]. \end{aligned} \tag{7.80}$$

From Eq. (7.34), we see that $T_{\mathcal{SS}}$ depends on the integral

$$\int_{t_{\rm hc}}^{t} \beta H dt' = \int_{N_*}^{N_{\rm hc}} \beta dN'. \tag{7.81}$$

Plugging in the expression for β from Eq. (7.80)

$$\begin{aligned}\int_{N_*}^{N_{\rm hc}} \beta dN' = \kappa(N_{\rm hc} - N_*) \\ - c_1 \ln\left(\frac{N_{\rm hc}}{N_*}\right) - c_2\left(\frac{1}{N_*} - \frac{1}{N_{\rm hc}}\right)\end{aligned} \tag{7.82}$$

where

$$c_1 = 1 - \frac{3\kappa}{4} - \frac{\varepsilon}{2} \tag{7.83}$$

$$c_2 = \frac{9}{8} - \frac{3\varepsilon}{8}. \tag{7.84}$$

Of course there is the ambiguity of stopping the integration one e-fold before the end of inflation. If one plots β vs. N_* and does a rough integration of the volume under the curve, one finds this area giving an extra contribution $\int_1^0 \beta dN \sim -1$. This is a change, but not a severe one. We will neglect it for now, keeping in mind that there is an $\mathcal{O}(1)$ multiplicative factor missing from the correct result. However since β varies over a few orders of magnitude, we can consider this factor a small price to pay for such a simple analytical result.

Bibliography

[1] A. H. Guth, "The inflationary universe: A possible solution to the horizon and flatness problems," Phys. Rev. D **23**, 347 (1981); A. D. Linde, "A new inflationary universe scenario: A possible solution to the horizon, flatness, homogeneity, isotropy and primordial monopole problems," Phys. Lett. B **108**, 389 (1982); A. Albrecht and P. J. Steinhardt, "Cosmology for grand unified theories with radiatively induced symmetry breaking," Phys. Rev. Lett. **38**, 1220 (1982).

[2] A. H. Guth and D. I. Kaiser, "Inflationary cosmology: Exporing the universe from the smallest to the largest scales," Science **307**, 884 (2005) [arXiv:astro-ph/0502328]; J. Martin, C. Ringeval, and V. Vennin, "Encyclopedia Inflationaris," arXiv:1303.3787 [astro-ph.CO].

[3] B. A. Bassett, S. Tsujikawa, and D. Wands, "Inflation dynamics and reheating," Rev. Mod. Phys. **78**, 537 (2006) [arXiv:astro-ph/0507632]; K. A. Malik and D. Wands, "Cosmological perturbations," Phys. Rept. **475**, 1 (2009) [arXiv:0809.4944 [astro-ph]].

[4] D. H. Lyth and A. Riotto, "Particle physics models of inflation and the cosmological density perturbation," Phys. Rept. **314**, 1 (1999) [arXiv:hep-ph/9807278]; C. P. Burgess, "Lectures on cosmic inflation and its potential stringy realizations," Class. Quant. Grav. **24**, S795 (2007) [arXiv:0708.2865 [hep-th]]; L. McAllister and E. Silverstein, "String cosmology: A review," Gen. Rel. Grav. **40**, 565 (2008) [arXiv:0710.2951 [hep-th]]; D. Baumann and L. McAllister, "Advances in inflation in string theory," Ann. Rev. Nucl. Part. Sci. **59**, 67 (2009) [arXiv:0901.0265 [hep-th]]; A. Mazumdar and J. Rocher, "Particle

physics models of inflation and curvaton scenarios," Phys. Rept. **497**, 85 (2011) [arXiv:1001.0993 [hep-ph]].

[5] C. G. Callan, Jr., S. R. Coleman, and R. Jackiw, "A new improved energy-momentum tensor," Ann. Phys. (N.Y.) **59**, 42 (1970); T. S. Bunch, P. Panangaden, and L. Parker, "On renormalisation of $\lambda\phi^4$ field theory in curved space-time, I," J. Phys. A **13**, 901 (1980); T. S. Bunch and P. Panangaden, "On renormalisation of $\lambda\phi^4$ field theory in curved space-time, II," J. Phys. A **13**, 919 (1980).

[6] N. D. Birrell and P. C. W. Davies, *Quantum Fields in Curved Space* (New York: Cambridge University Press, 1982).

[7] I. L. Buchbinder, S. D. Odintsov, and I. L. Shapiro, *Effective Action in Quantum Gravity* (New York: Taylor and Francis, 1992).

[8] V. Faraoni, "A crucial ingredient for inflation," Int. J. Theo. Phys. **40**, 2259 (2001) [arXiv:hep-th/0009053].

[9] D. S. Salopek, J. R. Bond, and J. M. Bardeen, "Designing density fluctuation spectra in inflation," Phys. Rev. D **40**, 1753 (1989); R. Fakir and W. G. Unruh, "Improvement on cosmological chaotic inflation through nonminimal coupling," Phys. Rev. D **41**, 1783 (1990); D. I. Kaiser, "Primordial spectral indices from generalized Einstein theories," Phys. Rev. D **52**, 4295 (1995) [arXiv:astro-ph/9408044]; E. Komatsu and T. Futamase, "Complete constraints on a nonminimally coupled chaotic inflationary scenario from the cosmic microwave background," Phys. Rev. D **59**, 064029 (1999) [arXiv:astro-ph/9901127]; A. Linde, M. Noorbala, and A. Westphal, "Observational consequences of chaotic inflation with nonminimal coupling to gravity," JCAP **1103**, 013 (2011) [arXiv:1101.2652 [hep-th]].

[10] F. L. Bezrukov and M. E. Shaposhnikov, "The Standard Model Higgs boson as the inflaton," Phys. Lett. B **659**, 703 (2008) [arXiv:0710.3755 [hep-th]].

[11] Planck collaboration, "*Planck* 2013 results, XXII. Constraints on inflation," arXiv:1303.5082 [astro-ph.CO].

[12] A. D. Linde, "Generation of isothermal density perturbations in the inflationary universe," Phys. Lett. B **158**, 375 (1985); D. Polarski and A. A. Starobinsky, "Isocurvature perturbations in multiple inflationary models," Phys. Rev. D **50**, 6123 (1994) [arXiv:astro-ph/9404061]; J García-Bellido and D. Wands, "Metric perturbations in two-field inflation," Phys. Rev. D **53**, 5437 (1996) [arXiv:astro-ph/9511029].

[13] C. Gordon, D. Wands, B. A. Bassett, and R. Maartens, "Adiabatic and entropy perturbations from inflation," Phys. Rev. D **63**, 023506 (2001) [arXiv:astro-ph/0009131]; S. Groot Nibbelink and B. J. W. van Tent, "Density perturbations arising from multiple field slow-roll inflation," arXiv:hep-ph/0011325; S. Groot Nibbelink and B. J. W. van Tent, "Scalar perturbations during multiple-field slow-roll inflation," Class. Quant. Grav. **19**, 613 (2002) [arXiv:hep-ph/0107272].

[14] D. Wands, N. Bartolo, S. Matarrese, and A. Riotto, "An observational test of two-field inflation," Phys. Rev. D **66** (2002): 043520 [arXiv:astro-ph/0205253].

[15] A. R. Liddle, A. Mazumdar, and F. E. Schunck, "Assisted inflation," Phys. Rev. D **58**, 061301 (1998) [arXiv:astro-ph/9804177]; A. Mazumdar and L. Wang, "Separable and non-separable multi-field inflation and large non-Gaussianity," JCAP **09**: 005 (2012) [arXiv:1203.3558 [astro-ph.CO]].

[16] D. Wands, "Multiple field inflation," Lect. Notes. Phys. **738**, 275 (2008) [arXiv:astro-ph/0702187].

[17] F. Di Marco, F. Finelli, and R. Brandenberger, "Adiabatic and isocurvature perturbations for multifield generalized Einstein models," Phys. Rev. D **67**, 063512 (2003) [arXiv:astro-ph/0211276]; D. Langlois and S. Renaux-Petel, "Perturbations in generalized multi-field inflation," JCAP **0804**, 017 (2008) [arXiv:0801.1085 [hep-th]]; D. I. Kaiser and A. T. Todhunter, "Primordial perturbations from multifield inflation with nonminimal couplings," Phys. Rev. D

81, 124037 (2010) [arXiv:1004.3805 [astro-ph.CO]]; L. McAllister, S. Renaux-Peterl, G. Xu, "A statistical approach to multifield inflation: Many-field perturbations beyond slow roll," arXiv:1207.0317 [astro-ph.CO].

[18] C. M. Peterson and M. Tegmark, "Testing two-field inflation," Phys. Rev. D **83**, 023522 (2011) [arXiv:1005.4056 [astro-ph.CO]]; "Non-Gaussianity in two-field inflation," Phys. Rev. D **84**, 023520 (2011) [arXiv:1011.6675 [astro-ph.CO]]; "Testing multifield inflation: A geometric approach," Phys. Rev. D **87**, 103507 (2013) [arXiv:1111.0927 [astro-ph.CO]].

[19] D. I. Kaiser and E. I. Sfakianakis, "Multifield Inflation after *Planck*: The Case for Nonminimal Couplings," Phys. Rev. Lett. **112**, 011302 (2014) [arXiv:1304.0363 [astro-ph.CO]].

[20] M. Bucher, K. Moodley, and N. Turok, "The general primordial cosmic perturbation," Phys. Rev. D **62**, 083508 (2000) [arXiv:astro-ph/9904231]; M. Bucher, K. Moodley, and N. Turok, "Characterising the primordial cosmic perturbations," Phys. Rev. D **66**, 023528 (2002) [arXiv:astro-ph/0007360]; H. Kurki-Suonio, V. Muhonen, and J. Väliviita, "Correlated primordial perturbations in light of CMB and large scale structure data," Phys. Rev. D **71**, 063005 (2005) [arXiv:astro-ph/0412439].

[21] D. I. Kaiser, "Conformal transformations with multiple scalar fields," Phys. Rev. D **81**, 084044 (2010) [arXiv:1003.1159 [gr-qc]].

[22] D. I. Kaiser, E. A. Mazenc, and E. I. Sfakianakis, "Primordial bispectrum from multifield inflation with nonminimal couplings," Phys. Rev. D **87**, 064004 (2013) [arXiv:1210.7487 [astro-ph.CO]].

[23] ATLAS Collaboration, "Observation of a new particle in the search for the Standard Model Higgs boson with the ATLAS detector at the LHC," Phys. Lett. B **716**, 1 (2012) [arXiv:1207.7214 [hep-ex]]; CMS Collaboration, "Observation of a new boson at a mass of 125 GeV with the CMS experiment at the LHC," Phys. Lett. B **716**, 30 (2012) [arXiv:1207.7235 [hep-ex]].

[24] Higgs inflation should be treated as a multifield model, and hence as a member of the class under consideration here, since the Goldstone modes remain in the spectrum at high energies in renormalizable gauges [25, 26, 27].

[25] S. Weinberg, *The Quantum Theory of Fields*, vol. 2, *Modern Applications* (New York: Cambridge University Press, 1996).

[26] S. Mooij and M. Postma, "Goldstone bosons and a dynamical Higgs field," JCAP **1109**, 006 (2011) [arXiv:1104.4897 [hep-ph]].

[27] R. N. Greenwood, D. I. Kaiser, and E. I. Sfakianakis, "Multifield dynamics of Higgs inflation," Phys. Rev. D **87**, 064021 (2013) [arXiv:1210.8190 [hep-ph]].

[28] A. O. Barvinsky, A. Yu. Kamenschchik, C. Kiefer, A. A. Starobinsky, and C. F. Steinwachs, "Asymptotic freedom in inflationary cosmology with a nonminimally coupled Higgs field," JCAP **0912**, 003 (2009) [arXiv:0904.1698 [hep-ph]]; A. O. Barvinsky, A. Yu. Kamenschcik, C. Kiefer, A. A. Starobinsky, and C. F. Steinwachs, "Higgs boson, renormalization group, and naturalness in cosmology," Euro. Phys. J. C **72**, 2219 (2012) [arXiv:0910.1041 [hep-ph]]; F. Bezrukov, M. Yu. Kalmykov, B. A. Kniehl, and M. Shaposhnikov, "Higgs boson mass and new physics," JHEP **1210**, 140 (2012) [arXiv:1205.2893 [hep-ph]].

[29] K. Allison, "Higgs ξ-inflation for the 125 - 126 GeV Higgs: A two-loop analysis," arXiv:1306.6931 [hep-ph].

[30] C. P. Burgess, H. M. Lee, and M. Trott, "Power-counting and the validity of the classical approximation during inflation," JHEP **0909**, 103 (2009) [arXiv:0902.4465 [hep-ph]]; C. P. Burgess, H. M. Lee, and M. Trott, "Comment on Higgs inflation and naturalness," JHEP **1007**, 007 (2010) [arXiv:1002.2730 [hep-ph]]; J. L. F. Barbon and J. R. Espinosa, "On the naturalness of Higgs inflation," Phys. Rev. D **79**, 081302 (2009) [arXiv:0903.0355 [hep-ph]]; M. P. Hertzberg, "On inflation with non-minimal coupling," JHEP **1011**, 023 (2010)[arXiv:1002.2995 [hep-ph]]; R. N. Lerner and J. McDonald, "A

unitarity-conserving Higgs inflation model," Phys. Rev. D **82**, 103525 (2010) [arXiv:1005.2978 [hep-ph]]; S. Ferrara, R. Kallosh, A. Linde, A. Marrani, and A. Van Proeyen, "Superconformal symmetry, NMSSM, and inflation," Phys. Rev. D **83**, 025008 (2011) [arXiv:1008.2942 [hep-th]]; F. Bezrukov, A. Magnin, M. Shaposhnikov, and S. Sibiryakov, "Higgs inflation: Consistency and generalizations," JHEP **1101**, 016 (2011) [arXiv:1008.5157 [hep-ph]]; F. Bezrukov, "The Higgs field as an inflaton," Class. Quantum Grav. **30**, 214001 (2013) [arXiv:1307.0708 [hep-ph]]; X. Calmet and R. Casadio, "Self-healing of unitarity in Higgs inflation," arXiv:1310.7410 [hep-ph].

[31] R. N. Lerner and J. McDonald, "Unitarity-violation in generalized Higgs inflation models," JCAP **11** (2012): 019 [arXiv:1112.0954 [hep-ph]]; F. Bezrukov, G. K. Karananas, J. Rubio, and M. Shaposhnikov, "Higgs-dilaton cosmology: An effective field theory approach," Phys. Rev. D **87**, 096001 (2013) [arXiv:1212.4148 [hep-ph]].

[32] G. F. Giudice and H. M. Lee, "Unitarizing Higgs inflation," Phys. Lett. B **694**, 294 (2011) [arXiv:1010.1417 [hep-ph]]; H. M. Lee, "Running inflation with unitary Higgs," Phys. Lett. B **722**, 198 (2013) [arXiv:1301.1787 [hep-ph]];

[33] D. J. H. Chung, L. L. Everett, G. L. Kane, S. F. King, J. Lykken, and L.-T. Wang, "The soft supersymmetry-breaking Lagrangian: Theory and applications," Phys. Rept. **407**, 1 (2005) [arXiv:hep-ph/0312378].

[34] WMAP collaboration, "Nine-year Wilkinson Microwave Anisotropy Probe (WMAP) observations: Cosmological parameter results," arXiv:1212.5226 [astro-ph.CO].

[35] Planck collaboration, "*Planck* 2013 results, XXIV. Constraints on primordial non-Gaussianity," arXiv:1303.5084 [astro-ph.CO].

[36] Planck collaboration, "*Planck* 2013 results, XV. CMB power spectra and likelihood," arXiv:1303.5075 [astro-ph.CO].

[37] F. Bezrukov, D. Gorbunov, and M. Shaposhnikov, "On initial conditions for the hot big bang," JCAP **0906**, 029 (2009) [arXiv:0812.3622 [hep-ph]]; J. García-Bellido, D. G. Figueroa, and J. Rubio, "Preheating in the Standard Model with the Higgs-inflaton coupled to gravity," Phys. Rev. D **79**, 063531 (2009) [arXiv:0812.4624 [hep-ph]]; J.-F. Dufaux, D. G. Figueroa, and J. García-Bellido, "Gravitational waves from Abelian gauge fields and cosmic strings at preheating," Phys. Rev. D **82**, 083518 (2010) [arXiv:1006.0217 [astro-ph.CO]].

[38] A. H. Guth and E. I. Sfakianakis, "Density Perturbations in Hybrid Inflation Using a Free Field Theory Time-Delay Approach," arXiv:1210.8128 [astro-ph.CO]

[39] R. Kallosh, A. Linde and D. Roest, "A universal attractor for inflation at strong coupling," arXiv:1310.3950 [hep-th]

[40] R. Kallosh and A. Linde, "Multi-field Conformal Cosmological Attractors," arXiv:1309.2015 [hep-th]

[41] R. Kallosh and A. Linde, "Non-minimal Inflationary Attractors," arXiv:1307.7938 [hep-th] R. Kallosh and A. Linde, "Universality Class in Conformal Inflation," JCAP **1307**, 002 (2013) [arXiv:1306.5220 [hep-th]] R. Kallosh and A. Linde, "Superconformal generalizations of the Starobinsky model," JCAP **1306**, 028 (2013) [arXiv:1306.3214 [hep-th]]

[42] R. Kallosh and A. Linde, "Superconformal generalization of the chaotic inflation model $\frac{\lambda}{4}\phi^4 - \frac{\xi}{2}\phi^2 R$," JCAP **1306**, 027 (2013) [arXiv:1306.3211 [hep-th]]

[43] B. A. Bassett, D. I. Kaiser, and R. Maartens, "General relativistic effects in preheating," Phys. Lett. B **455**, 84 (1999) [arXiv:hep-ph/9808404]; F. Finelli and R. Brandenberger, "Parametric amplication of gravitational fluctuations during reheating," Phys. Rev. Lett. **82**, 1362 (1999) [arXiv:hep-ph/9809490]; B. A. Bassett, F. Tamburini, D. I. Kaiser, and R. Maartens, "Metric preheating and limitations of linearized gravity," Nucl. Phys. B **561**, 188 (1999) [arXiv:hep-ph/9901319]; B. A. Bassett, C. Gordon, R. Maartens, and D. I. Kaiser, "Restor-

ing the sting to metric preheating," Phys. Rev. D **61**, 061302 (2000) [arXiv:hep-ph/9909482]; S. Tsujikawa and B. A. Bassett, "When can preheating affect the CMB?," Phys. Lett. B **536**, 9 (2002) [arXiv:astro-ph/0204031].

[44] F. Finelli and R. Brandenberger, "Parametric amplification of metric fluctuations during reheating in two field models," Phys. Rev. D **62**, 083502 (2000) [arXiv:hep-ph/0003172]; F. Finelli and S. Khlebnikov, "Large metric perturbations from rescattering," Phys. Lett. B **504**, 309 (2001) [arXiv:hep-ph/0009093]; F. Finelli and S. Khlebnikov, "Metric perturbations at reheating: The use of spherical symmetry," Phys. Rev. D **65**, 043505 (2002) [arXiv:hep-ph/0107143]; J. Lachapelle and R. H. Brandenberger, "Preheating with non-standard kinetic term," JCAP **0904**, 020 (2009) [arXiv:0808.0936 [hep-th]]; J. Garcia-Bellido, J. Rubio, and M. Shaposhnikov, "Higgs-dilaton cosmology: Are there extra relativistic species?," Phys. Lett. B **718**, 507 (2012) [arXiv:1209.2119 [hep-ph]].